

Lawrence Berkeley National Laboratory

Recent Work

Title

Nuclear Science Division Annual Report 1992

Permalink

<https://escholarship.org/uc/item/5w2124c1>

Author

Symons, T.J.M.

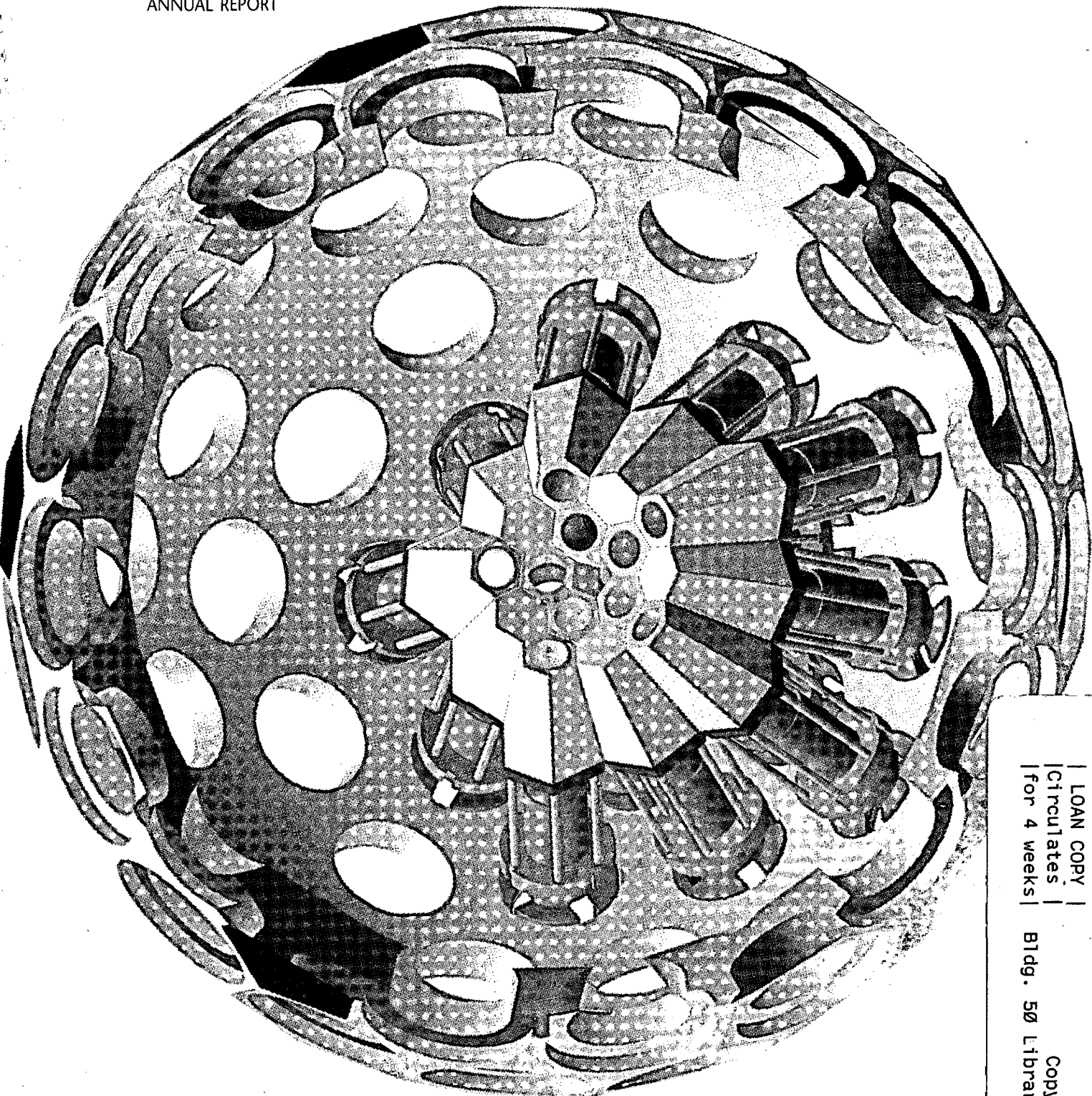
Publication Date

1993-06-01

NUCLEAR
SCIENCE
DIVISION

1992

ANNUAL REPORT



| LOAN COPY |
| Circulates |
| for 4 weeks |

Bldg. 50 Library.

LBL-33333

DISCLAIMER

This document was prepared as an account of work sponsored by the United States Government. While this document is believed to contain correct information, neither the United States Government nor any agency thereof, nor the Regents of the University of California, nor any of their employees, makes any warranty, express or implied, or assumes any legal responsibility for the accuracy, completeness, or usefulness of any information, apparatus, product, or process disclosed, or represents that its use would not infringe privately owned rights. Reference herein to any specific commercial product, process, or service by its trade name, trademark, manufacturer, or otherwise, does not necessarily constitute or imply its endorsement, recommendation, or favoring by the United States Government or any agency thereof, or the Regents of the University of California. The views and opinions of authors expressed herein do not necessarily state or reflect those of the United States Government or any agency thereof or the Regents of the University of California.

LBL-33333
UC-413
April 1993

NUCLEAR
SCIENCE
DIVISION
1992
ANNUAL REPORT

Division Director
T. J. M. Symons

Deputy Division Director
Janis M. Dairiki

Editor
W. D. Myers

Table of Contents

Introduction	1
<i>T.J.M. Symons</i>	
Overviews	3
Low-Energy Research Program	3
<i>G.J. Wozniak</i>	
Bevalac Research Program	9
<i>H.G. Ritter</i>	
Relativistic Nuclear Collisions Program	13
<i>A.M. Poskanzer</i>	
Nuclear Theory Program	19
<i>N.K. Glendenning</i>	
Nuclear Data Evaluation Program	25
<i>R.B. Firestone and E. Browne</i>	
88-Inch Cyclotron Operations	27
<i>C.M. Lyneis, D.J. Clark, D. Collins, A. Guy, S.A. Lundgren, R.J. McDonald, P. McMahan, and Z.Q. Xie</i>	
Group Lists	33
Low Energy Experiments	39
The IsoSpin Laboratory	41
<i>J. Michael Nitschke</i>	
Evidence for M1 Transitions Between Superdeformed States in ^{193}Hg	42
<i>P. Fallon, J. Burde, B. Cederwall, M.A. Deleplanque, R.M. Diamond, I.Y. Lee, J.R.B. Oliveira, F.S. Stephens, J.A. Becker, M.J. Brinkman, E.A. Henry, A. Kuhnert, M.A. Stoyer, J.E. Draper, C. Duyar and E. Rubel</i>	
Superdeformation in ^{191}Au	43
<i>D.T. Vo, W.H. Kelley, F.K. Wohn, J.C. Hill, M.A. Deleplanque, R.M. Diamond, F.S. Stephens, J.R.B. Oliveira, J. Burde, A.O. Macchiavelli, J. deBoer, J.A. Becker, E.A. Henry, M.J. Brinkman, A. Kuhnert, M.A. Stoyer, J.R. Hughes, J.E. Draper, C. Duyar, and E. Rubel</i>	
Oblate Collective Band in ^{193}Hg	44
<i>N. Roy, J.A. Becker, E.A. Henry, M. Brinkman, M.A. Stoyer, J.A. Cizewski, R.M. Diamond, M.A. Deleplanque, F.S. Stephens, C.W. Beausang, and J.E. Draper</i>	

A New Oblate Band in ^{196}Hg with Quenched M1 Strength	45
<i>B. Cederwall, M.-A. Deleplanque, F. Azaiez, R.M. Diamond, P. Fallon, W. Korten, I.-Y. Lee, A.O. Macchiavelli, J.R.B. Oliveira, F.S. Stephens, W.H. Kelly, D.T. Vo, J.A. Becker, M.J. Brinkman, E.A. Henry, J.R. Hughes, A. Kuhnert, M.A. Stoyer, T.F. Wang, J.E. Draper, C. Duyar, E. Rubel, J. deBoer</i>	
Collective Oblate Bands in ^{196}Pb	46
<i>J.R. Hughes, Y. Liang, R.V. F. Janssens, A. Kuhnert, J.A. Becker, I. Ahmad, I.G. Bearden, M.J. Brinkman, J. Burde, M.P. Carpenter, J.A. Cizewski, P.J. Daly, M.A. Deleplanque, R.M. Diamond, J.E. Draper, C. Duyar, B. Fornal, U. Garg, Z.W. Garbowski, E.A. Henry, R.G. Henry, W. Hesselink, N. Kalantar-Nayestanaki, W.H. Kelly, T.L. Khoo, T. Lauritsen, R.H. Mayer, D. Nissius, J.R.B. Oliveira, A.J.M. Plompen, W. Reviol, E. Rubel, F. Soramel, F.S. Stephens, M.A. Stoyer, D. Vo, and T.F. Wang</i>	
Rotation-Induced Transition from Superfluid to Normal Phase in Mesoscopic Systems: ^{168}Yb and Adjacent Nuclei	47
<i>J.R.B. Oliveira, S. Frauendorf, M.A. Deleplanque, R.M. Diamond, F.S. Stephens, C.W. Beausang, J.E. Draper, C. Duyar, E. Rubel, J.A. Becker, E.A. Henry, and N. Roy</i>	
High-Spin States in ^{179}Os	48
<i>J. Burde, M.-A. Deleplanque, R.M. Diamond, A.O. Macchiavelli, F.S. Stephens, and C.W. Beausang</i>	
Spectroscopy of Very Neutron-Deficient Hafnium and Tungsten Isotopes	49
<i>G.D. Dracoulis, B. Fabricius, P.M. Davidson, A.O. Macchiavelli, J. Oliveira, J. Burde, F.S. Stephens, and M.-A. Deleplanque</i>	
Construction of a Remote LIPAS Apparatus for Determining Equilibrium Constants of Cation-Cation Complexes	50
<i>N.J. Hannink, D.C. Hoffman, R.J. Silva, and R.E. Russo</i>	
Solubility and Speciation of Plutonium(V) and Plutonium(VI) in Carbonate Solution	51
<i>M.P. Neu, H. Nitsche, R.J. Silva, and D.C. Hoffman</i>	
Surface Sorption Technique for Separation of Rutherfordium (Element 104)	52
<i>C.D. Kacher, A. Bilewicz, and D.C. Hoffman</i>	
Comparison of TBP/HCl and TBP/HNO_3 Extraction Systems for Rf	53
<i>C.D. Kacher, K.E. Gregorich, N.J. Hannink, M.P. Neu, B.A. Kadkhodayan, S.A. Kreek, M.R. Lane, E.R. Sylwester, M.F. Mohar, D.M. Lee, and D.C. Hoffman</i>	
On-Line Gas Phase Isothermal Chromatography of Zirconium and Niobium Chlorides	54
<i>B. Kadkhodayan, D.C. Hoffman, B. Eichler, H.W. Gäggeler, and A. Kovacs</i>	

On-Line Gas Phase Isothermal Chromatography of Hafnium and Tantalum Chlorides	55
<i>B. Kadkhodayan, A. Türler, K.E. Gregorich, E. Sylwester, C.D. Kacher, S.A. Kreek, M.R. Lane, D.M. Lee, M.P. Neu, and D.C. Hoffman</i>	
On-Line Gas Phase Isothermal Chromatography of Rutherfordium (Element 104) Chlorides	56
<i>B. Kadkhodayan, A. Türler, K.E. Gregorich, E. Sylwester, C.D. Kacher, S.A. Kreek, M.R. Lane, D.M. Lee, M.F. Mohar, M.P. Neu, D.C. Hoffman</i>	
On-Line Gas Phase Isothermal Chromatography of Hahnium (Element 105) Chlorides	57
<i>B. Kadkhodayan, A. Türler, H.W. Gäggeler, B. Eichler, D.T. Jost, A. Kovacs, D. Vermeulen, K.E. Gregorich, S.A. Kreek, D.M. Lee, D.C. Hoffman, P. Baisden, J.V. Kratz, H.U. Becker, M.K. Gober, H.P. Zimmerman, M. Schädel, W. Brüchle, E. Jäger, V. Pershina, B. Schausten, E. Schimpf</i>	
Discovery of ²⁵²Bk	58
<i>S.A. Kreek, K.E. Gregorich, B. Kadkhodayan, M.P. Neu, C.D. Kacher, M.R. Lane, E.R. Sylwester, D.M. Lee, and D.C. Hoffman</i>	
Review of Spontaneous Fission	59
<i>D.C. Hoffman, T.M. Hamilton, and M.R. Lane</i>	
Electron-Capture Delayed Fission in ²²⁸Np	60
<i>S.A. Kreek, K.E. Gregorich, H.L. Hall, K.R. Czerwinski, T.M. Hamilton, R.A. Henderson, B. Kadkhodayan, C.D. Kacher, M.R. Lane, J.D. Leyba, M.P. Neu, E.R. Sylwester, A. Türler, D.M. Lee, M.J. Nurmi and D.C. Hoffman</i>	
Electron-Capture Delayed Fission in ²³⁸Bk	61
<i>S.A. Kreek, K.E. Gregorich, H.L. Hall, K.R. Czerwinski, T.M. Hamilton, R.A. Henderson, B. Kadkhodayan, C.D. Kacher, M.R. Lane, J.D. Leyba, M.P. Neu, E.R. Sylwester, A. Türler, D.M. Lee, M.J. Nurmi, and D.C. Hoffman</i>	
Tests of a Macintosh-Driven CAMAC Data Acquisition System	62
<i>M.F. Mohar and K.E. Gregorich</i>	
Conditional Barriers for Neutron-Rich and Neutron-Poor Compound Nuclei ^{98,90}Mo	63
<i>A. Veeck, K. Hanold, N. Colonna, D. Delis, Q. Sui, K. Tso, W. Skulski, G.J. Wozniak, and L.G. Moretto</i>	
Heavy Residues from the Reaction of ¹²⁹Xe + Be, C, Al at 26, 40, and 50 MeV/nucleon	64
<i>K. Hanold, L.G. Moretto, G.J. Wozniak, D. Bazin, D.J. Morrissey, N.A. Orr, B.M. Sherrill, J.A. Winger</i>	

Complex Fragment Production and Multifragmentation in ^{139}La-Induced Reactions at 35, 40, 45 and 55 MeV/u	65
<i>P. Roussel-Chomaz, N. Colonna, Y. Blumenfeld, B. Libby, G.F. Peaslee, D.N. Delis, K. Hanold, M.A. McMahan, J.C. Meng, Q.C. Sui, G.J. Wozniak, L.G. Moretto, H. Madan, A.A. Marchetti, A.C. Mignerey, G. Guarino, N. Santoruvo, I. Iori, and S. Bradley</i>	
Dynamics and Statistics in Multifragmentation Production	66
<i>M. Colonna, P. Roussel-Chomaz, N. Colonna, M. DiToro, L.G. Moretto, and G.J. Wozniak</i>	
Evolution of the 60 MeV/u $^{129}\text{Xe} + ^{27}\text{Al}$, ^{89}Y & ^{197}Au Reactions with Impact Parameter	67
<i>W. Skulski, N. Colonna, K. Tso, G.J. Wozniak, L.G. Moretto, D.R. Bowman, M. Chartier, C.K. Gelbke, W.C. Hsi, M.A. Lisa, W.G. Lynch, G.F. Peaslee, L. Phair, C. Schwarz, and M.B. Tsang</i>	
Intermediate Mass Fragment Emission as a Probe of Nuclear Dynamics	68
<i>D.R. Bowman, C. Mader, G.F. Peaslee, W. Bauer, N. Carlin, R.T. deSouza, C.K. Gelbke, W.G. Gong, Y.D. Kim, M.A. Lisa, W.G. Lynch, L. Phair, M.B. Tsang, C. Williams, N. Colonna, K. Hanold, M.A. McMahan, G.J. Wozniak, and L.G. Moretto</i>	
Excitation of Eigenmodes and Surface Instabilities in Disk Fragmentation	69
<i>L.G. Moretto, K. Tso, N. Colonna, and G.J. Wozniak</i>	
Multifragmentation in 60 MeV/u $^{197}\text{Au} + ^{\text{nat}}\text{Cu}$ Reactions	70
<i>D.N. Delis, N. Colonna, Q. Sui, K. Tso, K. Hanold, M. Justice, G.J. Wozniak, L.G. Moretto, B. Libby, A.C. Mignerey, A. Pantaleo, G. D'Erasmus, V. Paticchio, L. Fiore, E.M. Fiore, I. Iori, and A. Moroni</i>	
Calibration of the Response Function of CsI(Tl) Scintillators to Intermediate-Energy Heavy Ions	71
<i>N. Colonna, G.J. Wozniak, A. Veeck, W. Skulski, G.W. Goth, L. Manduci, P.M. Milazzo, and P.F. Mastinu</i>	
The Beta-Delayed Proton Emission of ^{65}Se	72
<i>J.C. Batchelder, D.M. Moltz, T.J. Ognibene, M.W. Rowe, and J. Cerny</i>	
The Beta-Delayed Proton Emission of ^{73}Sr	73
<i>J.C. Batchelder, D.M. Moltz, T.J. Ognibene, M.W. Rowe, and J. Cerny</i>	
Development of a New Low-Energy Proton Detector Ball	74
<i>D.M. Moltz, J.C. Batchelder, T.J. Ognibene, M.W. Rowe, R.J. Tighe, and Joseph Cerny</i>	
Present and Future Improvements to RAMA	75
<i>T.J. Ognibene, D.M. Moltz, J.C. Batchelder, M.W. Rowe, R. Tighe, and Joseph Cerny</i>	
Search for a 17 keV Neutrino in the Electron-Capture Decay of ^{55}Fe	76
<i>F.E. Wietfeldt, Y.D. Chan, M.T.F. da Cruz, A. García, R.-M. Larimer, K.T. Lesko, E.B. Norman, R.G. Stokstad, and I. Žliment</i>	

Second-Forbidden Electron-Capture Decay of ^{55}Fe	77
<i>I. Žlimen, E. Browne, Y. Chan, M.T.F. da Cruz, A. García, R.-M. Larimer, K. T. Lesko, E.B. Norman, R.G. Stokstad, and F.E. Wietfeldt</i>	
Electron-Capture Decay of ^{100}Tc and the $2\nu\text{-}\beta$-Decay of ^{100}Mo	78
<i>A. García, Y-D Chan, M.T.F. da Cruz, M.M. Hindi, R.M. Larimer, K.T. Lesko, E.B. Norman, R.G. Stokstad, F.E. Wietfeldt, I. Žlimen, D.M. Moltz, J. Batchelder, T.J. Ognibene</i>	
Thick-Target Yields of Iodine from Proton Interactions in Te, and the Double-β Decay of $^{128,130}\text{Te}$	79
<i>M.T.F. da Cruz, D.W. Bardayan, Y. Chan, A. García, M.M. Hindi, R.-M. Larimer, K.T. Lesko, E.B. Norman, R.G. Stokstad, F.E. Wietfeldt, and I. Žlimen</i>	
β^+ Decay and Cosmic-Ray Half-Life of ^{54}Mn	80
<i>M.T.F. da Cruz, D.W. Bardayan, Y. Chan, A. García, M.M. Hindi, R.-M. Larimer, K.T. Lesko, E.B. Norman, R.G. Stokstad, F.E. Wietfeldt, and I. Žlimen</i>	
β^+ Decay and Cosmic-Ray Half-Lives of $^{143,144}\text{Pm}$	81
<i>M.M. Hindi, A.E. Champagne, M.T.F. da Cruz, E.B. Norman, K.T. Lesko, R.M. Larimer, and B. Sur</i>	
Sudbury Neutrino Observatory, Photomultiplier Tube Support Structure	82
<i>K.T. Lesko, D. Beck, Y.D. Chan, T. de Cruz, Fred Dycus, A. García, Y. Kajiyama, G. Koehler, A. Ozeroff, E. Norman, P. Purgalis, A. Smith, R. Stokstad, I. Žlimen, and the Sudbury Neutrino Observatory Collaboration</i>	
Neural Network for Recognizing Čerenkov Radiation Patterns	83
<i>D.W. Dong, Y. Chan, M.T.F. da Cruz, A. García, K.T. Lesko, R.M. Larimer, E.B. Norman, R.G. Stokstad, F.E. Wietfeldt, and I. Žlimen</i>	
Two-Particle Correlation Functions in $^{14}\text{N} + ^{27}\text{Al}$ collisions at $E/A = 75$ MeV	84
<i>W.G. Gong, P. Danielewicz, C.K. Gelbke, and S. Pratt</i>	
Performance of the LBL AECR Source at Various Frequencies	85
<i>Z.Q. Xie, C.M. Lyneis, S.A. Lundgren, and D. Collins</i>	
Angular Distribution of ^{23}Mg Produced from 9.7 A MeV ^{24}Mg on Pt	86
<i>K. Matsuta, S. Fukuda, T. Izumikawa, M. Tanigaki, M. Fukuda, T. Ohtsubo, Y. Nojiri, T. Minamisono, J.R. Alonso, G.F. Krebs, R.J. McDonald, and T.J.M. Symons</i>	
Controlling Surface Radioactivity at SNO	87
<i>LBL-SNO Group</i>	
Emission of ^{23}F and ^{24}Ne in Cluster Radioactivity of ^{231}Pa	88
<i>P.B. Price, R. Bonetti, A. Guglielmetti, C. Chiesa, R. Matheoud, C. Migliorino, and K.J. Moody</i>	
Search for Cluster Radioactivity of ^{237}Np	88
<i>K.J. Moody, E.K. Hulet, and P.B. Price</i>	

Bevalac Experiments	89
Neutron Momentum Distribution from the Fragmentation of Neutron Rich Nuclei	91
<i>T. Kobayashi, I. Tanihata, K. Yoshida, T. Suzuki, S. Shimoura, K. Sugimoto, K. Matsuta, S. Fukuda, H. Weiman, W. Christie, and D.L. Olson</i>	
Revelation of Thick Neutron Skins in Nuclei	92
<i>I. Tanihata, D. Hirata, T. Kobayashi, S. Shimoura, K. Sugimoto, and H. Toki</i>	
Proton-Like Cross Section from 757 MeV/n La on La Collisions	93
<i>J. Bistirlich, R. Bossingham, H. Bossy, A. Chacon, T. Case, K. Crowe, Y. Dardenne, J. Friedrich, W. McHarris, J. Rasmussen, M. Stoyer</i>	
The EOS Experimental Program	94
<i>G. Rai and the EOS Collaboration</i>	
dE/dx Response and Particle Identification in the EOS Time Projection Chamber	95
<i>A. Scott, S. Wang, D. Keane, and the EOS Collaboration</i>	
Study of Multifragmentation	96
<i>The EOS Collaboration</i>	
Preliminary Results of Collective Flow from Au + Au	97
<i>M. Partlan and the EOS collaboration</i>	
Relative Dielectron Yields in p+p and p+d Interactions from $E_{\text{beam}} = 1.0$	98
<i>W.K. Wilson and the DLS Collaboration</i>	
Electron Pair Production in C+C, α+Ca and d+Ca Collisions	99
<i>C.J. Naudet and the DLS Collaboration</i>	
Dielectron Production in Ca+Ca Collisions, $E_{\text{beam}} = 1.05$ GeV/A	100
<i>R.J. Porter and the DLS Collaboration</i>	
Development of a Simple Device to Restandardize ECL Signals	101
<i>H.S. Matis, B.T. Turko, J.E. Galvin, G.J. Zizka, and the DLS Collaboration</i>	
Upper Limit on the Cross Section for Nuclear Charge Pickup by Relativistic Uranium Ions	102
<i>A.J. Westphal, P.B. Price, and D.P. Snowden-Ifft</i>	
Sensitivity Study of CR-39 Plastic Track Detectors	102
<i>Y.D. He and P.B. Price</i>	
Ultrarelativistic Experiments	103
The STAR Experiment at RHIC	105
<i>The STAR Collaboration</i>	

STAR Time Projection Chamber	106
<i>H. Wieman, J. Bercovitz, D. Cebra, W. Gong, E. Hjort, H. Huang, P. Jones, D. Keane, J. Mitchell, R. Morse, G. Rai, I. Sakrejda, R. Scharenberg, D. Shuman, A. Sobel, R. Stone, B. Stringfellow, and the STAR Collaboration</i>	
The Silicon Vertex Tracker for STAR	107
<i>W. Christie, S. Margetis, C. Naudet, G. Odyniec, J. Schambach, K. Wilson, and the STAR Collaboration</i>	
A Simulation Package for the STAR Time Projection Chamber	108
<i>P.G. Jones, I. Sakrejda, and the STAR Collaboration</i>	
The SVT Resolution Simulator (SRS)	109
<i>W.K. Wilson, S. Margetis, C. Naudet, G. Odyniec, and J. Walton</i>	
Main Vertex Reconstruction in STAR	110
<i>S. Margetis, D. Cebra, and The STAR Collaboration</i>	
Feasibility of Single-Event Bose-Einstein Correlations in STAR	111
<i>R.J. Morse and The STAR Collaboration</i>	
Temperature Dependence of the Gas Gain of Proportional Counters	112
<i>W.G. Gong, A. Sobel, H. Wieman, E. Hjort, J. Mitchell</i>	
A $J^{PC} = 0^{++}$ Resonance at 1560 MeV/c²	113
<i>K.M. Crowe, D.S. Armstrong, J. Bistirlich, R. Bossingham, H. Bossy, T. Case, and the Crystal Barrel Collaboration</i>	
The Pseudoscalar Mixing Angle from $\bar{p}p$ Annihilation at Rest	114
<i>K.M. Crowe, D.S. Armstrong, J. Bistirlich, R. Bossingham, H. Bossy, T. Case, and the Crystal Barrel Collaboration</i>	
Correlations in ³²S+S and ³²S+Au Collisions at the CERN SPS	115
<i>M.A. Bloomer, P. Jacobs, A.M. Poskanzer, and WA80 Collaboration</i>	
Multiplicity Dependence of the Strangeness Production from the CERN Experiment NA-36	116
<i>D.E. Greiner, C.R. Gruhn, I. Sakrejda, P.G. Jones, and E.G. Judd</i>	
Doubly Strange Baryons in CERN Experiment NA-36	117
<i>D.E. Greiner, C.R. Gruhn, P.G. Jones, E.G. Judd, and I. Sakrejda</i>	
Antilambda Production near Midrapidity in Central S+Au Collisions at 200 GeV/Nucleon	118
<i>NA35 Collaboration</i>	
Impact Parameter Dependence of Bose-Einstein Correlations at 200 GeV/Nucleon	119
<i>The NA35 Collaboration</i>	
Electronics for the NA35 TPC	120
<i>NA35 Collaboration</i>	

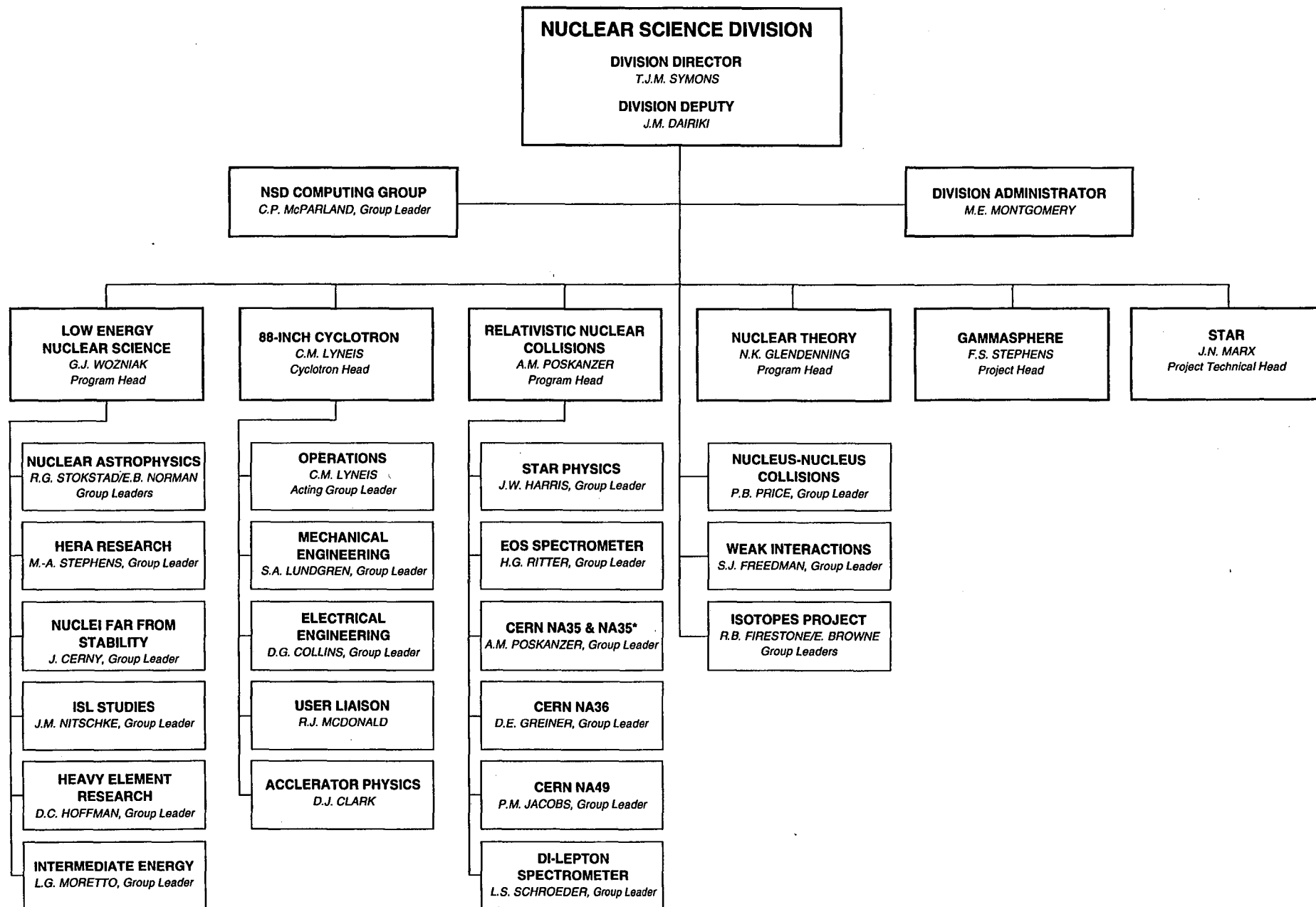
The NA49 Experiment for Lead Beams at the CERN SPS	121
<i>The NA49 Collaboration</i>	
Electronics for the NA49 TPCs	122
<i>The NA49 Collaboration</i>	
Advances in Solid State Nuclear Track Detectors	123
<i>P.B. Price</i>	
First Measurement of Cross Sections for Electron Capture and Stripping by Ultrarelativistic Ions	123
Search for Abnormal Nucleus production in Heavy-Ion Collisions	124
<i>Y.D. He and P.B. Price</i>	
Measurement of Cross Section for Charge Pickup by 11.4 A GeV Gold Ions	125
<i>Y.D. He and P.B. Price</i>	
Nuclear and Electromagnetic Fragmentation of 2.25-TeV ¹⁹⁷Au Nuclei	126
<i>Y.D. He and P.B. Price</i>	
Theory	127
Scale Dependence of Nuclear Gluon Structure	129
<i>K.J. Eskola</i>	
Color Conductivity and the Evolution of the Minijet Plasma at RHIC	130
<i>K.J. Eskola and M. Gyulassy</i>	
HIJING: A Monte Carlo Model for Multiple Jet Production in pp, pA and AA Collisions	131
<i>X.-N. Wang and M. Gyulassy</i>	
Transverse Flow Due to Minijets in $p\bar{p}$ Collisions at $\sqrt{s} = 1.8$ TeV	131
<i>X.-N. Wang and M. Gyulassy</i>	
Studying Minijets via the p_T Dependence of Two Particle Correlation in Azimuthal Angle Φ	131
<i>X.-N. Wang</i>	
Gluon Shadowing and Jet Quenching in A+A Collisions at $\sqrt{s} = 200$ A GeV	132
<i>X.-N. Wang and M. Gyulassy</i>	
Dynamical versus Decay Photons in A + A Collisions at $\sqrt{s} = 200$ GeV	132
<i>D.K. Srivasta, M. Gyulassy, and X.-N. Wang</i>	
Interpretation of Rapidly Rotating Pulsars	132
<i>F. Weber and N.K. Glendenning</i>	

Relativistic Mean-Field Calculations of Λ and Σ Hypernuclei	133
<i>N.K. Glendenning, D. Von-Eiff, M. Haft, H. Lenske, and M.K. Weigel</i>	
Application of the Improved Hartle Method for the Construction of General Relativistic Rotating Neutron Star Models	133
<i>F. Weber and N.K. Glendenning</i>	
Neutron Stars in the Derivative Coupling Model	133
<i>N.K. Glendenning, F. Weber, and S.A. Moszkowski</i>	
Reconciliation of Neutron-Star Masses and Binding of the Λ in Hypernuclei	134
<i>N.K. Glendenning and S.A. Moszkowski</i>	
Nuclear Solid Crust on Rotating Stage Quark Stars	134
<i>F. Weber and N.K. Glendenning</i>	
First-Order Phase Transitions with More than One Conserved Charge: Consequences for Neutron Stars	135
<i>N.K. Glendenning</i>	
Limiting Rotational Period of Neutron Stars	135
<i>N.K. Glendenning</i>	
Neutron Stars, Strange Stars and the Nuclear Equation of State	136
<i>F. Weber and N.K. Glendenning</i>	
Early Cluster Recognition in Molecular Dynamics	137
<i>C. Dorso and J. Randrup</i>	
Simulating the Langevin Force by Simple Noise in Nuclear One-Body Dynamics	138
<i>M. Colonna, G.F. Burgio, Ph. Chomaz, M. Di Toro, and J. Randrup</i>	
Linear Response in Stochastic Mean-Field Theories and the Onset of Instabilities	139
<i>M. Colonna, P. Chomaz, and J. Randrup</i>	
Effect of N-Body Collisions on Subthreshold Kaon Production in High-Energy Nuclear Reactions	140
<i>G. Batko, J. Randrup, and T. Vetter</i>	
BUU Dynamics of Unbound Spherical Nuclei	141
<i>G. Batko and J. Randrup</i>	
Refinements of the Nucleon-Exchange Transport Model for the Emission of Hard Photons and Nucleons	142
<i>S.J. Luke, R. Vandenbosch, and J. Randrup</i>	
The Order of Chaos Transition in Axially Symmetric Nuclear Shapes	143
<i>J. Blocki, F. Brut, T. Srokiwski, and W.J. Swiatecki</i>	

A Numerical Verification of the Prediction of an Exponential Velocity Spectrum for a Gas of Particles in a Time Dependent Potential Well	143
<i>J. Blocki, F. Brut, and W.J. Swiatecki</i>	
A Diffusion Equation for Energy in Ergodic Adiabatic Ensembles	144
<i>C. Jarzynski</i>	
Theory of Rotational Population Patterns in Heavy-Ion Transfer Reactions: Even- Even Thorium Nuclei	145
<i>S.Y. Chu, J.O. Rasmussen, R. Donangelo, M.A. Stoyer, S. Frauendorf, and Y.R. Shimizu</i>	
Seminars	147
Nuclear Science Division	149
Nuclear Theory	152
Author Index	155

INTRODUCTION AND OVERVIEWS

LAWRENCE BERKELEY LABORATORY • UNIVERSITY OF CALIFORNIA



Introduction

This report describes the activities of the Nuclear Science Division for the year ending December 31, 1992. This was a busy time and considerable progress was made on projects which will provide the scientific heart of the Division for the remainder of the decade.

The STAR detector for RHIC made excellent progress during the year, passing its final hurdle in January 1993 on the way to a formal construction start. STAR is now a collaboration involving 29 institutions and over 200 scientists and engineers. The success of this initiative owes much to John Harris who has carried a heavy burden as spokesperson of the collaboration for the past three years.

The Sudbury Neutrino Observatory is another large project in which the Division is playing a major role. This experiment will be located 6800 feet underground in a nickel mine in Canada and will use 1000 tons of heavy water as a neutrino detector. Our responsibility is to construct the geodesic structure, some 20 m in diameter, which will support the photomultiplier tubes used in the experiment. Work is proceeding well and installation at Sudbury is expected to begin in the fall of 1993.

Gammasphere also moved ahead quickly. In its final form this device will be an array of 110 Compton-suppressed germanium detectors with unprecedented sensitivity for the study of nuclear structure. The mechanical specifications were finalized during the year and the first thirty detectors ordered. Preparation for Gammasphere was a major activity at the 88-Inch Cyclotron. Engineering modifications were made to the shielding to improve the earthquake safety of the facility; the counting area was redecorated and preparations began for construction of new offices to accommodate outside users.

The progress of these new projects is significant, but should not overshadow the ongoing research program. Both the Bevalac and the 88-Inch Cyclotron had outstanding years. This was the last full year of Bevalac operation and an astonishing amount was accomplished. The EOS TPC was commissioned and took a large quantity of unique data. Given the complexity of the device, everyone involved should be congratulated on a job very well done. The dilepton spectrometer also ran extensively and completed a very successful program.

We were fortunate to have several new staff members join us during the year. At the senior level, Jay Marx and I-Yang Lee came on board. Jay is leading the construction of STAR and I-Yang is Project Scientist for Gammasphere. Both these projects are fortunate to have attracted such experienced and talented scientists. In addition, three new Divisional fellows started work in the fall: Peter Jacobs, Paul Fallon and Xin-Nian Wang.

Although there are still difficulties in the funding of nuclear physics at the national level, the outlook for the Division is bright. We are fortunate to have a dedicated staff and a steady stream of outstanding visitors and the pages which follow attest to their enthusiasm and productivity. In closing, I would like to thank Bill Myers for editing this report once again.

Low-Energy Research Program

G. J. Wozniak

The Nuclear Science Division's efforts in the broad area of low-energy nuclear science include studies of nuclear structure, chemistry, astrophysics, weak interactions, and heavy-ion reaction mechanisms. Main themes are the effects of high angular momentum, extremes in isospin and nuclear charge (the heaviest elements), exotic modes of decay, and weak interactions. Some of these programs are carried out exclusively at the 88-Inch Cyclotron, portions at other accelerators, and others are non-accelerator based. Scientific staff are playing important roles in the construction of two major new facilities: Gammasphere and the Sudbury Neutrino Observatory (SNO). Staff scientists are also involved in planning for the IsoSpin Laboratory, a proposed major new national initiative. During the last year, many exciting results have emerged from these programs. A brief overview is given below followed by more detailed descriptions in later sections.

Nuclear Structure

During the last year the Nuclear Structure Group hired a new Divisional Fellow (Paul Fallon) to replace Dick Diamond who retired. In addition, two staff scientists (I. Y. Lee and A. O. Macchiavelli) were hired to help construct Gammasphere. The group has focused on the structure of the nucleus at very high angular momentum, where its properties are different from the well-known ones at lower spin and excitation energy. The group is particularly interested in the structure of superdeformed nuclei and the new oblate bands in the mass 190 region.

The Nuclear Structure Group is heavily involved in the construction of Gammasphere and its early implementation which is planned for spring of 1993. This interim device will have a resolving power a factor of ten higher than HERA and may answer some of the current puzzles in superdeformed nuclei. Recently, a group led by John Rasmussen has joined the Gammasphere effort and proposed off-line studies of rotational-band population patterns in spontaneous fission using radioactive sources.

Heavy-Element Nuclear and Radiochemistry

Several factors have combined to make the 88-Inch Cyclotron facility one of the leading laboratories in the world for production and study of transuranic nuclei. One factor is the availability of intense (microampere) beams of ions from ^1H through ^{48}Ca . Another is the technology developed at LBL and LLNL for producing, handling, and irradiating radioactive targets of isotopes from uranium through einsteinium. The Heavy Element Nuclear and Radiochemistry Group uses the Cyclotron to produce and characterize new elements and isotopes, to study nuclear reaction mechanisms, and to train students in modern nuclear and radiochemical techniques. During the last year, this group has continued its investigations of the nuclear and chemical properties of heavy elements.

Heavy-Ion Reactions

With the shutdown of the Bevalac, the Moretto/Wozniak group's multifragmentation program has been transferred to the K1200 Cyclotron at Michigan State University. There, in collaboration with the Miniball and the A1200 groups, several experiments on multifragmentation and complex fragment emission have been performed. The group maintains a parallel program at the 88-Inch Cyclotron to determine the emission barriers for complex fragment emission from medium mass nuclei. More recently, a collaboration has been established with the Washington University group to build a 4π charged particle detector (Microball) that will fit inside Gammasphere. The combination of the Microball and Gammasphere will be a very powerful tool for spectroscopic and reaction studies at the Cyclotron. In particular, studies of angular momentum transfer and alignment in deep-inelastic reactions with discrete γ -rays that, in the past, were hindered by poor statistics, will now become feasible. Furthermore, the availability of beams of different isotopes will allow studies of the N/Z equilibration in deep-inelastic reactions.

Nuclei Far From Stability

The Cerny Group has recently completed the construction of a new low-energy, proton-detector array. This large solid angle device (1π) has very low thresholds (0.18 MeV protons) enabling the measurement of decay branches that were below the detector thresholds of previous studies. This detector array has been successfully tested and several new decay lines observed. To extend the range of half lives that can be studied with the on-line mass separator RAMA, the

ion-source region is being relocated into the cave area to minimize the transit time in the helium jet. This improvement will allow the study of short-lived beta emitters.

With the shutdown of the Bevalac, the Matsuta Group has transferred their mirror magnetic moment and nuclear polarization programs to the 88-Inch Cyclotron. A first measurement of the quadrupole moment of ^{23}Mg has been made using a 9 MeV/nucleon ^{24}Mg beam on various targets. Efforts are under way to reduce the background and improve the accuracy of the measurement.

For several years, the Price Group has been measuring the spontaneous emission of heavy clusters from various actinide nuclei. Typically, even isotopes from C to Ne are observed as a very rare decay branch competing with alpha decay. Most recently, they found evidence for emission of an odd-Z cluster.

A new program focused on the proposed IsoSpin Laboratory (ISL) has begun under the leadership of Mike Nitschke. Mike is a member of the ISL steering committee that organized a Workshop on the Use of Intense RNBs at the ISL last fall at Oak Ridge. Together with a consultant, he has prepared a study of the radiation assessment of the ISL. The group is currently constructing a high-intensity-target test stand to study target cooling problems associated with the intense proton beams from the ISL.

Nuclear Astrophysics/Weak Interactions

In collaboration with eleven other institutions from Canada, the U.S. and the United Kingdom, LBL is participating in the Sudbury Neutrino Observatory, an experiment to detect neutrinos from the sun and supernovae. SNO is designed to address the solar neutrino problem, the question of neutrino oscillations, and neutrino production in stellar collapse. The LBL group is playing a major role and two of its members are SNO group leaders: one for the photomultiplier tube (PMT) support structure and the other for contamination control. The group is also involved in preparing an on-line monitoring program, a graphics interface, and a data analysis program.

Several years ago, the Norman Group demonstrated that the beta spectrum from a ^{14}C -doped germanium detector showed a distortion, consistent with the emission of a 17-keV neutrino with a probability of 1.25%. A recent very high statistics measurement of the inner bremsstrahlung (IB) spectrum of ^{55}Fe shows no evidence for this distortion. This is strong evidence against the existence of a 17-keV neutrino, since a similar distortion should show up in both beta and IB spectra. The group is continuing its work on double beta decay and cosmic chronometers.

The new weak interaction group, under the leadership of Stuart Freedman, has started a program in laser trapping. A laser laboratory has been set up in Building 88. Efforts are under way to trap ^{21}Na produced in a nuclear reaction. A ^{21}Na beam has been successfully focused by transverse cooling with a dye laser. In addition, this group has several off-site projects. Most notable is their

elegant measurement of the beta decay spectrum of ^{35}S . Using a high field solenoid spectrometer with no collimators, they were able to set very stringent limits on the emission of a 17-keV neutrino in beta decay.

SNO

The Sudbury Neutrino Observatory (SNO) is based on a 1000 tonne heavy water Čerenkov detector and is designed to measure the intensity, energy, and direction of neutrinos from the sun and other astrophysical sources such as supernovae. It is presently under construction in a very low background laboratory 2000 m underground in the Creighton mine near Sudbury, Ontario, Canada. This is an operating nickel mine owned by INCO. The heavy water used in the detector will be on loan from Atomic Energy of Canada Limited. The construction of the detector is expected to be completed in late 1994, and data taking is scheduled to start in 1995.

The most important and unique feature of the SNO detector is the use of heavy water as the detection medium. The neutrinos interact with the deuterons in the heavy water three ways: elastic scattering from electrons, charged current reactions with the deuterons, and neutral current breakup of the deuterons. These three reactions enable measurement of both the electron neutrino flux and the total neutrino flux of all types of neutrinos that reach the detector. If an electron neutrino produced at the center of the sun changes into another type of neutrino, this process will be detected and neutrino oscillations observed. In addition to neutrino oscillations in vacuum, the SNO experiment can detect matter enhanced oscillations, the MSW effect, by observing the energy spectrum shape of the electron neutrinos reaching the earth.

The basic measurements that will be made are:

- 1) the flux and energy spectrum of electron neutrinos reaching the earth, and
- 2) the total flux of all neutrino types above an energy of 2.2 MeV.

With these two measurements, it will be possible to

- 1) show clearly if neutrino oscillations are occurring, and
- 2) independently test solar models by determining the production rate of high energy electron neutrinos in the solar core.

The use of heavy water provides an opportunity to use the sun as a calibrated source of neutrinos. Using the sun as a distant source of neutrinos would increase the sensitivity of the search for neutrino oscillations by many orders of magnitude, compared to present measurements at reactors and accelerators. The detection of both electron neutrinos and all types of neutrinos from a supernova would give new information on the mechanism of stellar collapse.

The collaboration is composed of Canadian, English, and the U.S. university and national laboratory research groups. LBL is responsible for designing, engineering, fabricating and supervising the installation of the geodesic support structure that positions the detector's 10,000 PMTs. LBL performs low level

counting of uranium and thorium concentrations in detector materials and is establishing the contamination control program for the project. We are working with the SNO collaboration in developing Monte Carlo, Data Acquisition, and Data Analysis codes.

Bevalac Research Program

H.G. Ritter

The Bevalac's ability to provide beams of the heaviest of ions in the GeV/nucleon range gave it a unique role in the U.S. nuclear-science program. The phase out of the Bevalac research program in February 1993 stimulated a concentration on the central scientific themes and a consolidation in the last year of running to three programs studying the properties of nuclear matter, and an atomic physics experiment. The emphasis was on using unique experimental equipment and beams. Data from these and previous experiments are now actively being analyzed.

The central focus of the Bevalac's research program has been the production and study of extreme conditions in nuclear matter. Early experiments with the Plastic Ball and Streamer Chamber provided the first definitive evidence for collective flow of nuclear matter at high temperatures (50-100 MeV) and nuclear densities (2-4 times normal) created in the central collision of two heavy nuclei. These experiments have allowed us to study the thermodynamic and transport properties of nuclear matter, and, from this, the nuclear matter equation of state (EOS), a quantity of fundamental importance in nuclear physics and of relevance to the understanding of the extreme conditions existing inside neutron stars.

The EOS time projection chamber (TPC), the next generation 4π detector, has completed its very successful data taking. EOS has pioneered the technique of tracking by pad-readout only in a magnetic field and high density electronics using custom designed integrated circuits. EOS expanded on existing 4π

measurements and provided new data for complete event analysis of the central collisions of the heaviest nuclei. In addition, in conjunction with the multiple sampling ionization chamber (MUSIC) and with a time-of-flight wall, the experiment studied multi-fragmentation.

Rare events can often provide insight into differing aspects of reaction dynamics. It is generally acknowledged that dileptons, because they interact only weakly, are a useful probe of the hot, compressed phase of the collision process. By contrast, pions and nucleons, which interact strongly with matter, suffer considerable scattering before being detected. Since dileptons are expected to be extremely rare, special detection techniques are required to sort them out from the myriad of other particles produced by the collision. The dilepton spectrometer (DLS) measured dilepton production in Ca+Ca, α +Ca, and C+C reactions at different energies. The DLS collaboration finished a systematic study of the elementary p-p and p-n interactions at different energies.

The production of radioactive beams and measurements of their ground-state properties were pioneered at the Bevalac by several groups from Japan. Initial work involved the measurement of the radii of light neutron-rich nuclei, culminating in the observation of the "neutron halo" associated with ^{11}Li . Work in this area continued to concentrate on measurements of the correlations between nuclear fragments from these exotic nuclei and played a worldwide leadership role in defining new directions for this line of research.

Following are the named collaborations in which the Nuclear Science Division participates. The spokespersons are indicated in **boldface**.

DLS Collaboration

S. Beedoe¹, M. Bougheb², J. Carroll¹, W. Christie³, W. Gong, T. Hallman¹, L. Heibronn, H.Z. Huang, G. Igo¹, P. Kirk⁴, G. Krebs, L. Madansky³, F. Manso², H.S. Matis, D. Miller⁵, J. Miller, C. Naudet, J. Porter, G. Roche², **L. Schroeder**, P.A. Seidl, M. Toy¹, W. K. Wilson, Z.F. Wang⁴, R. Welsh³, A. Yegneswaran⁶

1. University of California at Los Angeles, Los Angeles, CA, USA
2. Université de Clermont II, Aubière, France
3. The Johns Hopkins University, Baltimore, MD, USA
4. Louisiana State University, Baton Rouge, LA, USA
5. Northwestern University, Evanston, IL, USA
6. CEBAF, Newport News, VA, USA

EOS Collaboration

F. Bieser, F. P. Brady¹, D. Cebra, A. D. Chacon³, J. Chance, Y. Choi², S. Costa⁵, J. Elliot², M. Gilkes², A. Hirsch², E. Hjort², D. Keane⁴, V. Lindenstrut⁶, U. Lynen⁶, H. S. Matis, M. McMahan, C. McParland, W. Mueller⁶, D. L. Olson, M. D. Partlan¹, N. Porile², R. Potenza⁵, G. Rai, J. Rasmussen, H. G. Ritter, J. L. Romero¹, H. Sann⁶, R. Scharenberg², A. Scott⁴, Y. Shao⁴, B. Srivastava², T.J.M. Symons, P. Warren², H. H. Wieman, K. Wolf³

1. U.C. Davis, Davis, CA, USA
2. Purdue University, West Lafayette, IN, USA
3. Texas A&M University, College Station, TX, USA
4. Kent State University, Kent, OH, USA
5. INFN Catania, Italy
6. GSI Darmstadt, Germany

Secondary Radioactive Beams Collaboration

K. Matsuta, J. R. Alonso, G. F. Krebs, T. J. M. Symons, H. H. Wieman, D. L. Olson, W. Christie, L. Greiner, R.J. McDonald, A. Ozawa¹, Y. Nojiri¹, T. Minamisono¹, M. Fukuda¹, A. Kitagawa¹, S. Momota¹, T. Ohtsubo¹, S. Fukuda¹, T. Izumikawa¹, M. Tanigaki¹, K. Sugimoto¹, I. Tanihata², K. Yoshida², T. Kobayashi², T. Suzuki², S. Shimoura³, K. Omata⁴, O. Testard⁵

1. Osaka University, Toyonaka, Osaka 560, Japan
2. RIKEN, Wako, Saitama 351-01, Japan
3. University of Tokyo, Bunkyo-ku, Tokyo 113, Japan
4. INS, University of Tokyo, Tanashi, Tokyo 188, Japan
5. Saclay, 91191 GIF-sur-YVETTE, Cedex, France

Relativistic Nuclear Collisions Program

A.M. Poskanzer

The main focus of the future high energy heavy ion research program at LBL is the Relativistic Heavy Ion Collider (RHIC) which will be completed at Brookhaven National Laboratory in 1997. For the nearer term, the various activities of LBL at the CERN laboratory in Geneva, Switzerland have finished data-taking with ^{32}S beams and have now consolidated into one experiment, NA49, for the Pb beams program in 1994.

The high energy program at CERN is attempting to compress nuclei sufficiently to produce a transition of the *nucleons* in the nuclei to a plasma of free quarks and gluons. At the higher energies expected at RHIC the density of the energy of the *produced particles* will be so high that a momentary state of the quark-gluon plasma is expected. It is believed that the quark-gluon plasma existed soon after the Big Bang at the creation of the Universe and may exist now in the cores of neutron stars.

The STAR (Solenoidal Tracker at RHIC) Collaboration now has 200 scientists from 28 institutions. The Spokesperson, the Project Director, and thirty of the scientists are from LBL. STAR is an experiment to study particle production and high momentum jet production at midrapidity to identify the phase transition from normal nuclear matter to quark matter. A measurement of the produced particles at midrapidity provides the opportunity to select events with extreme values of temperature (particle spectrum), flavor (strangeness content), shape (particle momenta), and size (two-particle correlations). The experiment will contain a Time Projection Chamber (TPC) located inside a solenoidal magnet for tracking, momentum analysis, and particle identification. A barrel of scintillators

surrounding the main TPC will provide the centrality trigger. It is hoped to also include a Silicon Vertex Tracker near the interaction region that will distinguish primary and secondary vertices, and improve the tracking and momentum resolution.

At the CERN Super Proton Synchrotron the emphasis of the recently completed program of 200 GeV/nucleon ^{32}S -induced reactions was to explore the possibility of producing a phase transition from hadronic matter to a quark-gluon plasma in central collisions of heavy ions at these energies. LBL effected a consolidation so that at the end of the ^{32}S data-taking it was participating in only one CERN experiment: NA35. Its TPC was the first such detector to operate in a magnetic field free region with pad readout only. LBL built and installed 6000 additional channels of modern electronics. This is a step on the way to a much larger contribution from LBL of integrated electronics for the TPCs of the NA49 Pb-beams experiment in 1994. NA49 will consist of two dipole magnets in series, two large volume TPCs for tracking and particle identification of charged particles, two high-resolution intermediate-size TPCs inside the magnets to detect neutral strange particle decays and wide angle pions, and a time-of-flight wall to complete the hadron identification scheme. This combination of detectors should allow enough coverage of the particles from the reaction to do event-by-event physics for the first time at a CERN experiment. Thus, it should be possible to correlate, on an event-by-event basis, such variables as the source radius from two-pion correlations, entropy from rapidity densities, temperature from slopes, and stopping from baryon distributions.

At the Brookhaven AGS the Nuclear Science Division is participating with the UC Space Sciences Laboratory in a search for rare negative particle production in Si + Au collisions. The main purpose is to study the space-time evolution of the reaction through coalescence yields.

Following are the named collaborations in which the Nuclear Science Division participates. The spokespersons are indicated in **boldface**.

NA35 Collaboration

J. Bächler⁷, J. Bartke⁴, H. Bialkowska¹¹, M. Bloomer, R. Bock⁵, R. Brockmann⁵, P. Buncic¹², S.I. Chase, J. Cramer¹³, I. Derado⁹, V. Eckardt⁹, J. Eschke⁶, D. Ferenc¹², B. Fleischmann⁵, P. Foka⁵, M. Fuchs^{5,6}, M. Gazdzicki¹⁰, E. Gladysz⁴, J.W. Harris, M. Hoffmann⁷, P. Jacobs, S. Kabana⁶, K. Kadija¹², R. Keidel⁸, J. Kosiec⁶, M. Kowalski⁹, A. Kühmichel⁶, M. Lahanas⁶, J.Y. Lee⁶, A. Ljubicic, Jr.¹², S. Margetis, R. Morse, E. Nappi², G. Odyniec, G. Paic¹², A.D. Panagiotou¹, A. Petridis¹, A. Piper⁸, F. Posa², A.M. Poskanzer, F. Pühlhofer⁸, G. Rai, W. Rauch⁹, R. Renfordt⁶, W. Retyk¹⁰, D. Röhrich⁶, G. Roland⁶, H. Rothard⁶, K. Runge⁷, A. Sandoval⁵, J. Schambach, E. Schmidt⁶, N. Schmitz⁹, E. Schmoetten⁷, I. Schneider⁶, **P. Seyboth**⁹, J. Seyerlein⁹, E. Skrzypczak¹⁰, P. Stefanski⁴, R. Stock⁶, H. Ströbele⁶, L. Teitelbaum, T. Trainor¹³, G. Vasileiadis¹, M. Vassiliou¹, G. Vesztergombi⁹, D. Vranic¹², S. Wenig⁶

¹ Department of Physics, University of Athens, Athens, Greece

² Dipartimento di Fisica, Università di Bari and INFN Bari, Bari, Italy

³ CERN, Geneva, Switzerland

- ⁴ Institute of Nuclear Physics, Cracow, Poland
⁵ Gesellschaft für Schwerionenforschung (GSI), Darmstadt, Germany
⁶ Fachbereich Physik der Universität, Frankfurt, Germany
⁷ Fakultät für Physik der Universität, Freiburg, Germany
⁸ Fachbereich Physik der Universität, Marburg, Germany
⁹ Max-Planck-Institut für Physik u. Astrophysik, München, Germany
¹⁰ Institute for Experimental Physics, University of Warsaw, Warsaw, Poland
¹¹ Institute for Nuclear Studies, Warsaw, Poland
¹² Rudjer Boskovic Institute, Zagreb, Croatia
¹³ Nuclear Physics Laboratory, University of Washington, Seattle, WA, USA

NA36 Collaboration

E. Andersen¹, R. Blaes⁸, H. Braun⁸, J.M. Brom⁸, M. Cherney⁶, B. de la Cruz⁵, G.E. Diebold⁷, B. Dulny⁴, C. Fernández⁷, C. Garabatos⁷, J.A. Garzón⁷, W.M. Geist⁸, D.E. Greiner, C. Gruhn, M. Hafidouni⁸, J. Hrubec⁹, P.G. Jones, E. Judd^{†,2}, J.P.M. Kuipers¹⁰, M. Ladrem⁸, P. Ladrón de Guevara⁵, G. Løvhøiden¹, J. MacNaughton⁹, A. Michalon⁸, M.E. Michalon-Mentzer⁸, J. Mosquera⁷, Z. Natkanic⁴, J.M. Nelson², G. Neuhofer⁹, C. Perez de los Heros⁵, M. Pló⁷, P. Porth⁹, B. Powell³, A. Ramil⁷, J.L. Riestler⁸, H. Rohringer⁹, I. Sakrejda, T. Thorsteinsen¹, J. Traxler⁹, C. Voltolini⁸, K. Wozniak⁴, A. Yañez⁷, R. Zybert²

¹ University of Bergen, Dept. of Physics, Bergen, Norway

² University of Birmingham, Dept. of Physics, Birmingham, UK

³ CERN, Geneva, Switzerland

⁴ Instytut Fizyki Jadrowej, Krakow, Poland

⁵ CIEMAT, Div. de Física de Partículas, Madrid, Spain

⁶ Creighton University, Department of Physics, Omaha, NE, USA

⁷ Universidad de Santiago, Dpto. Física de Partículas, Santiago de Compostela, Spain

⁸ Centre de Recherches Nucléaires, IN2P3-CNRS/Université L. Pasteur, Strasbourg, France

⁹ Institut für Hochenergiephysik (HEPHY), Wien, Austria

¹⁰ University of York, Dept. of Physics, York, UK

[†]Present address: Lawrence Berkeley Laboratory, Berkeley CA, USA

NA49 Collaboration

J. Bächler⁷, J. Bartke⁵, H. Bialkowska¹¹, M. Bloomer, R. Bock⁸, L. Boroczky³, W.J. Braithwaite¹³, D. Brinkman⁶, R. Brockmann⁸, P. Buncic¹⁴, S.I. Chase, J. Cramer¹³, I. Derado¹⁰, W. Dominik¹², V. Eckardt¹⁰, F. Eckhardt⁹, J. Eschke⁶, D. Ferenc^{14,6}, H. Fessler¹⁰, H.G. Fischer⁴, B. Fleischmann⁸, P. Foka⁸, M. Fuchs⁸, M. Gazdzicki⁶, H.J. Gebauer¹¹, E. Gladysz⁵, J.W. Harris, S. Hegyi³, M. Hoffmann⁷, P. Jacobs, P.G. Jones, E. Judd², S. Kabana⁶, K. Kadija¹⁴, A. Karabarbounis¹, R. Keidel⁹, J. Kosiec¹², M. Kowalski⁵, A. Kühmichel⁶, J.Y. Lee⁶, A. Ljubicic, Jr.¹⁴, V. Manske⁹, S. Margetis, R. Morse, J.M. Nelson², G. Odyniec, G. Paic¹⁴, A.D. Panagiotou¹, A. Petridis¹, A. Piper⁹, A.M. Poskanzer, F. Pühlhofer⁹, G. Rai, W. Rauch¹⁰, R. Renfordt⁶, W. Retyk¹², H.G. Ritter, D. Röhrich⁶, G. Roland⁶, H. Rothard⁶, K. Runge⁷, A. Sandoval⁸, J. Schambach, N. Schmitz¹⁰, E. Schmoetten⁷, J. Seyboth⁹, P. Seyboth⁹, J. Seyerlein¹⁰, E. Skrzypczak¹², I. Szenpetery³, J. Sziklai³, P.

Stefanski⁵, R. Stock⁶, H. Ströbele⁶, T. Trainor¹³, G. Vasileiadis¹, M. Vassiliou¹, G. Vesztergombi³, D. Vranic¹⁴, S. Wenig⁶, H. Wieman, J. Zimanyi³, X.-Y. Zhu¹³, R. Zybert²

¹ Department of Physics, University of Athens, Athens, Greece

² School of Physics, University of Birmingham, Birmingham, UK

³ Central Research Institute of Physics, Budapest, Hungary

⁴ CERN, Geneva, Switzerland

⁵ Institute of Nuclear Physics, Cracow, Poland

⁶ Fachbereich Physik der Universität, Frankfurt, Germany

⁷ Fakultät für Physik der Universität, Freiburg, Germany

⁸ Gesellschaft für Schwerionenforschung (GSI), Darmstadt, Germany

⁹ Fachbereich Physik der Universität, Marburg, Germany

¹⁰ Max-Planck-Institut für Physik u. Astrophysik, München, Germany

¹¹ Institute for Nuclear Studies, Warsaw, Poland

¹² Institute for Experimental Physics, University of Warsaw, Warsaw, Poland

¹³ Nuclear Physics Laboratory, University of Washington, Seattle, WA, USA

¹⁴ Rudjer Boskovic Institute, Zagreb, Croatia

STAR ★ Collaboration

D.L. Adams¹⁷, S. Ahmad¹⁷, S.A. Akimenko¹⁵, B.D. Anderson¹¹, A. Arahamian¹³, Y.I. Arestov¹⁵, M.E. Beddo¹, N.I. Belikov¹⁵, R. Bellwied²², S. Bennett²², J. Berkovitz, J. Bielecki²², F. Bieser, N.N. Biswas¹³, M.A. Bloomer, B.E. Bonner¹⁷, F.P. Brady⁵, W.J. Braithwaite²¹, J.A. Buchanan¹⁷, P. Buncic², D.D. Carmony¹⁶, J. Carroll⁶, D.A. Cebra, A.D. Chacon¹⁸, C.S. Chan¹², S.I. Chase, M.G. Cherney⁸, C.N. Chiou¹⁷, Y. Choi¹⁶, R.K. Choudhury¹⁸, W. Christie, J.M. Clement¹⁷, M.D. Corcoran¹⁷, T.M. Cormier²², H.J. Crawford⁴, J.G. Cramer²¹, A.M. Davidenko¹⁵, J.W. Dawson¹, A.A. Dereschikov¹⁵, W. Dominik¹⁹, J.E. Draper⁵, W.R. Edwards, S.E. Eiseman³, T. Empl¹⁷, J.M. Engelage⁴, V. Erin¹⁵, A. Etkin³, D. Ferenc², K.J. Foley³, Z. Fraenkel²³, F. Gang²², U. Garg¹³, M. Gazdzicki⁹, V. Ghazikhanian⁶, A. Grachov¹⁵, M. Green, D. Greiner, L. Greiner⁴, D.P. Grosnick¹, V.J. Guarino¹, E. Gulmez⁶, W.N. Haberichter¹, R.W. Hackenberg³, J. Hall²², T.J. Hallman⁶, J.W. Harris, D.A. Hill¹, N. Hill¹, A.S. Hirsch¹⁶, E. Hjort¹⁶, H. Huang, T. Humanic¹⁴, G.J. Igo⁶, P.M. Jacobs, P.G. Jones, M.L. Justice¹¹, K. Kadija², M. Kaplan⁷, P.J. Karol⁷, T. Kasprzyk¹, D. Keane¹¹, V.P. Kenney¹³, S. Kleinfelder, M.A. Kramer¹², M.J. LeVine³, R. LaPierre, Q. Li²², S.J. Lindenbaum¹², P.J. Lindstrom, R.S. Longacre³, D.X. Lopiano¹, W.A. Love³, A. Lukaszew²², L. Madansky¹⁰, S. Margetis, J. Marx, R. Matheus²², H.S. Matis, C. McParland, T.S. McShane⁸, P. Meschanin¹⁵, H.E. Miettinen¹⁷, Z. Milosevich⁷, J. Mitchell, T. Moore, R. Morse, G.S. Mutchler¹⁷, J. Nasiatka¹, C.J. Naudet, T. Noggle, S.B. Nurushev¹⁵, G. Odyniec, D.L. Olson, G. Paic², T. Pawlak²⁰, W. Peryt²⁰, E. Petereit¹, J. Piekarczyk¹³, E.D. Platner³, J. Pluta²⁰, N.T. Porile¹⁶, A.M. Poskanzer, D. Prindle²¹, C. Pruneau²², G. Rai, J. Rasson, P. Rehak³, R.E. Renfordt⁹, H.-G. Ritter, J.B. Roberts¹⁷, G. Roger²², D. Röhrich⁹, J.L. Romero⁵, A.I. Ronjin¹⁵, V.L. Rykov¹⁵, I. Sakrejda, A.C. Saulys³, J. Schambach, R.P. Scharenberg¹⁶, L.S. Schroeder, J. Seger⁸, Y.P. Shao¹¹, D. Shuman, J. Skeens¹⁷, H.M. Spinka¹, B. Srivastava¹⁶, I. Stancu¹⁷, R. Stock⁹, R. Stone, H. Stroebele⁹, T.J.M. Symons, L. Teitelbaum, M.L. Tincknell¹⁶, T.A. Trainor²¹, S. Trentalange⁶, I. Tserruya²³, D.G. Underwood¹, J.H. Van Dijk³, E. Vardaci⁷, A.N. Vasiliev¹⁵, D. Vranic², J.W. Watson¹¹, R.C. Welsh¹⁰

S. Wenig⁹, C. Whitten, Jr.⁶, H. Wieman, W.K. Wilson, K.L. Wolf¹⁸, A. Yokosawa¹,
K.H. Zhao¹², X.-Z. Zhu²¹, Y. Zhu¹²

¹ Argonne National Laboratory, Argonne, IL, USA

² Rudjer Boskovic Institute, Zagreb, Croatia

³ Brookhaven National Laboratory, Upton, NY, USA

⁴ Univ. of California at Berkeley, Space Science Laboratory, Berkeley, CA, USA

⁵ Univ. of California at Davis, Davis, CA, USA

⁶ Univ. of California at Los Angeles, Los Angeles, CA, USA

⁷ Carnegie Mellon University, Pittsburgh, PA, USA

⁸ Creighton University, Omaha, NE, USA

⁹ University of Frankfurt, Frankfurt, Germany

¹⁰ Johns Hopkins University, Baltimore, MD, USA

¹¹ Kent State University, Kent, OH, USA

¹² City College of New York, New York, NY, USA

¹³ University of Notre Dame, Notre Dame, IN, USA

¹⁴ University of Pittsburgh, Pittsburgh, PA, USA

¹⁵ Institute of High Energy Physics, Protvino, Russia

¹⁶ Purdue University, West Lafayette, IN, USA

¹⁷ Rice University, Houston, TX, USA

¹⁸ Texas A & M University, College Station, TX, USA

¹⁹ Warsaw University, Warsaw, Poland

²⁰ Warsaw University of Technology, Warsaw, Poland

²¹ University of Washington, Seattle, WA, USA

²² Wayne State University, Detroit, MI, USA

²³ Weizmann Institute of Science, Rehovot, Israel

Nuclear Theory Program

N.K. Glendenning

The goal of the nuclear theory program at LBL is to develop the theory and methods necessary for the analysis and interpretation of experiments involving nuclei and for the prediction of as yet unobserved phenomena. These include nuclear reactions at low to ultra-relativistic energies, and lepton-nucleus and hadron-nucleus reactions. In addition, the program aims at adding breadth to the Division's overall nuclear research program by concentrated effort also in nuclear astrophysics, macroscopic nuclear models, QCD and hydrodynamic theories of ultra-dense matter and phase transitions, and an interdisciplinary program in the order-to-chaos transition.

Ultrarelativistic Nuclear Collisions

With the advent of new and proposed experimental facilities in the U.S. and elsewhere for accelerating heavy ions to relativistic energies, nuclear physics is entering an era of investigations focusing on the quark-gluon substructure of nuclear matter and the possibility of a phase transition from hadronic matter to quark-gluon plasma at extremely high energy density. The results from those laboratory-based investigations will have profound influences on a broad range of physical science, from astrophysics to cosmology. To assist the analysis and understanding of both the existing and future experimental data, to find a promising, reliable set of signatures for the phase transition, and to predict new results from fundamental theories under the extreme conditions, an extended and rigorous research program has been planned and carried out in the nuclear theory group.

This program includes two interconnected efforts, one along formal field theoretical lines and the other on phenomenological lines closely connected to the experimental data. Some aspects of the formal theoretical work is directly related to the problems that we encounter in developing phenomenological models. The ultimate goal along this direction is to include all major features of the fundamental theories into a model which can describe ultrarelativistic heavy ion reactions from energies at presently available facilities to the future proposed colliders. The development of such a Monte Carlo model can also guide experimentalists to design their detectors for the forthcoming RHIC collider and proposed LHC to best take into account of the new physics in that energy regime. The existence of a major experimental effort within the Nuclear Science Division utilizing CERN and BNL facilities naturally leads to close interactions between theorists and experimentalists in this area. A proposed summer study workshop on Pre-equilibrium Parton Dynamics to be held at LBL in 1993 has been approved by the Nuclear Science Division. We hope this workshop will bring experts in the field to discuss the issues related to thermalization and equilibration of the dense system created in the high energy heavy ion collisions.

Nuclear Astrophysics

The research in nuclear astrophysics has recently dealt with various aspects of compact stars falling into three categories, which have to do with (1) neutron stars and pulsars, (2) a deepened understanding of general relativity relating to the phenomenon of frame dragging, (3) speculations having to do with the strange matter hypothesis. In particular for neutron stars the research has concerned: (a) A model independent limit on rotation of neutron stars which provides a rigorous bound on neutron stars, and hence provides a means of identifying strange quark stars if they exist and any are discovered with high rotational frequency. (b) The coexistence phase of confined hadrons and deconfined quark matter which in the work of the last decade had been inadvertently excluded by a seemingly innocuous assumption, (c) The baryon composition of neutron stars as constrained by hypernuclear physics. As an adjunct to this work we have computed the spectroscopy of Σ hypernuclei hoping to encourage more experimentation in this area, since it is a source of information on the relative couplings of hyperons among themselves and nucleons, and impacts such neutron star properties as mass, cooling rates, lifetimes of pulsar magnetic fields and hence their active lifetimes. (d) The limits imposed on rotation by gravitational radiation instabilities as moderated by viscosity.

In the category of the theory of general relativity, the role of dragging of local inertial frames in determining the Kepler frequency of massive stars has been clarified by both an analytic and numerical analysis. In the category of strange stars and the strange quark matter hypothesis of Witten, (a) computations of the heavy ion crust on rotating strange stars and the reconciliation of the observation of pulsar glitches with strange stars, which was the outstanding astrophysical evidence that may have ruled out the hypothesis had strange stars been unable to glitch; (b) hypothetical strange white dwarfs, their minimum mass, and how this sequence is related to ordinary white dwarfs. In addition to this, we are taking

up a study of the supernova mechanism including improvements in the handling of the neutrino transport during the explosion, that relate to several controversial issues.

Nuclear Dynamics

The theory of nuclear dynamics is another major thrust of the LBL nuclear theory effort. This line of research aims to develop new dynamical theories for quantal many-body systems and to invoke these in the planning and interpretation of heavy-ion experiments. A considerable fraction of the recent effort has been carried out within the framework of semi-classical one-body dynamics, in which the nucleon phase-space density is propagated in its self-consistent effective field, while the individual nucleons experience stochastic two-body collisions subject to Pauli blocking. The efforts are continuing towards extending this approach to incorporate the fluctuating part of the collision integral and thus develop a stochastic theory of nuclear dynamics, the Boltzmann-Langevin model. In addition to being formally well based, such an extension is required in order to address such processes as nuclear multifragmentation where spontaneous symmetry breaking and catastrophic evolution occur.

After developing and testing a novel simulation model based on a lattice in phase-space, attention has been turned more towards the clusterization process in unstable matter, such as may occur as the collision system decompresses. The self-consistent propagation of the spontaneous fluctuations restores the predictive power of the stochastic one-body approach, even when such catastrophic phenomena as cluster formation are addressed.

The fact that several nucleons are within range whenever two nucleons collide makes the assumption of isolated two-body scatterings dubious. We have clarified the situation in two stages. First the simplest pion-exchange diagrams for elastic three-nucleon processes have been calculated and employed to illustrate the evolution in momentum space. Then the collision integral was generalized to include many-body scatterings by assuming a complete microcanonical sharing of the available energy between the N participating nucleons, the number of which is determined by a simple examination of the neighborhood of the collision partners, using a standard pseudo-particle simulation model as a basis. With this extended model, the effect on anisotropy, flow angle, sideways momentum, and backwards yield have been ascertained and are found to be generally small, which is understood as a consequence of detailed balance in the basic N -body processes.

Nuclear Properties

A Thomas-Fermi model of nuclei is under development, that can serve as the basis for the extrapolation of nuclear theories into regimes of high temperatures, very high spins, extreme combinations of neutron and proton numbers, etc. The parameters of the effective nucleon-nucleon interaction used in the model are determined by comparing the theory to measured values of nuclear sizes, charge

distributions, binding energies, and optical model potential depths. Currently this statistical model serves as a reliable basis for a broad spectrum of extrapolations. A recent application of the Thomas-Fermi model has been to deformed nuclei, in particular to the calculation of nuclear fission barriers. The calculations can include the effects of angular momentum and could even be turned around to investigate the effect of diffuseness and polarization on fusion barriers.

In addition to the extensive applications of the current model we are continuing to improve the model itself. An important extension would improve our description of the nuclear surface by treating the quantal penetration of matter into the classically forbidden region of space. To this end we have developed an improved Thomas-Fermi model—simpler than other existing refinements—in order to be able to describe the presence on the fringes of the nuclear surface of such a quantal halo, characterized by matter at positive density but negative energy density. The implementation of these new ideas is still in progress. The resulting model should have improved predicting power for its extrapolations and may be able to clear up the long standing problem concerning current estimates for the value of the curvature correction to the nuclear surface energy.

Transition from Order to Chaos in Nuclei

A principal theme underlying our work on nuclear dynamics is the relevance of the order to chaos transition in nucleonic motions to the collective behavior of the nucleus as a whole. This insight has led to the mounting of a special initiative in our group, whose aim is to broaden the contacts between nuclear physics and the research in chaos and nonlinear dynamics. The result has been a number of collaborations with scientists in the United Kingdom, Poland, France, and China. We have recently obtained a State Department Curie-Sklodowski Grant to cover expenses in connection with our Polish collaboration. The topics of research range from the properties of random matrices as representations of nuclear spectra, to dissipative effects in classical and quantal systems of independent particles driven by a time-dependent mean-field potential, to aspects of Berry's phase in spinning nuclei and optical fibers. Recent results of particular interest concern the study of the wall formula for dissipation in the case of quantized particles in a potential well, and the derivation of a universal asymptotic velocity distribution (an exponential) for independent particles in an irregular time-dependent container. A general equation for the diffusion of energy in time dependent dynamical systems was derived and is being applied to a variety of problems of interest.

Neural Networks

We are concluding a three year project on neurocomputing methods applied to pattern recognition in high energy physics. This year we developed a feed forward network to estimate jet energies in the presence of a very high level of low energy noise expected in nuclear collisions at high energies. We showed that the neural filter can be trained to provide a nearly bias free estimator of the jet

energy distribution and developed a constrained deconvolution method to uncover accurately the primordial jet distribution and to analyze jet energy loss quantitatively. The network learns by error propagation from training data to do jet recognition in raw input particle data. The project has succeeded in demonstrating the usefulness of neural network in pattern recognition confronted in high energy and nuclear physics experiments. The results of our work should be useful for future physics experiment at RHIC, LHC, and SSC.

Nuclear Data Evaluation Program

R.B. Firestone and E. Browne

The Isotopes Project compiles, evaluates, and disseminates nuclear structure and radioactive-decay data for basic and applied research, and for diverse technical applications. Since 1979, the project has coordinated its efforts with the national and the international nuclear data networks, and is responsible for the evaluation of properties of nuclei with mass numbers $A=89-93$, $167-194$, 206 , $210-212$, 215 , 219 , 223 , and 227 . This responsibility includes preparing data in computerized form for entry into the Evaluated Nuclear Structure Data File (ENSDF). The project has also started a coordinated effort with other data groups to update the high-spin data in ENSDF for use at Gammasphere and other new large detector arrays.

Spectroscopic data from radioactive decay and nuclear reactions — after verification of completeness, correctness, and self-consistency — serve as input data for determining recommended adopted values of specific nuclear properties. These “best values,” deduced with the aid of statistical procedures, the application of systematics and the use of nuclear models, constitute the main scientific contribution of the data evaluation effort. The project’s data and corresponding bibliographic references are both computer retrievable and available in published form.

Comprehensive evaluations, produced from ENSDF, are subsequently published in *Nuclear Data Sheets*. Concurrent with evaluation of data, the Isotopes Project develops methods and computer codes for data analysis. These include minimization procedures for deducing best values from various sets of data, and data-verification codes for ensuring correctness and uniformity. The project has a continuing interest in methods for propagation of the experimental uncertainties reported for nuclear properties. Their application in nuclear data

evaluation leads to uniform and rigorous interpretation of the data, and results in consistently reliable recommended values.

The Isotopes Project produced seven editions of the *Table of Isotopes* from 1940 to 1978, the sixth and seventh in book form. Each edition provided a comprehensive and critical evaluation of the known nuclear properties deduced from radioactive decay and reaction data. The project is also responsible for the production of the *Table of Radioactive Isotopes*, first published in 1986. This book provides a concise source of recommended data derived from ENSDF, and is tailored to the needs of applied users in industry, biology, medicine, and other fields. It has also proved itself as an indispensable reference for nuclear physicists and chemists in basic research. The Isotopes Project is preparing an 8th edition of the *Table of Isotopes* scheduled for completion in 1993. This book will primarily emphasize nuclear structure and decay data. The 8th edition of the *Table of Isotopes* is planned to be updated regularly and provided, on various computer media, for remote printing. Future editions are expected to be published on approximately a 5-year cycle.

The Isotopes Project has accepted responsibility for developing an electronic nuclear data dissemination system to display nuclear data on personal computers and workstations. This program will provide a chart-of-the-nuclides graphical interface to the ENSDF file including full searching capabilities for all data, graphical and tabular display of information, calculation utilities, and access to the Nuclear Structure Reference library (NSR). A preliminary version of this program, supporting menu-driven access to the numerical data and level scheme drawings based on ENSDF, will be available in 1993 and the full version is expected to be completed by 1996.

The Isotopes Project serves a broad user community and plays an active role in promoting the science of nuclear data evaluation. It has developed, and makes available, an extensive computerized database of nuclear structure and radioactive decay information (LBL/ENSDF) based on ENSDF.

Publications:

1. C.M. Baglin, Nuclear Data Sheets 66 347 (1992).
2. E. Browne, Nuclear Data Sheets 65, 209 (1992).
3. V.S. Shirley, Nuclear Data Sheets 66, 69 (1992).
4. E. Browne, Nuclear Data Sheets 65, 669 (1992).
5. B. Singh, Nuclear Data Sheets 66, 623 (1992).
6. E. Browne, Nuclear Data Sheets 66, 281 (1992).
7. R.B. Firestone, Nuclear Data Sheets 65, 589 (1992).
8. V.S. Shirley, *Alpha Particles*, McGraw-Hill Encyclopedia of Science and Technology, 7th Edition, Vol. 1, 416 (1992).
9. R.B. Firestone and B. Singh, *Nuclear Data for the High-Spin Community*, International Conference on Nuclear Structure at High Angular Momentum, Ottawa, Canada, May 18-21, 1992.
10. I. Zlimer, E. Browne, Y. Chan, M.T.F. da Cruz, A. Garcia, R.-M. Larimer, K.T. Lesko, E.B. Norman, R.G. Stokstad, and F.E. Wietfeldt, *Second-forbidden Electron Capture Decay of ^{55}Fe* , Phys. Rev. C46, 1136 (1992).

88-Inch Cyclotron Operations

*C.M. Lyneis, D.J. Clark, D. Collins,
A. Guy, S.A. Lundgren, R.J. McDonald,
P. McMahan, and Z.Q. Xie*

The 88-Inch Cyclotron is operated by the Nuclear Science Division as a national facility in support of U.S. Department of Energy programs in basic nuclear science. Written proposals for experiments in nuclear science are evaluated by a Program Advisory Committee on the basis of the science proposed. Current members are R. Janssens (ANL), R.W. Hoff (LLNL), J. Waddington (McMaster), N. Koeller (Rutgers), R.L. McGrath (SUNY), and L. Sobotka (Wash. U.). The current membership of the Users' Executive Committee is J.M. Alexander (SUNY), J.A. Becker (LLNL), K.E. Gregorich (LBL), W.D. Loveland (Oregon State University, chairman), and H.R. Weller (Duke University).

Research at the Cyclotron is conducted by scientists from many institutions in addition to those from LBL and the University of California at Berkeley. During FY 92, the Cyclotron was used by 110 scientists from 24 institutions. About 60% of the total beam time was used by scientists from institutions other than LBL. The Cyclotron also plays an important role in the education and training of young scientists at the undergraduate, graduate, and postdoctoral stages of their careers.

The central component of this facility is a sector-focused, variable-energy cyclotron that has been upgraded by the addition of an Electron Cyclotron Resonance (ECR) high-charge-state ion source. This versatile combination produces heavy ion beams from helium to oxygen with energies up to 32 MeV/nucleon. For heavier ions the maximum energy per nucleon decreases with increasing mass. Typical ions and maximum energy are argon at 17 MeV/u, krypton at 8 MeV/u, and xenon at 5 MeV/u. Most metallic ions and all

other gaseous ions up to mass 150 either have been accelerated or can be developed with energies high enough for nuclear physics experiments. Light ions—p, d, ^3He , and ^4He —are produced up to total energies of 55, 65, 135, and 130 MeV, respectively. Polarized proton and deuteron beams at intensities of up to 0.5 microampere are also available. Beams directly from the ECR source at up to 10 keV per charge state can be delivered by a transport system on the vault roof to target stations for atomic physics research.

Accelerator Use

The Cyclotron operating efficiency continued to benefit from the ECR source. There are long periods of steady operation, and only one operator per shift is required. The range of ions available from the ECR source has continued to expand. Table 1 summarizes the time distribution. The Accelerator Operation Summary shows that cyclotron reliability was very high, with only 5% of the operating time being lost to unscheduled maintenance. The "Other Research" category under "Experiment Summary" consists mainly of testing electronic integrated circuits in partnership with the aerospace industry by using cyclotron beams to simulate space radiation.

Ions and Energies

The cyclotron fed by the ECR source provides a wide range of ions, energies, and intensities in support of the experimental program at the 88-Inch Cyclotron. Using the low and high temperature ovens in the LBL ECR, most elements can be accelerated. A partial list of beams, energies, and intensities is given in Table 2. In addition to those listed, many isotopic beams such as ^{26}Mg , ^{29}Si , ^{30}Si , ^{34}S , ^{37}Cl , ^{65}Cu , and ^{70}Ge can be produced from natural feed. Other isotopes such as ^3He , ^{13}C , ^{15}N , ^{18}O , ^{22}Ne , ^{44}Ca , ^{54}Fe , and ^{235}U can be run economically from enriched isotopes because of the high efficiency of the ECR source.

The beams developed and listed in Table 2 are generally developed as needed by the wide range of experiments proposed by the users of the 88-Inch Cyclotron. As the Gammastat detector comes into operation we expect to develop an even wider range of ion species, particularly neutron-rich isotopes, which are used to produce high spin states in compound nuclei. Heavy element radiochemistry experiments require several μA of beams up to mass 48 at 6-8 MeV/nucleon. Groups studying heavy-ion reaction mechanism and complex fragmentation of highly excited nuclei use higher energy beams such as nitrogen and oxygen at 32 MeV/nucleon, neon at 25 MeV/nucleon, and krypton at 13 MeV/nucleon. In addition to the heavy-ion beams used with the cyclotron, the light ion beams continue to be frequently utilized. For example, the project to develop laser trapping of radioactive sodium beams requires 25 MeV proton beams. The study of β -delayed proton emission requires several μA beams of ^3He at 40 to 110 MeV. The nuclear astrophysics group typically uses beams of protons, deuterons, ^3He , and ^4He at 8-25 MeV/nucleon.

ECR Ion Source Development

The new Advanced Electron Cyclotron Resonance ion source (AECR), which was built as an AIP project, can be used to provide beams of greater intensity and higher charge states than are available from the LBL ECR. The AECR operates at 14 GHz, compared to 6 GHz for the LBL ECR, and incorporates an electron gun to inject cold electrons into the plasma and boost the production of high charge state ions. In the last year development of the source has greatly improved its short and long term stability. Several nuclear physics experiments have been run with AECR-generated beams, and it will be in regular operation with the Cyclotron in early 1993. Development of the source for the production of beams from solids, with special emphasis on the efficiency of source feed, is continuing.

Gammasphere

A number of modifications to Bldg. 88 have been undertaken to provide space and capabilities for the Gammasphere project. A laboratory area was set up to assemble, test, anneal, and store the new Gammasphere detectors. The Cave 4C counting area has been remodeled to provide a good working environment for Gammasphere users. The beamline to Cave 4C has been rebuilt with stainless steel beam pipe and cryopumps to provide the high vacuum required for good transmission of the heavy-ion beams. The beam optics system has been redesigned to improve transmission and meet the beam emittance requirements for Gammasphere. Additional quadrupoles and diagnostic devices will be installed during FY 93 to aid in the tuning of the beamline to Cave 4C.

Applied Research

The 88-Inch is a major source of heavy-ion beams for Single-Event Upset (SEU) testing of solid-state components for the U.S. Space program. Because of the ability to run "cocktails" of beams, allowing one to switch from one ion to another in a matter of minutes, it is possible to quickly establish the energy deposition level at which a SEU will occur. The availability of proton beams, used for studying radiation effects on charged-coupled devices, has further increased the demand for use of the Cyclotron.

The Aerospace Corporation, in cooperation with 88-Inch Operations, is presently installing a specially instrumented scattering chamber on a dedicated beamline. When completed, the 88-Inch will be able to support a state-of-the-art, user-friendly facility for the use of industrial and government users on a cost recovery basis.

User Support

88-Inch Cyclotron Research Group provides information, assistance, and coordination to outside users of the 88-Inch Cyclotron. It is the main contact between the Cyclotron operations staff and outside users. As such, they are responsible for the development and maintenance of experimental facilities at the

Cyclotron, and for making these facilities attractive to a diverse group of users from around the country, and in some cases, around the world.

Our users fall into two classes: 1) scientific users whose experimental proposals are reviewed by a Program Advisory Committee (PAC), and who are awarded time based on the scientific merits of these proposals, and 2) industrial users who purchase beam time for their own proprietary use.

The 88-Inch Cyclotron Research Users Group coordinates the PAC, which meets three times a year to review proposals for beam time. It supports both the 88-Inch Users' Association and the Gammasphere Users' Association and their Executive Committees through 1) holding annual Users' meetings at the fall meeting of the Division of Nuclear Physics of the American Physical Society, 2) sponsoring periodic telephone conferences of the Executive Committee to carry user concerns to the Cyclotron management, and 3) publishing a monthly newsletter which is distributed to all users. This 88-Inch Users Group also maintains the NSD Equipment Pool.

A low-energy computer support effort is aimed at developing and maintaining general hardware and software for experimental data acquisition, on-line diagnostics, and general data analysis capabilities at the 88-Inch Cyclotron. The group is presently exploring the possibility of adapting the Unix-based acquisition being developed for Gammasphere as the next general purpose acquisition system for the 88-Inch, and is in the process of acquiring a DEC Alpha computer as the next generation analysis machine.

Safety

We continue to devote significant effort to improving the safety and conduct of operations at the Cyclotron. Ninety-five percent of the self-assessment items from 1991 have been corrected. Procedures for controlling access to the Cyclotron have been improved, and a new radiation gate has been installed. Coordination of the safety effort with the EH&S Division has improved substantially as their staff has been increased. We have also put in a revised proposal for FY 94 AIP to modernize the radiation safety interlock system.

Publications

D.J. Clark, A Conceptual Design for a Primary Cyclotron for the ISL Radioactive Beam Project, Proceedings of the XIII International Conference on Cyclotrons and Their Applications, Vancouver, Canada July 6-10, 1992 (to be published).

A.T. Young, K.J. Bertsche, D.J. Clark, K. Halbach, W.B. Kunkel, K.G. Leung, C.Y. Li, Design of a Compact Permanent Magnet Cyclotron Mass Spectrometer for the Detection and Measurement of Trace Isotopes, Proceedings of the XIII International Conference on Cyclotrons and Their Applications, Vancouver, Canada, July 6-10, 1992 (to be published).

D.J. Clark, Conference Summary, Proceedings of the XIII International Conference on Cyclotrons and Their Applications, Vancouver, Canada July 6-10, 1992 (to be published).

C.M. Lyneis, ECR Ion Sources for Accelerators, Proceedings of the XIII International Conference on Cyclotrons and Their Applications, Vancouver, Canada, July 6-10, 1992 (to be published).

Z.Q. Xie and C.M. Lyneis, Performance of the LBL ECR Source at Various Frequencies, Proceedings of the XIII International Conference on Cyclotrons and Their Applications, Vancouver, Canada, July 6-10, 1992 (to be published).

J.D. Molitoris, W.E. Meyerhof, C. Stoller, R. Anholt, D.W. Spooner, L.G. Moretto, L.G. Sobotka, R.J. McDonald, G. J. Wozniak, M.A. McMahan, L. Blumenfeld, N. Colonna, M. Nessi and E. Morenzoni, *Phys. Rev. Lett.* (1992) (to be published).

Table 1. FY 92

<u>Accelerator Operation Summary</u>	
Research	4017 hours
Tuning	608
Machine Studies	32
Unscheduled Shutdowns	251
Scheduled Shutdowns	3876
Electrical Energy Consumption	6.9 GWH
<u>Experiment Summary</u>	
Beam Utilization for Research	
Nuclear Research	3326 hours
Other Research	<u>691</u>
Total	4017
Number of Nuclear Science Experiments	68
Number of Scientists	110
Number of Students	30
Institutions Represented	
Universities	12
Other DOE National Laboratories	2
Other	10
Percentage of Beam Time	
In-House Staff	42%
Universities	21
DOE National Laboratories	20
Other Institutions	<u>17</u>
Total	100

Table 2. 88-Inch Cyclotron Beam List

Ion	Charge State	External Beam (eμA)	E/A Range or Max (MeV/u)	Ion	Charge State	External Beam (eμA)	E/A Max (MeV/u)
p	1	100-5	.2-55				
p (pol.)	1	.7-.4	6-50	31P	8	.5	9
d	1	100-5	.3-32		10	.1	15
d (pol.)	1	.7-.4	5-32	32S	7	3.5	7
³ He	2	100-5	1-47		8	2.0	9
⁴ He	2	100-5	1-32		9	1.0	11
⁷ Li	2	.5	11		10	.4	14
	3	.03	26		11	.1	17
⁹ Be	2	.5	7		12	.02	20
	3	.3	15		13	.003	23
	4	.2	28	35Cl	9	.4	9
¹² C	4	10	6		10	.1	11
	4	5.0	16		11	.02	14
	5	.1	24		12	.005	16
	6	.01	32	39K	9	.4	7
¹⁴ N	5	5.0	18		10	2	9
	6	.15	26		11	1	11
	7	.01	32		12	.02	13
¹⁶ O	5	10	9	40Ar	9	3.0	7
	5	5	14		10	1.5	9
	6	3.0	20		11	.6	11
	7	.1	27		12	.4	13
	8	.03	32		13	.09	15
¹⁹ F	6	2	9		14	.015	17
	6	1	14	40Ca	9	1.5	7
	7	.6	19		10	1.0	9
²⁰ Ne	6	5	8		11	.8	11
	6	2.0	13		12	.4	13
	7	.4	17		13	.06	15
	8	.1	22		14	.006	17
	9	.02	28	63Cu	15	.1	8
²⁴ Mg	6	1.5	9		19	.03	13
	7	.7	12	84Kr	17	.2	6
	8	.2	16		19	.08	7
	9	.1	20		20	.04	8
	10	.03	24	129Xe	23	.01	4
²⁸ Si	6	2.0	6		27	.01	6
	7	1.0	9	159Tb	30	.005	5
	8	.7	11	238U	21	.010	.7
	9	.5	14		30	.001	2.2
	10	.2	18				
	11	.05	22				

The listed currents are based on natural isotopic source feed, except for ³He. Beam intensity on target will vary according to beam line optics, collimation, and energy resolution requirements. Other elements run include ¹¹B, ²³Na, ²⁷Al, ⁴⁵Sc, ⁴⁸Ti, ⁵²Cr, ⁵⁵Mn, ⁵⁶Fe, ⁵⁸Ni, ⁷⁰Ge, ¹⁰⁷Ag, ¹²⁰Sn, ¹²⁷I, ¹³⁹La, and ²⁰⁹Bi. Many isotopes of these, including ⁴⁴Ca, ⁴⁸Ca, and ²³⁵U, have also been run. These and other ions have energies and intensities similar to those in the table in the same mass range. Beam energies down to below 0.3 MeV/u are available.

GROUP LISTS

Group Lists

Following are the lists of people in the Nuclear Science Division groups. At the end of each list are the long-term visitors with their home institutions in parentheses.

Administrative Staff

J.M. Dairiki, Assistant Director

L.J. Davis

R.E. Hodges

R.E. Jahnigen

J.B. Lofdahl

M.E. Montgomery

A. Nellis

B.E. Phillips

T.S. Pouncey

W.J. Smith-Burnett

M.B. Star

C.J. Sterling

J.C. Sterling

T.J.M. Symons, Director

J.M. Tarzian

For Glenn T. Seaborg,

Associate Director at Large:

N.B. Lockhart

D. Yan

S.L. Whyte

Exotic Nuclei: RAMA

J. Cerny

J.C. Batchelder*

D.M. Moltz

T.J. Ognibene*

M. Rowe*

S.K. Thompson*

R. J. Tighe

E. Y. Wang**

OASIS

J.M. Nitschke

High-Spin Studies

B.W. Cederwall

M.A. Deleplanque-Stephens

R.M. Diamond

P. Fallon

F.S. Stephens

I.Y. Lee

J.R.B. Oliveira

J.E. Draper (UC Davis)

C. Duyar* (UC Davis)

E. Rubel* (UC Davis)

Nuclear Astrophysics and Fundamental Symmetries

Y.D. Chan

A. Garcia

K.T. Lesko

E.B. Norman

R.G. Stokstad

F.E. Wietfeldt*

I. Zlimer

Heavy Element Nuclear & Radiochemistry

A. Ghiorso

K.E. Gregorich

N.J. Hannink*

D.C. Hoffman

C.D. Kacher*

B.A. Kadkhodayan*

S.A. Kreek*

M.R. Lane*

D.M. Lee

M.F. Mohar

M.P. Neu*

G.T. Seaborg

E. R. Sylwester*

H.L. Hall (LLNL)

W.D. Loveland (Oregon State)

Weak Interactions

S.J. Freedman

C.J. Bowers*

B.K. Fujikawa

Z. Lu*

J. Mortara*

S. Shang

M. Rowe*

*Graduate student, **undergraduate student, **group leader in boldface.**

88-Inch Cyclotron Operations

D.J. Clark
D.E. Deutscher
A.P. Guy
R.M. Larimer
G.L. Low, Jr.
C.M. Lyneis
R.J. McDonald
S.A. Meaney
V.L. Saling
Z.Q. Xie

Isotopes Project

R.B. Firestone
E. Browne-Moreno
V.A. Shirley
C.M. Baglin (Morgan Hill, CA)
B. Singh (McMaster)
J.Z. James (UCB)
C.A. Stone (San Jose State)

Theory

J. Cernohorsky
K.J. Eskola
N.K. Glendenning
M. Gyulassy
C. Jarzynski
W.D. Myers
J. Randrup
W.J. Swiatecki
X. Wang
F. Weber (Munich)
D. Dong

Software Group

R.A. Belshe
S. Jacobson
C.P. McParland
W.H. Rathbun
E.B. Yee

Intermediate Energy

D.N. Delis*
K.A. Hanold*
K. Jing
L.G. Moretto
W. Skulski
Q.C. Sui
K. Tso*

A.C. Veeck*
G.J. Wozniak

Crystal Barrel

D. Armstrong
R.R. Bossingham
T.A. Case*
K. Crowe
Y. Dardennes*

Transfer Reactions & Rotational Inelastic Scattering

J.O. Rasmussen
S.Y. Chu* (Yale)
Z. Guo (Fudan)

Plastic Track Detectors

Y.D. He
D.M. Lowder
T.C. Miller
P.B. Price
A.A. Richards
D. Snowden-Ifft
A. Westphal
W.T. Williams

Secondary Radioactive Beams

K. Matsuta
M. Fukuda

Subthreshold Kaons & Antiprotons

V. Perez-Mendez
J. Drewery
S.N. Kaplan

Nuclear & Astrophysics

R.L. Gan**
C.T. Milling**
C. Chen (LSU)
S. Costa (Catania)
H.J. Crawford (UCSSL)
J.M. Engelage (UCSSL)
I. Flores (UCSSL)
L.C. Greiner (UCSSL)
J. Romanski
C.E. Tull (LSU)

Di-Lepton Spectrometer

H.Z. Huang
H.S. Matis
C.J. Naudet
R.J. Porter*
L.S. Schroeder
W.K. Wilson
J. Carroll (UCLA)
G. Roche (Clermont II)
M.V. Toy* (UCLA)

Relativistic Nuclear Collisions

F.S. Bieser
M.A. Bloomer
S. Chase*
W.B. Christie
E.M. Friedlander
W. Gong
D.E. Greiner
J.W. Harris
P.M. Jacobs
P.G. Jones
P.J. Lindstrom
S. Margetis
J.N. Marx
H.S. Matis

J.T. Mitchell
R.J. Morse
G. Odyniec
W. Ogle**
D.L. Olson
M. Partlan*
A.M. Poskanzer
G. Rai
H-G. Ritter
A. Sobel**
I. Sakrejda
J.J. Schambach
L.P. Teitelbaum*
H.H. Wieman
J.D. Wolf
C.F. Bormann (GSI)
D.A. Cebra (UC Davis)
A.D. Chacon (Texas A&M)
S. Costa (Catania)
T.J. Hallman (UCLA)
E.C. Hjort (Purdue)
M.L. Justice (Kent State)
D.F. Keane (Kent State)
L.M. Lerman (Phillips)
N. Porile (Purdue)
A. Scott* (Kent State)
Y. Shao* (Kent State)

LOW ENERGY EXPERIMENTS

The IsoSpin Laboratory

J. Michael Nitschke

The science of Radioactive Nuclear Beams (RNB) is evolving rapidly. RNBs produced through projectile fragmentation are being used routinely. The first RNB facility based on the ISOL (Isotope Separator On-Line) principle¹ has obtained its first results with low energy light ion beams of interest in astrophysics. An ISOL-RNB facility is under construction at ORNL² and ten others are in various proposal states world-wide.

Since its inception in 1989 the plan for the IsoSpin Laboratory (ISL)³ has advanced both scientifically and technically, mainly due to the activities of the ISL Steering committee and a Users community that now numbers almost 500. In October 1992 a Workshop on the Production and Use of Intense RNBs was held in Oak Ridge⁴. It concentrated on the technical aspects of constructing a high-intensity, broad-mass-range, second generation RNB facility, and addressed specifically issues related to target/ion sources and mass separation, primary and secondary accelerators, and experiments using RNBs. Feedback from the participants led to a refinement of the specifications for the ISL over those outlined in the White Paper.³ The most important change was in the top energy. While it was thought previously that a flat 10MeV/u output energy over the entire mass range would be appropriate, transfer- and deep inelastic reactions in inverse kinematics, for example $p(^{11}\text{Li}, d)^{10}\text{Li}$, will require energies up to 30 MeV/u. The study of shell model states near ^{132}Sn with reactions of the type $d(^{132}\text{Sn}, p)^{133}\text{Sn}$ will require ~15 MeV/u. Consequently, from various physics requirements, an output energy profile has emerged with ~30MeV/u for the lightest masses, 20-25MeV/u for $A\sim 130$ and ~8MeV/u for the heaviest masses up to $A\lesssim 240$.

Another post-accelerator parameter that will demand special attention is beam purity. For some astrophysical experiments it will have to be as high as 10^{-5} . This will require chemically

selective targets and ionization, and electromagnetic- and gas-filled separators. For the separation of isobars a high resolution ($m/\Delta m = 30.000$) Mattauch-Herzog-type separator will be needed.

Transverse beam emittances should be as low as possible ($\sim 1-2 \pi$ mm mrad) for beam containment and background reduction. Longitudinal emittances should be better than 50 keV ns with a micro structure of 100 ns for time-of-flight experiments.

Several key R&D areas have been identified and three working groups have been established to address the following topics: target/ion sources, post-accelerators, and experiments.

At LBL, ISL related work is being carried out in the following areas: cyclotron design studies for primary beam production, high intensity target designs and tests, radiological studies⁵, low- β accelerators, ECR sources, charge state enforcers, system analysis, and experiment preparations in nuclear structure and heavy element science.

A target test stand for 50 kW, using electrons to simulate the primary proton beam, has been completed and the first experiments have started.

References

1. Bruandet, J.F., Fernandez, B. and Bex, M. *Proceedings of the Intl. Workshop on the Physics and Techniques of Secondary Nuclear Beams*, Edition Frontiers, Gif-sur-Ivette, Dourdan, France, 1992.
2. Garrett, J.D. and Olsen, D.K. *A proposal for Physics with Exotic Beams at the Holifield Heavy Ion Research Facility*, Oak Ridge National Laboratory, 1991.
3. *The IsoSpin Laboratory, Research Opportunities with Radioactive Nuclear Beams*, LALP 91-51, 1991.
4. Garrett, J.D. *Proceedings of the Workshop on the Production and Use of Intense Radioactive Beams*, ORNL, Oak Ridge TN, 1992, to be published.
5. Barbier, M.M. *IsoSpin Laboratory Radiation Assessment*, Marcel M. Barbier Inc., MMB-53, 1992.

Evidence for M1 Transitions Between Superdeformed States in $^{193}\text{Hg}^*$

P. Fallon, J. Burde, B. Cederwall, M.A. Deleplanque, R.M. Diamond, I.Y. Lee, J.R.B. Oliveira, F.S. Stephens.[†]

*J.A. Becker, M.J. Brinkman, E.A. Henry, A. Kuhnert, M.A. Stoyer.[‡]
J.E. Draper, C. Duyar and E. Rubel.[§]*

Superdeformed states are associated with extremely large quadrupole deformations, typically $\beta_2 \approx 0.6$ in the mass 150 region and $\beta_2 \approx 0.47$ in the mass 190 region. The large quadrupole deformations enhance stretched E2 transition rates and consequently one would not expect the 'slower' inter-band transitions to compete with these highly collective 'fast' inband decays.

Superdeformed bands around mass 190 extend to low frequencies ($\hbar\omega \sim 0.15$ MeV) and spins ($I_f \sim 8$). The large electron conversion coefficients associated with low energy M1 decays enhance the total M1 transition probability and the E2 transition probabilities decrease with decreasing transition energy ($B(E2) \propto E_\gamma^5$). Thus it is more likely for M1 decays to compete with stretched E2 decays, resulting in cross talk between superdeformed states. The first evidence for transitions between superdeformed bands was in ^{193}Hg ¹, although in this previous work the cross talk was only observed from one band to another and not vice-versa.

High spin states in ^{193}Hg were populated by the reaction $^{176}\text{Yb}(^{22}\text{Ne}, 5n)^{193}\text{Hg}$ at a beam energy of 116 MeV using the HERA Ge detector array at the LBL 88-Inch Cyclotron. Approximately 680 million events were contained in a 'high-fold' correlation matrix of which $\sim 60\%$ belonged to ^{193}Hg .

This experiment shows, for the first time, that the cross-talk between superdeformed bands in ^{193}Hg is two-way and as a result the inter-band

transitions are most likely to have M1 multipolarity and connect signature partner bands. The intensity of the cross-talk is $\sim 30\%$ of the inband decay. The proposed M1 decays between bands are shown in figure 1.

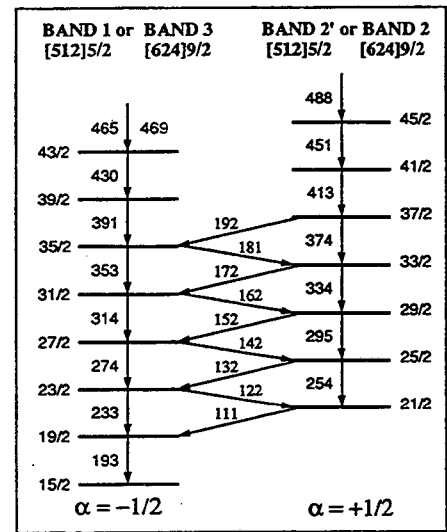


Fig. 1. Schematic partial level scheme for the proposed signature partner bands in ^{193}Hg . The M1 energies are calculated in the limit that the bands are strongly coupled.

The M1 gamma-rays are extremely weak, indeed only the the 142 and 152 keV transitions occur in regions of the spectrum free from large contaminant peaks. The individual intensities for the 142 and 152 keV M1 gamma-rays are 14(6)% and 15(6)% of the full superdeformed inband intensity respectively. That is they are $\sim 1/2$ of the total cross-talk intensity and thus they are consistent with what one may expect for M1 decays.

Footnotes and References

*Submitted to Phys. Rev. Lett.

[†]Lawrence Berkeley Laboratory.

[‡]Lawrence Livermore National Laboratory.

[§]UC Davis

¹D.M.Cullen et al., Phys. Rev. Lett. C 47 (1991).

Superdeformation in $^{191}\text{Au}^*$

D.T. Vo[†], W.H. Kelly[†], F.K. Wohn[†], J.C. Hill[†], M.A. Deleplanque, R.M. Diamond, F.S. Stephens, J.R.B. Oliveira[‡], J. Burde[§], A.O. Macchiavelli^{**}, J. deBoer^{††}, J.A. Becker^{‡‡}, E.A. Henry^{‡‡}, M.J. Brinkman^{‡‡}, A. Kuhnert^{‡‡}, M.A. Stoyer^{‡‡}, J.R. Hughes^{‡‡}, J.E. Draper[#], C. Duyar[#], and E. Rubel[#]

A superdeformed (SD) band has been observed for the first time in a Au isotope, extending the SD mass-190 region from $Z=80-82$ to include $Z=79$. The experiments were carried out at the LBL 88-Inch Cyclotron and made use of HERA. States in $^{190,191,192}\text{Au}$ were populated in the reaction $^{186}\text{W}(^{11}\text{B}, xn)$ at 86, 84, and 78 MeV. All three- and higher-fold γ -ray coincidences were recorded, as well as two-fold events if in coincidence with at least six inner-ball detectors.

Matrices of $\gamma\gamma$ coincidences were constructed with various sum-energy and multiplicity requirements. A channel-by-channel search of the matrices revealed a band of at least 13 transitions ranging in energy from 229 to 678 keV in the 86- and 84-MeV data sets (Fig. 1). The relative intensity pattern of the band (inset) and the energy spacings of the transitions are similar to those of other SD bands in this region, but it is one of the weakest found to date.

Assignment of this band to ^{191}Au is based on the excitation function and cross bombardment results. From the fact that the SD band is so weak in the 78-MeV reaction where ^{192}Au is most intense, one can rule out that the SD band belongs to ^{192}Au . In an earlier experiment, $^{176}\text{Yb}(^{19}\text{F}, 5n)^{190}\text{Au}$ at bombarding energies of 100 and 105 MeV, normal deformed states with similar spins as in the ^{11}B irradiations were obtained. Although the statistics for ^{190}Au at both energies are better and the ^{191}Au populations are smaller than those in the ^{11}B reaction, searches for the SD band were unsuccessful. Thus it does not belong to ^{190}Au , and is assigned to ^{191}Au .

Except for the highest one, all transitions in this ^{191}Au band are within 2 keV of those in the $^{191}\text{Hg}^*$ SD band. It is somewhat surprising that a single proton hole in the ^{192}Hg core (^{191}Au) would give the same effect as a single neutron

hole ($^{191}\text{Hg}^*$). But, unpaired single-particle Routhian calculations show that the SD band in ^{191}Au may be assigned to the $[411]1/2$ orbital, and that a proton hole in such an orbital would produce a similar effect as a neutron hole in the $^{191}\text{Hg}^*$ $[642]3/2$ orbital because both Routhians have small slopes and curvatures. This may explain the absence of the signature partner of the ^{191}Au band, since the $[411]1/2$ orbital does have some signature splitting.

Footnotes and References

* Condensed from article submitted for publication

† Iowa State University, Ames, IA 50011

‡ Universidade de Sao Paulo, S. Paulo, SP, Brazil

§ The Hebrew University, Jerusalem, Israel

** CNEA 1429-Buenos Aires, Argentina

†† Universitat Munchen, D-8046 Garching, Germany
& LLNL, Livermore, CA 94550

University of California, Davis, CA 94550

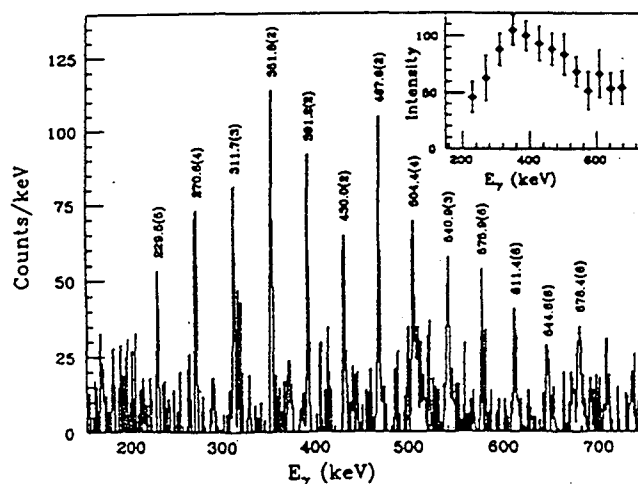


Fig. 1. Spectrum of the SD band produced in the $^{186}\text{W}(^{11}\text{B}, 6n)$ reaction from double-gated three- and higher-fold events. The inset shows the transition intensities (with internal conversion).

Oblate Collective Band in ^{193}Hg

N. Roy, J. A. Becker,* E. A. Henry,* M. J. Brinkman,* M. A. Stoyer,* J. A. Cizewski,†
R. M. Diamond, M. A. Deleplanque, F. S. Stephens, C. W. Beausang, and J. E. Draper.‡*

A new collective band has been observed in ^{193}Hg with $E_x > 5.7$ MeV. The states have spin extending from $I \geq 47/2$ to $I + 10$, and the γ -ray cascade includes competing dipole and quadrupole transitions. The band has been interpreted as collective oblate, involving deformation aligned high- j proton configurations such as $\pi(s_{1/2}^{-2}h_{9/2}i_{13/2})$, and rotation aligned $i_{13/2}^{-n}$ neutrons.

The experimental data were obtained at the LBL 88-Inch Cyclotron Facility. ^{193}Hg was populated in the reaction $^{176}\text{Yb}(^{22}\text{Ne}, 5n)$ at $E(^{22}\text{Ne}) = 110$ MeV. Reaction γ rays were detected with the Ge detector array HERA. The evidence for the new band was obtained in an analysis of a symmetrized E_γ vs E_γ matrix.

The collective cascade illustrated in Fig. 1 suggests signature partners of the same intrinsic state with some signature splitting. Both partners undergo band crossing with an alignment gain $\sim 4\hbar$ (most likely $i_{13/2}$ neutrons). The small dynamic moment-of-inertia ($\mathcal{J}^{(2)} \sim 16\hbar^2/\text{MeV}$) is typical of similar bands in this region that are oblate. Weak interaction between crossing bands is typical of this mass region; the closeness of the two $I + 4$ levels provides an upper limit of 4 keV for the interaction strength of the band crossing.

Intensity balance arguments, in general, favor multipolarity $M1$ for the $L = 1$ transitions, since low-energy $M1$ transitions are highly converted in this nucleus. We assume all $L = 1$ transitions are $M1$ and all $L = 2$ transitions are $E2$. The $M1$ transitions suggest that high- K proton excitations are important in the structure, since g_K is large and positive for proton orbitals and the $M1$ transition rate increases with K^2 . High- K

proton orbitals are present above the spherical $Z = 82$ gap for oblate deformation, based on eg., $h_{9/2}$, $i_{13/2}$, and $f_{7/2}$ orbitals.

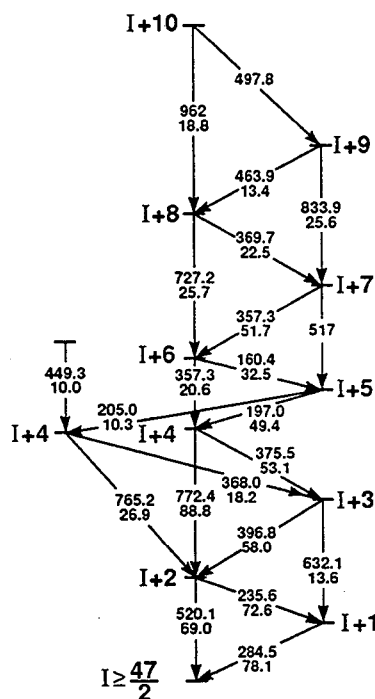


Fig. 1. Partial level scheme for the irregular band in ^{193}Hg . The γ -rays are labeled with transition energy and intensity (relative to the population of the yrast $13/2^+$ level, taken as 1000).

There are now a number of reports of $\Delta L = 1$ bands including ^{196}Hg ,¹ neutron deficient Tl, and (neutron deficient) $^{192,194,196-201}\text{Pb}$. These data provide a new systematic testing ground for shape coexistence and the onset of deformation near the magic number $Z = 82$.

Footnotes and References

*Lawrence Livermore National Laboratory.

†Rutgers University.

‡UC Davis.

Footnotes and References

¹B. Cederwall et al. LBL Annual Report 1992.

A New Oblate Band in ^{196}Hg With Quenched M1 Strength *

B.Cederwall,[†] M.-A.Deleplanque,[†] F.Azaiez,[†] R.M.Diamond,[†] P.Fallon,[†]
 W.Korten,[†] I.-Y.Lee,[†] A.O.Macchiavelli,[†] J.R.B.Oliveira,[†] F.S. Stephens[†]
 W.H.Kelly[‡], D.T.Vo,[‡] J.A.Becker,[§] M.J.Brinkman,[§] E.A.Henry,[§]
 J.R.Hughes,[§] A.Kuhnert,[§] M.A.Stoyer,[§] T.F.Wang,[§] J.E.Draper,^{**}
 C.Duyar,^{**} E.Rubel^{**} J.deBoer^{††}

High spin states in the nucleus ^{196}Hg were populated in $^{192}\text{Os}(^9\text{Be},5n)$ reactions at 65 MeV beam energy. The γ rays emitted from the excited nuclei were detected in the HERA array at the Lawrence Berkeley Laboratory 88-Inch Cyclotron facility. A new band structure is observed in ^{196}Hg showing the characteristics of a $\Delta I = 1$ rotational band with a moderate, almost spin-independent, signature splitting. A sum of coincidence-gated spectra is shown in fig. 1. Similarly to what was found for the $\Delta I = 1$ band in $^{193}\text{Hg}^1$ the observed $B(M1)/B(E2)$ values are significantly smaller than the ones measured for the recently discovered "oblate" bands in the lead isotopes. We have calculated theoretical estimates of the $B(M1)/B(E2)$ values based on the Dönau - Frauendorf formalism² and TRS calculations³. The calculated values for the $\pi h_{9/2}i_{13/2}h_{11/2}^{-2} \otimes \nu i_{13/2}^{-2}$ configuration are in reasonable agreement with the experimental values for the ^{196}Hg $\Delta I = 1$ band. Furthermore, the estimate for the $\pi h_{9/2}i_{13/2} \otimes \nu i_{13/2}^{-2}$ configuration follows well the larger $B(M1)/B(E2)$ ratios measured in the lead nuclei, suggesting that there is

a difference in the proton structure between the Pb and Hg nuclei involving aligned $h_{11/2}$ proton orbitals.

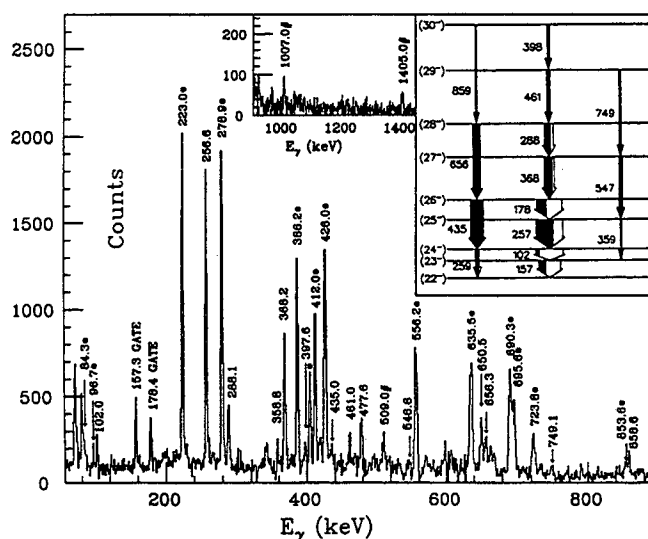


Fig. 1. Gamma-ray spectrum gated on the 157.3 keV and 178.4 keV transitions. Peaks marked with a "*" are from the decay within the previously established level scheme⁴ and the peaks marked with a "#" are connected to the depopulation of the band. The partial level scheme obtained in the present work is shown in the right inset. The γ -ray transitions are labeled by their energy in keV.

Footnotes and References

*Condensed from a Letter submitted to Phys. Rev. C, Rapid Comm.

[†]Lawrence Berkeley Laboratory

[‡]Iowa State University

[§]Lawrence Livermore National Laboratory

^{**}University of California, Davis

^{††}University of Munich

¹N. Roy et al., Phys. Rev. C, accepted

²F. Dönau and S. Frauendorf, *Proceedings of the Conference on High Angular Momentum Properties of Nuclei, Oak Ridge, 1982*, editor N.R. Johnson (Harwood Academic, New York, 1983), p. 143

³W. Nazarewicz et al., Nucl. Phys. A435 (1985) 397

Footnotes and References

⁴D. Mehta et al., Z. Phys. A339 (1991) 317

Collective Oblate Bands in ^{196}Pb

J.R. Hughes,* Y. Liang,[†] R.V.F. Janssens,[†] A. Kuhnert,* J.A. Becker,*
 I. Ahmad,[†] I.G. Bearden,[‡] M.J. Brinkman,* J. Burde, M.P. Carpenter,[†]
 J.A. Cizewski,[§] P.J. Daly,[‡] M.A. Deleplanque, R.M. Diamond, J.E. Draper,**
 C. Duyar,** B. Fornal,[‡] U. Garg,^{††} Z.W. Grabowski,[‡] E.A. Henry,* R.G. Henry,[†]
 W. Hesselink,^{‡‡} N. Kalantar-Nayestanaki,^{‡‡} W.H. Kelly,[¶] T.L. Khoo,[†] T. Lauritsen,[†]
 R.H. Mayer,[‡] D. Nissius,[‡] J.R.B. Oliveira, A.J.M. Plompen,^{‡‡} W. Reviol,^{††}
 E. Rubel,** F. Soramel,[†] F.S. Stephens, M.A. Stoyer,* D. Vo,[¶] and T.F. Wang*

Recent experimental data on the Pb isotopes have revealed a number of interesting features. In particular, a number of “regular” and “irregular” dipole bands have been observed¹ at higher angular momentum in both the even $^{192,194,198,200}\text{Pb}$ and odd $^{197-201}\text{Pb}$ nuclei. Such collective excitations are rather surprising in the singly-magic Pb nuclei, and, indeed, are thought to involve proton excitations across the spherical $Z = 82$ shell closure.

High-spin states in ^{196}Pb were investigated by our collaboration to further investigate these collective features. ^{196}Pb was populated² with the $^{170}\text{Er}(^{30}\text{Si}, 4n)$, and the $^{176}\text{Yb}(^{26}\text{Mg}, 6n)$ reactions. The Si-induced reaction was studied at the Argonne superconducting linear accelerator, ATLAS, and the Mg-induced reaction, was studied at the Lawrence Berkeley Laboratory 88-Inch Cyclotron. Large Compton-suppressed Ge arrays were used at both facilities for γ -ray spectroscopy.

Fig. 1 shows the partial level scheme for ^{196}Pb deduced from these data. Two regular (bands 1 and 2) and one irregular (band 3) band structure is observed.

In each case measured γ -ray angular correlation ratios and transition intensities suggest that the in-band γ -rays are of M1 nature. Transitions linking Band 2 to the previously identified yrast states have been observed, allowing tentative spin and parity assignments to be made. The large $B(M1)/B(E2)$ ratios for this band suggest a high- K proton configuration, and along with the regular rotational energy spacings, and the relatively small dynamic moment of inertia, an oblate deformed $\pi(i_{13/2} \otimes h_{9/2}) \otimes \nu(i_{13/2})^2$ structure is suggested.

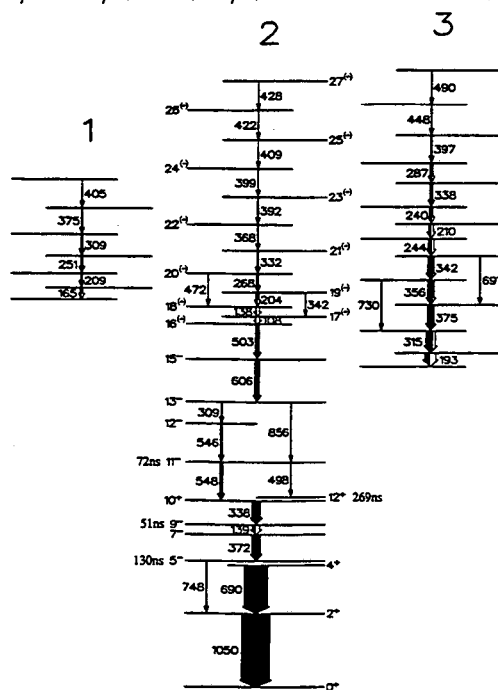


Fig. 1. Partial level scheme for ^{196}Pb . Transition energies are given in keV. Arrow widths represent relative intensities from the thick target data.

Footnotes and References

*Lawrence Livermore National Laboratory.

[†]Argonne National Laboratory.

[‡]Purdue University.

[§]Rutgers University.

**UC Davis.

^{††}Notre Dame.

^{‡‡}Vrije Universiteit, Netherlands.

[¶]Iowa State.

¹M.J. Brinkman *et al.*, Bull. Am. Phys. Soc. 37, 1312 (1992), and references therein.

²J.R. Hughes, *et al.*, accepted for publication in Phys. Rev. C.

Rotation-Induced Transition from Superfluid to Normal Phase in Mesoscopic Systems: ^{168}Yb and Adjacent Nuclei *

J.R.B.Oliveira, [†] S.Frauentorf, [‡] M.A.Deleplanque, R.M.Diamond, F.S.Stephens, C.W.Beausang, [§] J.E.Draper, ^{**} C.Duyar, ^{**} E.Rubel, ^{**} J.A.Becker, ^{††} E.A.Henry, ^{††} N.Roy ^{††}

Shortly after the discovery of pair correlations of the BCS type in nuclei, Mottelson and Valatin predicted that pairing should collapse in rapidly rotating nuclei much like superconductivity in a strong magnetic field. In nuclei only a small number of particles participate in the pairing correlations and the adequacy of the phase transition concept is questionable. The disappearance of static pairing corresponds to a major change of the excitation spectrum, from the quasiparticle (qp) to the particle-hole (ph) scheme.

The high-spin states of ^{168}Yb have been measured with the HERA system at the 88-Inch Cyclotron of the LBL, which consists of 20 Compton-suppressed GeHP detectors and an inner ball of 40 BGO detectors. The ^{168}Yb nucleus was produced in the reaction $^{124}\text{Sn}(^{48}\text{Ca},4n)$ at 210 MeV. Five bands previously reported by Bacelar *et al.* ¹ were confirmed and extended by one or two higher-lying transitions. In addition, four new bands, two extending up to $I \approx 40\hbar$, were observed.

The expected change of the neutron spectrum is calculated from the qp energies in a deformed rotating potential (Cranked Shell Model), in which the static pairing-gap parameter Δ decreases linearly from the full value (0.8 MeV) at $\omega = 0.25$ MeV, to zero at $\omega = 0.5$ MeV (fig. 1 (a)). This approach describes well the excita-

tion spectra in ^{168}Yb , as it is apparent from the figure, and in the adjacent Yb isotopes.

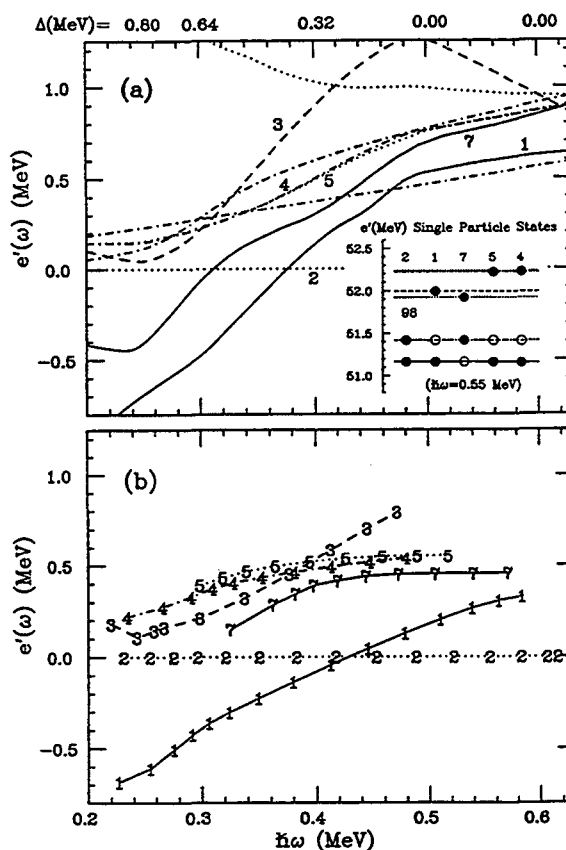


Fig. 1. Band structure of ^{168}Yb - Comparison between (a) the calculated states; and (b) the experimental results. The Routhians (energies in the rotating frame) are plotted relative to the lowest $(\pi, \alpha) = (-, 1)$ configuration (band 2). The solid, dashed, dot-dashed and dotted lines correspond to $(\pi, \alpha) = (+, 0), (+, 1), (-, 0),$ and $(-, 1)$, respectively. On the inset at the bottom right of (a), the particle-hole excitations of the $(-, 1)$ core (band 2) are shown; they are strictly valid only above $\omega = 0.5$ MeV where $\Delta = 0$.

Footnotes and References

*Condensed from Rapid Comm. - Phys. Rev. C, to be published in March 1993.

[†]On leave from the Univ. de S.Paulo, Brazil

[‡]On leave from the Institut für Kern und Hadronen Physik, Rossendorf, Germany

[§]University of Liverpool, Liverpool, United Kingdom

^{**}UC-Davis

^{††}LLNL

¹J. C. Bacelar *et al.*, Nucl. Phys. A442, 509 (1985).

High-spin states in $^{179}\text{Os}^*$

J. Burde[†], M.A. Deleplanque, R.M. Diamond, A.O. Macchiavelli[‡], F.S. Stephens, and C.W. Beausang[§]

The nucleus ^{179}Os was produced at the 88-Inch Cyclotron via the reaction $^{154}\text{Sm}(^{30}\text{Si},5n)$. Five new bands were found and those already known were extended towards higher spins. The results were analyzed using the Cranked-shell model, and by comparing signature splittings and $B(M1)/B(E2)$ ratios with theoretical predictions.

The first band crossing observed in nine out of the ten bands is most probably due to the alignment of a pair of $i_{13/2}$ neutrons. A second band crossing observed in three bands is likely caused by the alignment of two $h_{9/2}$ protons.

The signature splitting in the $9/2^+[624]$ band suggests that there is some hexadecapole deformation that brings the low- Ω components of the $i_{13/2}$ orbital together and mixes them.

The most interesting bands in that nucleus are the two pairs of pseudo-spin partners, namely the $5/2^- [512]$ signature pair and the $7/2^- [514]$ signature pair. The results suggest that these bands, which are close to each other in energy because of the pairing correlations, are fully mixed at low spins by the Coriolis interaction. However, as the pairing decreases at higher spins, these two bands have different properties as shown in Fig.1 where the alignments are plotted. The reason may be that for a smaller pairing, the $7/2$ orbital has a "particle" character, and therefore a core which is different from that of the $5/2$ orbital which has a "hole" character.

Footnotes and References

*Condensed from Phys. Rev. C46, 1642 (1992)

† University of Jerusalem, Israel

‡ Comisión Nacional de Energía Atómica, Buenos-Aires, Argentina

§ University of Liverpool, UK

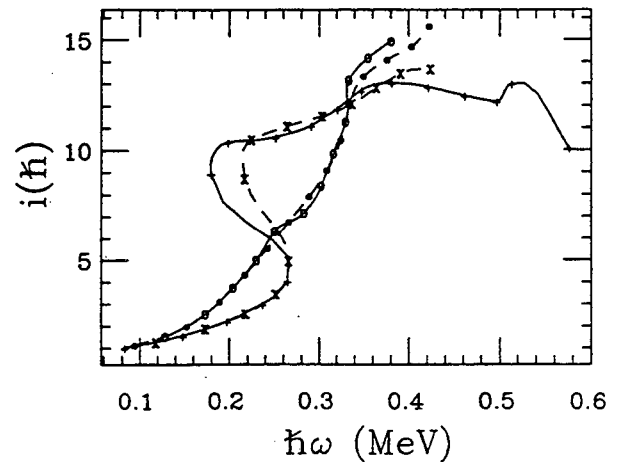


Fig. 1. Alignments i as a function of frequency for the two pseudo-spin partners $5/2^- [512]$ (crosses and pluses) and $7/2^- [514]$ (asterisks and circles). The $\alpha = -1/2$ signatures are shown as dashed lines and the $\alpha = 1/2$ signatures as solid lines. The reference parameters are $J_0 = 25 \text{ MeV}^{-1} \hbar^2$ and $J_1 = 60 \text{ MeV}^{-3} \hbar^4$.

Spectroscopy of Very Neutron-Deficient Hafnium and Tungsten Isotopes*

G.D. Dracoulis[†], B.Fabricius[†], P.M. Davidson[†], A.O. Macchiavelli, J. Oliveira, J. Burde, F.S. Stephens and M.A. Deleplanque

As the neutron number approaches the closed shell at $N=82$, the isotopes of W and Hf should correspondingly be less deformed. For the predicted deformation $\beta \leq 0.1$ and a neutron number around $N=86$, the Fermi level becomes close to the low- Ω components of the $h_{9/2}$ orbital, and is well below those for the $i_{13/2}$ orbital. Therefore, the first backbend is expected to result from the alignment of an $h_{9/2}$ neutron pair rather than that of an $i_{13/2}$ neutron pair observed for heavier isotopes.

The nuclei ^{158}Hf and ^{162}W were produced at the 88-Inch cyclotron in the reactions $^{107}\text{Ag}(^{54}\text{Fe}, p2n)$ and $^{107}\text{Ag}(^{58}\text{Ni}, p2n)$ respectively. Gamma-rays were observed with the HERA array of 21 Compton-suppressed Ge detectors. The identification of the product proton number was made on the basis of coincidences between the main transitions and the characteristic X-rays.

Fig. 1 shows plots of alignment as a function of frequency for several nuclei in the vicinity of ^{158}Hf and ^{162}W . The alignment in the positive parity band of ^{162}W is around $8\hbar$, compatible with the value obtained for a pair of $h_{9/2}$ neutrons, and significantly smaller than the value of $12\hbar$ seen in ^{164}W where a pair of $i_{13/2}$ neutrons align. The predicted deformations as well as blocking effects in the negative parity bands of even nuclei and in the odd neighboring nucleus ^{163}W support these assignments. The increase in alignment above the first backbend in ^{164}W is attributed to alignments of $h_{9/2}$ neutron and $h_{11/2}$ proton orbitals using the same arguments. The side band in ^{162}W and all the bands in ^{158}Hf appear to be irregular. More needs to be done to understand them.

Footnotes and References

*Condensed from Int.Conf. on Nucl. Struct. at High Angular Momentum, Ottawa, 1992, p.94.

[†] Australian National University, Canberra, Australia.

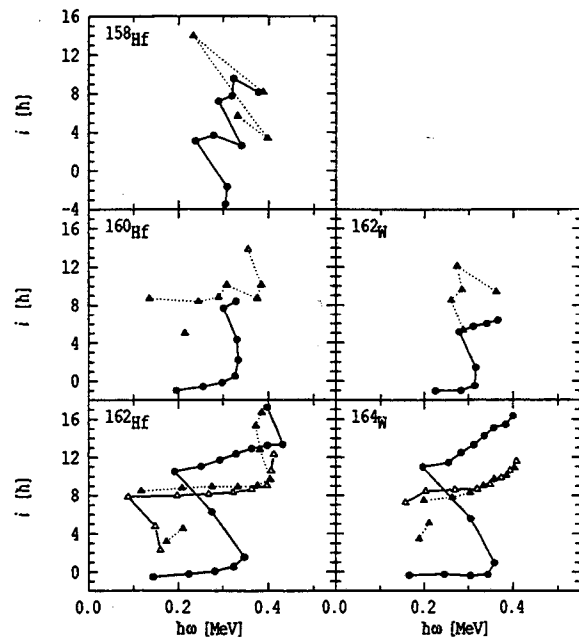


Fig. 1. Alignments as a function of frequency for several even-even isotopes. The positive parity states are shown by circles, and the negative parity ones by triangles.

Construction of a Remote LIPAS Apparatus for Determining Equilibrium Constants of Cation-Cation Complexes *

N.J. Hannink, D.C. Hoffman, R.J. Silva[†], and R.E. Russo[‡]

We constructed a remote Laser Induced PhotoAcoustic Spectroscopy(LIPAS) apparatus to use in an inert atmosphere glove box about 50 meters from the laser. This LIPAS apparatus is similar to that of Russo, Rojas, Robouch, and Silva¹. Our apparatus will be used to determine equilibrium constants of cation-cation complexes² involving uranium, neptunium, and plutonium.

A schematic of the LIPAS apparatus is shown in Fig. 1. The fiber optic cable connecting the laser to the LIPAS apparatus was also installed.

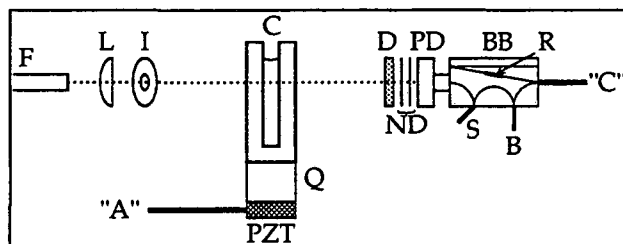


Fig. 1. Schematic of the LIPAS apparatus. Dotted line is the laser beam. Symbols are explained in the text.

The laser beam(from a Nd:YAG pumped dye laser) enters the LIPAS apparatus via the fiber optic cable(F). It is focused using a plano-convex lens(L, Oriel, $f=50$) to a point in or near the cuvette(C). The iris(I) removes stray, unfocused light. The beam passes through a reduced-volume quartz cuvette containing the sample. The laser beam is about 2 mm in diameter

Footnotes and References

*Work partially supported by The Glenn T. Seaborg Institute for Transactinium Science.

[†]Nuclear Chemistry Division, Lawrence Livermore National Laboratory, Livermore CA 94550

[‡]Energy and Environment Division, Lawrence Berkeley Laboratory, Berkeley CA 94720

¹R.E. Russo, D. Rojas, P. Robouch, and R.J. Silva, *Rev. Sci. Instrum.* **61**, 3729 (1990).

²Discovery documented in J.C. Sullivan, J.C. Hindman, and A.J. Zielen, *J. Amer. Chem. Soc.* **83**, 3373 (1961).

and aligned so that it does not hit the cuvette walls. The sample absorbs some of the light; then it non-radiatively releases some of the energy as heat which produces an acoustic wave. The acoustic wave travels through the solution, the cuvette, the quartz rod(Q) which is epoxied to the cuvette, and to the piezoelectric transducer(PZT) which is epoxied to the quartz rod. The PZT converts the acoustic wave to an electrical signal("A"); which goes to a preamplifier(Ortec 142C), located in the glove box, before going to the amplifier(Ortec 570), located in the laser laboratory.

After the laser beam emerges from the cuvette, it enters the photodiode assembly. The photodiode assembly has a diffuser(D) and two neutral density filters(ND) placed before the photodiode(PD) to reduce the light intensity by 7 orders of magnitude, allowing the photodiode to operate in its linear range. The photodiode has a 9 V reverse bias(input at B) to increase its sensitivity. The bias box(BB) produces the reverse bias; we constructed it with a 1 M Ω resistor(R) and included a switch(S). The photodiode signal("C") is sent to a boxcar (SRS Gated Integrator & Boxcar Averager) in the laser lab. Both the PZT and photodiode signals are processed by boxcars after appropriate amplification to allow triggering on the laser pulse and gating on the peaks of interest; these data are sent to the computer where they are stored and spectra displayed. The PAS signal is defined as "A"/"C", normalized to the laser power.

LIPAS is 100 to 1000 times more sensitive than conventional spectroscopy and yields the same information; therefore, its use in the study of cation-cation complexes allows lower concentrations to be used and fairly small equilibrium constants to be observed.

Solubility and Speciation of Plutonium(V) and Plutonium(VI) in Carbonate Solution*

M.P. Neu, H. Nitsche, R.J. Silva, and D.C. Hoffman

Plutonium migration in the geosphere and biosphere depends on its solubility and chemical form. Because plutonium has low solubility in near neutral solutions, nontraditional methods must be used to accurately characterize plutonium ions and complexes. We are using liquid scintillation counting and remote laser-induced photoacoustic spectroscopy (LIPAS) to study the behaviour of ^{242}Pu in 2 mM carbonate solution from supersaturation.¹ (The spectrometer, reported previously,¹ is similar to the apparatus described in the following report by Hannink, et al.) To afford comparison with speciation studies done in actual Yucca Mountain groundwaters,^{2,3} experimental solutions at pH 6.0 were produced by equilibrating 0.10 M sodium perchlorate with 5.71% CO_2 at 30.0°C and adding the ion of interest to yield an initial concentration of 3×10^{-5} M Pu(V), or 3×10^{-4} M Pu(VI).

A Pu(V)/carbonate solution was monitored for 7.5 weeks. Virtually all of the Pu remaining in solution was Pu(V); The Pu(V) concentration was determined to be 2.3×10^{-5} by spectral analysis of standards and a filtered aliquot of the solution. This value compares well with the upper solubility limit of 5×10^{-5} M for Pu in J-13 groundwater determined previously.³

We have begun Pu(VI) experiments. Initial spectral data show the disappearance of the characteristic Pu(VI) absorbance peak at 830 nm and a new peak at 841 nm, indicating the formation of a Pu(VI) carbonate complex. A peak at 569 nm, assigned to Pu(V), grows in within 7 hours.

Footnotes and References

*Work partially supported by Glenn T. Seaborg Institute for Transactinium Science.

1. M.P. Neu, H. Nitsche, R.J. Silva, R.E. Russo and D.C. Hoffman, L.B.L. Annual Reports, 1991-1992.

2. H. Nitsche, A. Muller, E.M. Standifer, R.S. Deinhammer, K. Becraft, T. Prussin, and R.C. Gatti, *Radiochim. Acta*, 58/59, 27 (1992).

3. H. Nitsche and N.M. Edelstein, *Radiochim. Acta*, 39, 23 (1985).

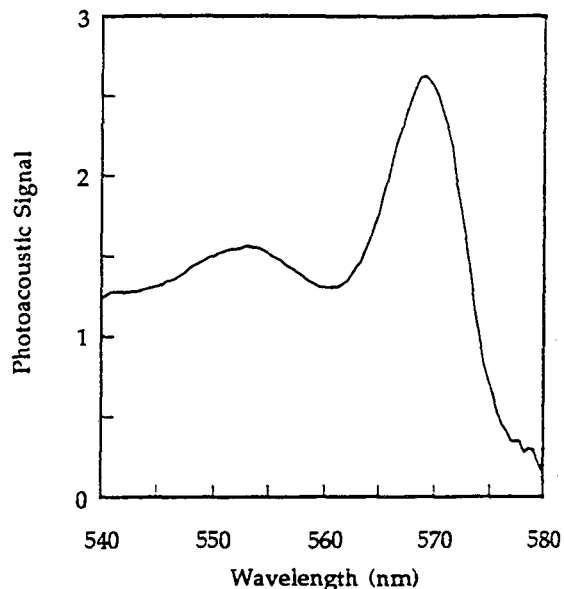


Fig. 1. Laser Photoacoustic Spectrum of a Pu(V) carbonate solution after 7.5 weeks.

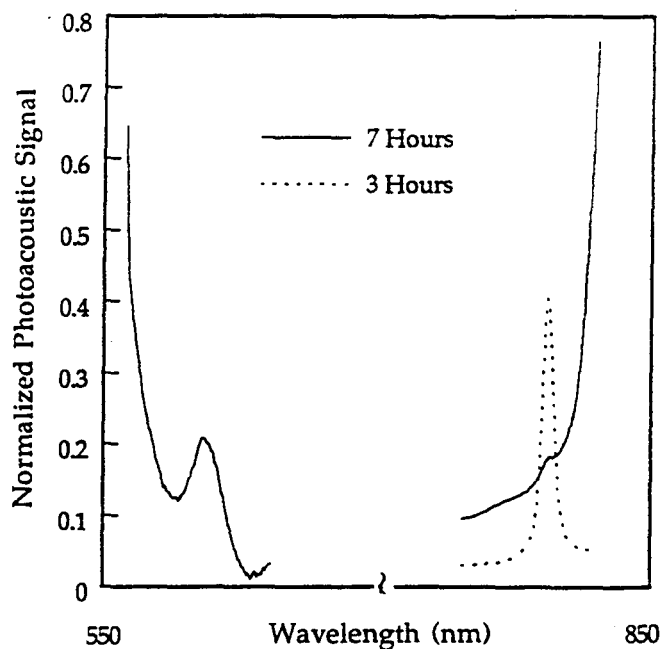


Fig. 2. Laser Photoacoustic spectra of Pu(V) and Pu(VI) species in the first hours of a Pu(VI) solubility/speciation experiment.

Surface Sorption Technique For Separation of Rutherfordium (Element 104)

C.D. Kacher, A. Bilewicz*, and D.C. Hoffman

Isotopes of transactinide elements can be formed in compound nucleus reactions between actinide targets and light-heavy ion beams at the 88-Inch Cyclotron. The products of interest, such as 65-s ^{261}Rf , are produced at rates of only about one atom per minute, along with large amounts of contaminant activities that interfere with the detection of the transactinides. Therefore, rapid and selective chemical separations are necessary for unambiguous isotope identification.

Surface sorption chemical separation is a fast and efficient method to separate 4+ ions such as Rf from 3+ actinide contaminants. The technique has the advantage over the liquid-liquid extractions used in the past in that it is fast and can be repeated on a one minute time scale. In these experiments, ^{261}Rf is produced in the $^{248}\text{Cm}(^{18}\text{O},5n)$ reaction and is transported to the chemical separation area on KCl aerosols via a He-jet. The Rf and other activities, along with the KCl from the gas transport system, are collected directly on a CoFeCN surface and allowed to sorb on the CoFeCN in a small volume of HCl solution. After waiting a few seconds for the sorption to take place, the surface is washed with more HCl to remove the actinides and other interfering activities which are not strongly sorbed. The surface is then dried, and the activities are detected directly from the surface by alpha and spontaneous fission pulse analysis.

In addition to Rf studies, tracer studies of the chloride complexation and hydrolysis of Zr, Hf, and Th have been performed using this sorption technique. We can then compare Rf behavior to the behavior of its lighter group 4 homologs, Zr and Hf, and to a 4+ actinide, Th.

Figs. 1 shows the effects of HCl concentration on sorption. Zr, Hf, Th, and Rf have 4+ ionic charges. These surfaces readily adsorb 4+ species while 2+ and 3+ species elute. In Fig. 1, Zr and Hf have low sorption percentages at low HCl

concentrations probably due to hydrolysis to form species such as $\text{Zr}(\text{OH})^{3+}$ or $\text{Hf}(\text{OH})^{3+}$. At higher HCl concentrations, the sorption of Zr and Hf seems to peak and then taper off. Th behaves differently. The sorption of Th remains high below 1M HCl then decreases between 1M and 6M HCl indicating the formation of chloride complexes such as ThCl_2^{2+} and ThCl^{3+} . The sorption of Rf increases between 0.5M and 4M HCl indicating that it, too, forms hydrolyzed species such as $\text{Rf}(\text{OH})^{3+}$ at lower HCl concentrations. Rf behaves more like its lighter homologs, Zr and Hf, than like Th. Rf forms hydrolyzed species as do Zr and Hf, but it is more sensitive to hydrolysis than Zr and Hf throughout a wider range of HCl concentrations.

*Institute of Nuclear Chem., Warsaw, Poland

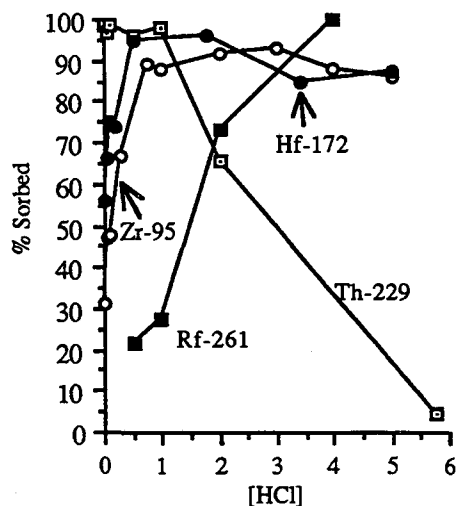


Fig. 1. Dependence of sorption of ^{229}Th , ^{95}Zr , ^{172}Hf , and ^{261}Rf on HCl concentration.

Comparison of TBP/HCl and TBP/HNO₃ Extraction Systems For Rf

C.D. Kacher, K.E. Gregorich, N.J. Hannink, M.P. Neu, B.A. Kadkhodayan, S.A. Kreek, M.R. Lane, E.R. Sylwester, M.F. Mohar, D.M. Lee, and D.C. Hoffman

Previous experiments at the 88-Inch Cyclotron showed that the extraction of ²⁶¹Rf into TBP from HCl solutions was an effective way to extract Rf. Unfortunately, approximately 2% of the actinides were extracted along with the Rf. The spontaneous fission (SF) activity from ²⁵⁶Fm made the determination of the SF and electron-capture (EC) branch of ²⁶¹Rf impossible. In addition, this SF contamination would make the identification of the new isotope ²⁶³Rf (which is expected to decay by SF) impossible with this extraction system.

Experiments at GSI and the University of Mainz demonstrated that extraction of Rf's lighter group 4 homologs, Hf and Zr, into TBP from HNO₃ solutions was very efficient, and that the actinide contamination in this system was very small.

It was therefore of interest to compare the TBP/HCl extraction system to the TBP/HNO₃ system. The extraction of rutherfordium by tributylphosphate (TBP) in benzene from separate aqueous 12M HCl and 10M HNO₃ environments was studied using 65-s ²⁶¹Rf produced at the LBL 88-Inch Cyclotron via the ²⁴⁸Cm (¹⁸O, 5n)²⁶¹Rf reaction. A 12M HCl concentration was used because a previous study¹ showed it best extracts Rf and a 10M HNO₃ concentration was used because the same study showed it best extracts Rf's lighter homolog, Zr. The TBP/HNO₃ separations were performed in parallel with the TBP/HCl separations to eliminate any systematic errors associated with factors such as uncertainty in the gas-jet transport efficiency.

The results showed that out of 130 TBP/HNO₃ experiments, only 4 events and 1 alpha-alpha correlation were observed compared to 12 events and 3 alpha-alpha correlations for the TBP/HCl system. The extraction of Rf using HNO₃ is unexpectedly small, indicating either that the NO₃⁻ complexation of Rf is significantly

weaker than for its lighter group 4 homologs, Zr and Hf, or that hydrolysis of Rf in HNO₃ dominates, possibly causing the hydrolyzed Rf species to adsorb onto the glass test tube used in the experiment. Performing the experiments in plastic rather than glass cones will minimize the surface sorption of hydrolyzed forms of Rf.

Footnotes and References

1. K. Czerwinski, *et.al.*, Studies of Fundamental Properties of Rutherfordium (Element 104) Using Organic Complexing Agents, LBL-32233, 76, 79 (1992).

On-Line Gas Phase Isothermal Chromatography of Zirconium and Niobium Chlorides

B. Kadkhodayan, D.C. Hoffman, B. Eichler[†], H.W. Gäggeler[†], A. Kovacs[†]

[†]Paul Scherrer Institute, CH - 5232 Villigen PSI, Switzerland

Gas-phase isothermal chromatography is a method by which volatile compounds of different chemical elements can be separated according to their volatilities. The technique, coupled with theoretical modeling of the processes occurring in the chromatography column¹ provides accurate determination of thermodynamic properties (adsorption enthalpies) for compounds of elements, such as the transactinides, which can only be produced on an atom-at-a-time basis. In addition, the chemical selectivity of the isothermal chromatography technique provides the decontamination from interfering activities, necessary for determination of the nuclear decay properties of the transactinides.

Theoretical calculations based on the relativistic Dirac-Fock method predict deviations from the normal periodic trends in the transactinide region. An intense effort in multi-configurational Dirac-Fock calculations relevant to the volatilities of halides of transactinide elements is now being carried out by Pershina et al. at Gesellschaft für Schwerionenforschung, Germany. While absolute values of the adsorption enthalpies from these calculations may not be accurate, the trends within a given group of the periodic table should be valid. This necessitates the experimental study of the volatilities of the homologous elements under the same conditions as for the transactinide elements. The comparison of calculations with experiments will help in the understanding of the role of relativistic effects in periodic trends.

The Heavy Element Volatility Instrument², HEVI, was used to investigate the volatility of Zr- and Nb-chlorides. These experiments were performed at the PSI SAPHIR reactor. The Zr and Nb isotopes were produced from the neutron induced fission of a ²³⁵U target. Tests were

performed using He/KCl and He/MoO₃ gas-jet transport systems and the following reactive gas mixtures as chlorinating agents: HCl, HCl/CCl₄, Cl₂, and Cl₂/CCl₄. The fission products were attached on aerosols and transported to HEVI. The activity-laden aerosols were stopped on a quartz wool placed in the beginning of a hollow quartz chromatography column. The wool was maintained at 900° C and the rest of the column was kept at various isothermal temperatures, ranging from 50 to 650° C. After leaving the column, the volatile species were reattached only KCl aerosols and transported to an intrinsic Ge detector to observe characteristic gamma activities. Figure 1 illustrates our results using MoO₃ as transport aerosol and Cl₂/CCl₄ as chlorinating agent. The solid lines drawn through the data points are from a theoretical Monte Carlo computer program¹.

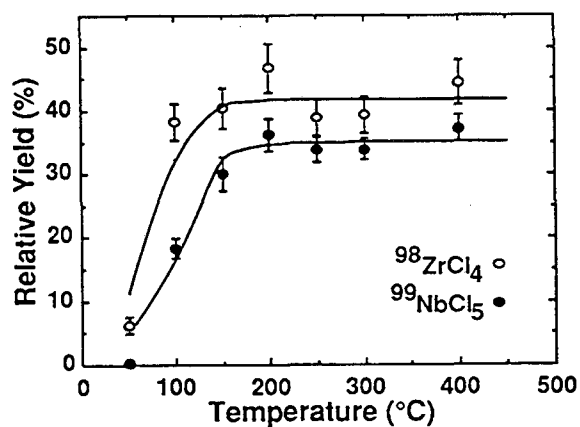


Fig. 1. Relative yield curves for ⁹⁸Zr and ⁹⁹Nb chloride molecules with a He/MoO₃ gas-jet and Cl₂/CCl₄ as chlorinating agent.

References

1. A. Türlér et al., LBL-31855, Annual Report (1991).
2. B. Kadkhodayan et al., *Nucl. Instr. Meth. A317*, 254 (1992).

On-Line Gas Phase Isothermal Chromatography of Hafnium and Tantalum Chlorides

B. Kadkhodayan, A. Türlér[†], K.E. Gregorich, E. Sylwester, C.D. Kacher, S.A. Kreek, M.R. Lane, D.M. Lee, M.P. Neu, D.C. Hoffman

[†]Paul Scherrer Institute, CH - 5232 Villigen PSI, Switzerland

A mixed target of ^{nat}Eu (47.8% ¹⁵¹Eu, 52.2% ¹⁵³Eu) and ¹⁴⁷Sm was used for the production of Hf and Ta isotopes by a (²⁰Ne,xn) reaction. The isotopes 41-s ¹⁶²Hf, 1.7-min ¹⁶⁵Hf, 32-s ¹⁶⁶Ta and 1.3-min ¹⁶⁷Ta were produced with cross section values of hundreds of milibarns. The Heavy Element Volatility Instrument¹ (HEVI) was used to investigate the volatility of Hf- and Ta-chlorides. HEVI is an on-line isothermal gas chromatography system which separates short lived volatile halides according to their volatility.

These experiments were performed at the LBL 88-Inch cyclotron. Experiments were carried out using He/KCl and He/MoO₃ gas-jet transport systems and reactive gas mixtures of HCl/CCl₄ and HCl/SOCl₂ as chlorinating agents. The experimental procedure from production to detection of the isotopes has been outlined in the previous page.

Figures 1 illustrate some of our results using the MoO₃ as transport aerosol and HCl/CCl₄ as the chlorinating agent. The solid lines drawn through the data points are from a theoretical Monte Carlo computer program². The calculated adsorption enthalpy values for the halide species of group 4 and 5 elements are presented in table 1. Most probably the Ta species under study here is TaOCl₃ rather than TaCl₅ because of its unusually low volatility.

In general the group 4 elements seem to be more volatile than the group 5 elements. Within the group 4 elements, the lighter halide species (ZrCl₄) is more volatile and has a larger ΔH_{ads} value than the heavier species (HfCl₄). Assuming similar molecular structures for chloride complexes within a periodic group, RfCl₄ should be the least volatile of the group 4 chlorides with

the smallest ΔH_{ads} value. A similar trend should exist within the group 5 chloride elements with TaCl₅ being the least volatile. However, it is not possible to arrive at such a conclusion since the Ta-chloride species under study is possibly an oxy-chloride complex.

References

1. B. Kadkhodayan et al., *Nucl. Instr. Meth. A317*, 254 (1992).
2. A. Türlér et al., LBL-31855, Annual Report (1991).

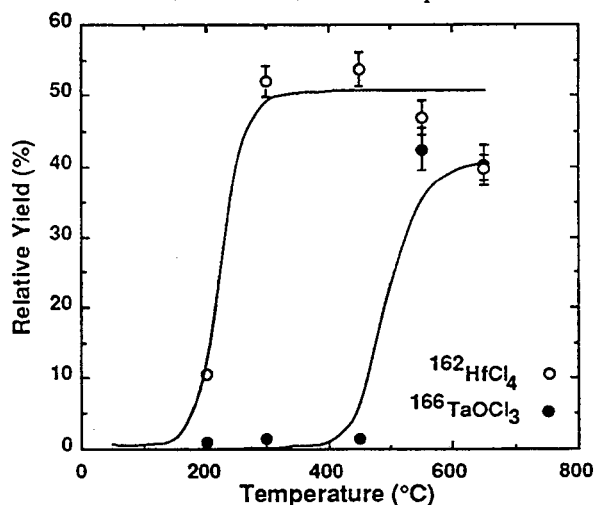


Fig. 1. Relative yield curves for ¹⁶²Hf and ¹⁶⁶Ta chloride molecules with a He/MoO₃ gas-jet and HCl/CCl₄ as chlorinating agent.

Table 1. Adsorption enthalpy values on SiO₂ surface calculated using the Monte Carlo computer program.

Compound	ΔH_{ads} (kJ/mole)
ZrCl ₄	-74 ± 5
NbCl ₅	-68 ± 5
HfCl ₄	-96 ± 5
TaOCl ₃	-149 ± 5

On-line Gas Phase Isothermal Chromatography of Rutherfordium (Element 104) Chlorides

B. Kadkhodayan, A. Türler[†], K.E. Gregorich, E. Sylwester, C.D. Kacher, S.A. Kreek, M.R. Lane, D.M. Lee, M.F. Mohar, M.P. Neu, D.C. Hoffman

[†]Paul Scherrer Institute, CH - 5232 Villigen PSI, Switzerland

The Heavy Element Volatility Instrument¹ (HEVI) was used to investigate the volatility of Rf tetrachlorides^{2,3}. HEVI is an On-line isothermal gas chromatography system which separates short lived volatile halides according to their volatility. 65-s ²⁶¹Rf was produced in fusion reactions of 94-MeV ¹⁸O + ²⁴⁸Cm at the LBL 88-Inch Cyclotron. Reaction products, transported by a He/MoO₃ gas jet system, were continuously collected on a quartz wool plug, kept at 900°C, inside a quartz chromatography column. The chlorides of Rf were formed by adding 100 ml/min HCl gas. Volatile species were carried to the cooler, isothermal section of the column by the He flow, where chromatography was performed. The separated species were attached on KCl aerosols in N₂, and transported through a capillary to the MG counting system⁴. Products were collected on thin polypropylene foils (40 μg/cm²) and subsequently stepped through 6 pairs of PIPS (Passivated Ion implanted Planar Silicon) detectors. A half-life of 78⁺¹¹₋₆ s was measured for ²⁶¹Rf. This value is slightly longer than the literature value of 65 s.

The volatility of Rf-chlorides, which has been determined with high accuracy, can be compared with the volatility of Zr- and Hf-chlorides^{2,3} measured under identical conditions. The following series in volatility of the group 4 element chlorides has been established: ZrCl₄ ≥ RfCl₄ > HfCl₄, with Zr- and Rf-chlorides similar in volatility and more volatile than Hf-chlorides. An adsorption enthalpy value of -79 ± 5 kJ/mole was calculated for RfCl₄ on a SiO₂ surface. Comparison of this value with the lighter group 4 elements gives the following series in adsorption enthalpy values: ZrCl₄ > RfCl₄ > HfCl₄ (Fig. 1). Assuming similar

molecular structures for chloride complexes within group 4 of the periodic table, a trend of decreasing volatility and ΔH_{ads} is observed as one moves down the group (noticed in Zr- and Hf-chlorides). Following this trend, RfCl₄ is then expected to be the least volatile of the group 4 chlorides with the smallest ΔH_{ads} value. As illustrated here, our results show a break in this expected trend. Further calculations are needed to assess whether this is due to relativistic effects in the transactinide region.

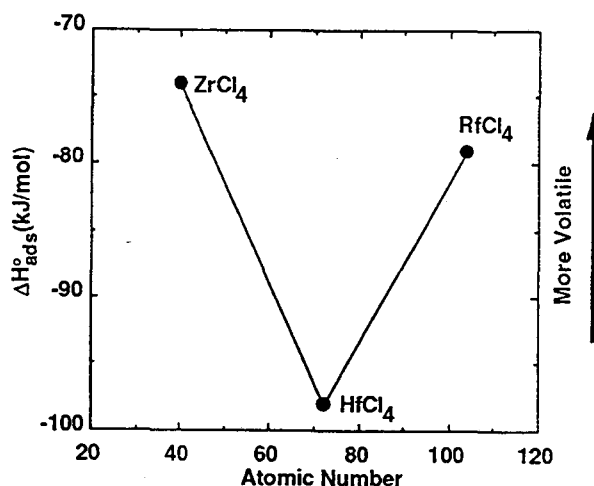


Fig. 1. A comparison of adsorption enthalpy values on SiO₂ for group 4 tetrachloride species.

References

1. B. Kadkhodayan et al., *Nucl. Instr. Meth.* **A317**, 254 (1992).
2. B. Kadkhodayan et al., this annual report.
3. B. Kadkhodayan PhD thesis, LBL (1993).
4. D.C. Hoffman et al., *Phys. Rev.* **C41**, 631 (1990).

On-Line Gas Phase Isothermal Chromatography of Hahnium (Element 105) Chlorides

B. Kadkhodayan, A. Türler*, H.W. Gäggeler*, B. Eichler*, D.T. Jost*, A. Kovacs*, D. Vermeulen*, K.E. Gregorich, S.A. Kreek, D.M. Lee, D.C. Hoffman, P. Baisden†, J.V. Kratz§, H.U. Becker§, M.K. Gober§, H.P. Zimmerman§, M. Schädel¶, W. Bröchle¶, E. Jäger¶, V. Pershina¶, B. Schausten¶, E. Schimpf¶

* Paul Scherrer Institute, CH - 5232 Villigen PSI, Switzerland

† Lawrence Livermore National Laboratory, CA 94550 (USA)

§ Institute für Kernchemie, Universität Mainz, D - 65 Mainz, Germany

¶ Gesellschaft für Schwerionenforschung mbH, D - 65 Darmstadt, Germany

We have used the Heavy Element Volatility Instrument¹ (HEVI) to investigate the volatility of Ha-chlorides. 34 s ²⁶²Ha and 27-s ²⁶³Ha were produced at the GSI UNILAC accelerator by bombarding a freshly prepared target of ²⁴⁹Bk with an intense beam of 99 MeV ¹⁸O. ²⁶²105 decays by 67% α -emission and 33% spontaneous fission (SF), whereas ²⁶³Ha decays by 43% α -emission and 57% SF.²

Reaction products, transported by a He/MoO₃ aerosol gas-jet system, were continuously collected on a quartz wool plug kept at 900°C inside the quartz chromatography column. The chlorides of element 105 were formed by adding 160 ml/min Cl₂ gas saturated with CCl₄. Volatile species were carried by the He flow to the cooler, isothermal section of the column where chromatography was performed. After the separation of the volatile halides, the molecules were attached on KCl aerosol particles in N₂, and transported through a capillary to the counting device (a modified magnetic tape station). The products were deposited on the surface of a conventional computer tape³. Every 20 seconds the tape was stepped to subsequently transport the activity in front of six 450 mm² PIPS (Passivated Ion implanted Planar Silicon) detectors.

The analysis of the experimental data is still in progress and only preliminary results will be reported here. A decay curve analysis of SF-activities observed in all gas chemistry runs at a beam energy of 99 MeV resulted in a half-life of 47^{+11}_{-8} s, assuming a minor contamination with

²⁵⁶Fm (²⁵⁶Md). This half-life is long compared to the literature value, but agrees well with the 44^{+19}_{-12} s half-life observed in earlier gas chemistry experiments.⁴ The analysis of α -spectra revealed 7 correlated α - α pairs, which resulted from the decay of 34-s ²⁶²Ha and its 3.93-s ²⁵⁸Lr daughter. Half-lives of 28^{+17}_{-8} s and $3.8^{+2.3}_{-1.0}$ s resulted for the mother and the daughter nuclides, respectively, in good agreement with the literature values. The observation of correlated mother-daughter pairs can be regarded as unambiguous proof that element 105 was observed after chemical separation. The chemical yield of Ha-chlorides at an isothermal temperature of 100°C was considerably lower than that measured at 250°C and higher temperatures. This indicates that the Ha chlorides are more volatile than their respective bromides,⁴ and probably similar in volatility to NbCl₅.⁵ In order to compare the volatility of Rf- and Ha-chlorides, additional experiments need to be performed at temperatures between 100°C and 250°C for a more accurate determination of the volatility of HaCl₅.

References

1. B. Kadkhodayan et al., *Nucl. Instr. Meth.* **A317**, 254 (1992).
2. J.V. Kratz et al., *Phys. Rev.* **C45**, 1064 (1992).
3. H.W. Gäggeler et al., *Nucl. Instr. Meth.* **A309**, 201 (1991).
4. H.W. Gäggeler et al., *Radiochim. Acta*, **57**, 93 (1992).
5. B. Kadkhodayan et al., this annual report.

Discovery of ^{252}Bk

S.A. Kreek, K.E. Gregorich, B. Kadkhodayan, M.P. Neu, C.D. Kacher, M.R. Lane, E.R. Sylwester, D.M. Lee, and D.C. Hoffman.

To discover ^{252}Bk , a growth experiment similar to that found in Ref. 1 was performed. This technique involves varying the irradiation time and separating Bk(IV) from all trivalent actinides using a bis-2-ethylhexyl-ortho-phosphoric acid (HDEHP) separation. The half-life of ^{252}Bk was determined from the growth of ^{252}Cf , the daughter of ^{252}Bk , as a function of the irradiation interval. The ^{252}Bk was produced at the 88-Inch Cyclotron in the reactions of 107-MeV ^{18}O with a ^{248}Cm target via the $^{248}\text{Cm}(^{18}\text{O}, ^{14}\text{N})^{252}\text{Bk}$ reaction and the collection times were 1, 3, 10, and 20 minutes. The samples were dissolved in 25 λ of HNO_3 and 25 λ of a saturated KBrO_3 solution to oxidize Bk(III) to Bk(IV) and the Bk(IV) was extracted into 50 λ of 0.5 M HDEHP solution in heptane. The HNO_3 contained ^{243}Am as a tracer to establish the level of contamination from trivalent actinides. The tracer was used in the HNO_3 to ensure that the daughters observed later were a result of the Bk decay and not contamination. The samples were stored according to the irradiation interval. After about 1 hour, the Bk daughters were back extracted with 3 M HCl . This reduced the activity level of ^{250}Cf (6.031 MeV alpha) and ^{248}Cf (6.26 MeV alpha) in the samples, which might mask the ^{252}Cf (6.118 MeV) alpha group. All of the samples with the same irradiation time were combined and electroplated on Pt with the method of Hoffman *et al.*² for alpha-pulse-height analysis.

A total of 8 samples was collected for each irradiation interval. The amount of ^{243}Am present in the samples indicated that the separation factor between the Bk(IV) and the trivalent actinides was better than 8×10^5 . The amount of ^{252}Cf and ^{250}Cf produced directly was expected to more than 10^2 times less than the observed activities. The number of ^{250}Bk and ^{252}Bk atoms calculated from the observed activities of ^{250}Cf and ^{252}Cf , respectively, in

the samples is plotted in Figure 1 as a function of the irradiation interval. A growth curve was fitted to each set of data by a least-squares analysis program. The ^{250}Cf activity (produced from the decay of the ^{250}Bk) was consistent with a ^{250}Bk half-life of 3.2 hours and a production cross section of 4 mb. This value is very close to the value of about 2 mb given by Lee *et al.*³ at a ^{18}O beam energy of 104 MeV. The ^{252}Cf activity was consistent with a ^{252}Bk half-life of 1.8 ± 0.5 minutes and a production cross section of $47 \pm 10 \mu\text{b}$.

Footnotes and References

1. B.Kadkhodayan *et al.*, *Radiochimica Acta* **56**, 1-5 (1992).
2. D.C. Hoffman in J. Kleinberg, Ed. Los Alamos National Laboratory Report LANL-1721, p.199, 1990.
3. D.M. Lee *et al.*, *Phys. Rev. C* **27**, 6 (1983).

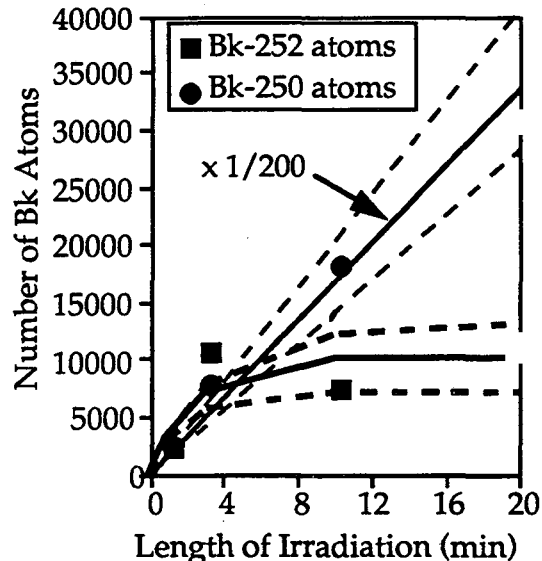


Fig. 1. Growth of ^{250}Cf and ^{252}Cf in separated Bk fractions. The number of atoms at each irradiation interval is indicated by the symbols. For each least-squares fit, the center curve is the fit to the data. The upper and lower dashed curves are the 1σ limits.

Review of Spontaneous Fission*

Darleane C. Hoffman, Todd M. Hamilton, and Michael R. Lane

A chapter on spontaneous fission has been prepared for publication in the CRC HANDBOOK OF NUCLEAR DECAY MODES. Comprehensive tables giving the recommended values of the half-lives and partial spontaneous fission (SF) half-lives or branches for all known spontaneously fissioning isotopes, half-lives and probabilities for known delayed fission emitters, properties of mass and total kinetic energy distributions for SF, and experimental values of average total neutron emission for SF and their variances are given

Plots of known SF half-lives for even-even nuclei, odd proton and odd neutron hindrance factors, schematic diagrams of mass-yield and TKE distributions, TKE systematics, average neutron emission vs. A of the fissioning nucleus, and contour plots of TKE vs. mass fraction are also included. Brief discussions of these topics as well as comparisons with various theoretical models are given.

References

*Condensed from LBL-33001, October, 1992, to be published in *Handbook of Nuclear Decay Modes*, D. N. Poenaru, editor, CRC Press, Inc., Boca Raton, Fl.

Electron-Capture Delayed Fission in ^{228}Np

S.A. Kreek, K.E. Gregorich, H.L. Hall^{*}, K.R. Czerwinski, T.M. Hamilton, R.A. Henderson[†],
B. Kadkhodayan, C.D. Kacher, M.R. Lane, J.D. Leyba[‡], M.P. Neu, E.R. Sylwester,
A. Türler[§], D.M. Lee, M.J. Nurmia and D.C. Hoffman.

We have continued our studies of electron-capture delayed fission (ECDF) of ^{228}Np which we first reported in 1990.¹ The ^{228}Np was produced at the 88-Inch Cyclotron in reactions of 50-MeV protons with twenty-three ^{233}U targets via the $^{233}\text{U}(p, 6n)^{228}\text{Np}$ reaction.

The half-life of ^{228}Np was determined to be 61.4 ± 1.4 seconds by measuring the ECDF rate with our rotating wheel system.² The fission properties were determined from measurement of the kinetic energies of coincident fission fragments. The mass-yield (MY) distribution is predominantly asymmetric. The most probable pre-neutron total kinetic energy (TKE) for the ECDF of ^{228}Np is 165 ± 5 MeV. The MY distribution and a contour plot of TKE vs. mass-fraction (MF) are shown in Figs 1 and 2, respectively. A decrease in TKE for symmetric mass splits (MF = 0.5) is seen in Fig. 2; this symmetric component constitutes about 2.5% of the total fissions. Symmetric mass division has been observed previously in isotopes with the same number of neutrons ($N = 136$) in the Ra region.³ However, this is the first observation of this effect for ECDF.

The production cross section of ^{228}Np is 35 ± 3 μb and the delayed fission probability is $(2.0 \pm 0.9) \times 10^{-4}$. The observed fission activity is attributed to the delayed fission of ^{228}Np based on an x-ray/fission correlation experiment. The mass number was assigned via observation of known progeny ^{216}Fr (related via alpha decay and ^{212}Po (related via electron-capture decay) in chemically separated Np samples.

Footnotes and References

^{*}Lawrence Livermore National Laboratory, Livermore, CA

[†]EG&G Rocky Flats, Inc., Golden, CO

[‡]Clemson Technical Center, Inc., Anderson, SC

[§]Paul Scherrer Institute, Würenlingen, Switzerland

1. H.L. Hall *et al.*, Lawrence Berkeley Laboratory Report No. LBL-30798 (1991).
2. D.C. Hoffman *et al.*, *Phys Rev. C* **22**, 1581 (1980).
3. E. Konecny *et al.*, *Nucl. Phys.* **A139**, 513 (1969).

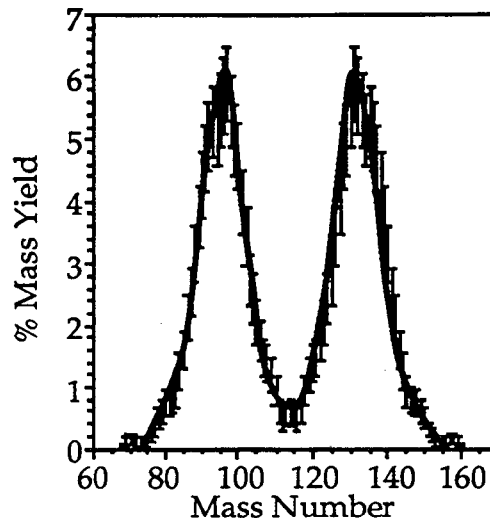


Fig. 1. Fragment MY distribution.

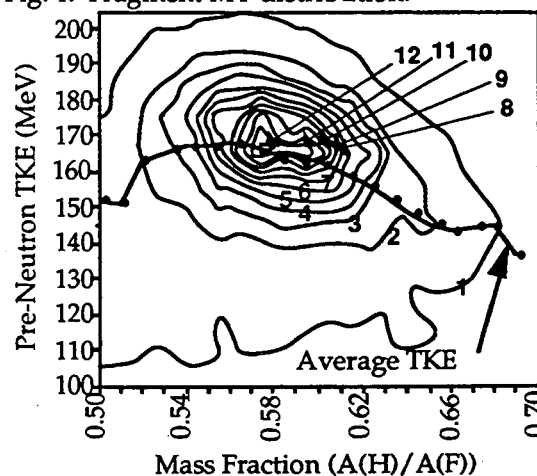


Fig. 2. TKE vs. MF contour plot for the ECDF of ^{228}Np . A(H) = mass number of heavy fragment; A(F) = mass number of fissioning nuclide. Data are grouped by 10 MeV and 0.01 units of mass fraction. Contours 1-12 indicate 10, 20, 30, 40, 50, 60, 70, 80, 90, 100, 110 and 120 events, respectively, based on a total of 2373 fissions.

Electron-Capture Delayed Fission in ^{238}Bk

S.A. Kreek, K.E. Gregorich, H.L. Hall*, K.R. Czerwinski, T.M. Hamilton, R.A. Henderson†, B. Kadkhodayan, C.D. Kacher, M.R. Lane, J.D. Leyba‡, M.P. Neu, E.R. Sylwester, A. Türler§, D.M. Lee, M.J. Nurmia and D.C. Hoffman.

We have continued our studies of electron-capture delayed fission (ECDF) of ^{238}Bk which we first reported in 1990.³ The ^{238}Bk was produced at the 88-Inch Cyclotron in reactions of 75-MeV ^4He with nine ^{241}Am targets via the $^{241}\text{Am}(^4\text{He}, 7n)^{238}\text{Bk}$ reaction.

The half-life of ^{238}Bk was determined to be 144 ± 6 seconds by measuring the ECDF rate with our rotating wheel system.⁴ The fission properties were determined from measurement of the kinetic energies of coincident fission fragments. The mass-yield (MY) distribution is predominantly asymmetric. The pre-neutron total kinetic energy (TKE) for the ECDF of ^{238}Bk is 174 ± 5 MeV. The (MY) distribution and a contour plot of TKE vs. mass fraction (MF) for ECDF of ^{238}Bk are shown in Figs. 1 and 2, respectively. The production cross section was 150 ± 10 nb with a delayed fission probability of $(4.8 \pm 2) \times 10^{-4}$. The observed fission activity was attributed to the delayed fission of ^{238}Bk via an x-ray/fission correlation experiment. The mass number was assigned via observation of the known ^{238}Cm in chemically separated Bk samples.

Footnotes and References

*Lawrence Livermore National Laboratory, Livermore, CA

†EG&G Rocky Flats, Inc., Golden, CO

‡Clemson Technical Center, Inc., Anderson, SC

§Paul Scherrer Institute, Würenlingen, Switzerland

1. B.S Meyer *et al.*, *Phys. Rev. C* **39**, 1876 (1989).
2. R.W. Hoff, *Inst. Phys. Conf. Ser. No. 88 / J. Phys. G: Nucl. Phys.* **27**, 475 (1986).
3. S.A. Kreek *et al.*, Lawrence Berkeley Laboratory Report No. LBL-30798 (1991).
4. D.C. Hoffman *et al.*, *Phys Rev. C* **22**, 1581 (1980).

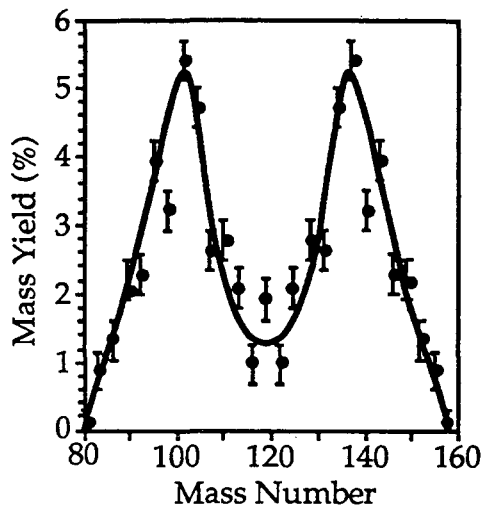


Fig. 1. Fragment MY distribution for ECDF of ^{238}Bk . Data were averaged over 5 mass numbers.

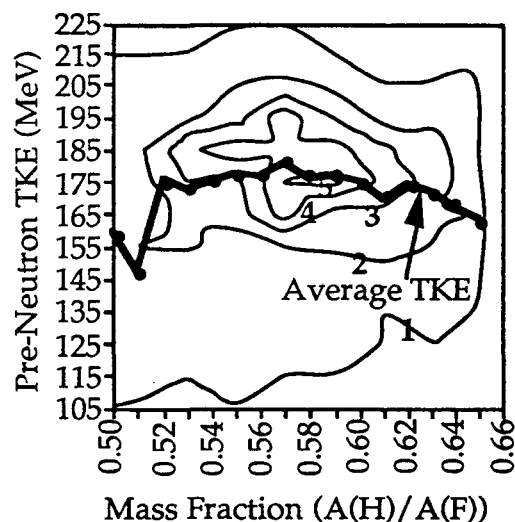


Fig. 2. TKE vs. MF contour plot for ECDF of ^{238}Bk . A(H) = mass number of heavy fragment; A(F) = mass number of fissioning nucleus. Data are grouped by 10 MeV and 0.02 units of mass fraction. Contours 1-5 indicate 5, 10, 15, 20, and 25 events, respectively, based on a total of 382 fissions.

Tests of a Macintosh-Driven CAMAC Data Acquisition System

M.F. Mohar and K.E. Gregorich

Testing has begun on a new data acquisition system to replace the antiquated PDP/11-based system presently used by the Heavy Element Nuclear and Radiochemistry Group at the 88-Inch Cyclotron. The new system is CAMAC based and read out by a Macintosh Quadra 700 interface. The Macintosh runs the commercially available software Kmax from SPARROW¹ to handle the data acquisition and storage as well as online and offline analysis. A SCSI port connection is made between the Mac and the Jorway 73A-1 CAMAC crate controller². An additional list processor, the Hytech 1340³, increases the data rate acceptance of the system by responding to the fast interrupts of incoming events and storing the data. This leaves the Kmax system free for on-line data processing with minimum deadtime due to the SCSI transfer.

Initial testing with only the Jorway 73A-1 crate controller and an Ortec AD811 analog-to-digital converter (ADC) in the CAMAC crate showed that the system could accept pulser data up to 150 single-word events per second. This rate reflects the data transfer limit of the SCSI interface due to the transfer protocol overhead. To go beyond this limit, the Hytech 1340 programmable list processor was installed. With this device programmed to read and store ADC events until 32,000-words of the 64k memory was filled, the system could run to approximately 10⁴ pulser events per second (the limit of the ADC conversion and readout time). There is still a deadtime associated with the block readout of the memory and transfer of data to the Macintosh for storage (about 250 milliseconds), and any online analysis on a block of data must be

completed before the arrival of a subsequent data block or further deadtime will result.

In the present experimental configurations run by the Heavy Element Nuclear and Radiochemistry Group, approximately 16 parameters (one word per parameter) of data are read for each event. Therefore, at the ADC-limited rate the memory will be filled in about 250 milliseconds with 2000 events. The subsequent readout and storage of the data without on-line analysis (250 milliseconds) will allow this cycle to occur twice per second. So the highest reasonable rate that can be accommodated is approximately 4000 events per second with roughly 60% deadtime. In reality, the experiments run with a maximum data rate of 100 events per second so that the deadtime should be less than 5%. Initial tests indicate that the 20 seconds between block reads, the time when data is accumulating in the list processor, is more than enough time for the Mac to perform the typical on-line analysis and to store the data onto the disk.

Future plans for more elaborate detection arrays (perhaps five- to ten-times the number of parameters) and more extensive on-line analyses have lead to discussions of writing the data in a zero-suppressed format to save disk space and reduce deadtime. An updated version of the list processor, the Hytech 1341, can be programmed such that it functions in a zero-suppressed mode with up to seven individual trigger conditions. However, it may be possible to modify the 1340 list processor to allow a less sophisticated suppression with only a single trigger. This will be investigated in the coming months with the assistance of the Hytech technical staff.

Footnotes and References

¹SPARROW, P.O.Box 6102, Mississippi State, MS 39762

²Jorway Corporation, 27 Bond St., Westbury, N.Y. 11590

³Hytech Electronics, LTD., 64 Amy St., Leicester, LE3 2FB England

Conditional Barriers for Neutron-Rich and Neutron-Poor Compound Nuclei $^{98,90}\text{Mo}$

A. Veeck, K. Hanold, N. Colonna^a, D. Delis, Q. Su^b, K. Tso, W. Skulski, G.J. Wozniak, and L.G. Moretto

Earlier work¹ by this group studied the mass-asymmetric, conditional-fission barriers for the nucleus ^{75}Br , and found that the Rotating Finite Range (RFR) Model predicts these barriers very accurately. To test the model for heavier systems, excitation functions have been measured for ^{98}Mo and ^{90}Mo , representing neutron-rich ($n/p=1.33$) and neutron-poor ($n/p=1.14$) nuclei of atomic number $Z=42$. Measurements at over six bombarding energies have been made to construct excitation functions that will be used in extracting the conditional barriers for each nucleus. These conditional barriers will be compared with RFR model calculations that predict a dependence on the neutron-to-proton (n/p) ratio. In addition, the conditional barriers can be used to improve the determination of the surface energy (a_s) and surface asymmetry (k_s) constants in the nuclear mass formula, and to improve sequential decay calculations of sequential multifragment emission.

To create the excited compound nuclei $^{98,90}\text{Mo}$, a carbon target was bombarded with beams of $^{86,78}\text{Kr}$ at several energies ranging from 6.4 MeV/u to 13.7 MeV/u. The 88-Inch Cyclotron with its new Advanced ECR (AEER) source provided steady beams of high charge states for these measurements. Eight telescopes, each consisting of a gas ΔE detector followed by a position-sensitive silicon detector, provided the energy, atomic number, and spatial location of each detected fragment. At each bombarding energy, the cross section for fragments from $Z = 4 - 32$ was measured over a large center-of-mass angular range. These cross sections were integrated to give experimental charge distributions like those shown in Fig. 1.

Simple predictions of the RFR model indicate that the emission barriers for ^{98}Mo are larger than those of ^{90}Mo . In addition, because ^{98}Mo has many more neutrons and they are more weakly bound than those in ^{90}Mo , neutron emission should be more favorable for ^{98}Mo . We see this clearly in Fig. 1 where the experimental cross

sections for complex fragment emission from ^{90}Mo are roughly a factor of five greater than those for ^{98}Mo . Calculations with the statistical code GEMINI, semi-quantitatively reproduce both the difference in the experimental cross sections for the two isotopes and the dependence on the Z -value of the emitted fragment.

Footnotes

^a INFN, Bari, Italy

^b Institute of Atomic Energy, Beijing, China

¹ D. Delis et al., Nucl. Phys. A534, 403 (1991)

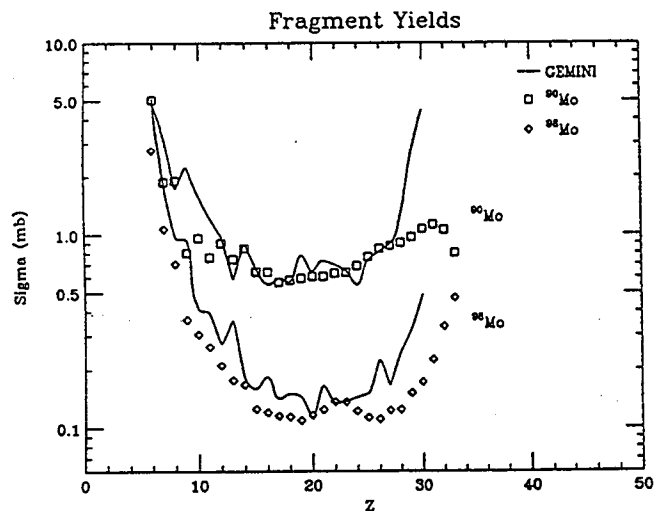


Fig. 1. This figure shows the charge distributions for the neutron-rich ^{98}Mo and the neutron-poor ^{90}Mo at excitation energies of 119 and 121 MeV, respectively. The points are the experimental data and the solid lines are calculations with the statistical code GEMINI, which incorporates finite-range model barriers.

Heavy residues from the reaction of $^{129}\text{Xe} + \text{Be, C, Al}$ at 26, 40, and 50 MeV/nucleon

K. Hanold, L.G. Moretto, G.J. Wozniak

D. Bazin, D.J. Morrissey*, N.A. Orr*, B.M. Sherrill*, J.A. Winger**

The yield of heavy residues from the very asymmetric systems 26, 40, 50 MeV/nucleon $^{129}\text{Xe} + \text{Be, C, Al}$ have been measured. These reactions have been studied extensively in the intermediate mass fragment region.^{1,2} The yields of the heavy residues will allow the further study of the relative amounts of complete and incomplete fusion. These residues were measured using the A1200 fragment separator as a 0 degree spectrometer. Relative yields for all isotopes with Z greater than 40 have been measured and the momentum distributions have been extracted.

Source velocity distributions from the similar reactions have been constructed using events with a multiplicity greater than 1.^{1,2} Preliminary comparison of the heavy residue velocity distributions with the source velocity distributions shows that the heavy residues will likely have a higher velocity and this might be taken to indicate that the heavy residues arise primarily from peripheral reactions.

The mass distributions have been found to be fairly broad and the lightest isotopes are near the limit of the known proton-rich nuclei. These distributions should allow a strict check of the predicted yields in Z and A from the statistical model. The modeling of these systems has been undertaken. These results and the rest of the experimental results will be described in a upcoming article.

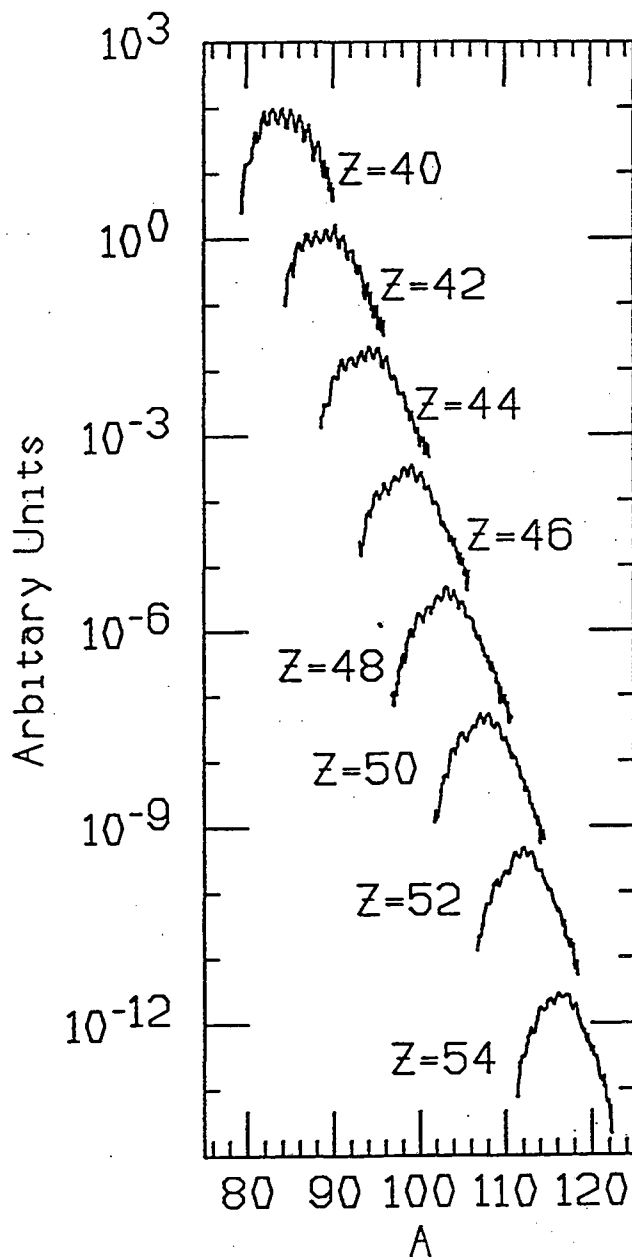


Fig. 1. Sample mass distributions from the Al target at 40 MeV/nucleon.

Footnotes and References

*NSCL, MSU, East Lansing, MI 48824

¹P. Roussel-chomaz et al., in press Nucl. Phys. A.

²D.R. Bowman et al., Nucl. Phys. A523, 386 (1991).

Complex Fragment Production and Multifragmentation in ^{139}La -induced Reactions at 35, 40, 45 and 55 MeV/u*

P. Roussel-Chomaz[†], N. Colonna⁺⁺, Y. Blumenfeld⁺⁺⁺, B. Libby[‡], G. F. Peaslee^{‡‡}, D. N. Delis, K. Hanold, M. A. McMahan, J. C. Meng^{‡‡‡}, Q. C. Sui^{‡‡‡}, G. J. Wozniak, L. G. Moretto, H. Madan[‡], A. A. Marchetti[‡], A. C. Mignerey[‡], G. Guarino⁺⁺, N. Santoruvo[§], I. Iori[§], and S. Bradley^{§§}

Complex-fragment emission is now a well established mode of decay for a compound nucleus. While it is quite rare at low excitation energy, due to the associated high barrier (typically 20 to 40 MeV), it becomes relatively abundant at high excitation energies and angular momenta.

Compound nuclei are formed in complete fusion reactions at low bombarding energies. As the bombarding energy increases, incomplete fusion sets in. Still, the product of the incomplete fusion can relax into a hot compound nucleus, which can be characterized in terms of its mass, excitation energy and, to a lesser extent, angular momentum, by detecting in coincidence the two fragments arising from its binary decay. For very mass-asymmetric entrance channels, the velocity distribution of the sources of binary complex fragment emission is very sharp, even at bombarding energies where incomplete fusion dominates.

For more symmetric entrance channels, the situation is more complex. In the reaction $^{139}\text{La} + ^{58}\text{Ni}$ at 18 MeV/u, the source velocity distribution determined from binary coincidences is very broad. In it one can distinguish a rather broad peak, corresponding to complete fusion, and a leading edge covering the velocity range corresponding to the entire range of mass transfers. This technique permits a direct selection of the excitation energy by setting a window on the source velocity. In the incomplete fusion picture, a given source velocity corresponds to a given mass transfer and that mass transfer corresponds to a given excitation energy, and, to a somewhat more uncertain degree, to a given angular momentum. Thus, at a fixed bombarding energy, we can "dial", as it were, the excitation energy of the fused product, and obtain an entire excitation function. This technique makes it possible to extend the study of the incomplete fu-

sion process along the two relevant "coordinates": the bombarding energy, and the entrance channel mass asymmetry.

With increasing bombarding energy, however, one encounters multifragment events that cannot be reduced to this "trivial" case. Thus, the question arises as to the origin of these multifragment events. Is it possible to characterize a source of multifragment events in terms of mass, charge, excitation energy, and angular momentum, similar to what was done for "binary" decays? In principle it is, and in fact the very same kinematics reconstruction used for "binary" events can be generalized to events with any number of fragments. If this kinematics reconstruction works, one would obtain, at any given bombarding energy, the relative excitation functions of binary, ternary, quaternary etc., events.

To achieve some of the goals illustrated above, we have investigated the sources of binary, ternary, quaternary etc., events in a series of ^{139}La -reactions. The roles of both the bombarding energy and the entrance-channel mass-asymmetry were investigated by means of the following reactions: 35, 40, 45, and 55 MeV/u $^{139}\text{La} + ^{12}\text{C}, ^{27}\text{Al}, ^{40}\text{Ca}, ^{51}\text{V}, \text{natCu}$ and ^{139}La .

Footnotes and References

*Condensed from Nucl. Phys A551, 508 (1993)

[†]SEPN, CEN, Saclay, France

⁺⁺INFN, Bari, Italy

⁺⁺⁺IPN, Orsay, France

[‡]University of Maryland, College Park, USA

^{‡‡}NSCL, Michigan State University, MI

^{‡‡‡}Institute of Atomic Energy, Beijing, China

[§]University of Milan, Milan, Italy

^{§§}Kaman Sciences, Alexandria, VA, USA

Dynamics and Statistics in Multifragmentation Production*

M. Colonna[†], P. Roussel-Chomaz^{††}, N. Colonna^{†††}, M. Di Toro[†], L. G. Moretto, and G.J. Wozniak

In contrast to lower energy reactions, intermediate-energy heavy-ion collisions are associated with abundant multifragment production. Several hypotheses have been put forward to explain such a process, some involving dynamical concepts, other statistical ones. Kinetic equations (Landau-Vlasov, Boltzmann-Uehling-Uhlenbeck or Boltzmann-Nordheim-Vlasov equations) have been widely used to simulate the evolution of heavy-ion collisions in the intermediate-energy range. So far, these transport theories have not been able to reproduce the yields of fragments in the mass range between the projectile and target. Conversely, statistical approaches, successfully used at low energy where complex fragments are assumed to be produced in the decay of compound nuclei formed in complete or incomplete fusion reactions, take minimal account of entrance-channel effects, and cannot reproduce the non-equilibrium features observed at intermediate energy.

The two approaches described above are complementary, and can be combined in a framework that incorporates both dynamical evolution and statistical decay. For the 55 MeV/u $^{139}\text{La} + ^{27}\text{Al}$ reaction, we have made a comparison between the experimental data and a "dynamical-statistical" approach by coupling the Boltzmann-Nordheim-Vlasov (BNV) and GEMINI codes.

Fig. 1 shows the angle-integrated cross section as a function of atomic number Z . The overall agreement between the data (open diamonds or vertical bars) and the simulation (solid line with filled diamonds) suggests that our approach correctly describes the mechanism of complex fragment production. The need for coupling the dynamical and statistical approaches is clearly illustrated by the comparison with the result of a purely dynamical simulation (dashed line), which fails completely to reproduce the experimental distribution. Small discrepancies are observed at intermediate Z values and above $Z = 35$. In addition, the other in-

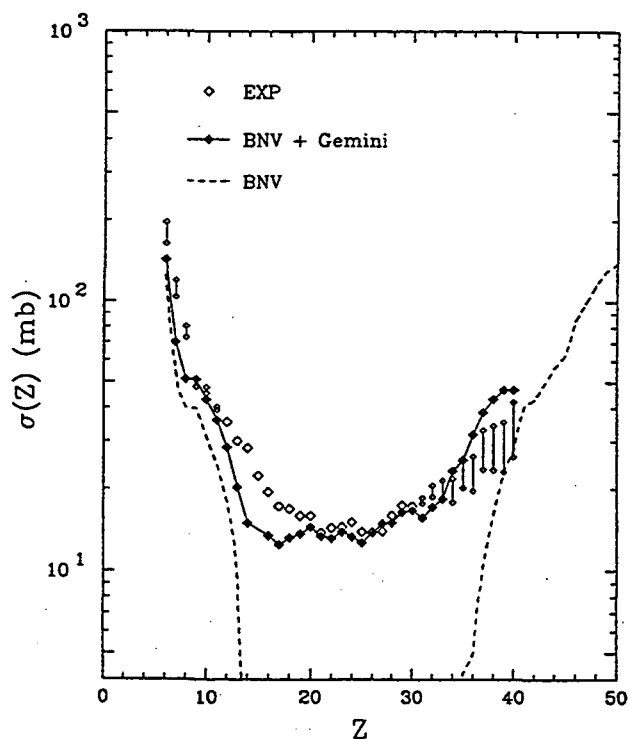
clusive observables of the reaction (angular distributions, emission velocities...) are reasonably well reproduced by the calculation, in both their equilibrium and non-equilibrium features.

Footnotes and References

*Condensed from Phys. Lett. B283, 180 (1992)

[†]INFN, LNS, Catania, Italy

^{††}SEPN, CEN Saclay, France



XBL 915-958A

Fig. 1. Comparison of the experimental (solid line) and calculated (dashed line) total charge (left-hand column) and source velocity (right-hand column) distributions for different fragment multiplicities for the 55 MeV/u $^{139}\text{La} + ^{27}\text{Al}$ reaction. The spectra have been normalized to the same maximum.

Evolution of the 60 MeV/u $^{129}\text{Xe} + ^{27}\text{Al}$, ^{89}Y & ^{197}Au Reactions with Impact Parameter

W. Skulski, N. Colonna, K. Tso, G. J. Wozniak, L. G. Moretto, D. R. Bowman, M. Chartier[†], C. K. Gelbke[†], W. C. Hsi[†], M. A. Lisa[†], W. G. Lynch[†], G. F. Peaslee[†], L. Phair[†], C. Schwarz[†], and M. B. Tsang[†]

Multifragment disintegration of highly excited nuclear systems is the subject of much interest, both experimentally and theoretically. In theoretical calculations, one can specify the range of impact parameters of the reaction or its "centrality". In experimental studies, one typically uses the light charged particle multiplicity as a measure of the centrality of the collision.

In the present experiment, we have utilized a combination of the 176-element MSU Miniball array with the forward angle (2° - 16°) LBL array. Together, the two detector arrays covered most of 4π , with the notable exception of the most forward angles below 2 degrees, where some of the projectile-like fragments (PLF) could escape. In addition, most of the slow-moving target-like fragments fell below Miniball detection thresholds.

To investigate the evolution of the reaction with impact parameter, we have plotted in Fig. 1 the detected total energy vs. total charged particle multiplicity. For the heavier targets, two branches are observed. In the upper branch, the total kinetic energy decreases with decreasing impact parameter as the forward going PLF has less energy due a smaller size (incomplete fusion) or an inelastic scattering. The lower branch, most likely corresponds to the case where the PLF is missed due to finite detection efficiency. This is most clear for the Al target where a bimodal distribution is observed. For the heavier targets, the two branches meet at high multiplicity, corresponding to the most central collisions, and the absence of PLF or TLF fragments. This distinct pattern of the evolution of the reaction with impact parameter should allow detailed comparisons with reaction models.

Footnotes and References

[†]NSCL, Michigan State University.

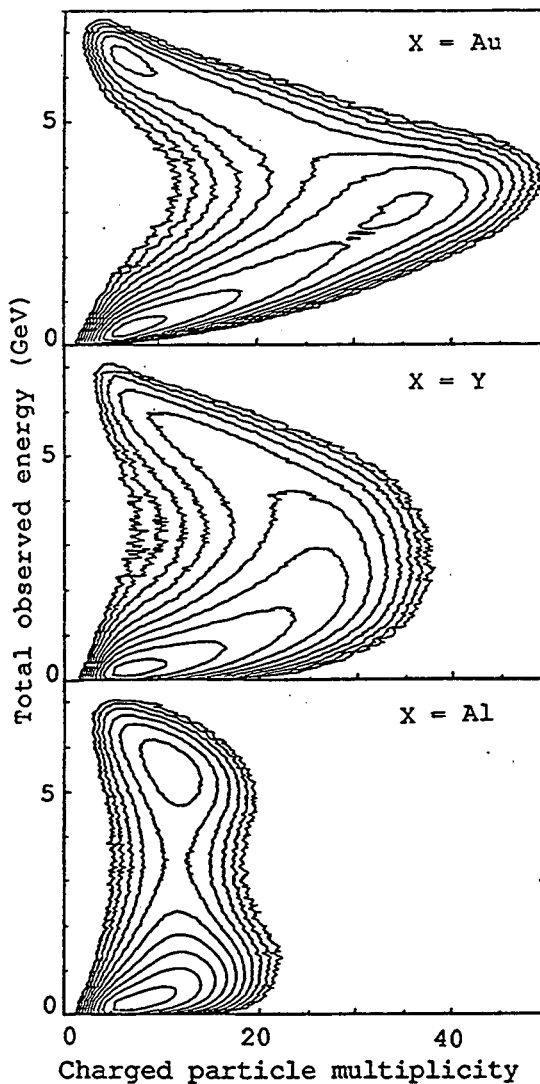


Fig. 1. For each event, the detected total energy is plotted vs. total charged particle multiplicity, for the 60 MeV/u $^{129}\text{Xe} + ^{27}\text{Al}$, ^{89}Y and ^{197}Au reactions.

Intermediate Mass Fragment Emission as a Probe of Nuclear Dynamics*

D. R. Bowman[†], C. Mader[†], G. F. Peaslee[†], W. Bauer[†], N. Carlin[†], R. T. de Souza^{††}, C. K. Gelbke[†], W. G. Gong[†], Y. D. Kim[†], M. A. Lisa[†], W. G. Lynch[†], L. Phair[†], M. B. Tsang[†], C. Williams[†], N. Colonna[‡], K. Hanold, M. A. McMahan, G. J. Wozniak, and L. G. Moretto,

Multifragment disintegration of highly excited nuclear systems has been recently studied using a new generation of electronic detectors. A number of theoretical investigations indicate that this process may become the dominant decay mode of nuclear systems at moderate temperatures ($T \sim 10$ MeV). These models predict fragment formation to occur as a result of volume instabilities at reduced nuclear density or surface instabilities of the Rayleigh-Taylor variety.

In the present experiment, we utilized a combination of the highly efficient 4π MSU MiniBall scintillation detector with the high resolution LBL Array consisting of 16 Si-Si-Plastic telescopes placed at forward laboratory angles between 2 and 16 degrees. Together, the two detection devices covered most of the solid angle, with the notable exception of the most forward angles below 2 degrees, where some of the PLFs could escape. Also, most of the slow-moving target-like fragments (TLF) fell below MiniBall detection thresholds.

Fig. 1 shows charge distributions gated on different values of the charge particle multiplicity N_c . For gates on small values of N_c , the charge distributions are very steep, and large yields of projectile-like fragments with $Z > 40$ are observed in the Si array at forward angles. With increasing charged particle multiplicity, the charge distributions become progressively less steep, and the heavy-fragment peak shifts to smaller Z values and becomes smaller in magnitude. Virtually no large fragments are observed for charged particle multiplicities $N_c \geq 25$, and the charge distributions become independent of the total charged particle multiplicity for $N_c > 20$.

To compare the decay properties of the six systems, we have fitted the charge distributions over the range of $3 \leq Z \leq 10$ with an exponential function $Y(Z) = Ae^{-\alpha Z}$. The extracted parameters α , are nearly independent of the target mass. However, α

decreases with increasing values of N_c and levels off for the largest values of N_c .

Footnotes and References

*Condensed from Phys. Rev. C46, 1834 (1992)

[†]NSCL, Michigan State University, MI

^{††}IUCF, Indiana University, Bloomington, IN

[‡]INFN, Bari, Italy

MSU-92-098

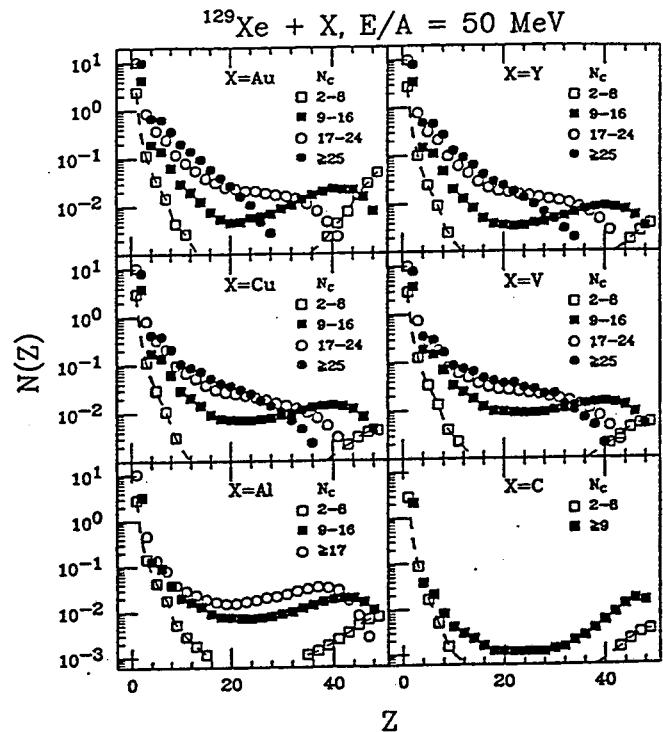


Fig. 1. Charge distributions measured for the $E/A = 50$ MeV $^{129}\text{Xe} + ^{197}\text{Au}$, ^{89}Y , ^{nat}Cu , ^{51}V , ^{27}Al and ^{12}C reactions for several gates N_c . The panels are labeled by target. The different symbols represent the indicated multiplicity gates. The solid and dashed lines guide the eye through the data points.

Excitation of Eigenmodes and Surface Instabilities in Disk Fragmentation

L. G. Moretto, Kin Tso, N. Colonna*, and G. J. Wozniak

Simulations using the Boltzmann-like kinetic equations show that under a variety of conditions, exotic nuclear structures like disks or bubbles are formed in central heavy-ion collisions, and proceed to break up into several fragments due to a new kind of Rayleigh-Taylor-like surface instability [1]. For example, disk fragmentation was observed in head-on collisions of two ^{90}Mo nuclei, as simulated by the Boltzmann-Nordheim-Vlasov (BNV) equation using different values of the nuclear incompressibility constant, K to cover the range currently believed appropriate for nuclear matter.

The nearly symmetric patterns of the fragments suggest the presence of stationary waves determined by the boundary conditions of the disk edge. It is possible that some of those higher order modes, which conserve symmetry of the equation, are excited by the very dynamics of the collisions. There is cylindrical symmetry in a head-on collision, so one should look for cylindrically symmetric eigenmodes, which, for a disk would be a combination of suitable cylindrical harmonics. Fig. 1 shows the radial profile of nuclear disks at $K = 540$ MeV, which appears to be strongly modulated by surface oscillations. The maxima of these oscillations eventually determine the position of the fragments, and they support the nodal patterns of cylindrical harmonics. Similar profiles are obtained for disks formed at lower values of K , but the upper value of 540 MeV essentially isolates surface effects from those associated with compression and expansion. Similar calculations have been performed for a range of bombarding energies and entrance-channel mass asymmetries with similar results.

Footnotes and References

* INFN, Bari, Italy

¹ L.G. Moretto *et al.*, Phys. Rev. Lett. 69, 1884 (1992)

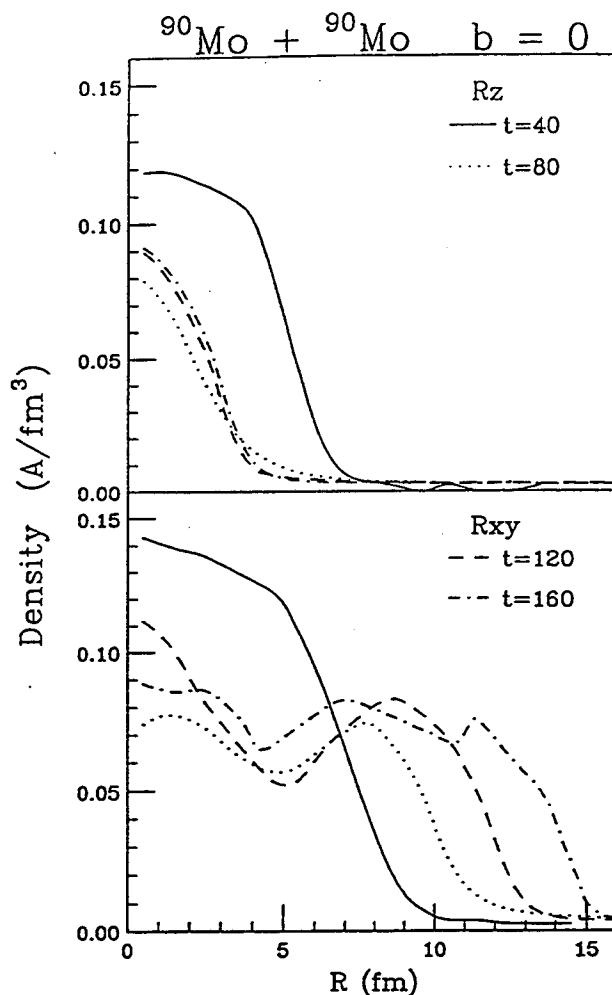


Fig. 1 shows the density profile of a nuclear disk along the beam axis (R_z) and the plane perpendicular to the beam axis (R_{xy}) at time steps of 40, 80, 120, and 160 fm/c. The disk is formed in a head-on collision ($b=0$) of 75 MeV/u $^{90}\text{Mo} + ^{90}\text{Mo}$ as simulated by the BNV equation with a stiff equation of state corresponding to $K = 540$ MeV.

Multifragmentation in 60 MeV/u $^{197}\text{Au} + \text{natCu}$ Reactions

D.N. Delis, N. Colonna, Q. Sui, K. Tso, K. Hanold, M. Justice, G.J. Wozniak, L.G. Moretto, B. Libby[†], A. C. Mignerey[†], A. Pantaleo^{††}, G. D'Erasmo^{††}, V. Patocchio^{††}, L. Fiore^{††}, E.M. Fiore^{††}, I. Iori^{†††}, and A. Moroni^{†††}

Nuclear fragmentation has been described in terms of percolation theory. In this approach, the nucleus is imagined to be composed of nucleons located in a crystal lattice. In a cold nucleus all sites are occupied. In an excited nucleus, one can introduce a probability for the occupation of lattice sites. Alternatively, one can consider a lattice whose bonds have a given probability p of being broken. Depending on the value of p , one observes connected clusters of nucleons that are identified with the observed fragments. For an infinite system, there is a critical value of p above which a cluster extending throughout the system (percolating cluster) exists. In a nucleus one can similarly define a critical value of p above which one major fragment is formed and below which many fragments are produced. The similarity of this result with the behaviors of systems exhibiting 2nd order phase transitions, like liquid-vapor systems at the critical temperature, has led to the use of percolation theory to model these transitions. The mass distribution of the clusters near the percolation threshold is given by a power law.

Campi has suggested¹ the study of the charge distribution in terms of their event-by-event moments. The k -th moment of the fragment size distribution $N(s, \epsilon)$ is given by: $M_k = \sum Z^k N(s, \epsilon)$. Near the critical point, the second and third moments (M_3, M_2) should fall on straight line in a doubly logarithmic plot, where the slope μ is expressed in terms of the critical exponent τ : $\mu = (\tau - 4)/(\tau - 3)$.

In Figure 1 we plot the logarithms of the third versus the second moments for multifragment events produced in the 60 MeV $^{197}\text{Au} + \text{natCu}$ reaction. In this plot only coincidence events (2-, 3-, 4-, 5-fold) are used. A strong correlation is observed between these two moments. The observed correlation allows one to extract a value for the slope of ~ 1.76 and a value for the critical

exponent of $\tau \sim 1.7$. This value is somewhat lower than the value predicted for a liquid gas phase transition of ~ 2.5 . A recent compilation² of values for τ obtained by fitting inclusive fragment distributions indicates that τ decreases with bombarding energy reaching a saturation value of 2 at $E_{\text{lab}} \sim 2$ GeV.

Footnotes and References

[†]University of Maryland, College Park, MD

^{††}INFN, Bari, Italy

^{†††}INFN, Milano, Italy

1 X. Campi, J. Phys. A 19 (1986) L917

2 W. Trautmann et al., GSI-92-44, Gesellschaft für Schwerionenforschung mbH (1992)

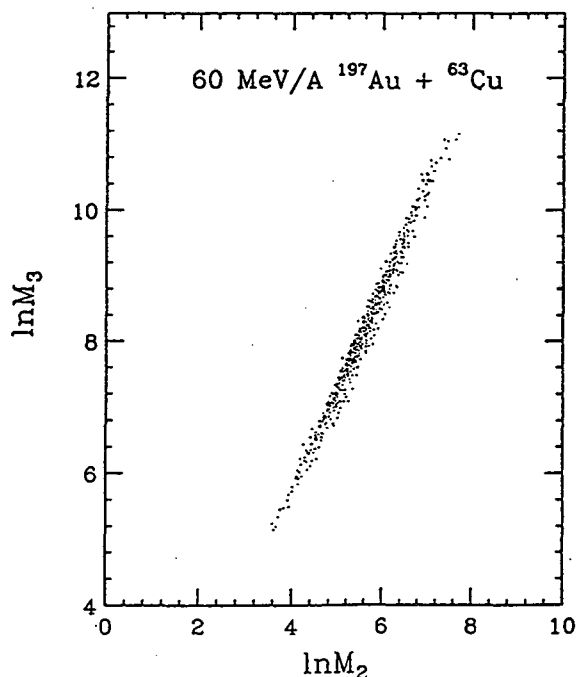


Fig. 1. The logarithms of the third moment M_3 versus the second moment M_2 of the charge distribution.

Calibration of the Response Function of CsI(Tl) Scintillators to Intermediate-Energy Heavy Ions*

N. Colonna⁺, G. J. Wozniak, A. Veeck, W. Skulski, G. W. Goth⁺⁺, L. Manduci⁺⁺⁺, P. M. Milazzo⁺⁺⁺, and P. F. Mastinu⁺⁺⁺

Intermediate-energy heavy-ion reactions, and multifragment emission processes in particular, are currently under intense investigation since they are expected to provide valuable information on the formation and decay of highly excited nuclear systems. The experimental characterization of these processes requires the simultaneous detection of many fragments, emitted over a large solid angle and with a broad range in mass and energy. A popular solution has been to construct an array of CsI(Tl) scintillators with photodiode readouts because of their compactness, reliability, high stopping power, and relatively low cost. Furthermore, CsI(Tl) crystals have the desirable properties of being only slightly hygroscopic, mechanically rugged, and easily machinable. However, because the light output from Cs(Tl) exhibits a strong dependence on the atomic number and energy of the detected ion, one needs to determine its response function to heavy ions at a variety of energies.

To study the response of Cs(Tl) scintillators to ions of different atomic number and energy, the detectors were directly exposed to low intensity beams (~100 particles/s) from the 88-Inch Cyclotron. Three "cocktail" beams with charge-to-mass ratios q/A of 1/2, 1/3 and 1/4 and energies of 25.5, 15.5 and 8.8 MeV/A, respectively, were accelerated and delivered on target. For each "cocktail" beam, several different ion species, over the range of $2 \leq Z \leq 36$, were simultaneously accelerated. To extend the measurement of the response to lower energies, and to fill in between the primary energies, the beams were degraded with aluminum foils.

Fig. 1 shows the measured light output, in arbitrary units, as a function of the energy for a set of representative ions, from ^4He to ^{84}Kr . The symbols represent the experimental data, while the

curves are the results of least square fits with the function:

$$L(E) = \gamma E + \beta [e^{-\alpha E} - 1].$$

For a large range of Z -values and over the whole energy range, satisfactory fits to the measured response functions are obtained with a linear-plus-exponential function. As can be seen from the figure, a linear function could also reproduce the highest energy data points.

Footnotes and References

*Condensed from Nucl. Instr. & Meth. Phys. Res. A321, 529 (1992)

⁺INFN, Bari, Italy

⁺⁺Skyline College, San Bruno, CA, USA

⁺⁺⁺INFN, Milan, Italy

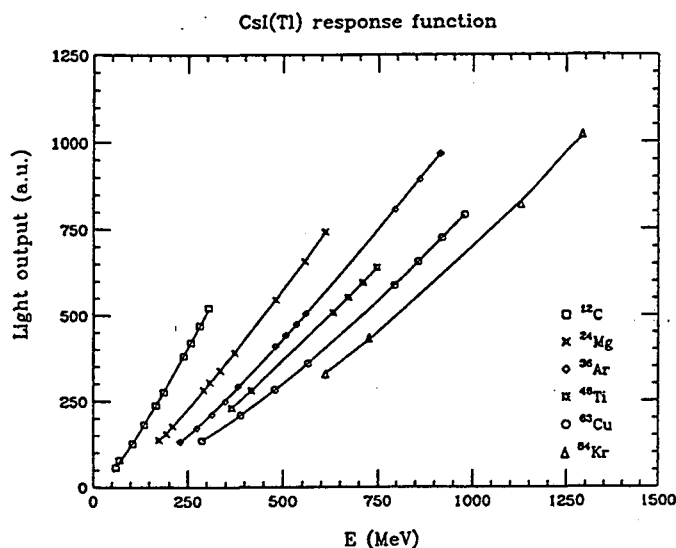


Fig. 1. Light output of the CsI(Tl) as a function of energy for some representative ions (filled diamonds). The solid lines are the results of fits (see text).

The Beta-delayed Proton Emission of ^{65}Se

J. C. Batchelder, D. M. Moltz, T. J. Ognibene, M. W. Rowe, and Joseph Cerny

The decays of many proton-rich light nuclei near the proton drip line have been identified by beta-delayed proton emission. All members of the $T_Z = -3/2$, $A = 4n+1$ series from ^9C to ^{61}Ge ¹ are strong delayed proton emitters, and most were discovered via their delayed-proton branches. The next member of this series, ^{65}Se , has been predicted by the Kelson-Garvey mass relation coupled with a formula for the Coulomb displacement energies, to be bound to ground state proton emission, while the IAS is unbound to proton emission by 3.61 ± 0.37 MeV (in the laboratory frame).

^{65}Se was produced via the $^{40}\text{Ca}(^{28}\text{Si},3n)$ reaction, utilizing a 175 MeV $^{28}\text{Si}^{6+}$ beam from the 88-Inch Cyclotron which was then degraded to two different on-target energies of 115 and 128 MeV. The recoil nuclei produced were transported by our He-jet system which has a transit time of about 30 ms. The activity was deposited on a moving tape (to remove long lived activity) directly in front of a Si ΔE -E telescope.

Observation of this decay proved to be difficult due to a continuing problem with oxygen contamination in the Ca targets used. The reaction of ^{28}Si on ^{16}O produces the well-known strong β -delayed proton emitter ^{41}Ti . ^{41}Ti has transitions at 3.69 MeV (15.5%), and at 3.75 MeV (31.0%), thereby creating a "background" peak precisely where it would interfere with the observation of ^{65}Se . To solve this problem, we used ^{nat}Ca targets that were produced as oxygen-free as possible.

The result of these bombardments are shown in figure 1. Figure 1a) shows the sum of the data taken at a target midpoint energy of 128 MeV. The spectra clearly shows a proton peak at 3.56 MeV with 21 counts, while the peak due to the 100% ^{41}Ti proton transition contains only 6 events. Figure 1b) shows the sum of the data taken at 115 MeV. There are considerably more "background" events due to ^{41}Ti . The broad peak at ≈ 3.7 MeV contains 125 counts compared to 119 counts in the main 100% ^{41}Ti peak at 4.74 MeV. The expected contribution from ^{41}Ti in the lower energy peak would be only 56 ± 7 counts. Fitting this peak as a double gaussian yields one centroid at 3.54 ± 0.06 MeV with 57 counts and a second centroid at 3.70 ± 0.06 MeV with 68 counts. The area and energy of the higher energy

gaussian are generally consistent with the 3.69-3.75 MeV ^{41}Ti doublet. Therefore the lower-energy gaussian may be preliminarily assigned to the β -delayed proton emission of ^{65}Se . A spectrum of ^{41}Ti (shown in black) is overlaid on top for comparison to show the extra events due to ^{65}Se . The weighted average of these two values is 3.55 ± 0.03 MeV. This mass is 60 keV lower than that predicted by the Kelson-Garvey mass relation. Although this is actually quite good agreement, it is also consistent with the observation that as one moves farther away from the valley of stability, the Kelson-Garvey mass formula under-predicts the stability of nuclei.

- 1.) M. A. C. Hotchkis, *et al.* Phys. Rev. C 35, 315 (1987)

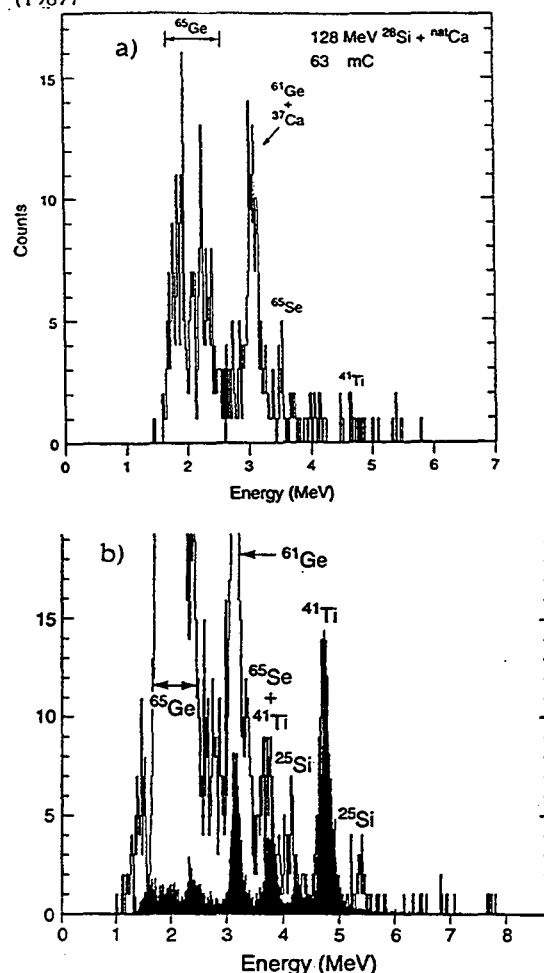


Fig. 1. Delayed proton spectra arising from 175 MeV $^{28}\text{Si} + ^{nat}\text{Ca}$ degraded to on-target energies of a) 128 MeV, and b) 115 MeV.

The Beta-delayed Proton Emission of ^{73}Sr

J. C. Batchelder, D. M. Moltz, T. J. Ognibene, M. W. Rowe, and Joseph Cerny

The $T_2 = -3/2$, $A = 4n+1$ series of nuclei is well known by their beta-delayed proton decay. All the members of this series from ^9C to ^{61}Ge have been observed to decay in this fashion. More recently the discovery of ^{65}Se has been reported¹. The next member of this series, ^{69}Kr , although predicted to be unbound to beta-delayed proton emission using the Kelson-Garvey mass relation coupled with a formula for the Coulomb displacement energies by 3.72 MeV (in the laboratory frame), Kr is a noble gas, and as such, cannot be transported via a He-jet system. The next member, ^{73}Sr , is predicted by the above formula to decay by beta-delayed proton decay from the Isobaric Analog State with an emitted proton energy of 3.80 MeV.

For this search, we have utilized our helium-jet system which has a transit time of around 25 ms. The activity was deposited on the edge of a slowly-moving wheel (to remove long lived activity), directly in front of a pair of Si ΔE -E telescopes at an angle of 120 degrees with respect to each other.

^{73}Sr was produced via the $^{40}\text{Ca}(^{36}\text{Ar},3n)$ reaction, utilizing a 245 MeV $^{36}\text{Ar}^{8+}$ beam from the 88-Inch Cyclotron which was then degraded to two different on-target energies of 115 and 128 MeV. There were two separate series of runs with different thicknesses for the ΔE 's.

The first set of runs utilized telescopes consisting of a $75\ \mu\text{m}$ ΔE and a $300\ \mu\text{m}$ E. The wheel speed was varied to get the optimum yield. Figure 1 shows the spectrum taken at a wheel speed of 27 seconds per revolution. This spectrum clearly shows a peak containing 17 counts at 3.77 ± 0.10 MeV, which we assign to the beta delayed proton decay of ^{73}Sr . The spectrum also contains 8 events due to the 100% ^{41}Ti transition arising from the $^{40}\text{Ca}(^{36}\text{Ar},\alpha 3n)$ reaction. ^{41}Ti also has transitions at 3.69 MeV (15.5%), and at 3.75 MeV (31.0%), so only 4 ± 2 events due to ^{41}Ti would be expected at 3.7 MeV.

The second set of runs utilizing telescopes consisting of a $27\ \mu\text{m}$ ΔE and a $300\ \mu\text{m}$ E, were taken with the same wheel speed. This gave a similar spectrum. At 3.73 ± 0.05 MeV there is a peak containing 13 events. Again the composite spectrum reveals ^{41}Ti , as well as lower energy

protons arising from ^{69}Se . The 100% ^{41}Ti peak contains 9 events, so 4 ± 2 events from ^{41}Ti would be expected in the 3.7 MeV region.

To prove that this peak cannot have arisen from a competing reaction channel such as $\alpha 3n$ or $\alpha 2n$, a 195 MeV ^{32}S beam (135 MeV at target midpoint) was bombarded on a ^{nat}Ca target. The resulting proton spectrum above 3 MeV contains only events due to ^{41}Ti .

Combining these two results gives a proton energy of 3.75 ± 0.05 MeV. We assign this peak to the beta-delayed proton emission of ^{73}Sr .

1.) J. C. Batchelder, et al. Submitted to Phys. Rev. C

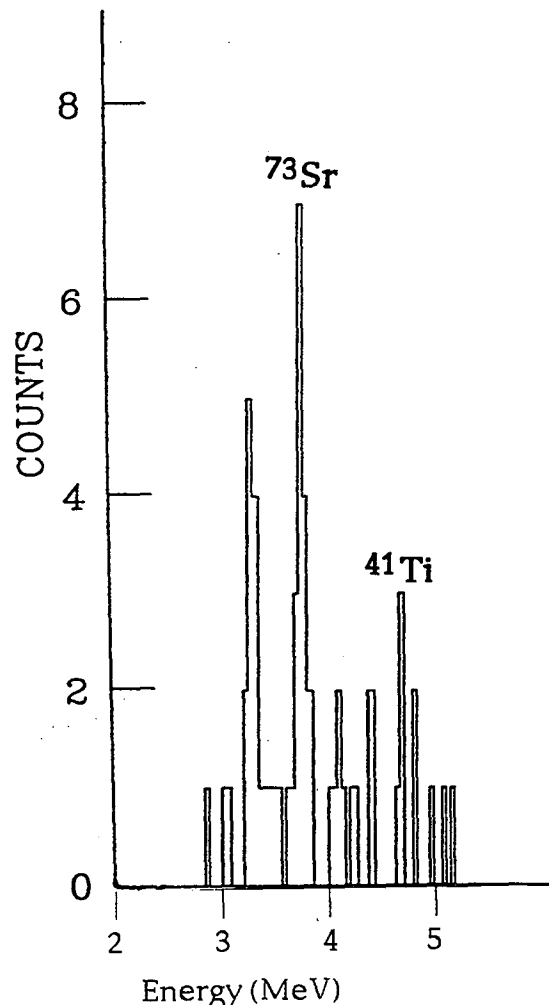


Fig. 1. Delayed proton spectra arising from 140 MeV $^{36}\text{Ar} + ^{nat}\text{Ca}$ target.

Development of a New Low-Energy Proton Detector Ball

D. M. Moltz, J. C. Batchelder, T. J. Ognibene, M. W. Rowe, R. J. Tighe, and Joseph Cerny

We have successfully developed a series of low-energy proton detectors over the last several years which have had the capability of detecting protons down to ~ 250 keV. The initial detector consisted of a single gas counter used as a ΔE and a silicon counter used as an E. Due to incomplete charge collection in the gas, the beta pulses are often large enough to place $\sim 1:10^4$ in the low-energy proton gate. For most experiments, this large contamination is unacceptable. Thus we pursued the design and construction of a two gas- ΔE - silicon E detector telescope. Since the high energy tail is a random event, it was thought that two gas counters would reduce the background to $1:10^8$ (measurements have shown that this is true to at least $1:10^6$) Five of these triple telescopes were built to fit on five faces of a cube. These detectors worked quite well for the duration of the beta-delayed two-proton decay measurement of ^{39}Ti ¹ (additional detector details may be found in ref. 1). Since these detectors incorporated two high voltage nickel foils as charge collectors, the effective proton threshold was ~ 300 keV. There exist three other lesser problems with these telescopes: 1) they are very difficult to assemble. 2) thermal cycling often broke the Ni foils. and 3) separate telescopes could not be placed closer than 90 degrees, thus making it difficult to attain a large geometrical counting efficiency. To solve all of these problems, we have constructed a low-energy proton ball out of a single piece of plastic with a common gas feed system.

This ball consists of six triples telescopes in a close-packed arrangement. Each telescope subtends $\sim 4\%$ of 4π solid angle for a total of $\sim 25\%$ of 4π for a thin collection foil at the center (such as might be used with the on-line mass separator RAMA beam). For a hard collection surface such as the small tape utilized with the helium-jet system, two telescopes are partially

eclipsed for a total solid angle of $\sim 19\%$ of 4π . By using a single high voltage grid (instead of two foils) and switching to DC-coupled preamps for the gas detectors, the low-energy threshold has been lowered to ~ 180 keV using CF_4 at 0.22 psia. Thermal cycling does not affect grid operation and assembly has also been made much simpler.

We have tested the ball extensively with delayed protons from ^{25}Si (0.37-5.40 MeV). We have also had two initial experiments where the detection of identified protons with $E < 300$ keV and identified alphas with $E < 2$ MeV was essential. (Improved particle energy resolution is also obtained with a single cooled silicon detector versus two room temperature silicon detectors (one of these is a very high capacitance ΔE detector). Clearly all of these improvements should permit a series of unique measurements heretofore inaccessible in any experiment. We intend to utilize this system with both the helium-jet and with RAMA.

Footnotes and References

- 1) D. M. Moltz, J. C. Batchelder, T. F. Lang, T. J. Ognibene, Joseph Cerny, P. E. Hausteine, and P. L. Reeder, *Z. Phys. A* 342, 273 (1992).

Present and Future Improvements to RAMA

T. J. Ognibene, D. M. Moltz, J. C. Batchelder, M. W. Rowe, R. Tighe and Joseph Cerny

Investigations of nuclei near the proton drip line must overcome two extreme difficulties: low production rates and short half-lives. One method that we use to separate the nuclide of interest from the other nuclei that are produced simultaneously in a nuclear reaction is to employ on-line mass separation. The RAMA¹ (Recoil Atom Mass Analyzer) system starts with a target chamber where radioactive recoils are thermalized onto a KCl aerosol in a helium-jet. The recoils are then transported, ionized, accelerated, mass separated and deposited in front of a detector setup at the Shielded Detector Station.²

We have recently completed improvements to our ion source/extraction region. We have realized an increase in the RAMA efficiency of 2 orders of magnitude and an increase in the FWTM mass resolution to 300. The previous $M/\Delta M$ was 200. In recent experiments, we measured an ~1% RAMA efficiency for gallium, zinc and copper.

In our current system, we use a 6m long capillary tube to transport the radioactivity from the target region to the entrance of RAMA. The relatively long transit time of ~180 ms precludes us from studying nuclei with

half-lives less than 150 ms.

To remedy this, we are presently involved in an upgrade to our RAMA system that is scheduled to be completed in the Spring of 1993 (Figure 1). The upgrade primarily involves moving the ion source region from the Cave 1 roof down to Cave 2 (our experimental area.) This will reduce the transit time to ~5 ms, essentially eliminating transit losses due to radioactive beta decay.

Included in the upgrade is a remote handling system, which will serve to minimize the radiation risk encountered when working on the ion source during an experiment. The helium-jet target chamber and the beam dump can be decoupled from the rest of the beam line and lowered with a scissors lift into a shielded sarcophagus.

We are redoing the RAMA computer monitoring and control system. The backbone of the new system is the Macintosh-based program LabVIEW[®].³ This is scheduled to be fully operational by the summer of 1993.

1. D. M. Moltz, *et al*, NIM **172**, 507 (1980).
2. F. B. Blönnigen, *et al*, NIM **B26**, 328 (1987).
3. National Instruments Corp. (Austin, TX)1990.

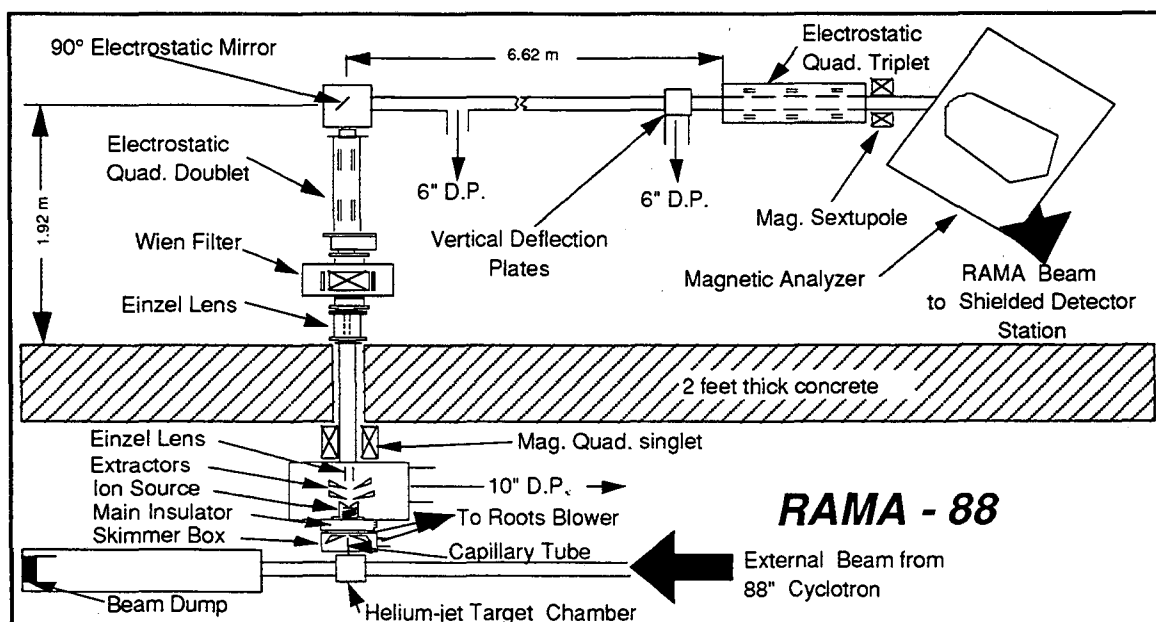


Fig. 1. Schematic view of the planned He-jet coupled on-line mass separator, RAMA

Search for a 17 keV Neutrino in the Electron-Capture Decay of $^{55}\text{Fe}^*$

F.E. Wietfeldt, Y.D. Chan, M.T.F. da Cruz, A. García, R.-M. Larimer, K.T. Lesko, E.B. Norman, R.G. Stokstad, and I. Žilim

In 1985, Simpson reported a distortion in the tritium β decay spectrum which he interpreted to be the result of emission of a 17 keV neutrino¹. In recent years several experiments have reported evidence of a 1% mixture of a 17 keV neutrino in β decay and electron capture internal bremsstrahlung (IB) spectra. A number of other experiments have not seen the effect. The signature of massive neutrino emission is a slope discontinuity, or kink, in the spectrum. Unfortunately, when a wide energy region of the spectrum is fit, smooth distortions caused by experimental systematics can mimic the effect of this kink.

A more effective test of the presence of a massive neutrino is to collect enough statistics to perform a local search for the kink, which should not be affected by smooth distortions. It is well known that the second derivative of a spectrum can reveal the presence of γ -ray lines too small to be seen easily in the raw data². We have found that the second derivative is also a powerful way to reveal the kink from a massive neutrino in a β or IB spectrum (see Fig. 1).

Using a chemically purified sample of ^{55}Fe and a coaxial Ge detector, we collected a high-statistics (1.13×10^7 counts/keV at 208 keV) internal-bremsstrahlung photon spectrum, and conducted a local search for departures from a smooth shape near the endpoint. We find no evidence for emission of a neutrino in the mass range 5–25 keV. In particular, a 1% 17 keV neutrino is excluded at the 7σ level.

Footnotes and References

*Condensed from LBL-33172 (submitted to Physical Review Letters).

¹J.J. Simpson, Phys. Rev. Lett. 54, 1891 (1985).

²M.A. Mariscotti, Nucl. Instr. and Meth. 50, 309 (1967).

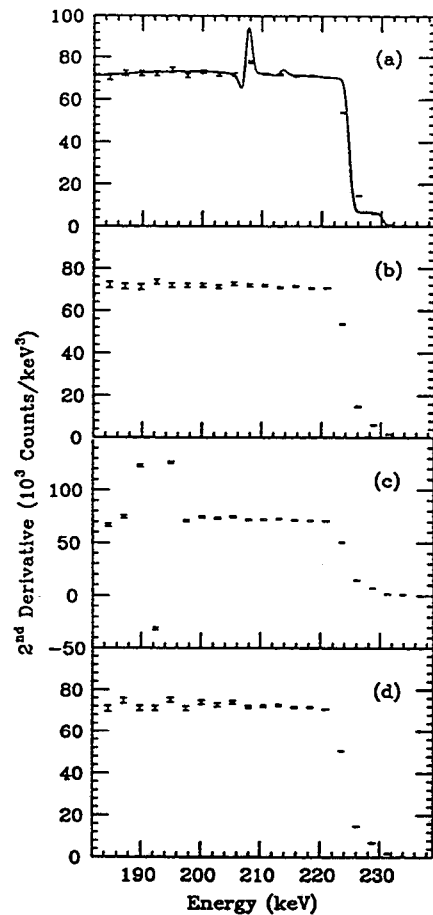


Fig. 1. Second derivatives of Monte Carlo spectra generated with (a) a 1% 17 keV neutrino and (b) no massive neutrino. The statistics are equivalent to those of the collected ^{55}Fe spectrum. Also shown in (a) is the second derivative of a Monte Carlo spectrum with infinite statistics (solid curve) generated with a 1% 17 keV neutrino. The structures at 208 and 214 keV are due to massive neutrino emission in the 1s and 2s-capture decays, respectively. Second derivatives of the ^{55}Fe spectrum (c) before background and impurity subtraction (revealing the ^{59}Fe line at 192 keV) and (d) after background and impurity subtraction.

Second-Forbidden Electron-Capture Decay of $^{55}\text{Fe}^*$

I. Žliment, E. Browne, Y. Chan, M.T.F. da Cruz, A. García, R.-M. Larimer, K.T. Lesko, E.B. Norman, R.G. Stokstad, and F.E. Wietfeldt

^{55}Fe undergoes a ground-state to ground-state electron-capture (EC) decay to ^{55}Mn with a $Q_{EC} = 231.7$ keV and $t_{1/2} = 2.73$ yr. The energetically allowed second-forbidden nonunique EC decay to the first excited state of ^{55}Mn (125.95 keV above the ground state) has not been observed so far, in part because of the continuous spectrum of the inner-bremsstrahlung (IB) (3.2×10^{-3} photons per 100 ^{55}Fe decays).

To carry out a detailed study of the IB spectrum of ^{55}Fe , in which we are looking for minute distortions from the theoretical spectrum, an ^{55}Fe sample was purchased from New England Nuclear Co. Because the sample contained impurities of ^{60}Co , ^{54}Mn and ^{59}Fe , we chemically purified it using ion-exchange techniques. ^{60}Co and ^{54}Mn were reduced to activity levels smaller than 1 nCi. The strength of the purified ^{55}Fe source was ~ 25 mCi. To subtract the contribution from ^{59}Fe , a separate source of ^{59}Fe was made.

We measured γ -ray spectra with a coaxial HPGe detector, placed inside an active shield of NaI scintillators which acted as veto for room background, coincident, and Compton scattered γ -rays. The iron source was placed in a 1-mm thick plastic container and an absorber made of Cu and Al foils was added between source and detector to reduce the Mn x-rays from EC decays. This assembly was then placed up against the Be window of the germanium detector. The data were taken during an eight month period and combined into nine successive runs. Room background and ^{59}Fe spectra were accumulated and recorded between the runs and normalized to the peaks in the ^{55}Fe data. Fig. 1 shows the spectrum of ^{55}Fe .

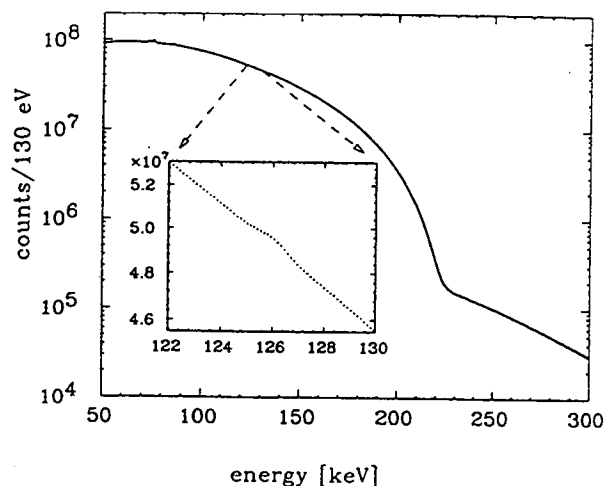


Fig. 1. Photon spectrum accumulated for eight months using the 25 mCi ^{55}Fe source after subtraction of room background and contributions from ^{59}Fe . The continuum above the IB endpoint is due to complete pileup events that are not removed by the pileup suppression. The inset shows an expanded view of the region around 126 keV.

In all nine sets of the data, we observed a peak at the energy ~ 126 keV. The intensity of the 126-keV line was normalized to the known intensity of the IB spectrum in the energy range from 121 to 131 keV ($1.66 \times 10^{-4}\%$). By following the decay of the 126 keV line, we find that its intensity does not change with respect to the intensity of the IB spectrum. *Ergo*, we attribute this γ -ray to the decay of ^{55}Fe .

Our deduced EC branching to the first excited state in ^{55}Mn is $(1.3 \pm 0.1) \times 10^{-7}\%$. The $\log ft$ value for this EC decay is 14.2, in agreement with systematics of allowed $\log ft$ values for second-forbidden nonunique transitions.

Condensed from Phys. Rev. C43 (1992) 1136

Electron-Capture Decay of ^{100}Tc and the 2ν - β -Decay of $^{100}\text{Mo}^*$

A. García, Y-D Chan, M.T.F. da Cruz,[†] M.M. Hindi,[‡] R.M. Larimer, K.T. Lesko, E.B. Norman, R.G. Stokstad, F.E. Wietfeldt, I. Žlimen,[§] D.M. Moltz, J. Batchelder, T.J. Ognibene

There is a long-standing discrepancy between calculated and measured double- β -decay rates. Abad *et al.*¹ have proposed that those decays are dominated by only the lowest excitation energy levels in the virtual intermediate nucleus. In particular, they suggested that $0^+ \rightarrow 0^+$ 2ν -decay rates can be calculated, in those cases where the intermediate nucleus has a 1^+ ground state, directly from the measured β^- and β^+/EC $\log ft$'s of the intermediate nucleus. The 2ν - β -decay of ^{100}Mo has been recently measured but in order to test the 'low-lying-state-dominance' hypothesis one needs to measure the EC $\log ft$ of ^{100}Tc (see Fig 1).

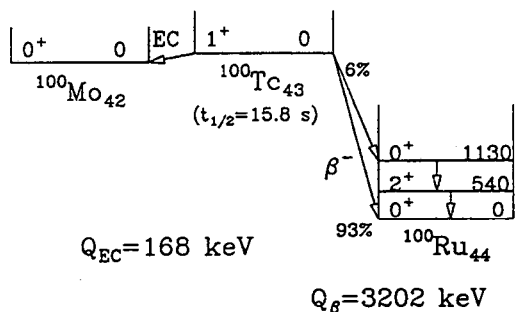


Fig. 1. Decay scheme of ^{100}Tc .

We have performed an experiment to measure the EC decay branch of ^{100}Tc by measuring the ratio of Mo $K\alpha$ x rays to 540-keV γ rays. The isotope was produced via the $^{100}\text{Mo}(p, n)$ reaction at the 88-Inch Cyclotron. A He-jet system was used to transport the radioactivity to a re-

Footnotes and References

*Condensed from LBL-33652 and submitted to Phys. Rev. C

[†]On leave from Instituto de Física, Universidade de São Paulo, SP, Brasil.

[‡]Phys. Dept., Tennessee Technological University.

[§]On leave from Rugjer Bošković Institute, Zagreb.

¹J. Abad *et al.*, An. Fis., 80, 9 (1984)

mote shielded counting station, where it was deposited onto a tape that was moved every 30 sec. by a computer tape drive unit and placed at the center of our counting station. At this position we had a 6 mm thick plastic detector surrounding the tape and a planar Ge detector to detect the x rays. A 33-cm diameter, 26-cm long annular NaI detector surrounded the Ge and plastic detectors. The mission of the NaI and plastic detectors was to reduce the profuse background created by bremsstrahlung from β 's and from x rays emitted by other Tc isotopes. Fig. 2 presents the low-energy portion of the Ge detector spectrum showing the Mo $K\alpha$ x ray.

Our result for the EC decay branch, $B(\text{EC}) = (1.8 \pm 0.9) \times 10^{-3}\%$, implies $\log ft = 4.40_{-0.30}^{+0.18}$.

The 2ν -decay-rate deduced using the 'low-lying-state-dominance' hypothesis is $t_{1/2} = (0.85 \pm 0.43) \times 10^{19}\text{y}$, which should be compared to the recently measured value² of $t_{1/2} = (1.16_{-0.08}^{+0.34}) \times 10^{19}\text{y}$.

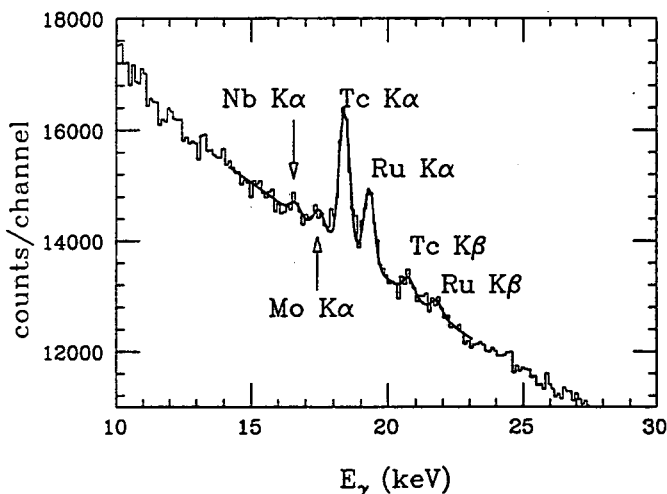


Fig. 2. Low-energy portion of Ge detector spectrum.

²S.R. Elliot *et al.*, J. Phys. G: 17, S145 (1991).

Thick-Target Yields of Iodine from Proton Interactions in Te, and the Double- β Decay of $^{128,130}\text{Te}$

M.T.F. da Cruz*, D.W. Bardayan†, Y. Chan, A. García, M.M. Hindi‡, R.-M. Larimer, K.T. Lesko, E.B. Norman, R.G. Stokstad, F.E. Wietfeldt and I. Žilimen‡

The geochemically inferred values for the double- β decay half-lives of $^{128,130}\text{Te}$ as obtained by Bernatowicz *et al.*¹ are based on the study of the isotopic abundances of the daughter-nuclei $^{128,130}\text{Xe}$, found in samples of tellurium ore from several locations. These abundances have to be corrected for contributions coming from several other origins: Xe trapping during the formation of the ore, fission, neutron capture, inverse- β decay, α - and cosmic-ray induced reactions.

The interactions of high-energy muons in rock would produce protons. Both muons and protons, reacting with the tellurium, would produce radioactive iodine isotopes, which β decay to xenon. After all other corrections applied to the xenon excesses, a small excess of ^{126}Xe , could only be explained by this mechanism. The motivation for this work was the fact that there are no experimental data one could use to infer the correction needed. A simple model, based on the hypotheses that (i) the protons produced are of very low energy, which restricts the possible reactions to (p, n) only, and (ii) all the cross sections are the same, suggests that the relative excesses of ^{126}Xe and ^{128}Xe are approximately 1 to 3.5.

We have measured the yields of proton-induced reactions on Te for several proton energies, to address the effect of cosmic rays in the ore. We measured the yields of iodine, and inferred those of Xe, for protons with energies of 15-, 30-, 45-, 50-, 1850-, and 5000-MeV. The rel-

Table 1: Relative $^{126,128,130}\text{Xe}$ yields inferred from the production of iodine in thick-targets of Te, $^{126}\text{Xe} \equiv 1$. (For the GeV-type protons the targets were not thick.)

E_p (MeV)	^{128}Xe	^{130}Xe
15	1.68(3)	1.86(4)
30	1.67(2)	0.32(1)
45	1.23(12)	0.19(2)
50	1.0(2)	0.16(3)
1850	1.4(5)	0.39(1)
5000	1.1(5)	0.28(1)

ative Xe yields obtained are displayed in Table 1, where it can be seen that the simple model described above does not seem to work.

We are now studying the effect of folding a muon energy spectrum with a nucleon-production cross section² in order to produce more realistic values for the relative excesses of ^{126}Xe and ^{128}Xe .

Footnotes and References

*On leave from Instituto de Física, Universidade de São Paulo, Caixa Postal 20516, 01498 São Paulo, SP, Brasil.

†Physics Department, Tennessee Technological University, Cookeville, TN 38505.

‡On leave from Rugjer Bošković Institute, Zagreb, Croatia.

¹T. Bernatowicz *et al.*, Phys. Rev. Lett. 69, 2341 (1992) and to appear in Phys. Rev. C

²H. Bilokon *et al.*, Nucl. Instrum. Methods Phys. Res. A303, 381 (1991).

β^+ Decay and Cosmic-Ray Half-Life of ^{54}Mn

M.T.F. da Cruz*, D.W. Bardayan†, Y. Chan, A. García, M.M. Hindi‡, R.-M. Larimer, K.T. Lesko, E.B. Norman, R.G. Stokstad, F.E. Wietfeldt and I. Žlimer‡

^{54}Mn is one of the radioactive species observed in cosmic rays. Its decay scheme is shown in Fig. 1, where it can be seen that the β^+ decay to ^{54}Cr ground state is energetically possible, and so is the β^- decay to ^{54}Fe ground state. However, these decays remain unobserved, with only an upper limit being set on the β^+ branch.¹

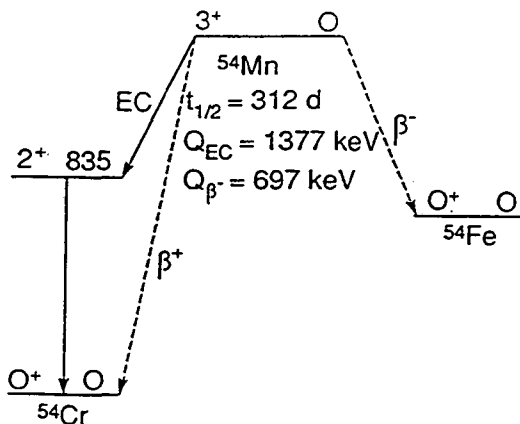


Fig. 1. Decay scheme of ^{54}Mn .

^{54}Mn decays in the laboratory with a half-life of 312 days, but as a high-energy cosmic ray, this nucleus would be stripped of its atomic electrons. This prevents its main decay mode to happen, leaving only the β^\pm decays. The knowledge of the branchings for both decays allows one to calculate the *cosmic-ray half-life* of ^{54}Mn . This half-life has been estimated to be on the order of 10^6 years and this would make ^{54}Mn a good “cosmic chronometer” for determining the confinement time of cosmic rays.

We have performed a search for the β^+ branch of ^{54}Mn decay, using the apparatus shown in

Footnotes and References

*On leave from Instituto de Física, Universidade de São Paulo, Caixa Postal 20516, 01498 São Paulo, SP, Brasil.

†Physics Department, Tennessee Technological University, Cookeville, TN 38505.

‡On leave from Rugjer Bošković Institute, Zagreb, Croatia.

¹B. Sur *et al.*, Phys. Rev. **C39**, 1511 (1989).

Fig. 2. Two HPGe detectors with $\sim 100\text{cm}^3$ were facing each other “sandwiching” a $5\ \mu\text{Ci}$ source. This was inside a NaI(Tl) annulus used as an active veto. The events of interest would be the detection of the two annihilation photons on the HPGe, with no signal coming from the annulus. The data were acquired in a MicroVAX, in multiparameter mode, with the master-gate being the firing of both HPGe detectors. All vetoing/gating conditions were set through software.

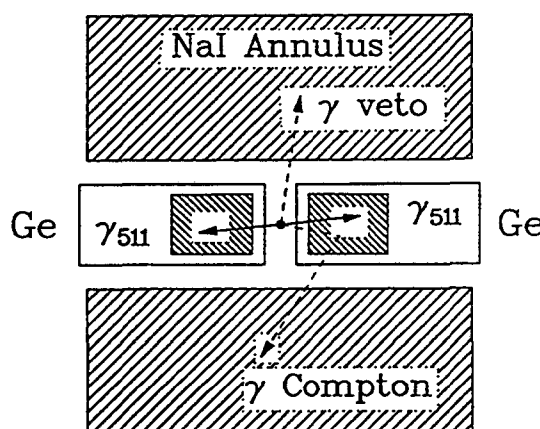


Fig. 2. Experimental setup.

The efficiency of the experimental setup for detecting events of the type considered was 1.0%, after correcting for the dead time and the accidental vetoing of good events. The presence of radioactive impurities in the source was investigated, especially for the β^+ emitters ^{22}Na and ^{65}Zn .

The measurement took ~ 870 hours, yielding an upper limit of 1.6×10^{-8} for the β^+ branch. We will now be searching for the β^- branch of ^{54}Mn .

β^+ Decays and Cosmic Ray Half-Lives of $^{143,144}\text{Pm}$

M. M. Hindi⁺, A. E. Champagne⁺⁺, M. T. F. da Cruz^{*}, E. B. Norman, K. T. Lesko, R. M. Larimer, and B. Sur^{**}

In the cosmic rays, $^{143,144}\text{Pm}$ are expected to be produced by fragmentation of heavy nuclei on interstellar hydrogen and helium.¹ Here, bereft of all atomic electrons, they cannot undergo their normal electron capture, but it is energetically possible for them to β^+ decay. Depending on how long these β^+ decay half lives are, the elemental abundance of Pm in the cosmic rays might be useful for determining the cosmic-ray confinement time. We have attempted to measure the crucial β^+ decay branches in the laboratory. $^{143,144}\text{Pm}$ were produced via the $^{141}\text{Pr}(\alpha, xn)$ reactions. The chemically purified Pm fraction was surrounded by an array of large Ge and NaI detectors. For ^{143}Pm , we looked for the two 511-keV annihilation photons in anticoincidence with any other radiation. For ^{144}Pm , we looked for the two annihilation photons in coincidence with the 696-keV nuclear gamma ray. No positive indication for either of these decay modes was observed. Our $1-\sigma$ limits are: for ^{143}Pm , $\text{BR}(\beta^+) < 5.7 \times 10^{-8}$, hence $t_{1/2} > 1.3 \times 10^7$ years; and for ^{144}Pm , $\text{BR}(\beta^+) < 8 \times 10^{-7}$, hence $t_{1/2} > 1.2 \times 10^6$ years. These results represent improvements by factors of 16 and 25, respectively, over the previously published² limits for these β^+ branches.

Footnotes and References

⁺ Physics Department, Tennessee Technological University, Cookeville, TN 38505

⁺⁺ Physics Department, University of North Carolina, Chapel Hill, NC 27599

^{*}On leave from Instituto de Fisica, Univ. de Sao Paulo, Sao Paulo, Brasil

^{**} AECL Research, Chalk River Laboratories, Chalk River, Ontario K0J 1J0, Canada

1. J. Drach and M. H. Salamon, *Astrophys. J.* **319**, 237 (1987).

2. D. Varga et al., *Nucl. Phys. A* **91**, 157 (1967).

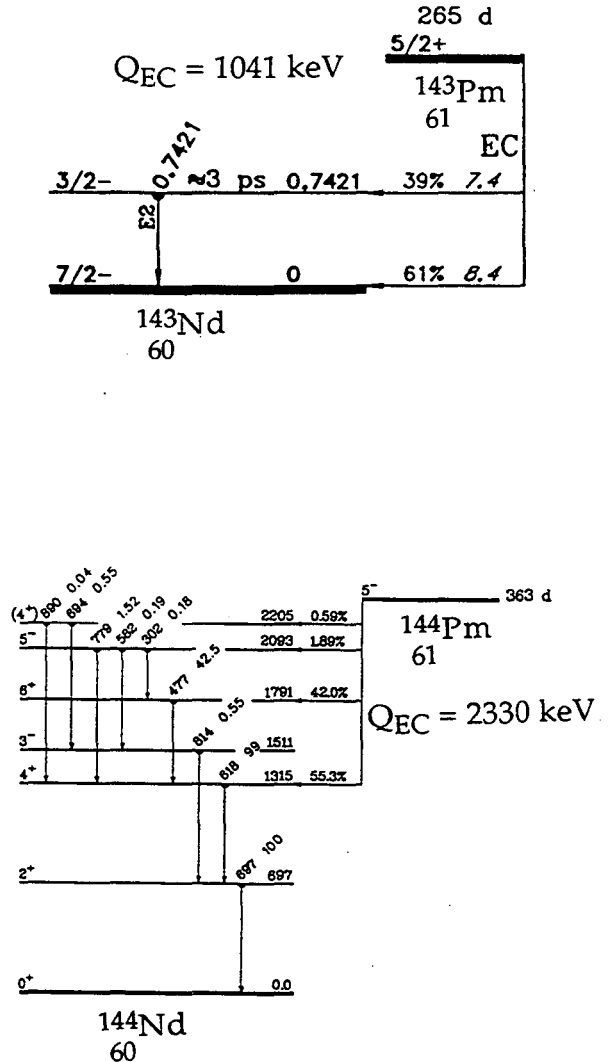


Fig. 1 Decay Schemes of $^{143,144}\text{Pm}$

Sudbury Neutrino Observatory, Photomultiplier Tube Support Structure

Kevin T. Lesko, David Beck[†], Yuen Dat Chan, Tiago de Cruz, Fred Dycus[†], Alejandro García, Yoichi Kajiyama[†], Gary Koehler[†], Alex Ozeroff[†], Eric Norman, Peter Purgalis[†], Alan Smith[†], Robert Stokstad, Igor Žlimen and the Sudbury Neutrino Observatory Collaboration

The Sudbury Neutrino Observatory (SNO) detector is a large heavy water Čerenkov detector designed to detect neutrinos in the 1000 ton D₂O target. The detector has sensitivity to the total neutrino flux, ν_x , regardless of family ($x = e, \mu, \tau$) and to the ν_e flux, separately, by measuring the elastic scattering, charged and neutral current signals. The detector is located in a mine two kilometers below ground near Sudbury, Ontario Canada. The mine is an active nickel mine operated by INCO, Ltd. The D₂O is contained in a thin-wall acrylic sphere, six meters radius, which is itself suspended in a 11 meter radius cavity filled with ~7000 tons of ultrapure light water.

The design of most of the detector components of was completed this year. Cavity excavation will be completed in April, 1993. Contracts for the acrylic vessel are in place as well as for a majority of the underground services and construction.

Lawrence Berkeley Laboratory is designing and supplying the Photomultiplier Tube Support Structure, which will position and secure the ~10000 PMTs used to detect the Čerenkov light generated by neutrino interactions in the D₂O. The experimental constraints on the design require an extremely low radioactivity contamination of detector components, submersion in ultrapure water for a period of at least ten years, restricted maintenance opportunities, and installation in an active nickel mine while simultaneously maintaining clean-room conditions.

The PMT Support Structure load bearing structure is based on a three-frequency icosahedron geodesic structure, 8.9 m radius. The structure is constructed of 270 stainless steel struts joined in 92 hubs. While weighing only 10000 kg it will support a maximum load of 66000 kg prior to filling the cavity with water. After filling the

cavity the structure will support a buoyant load of 14000 kg for the ten years of the experiment.

All components which make up the PMT Support Structure are specially selected to assure compatibility with the aggressive ultrapure water environment and to guarantee very low radioactive element contamination.

The contract for the fabrication of the geodesic sphere was released this year and construction has begun. The stainless steel used in the structure has been monitored for U and Th contamination and is well below project limits. The steel structure will undergo a complete test assembly prior to shipping it to Canada in mid-1993.

The design of the hexagon panels, which align and secure the PMTs and reflectors to the geodesic structure was completed this year. The interfaces with many of the other SNO provided components complicated the design of the panels and basic hexagon structures. The contracts for the 10000 hexagons will be let early in 1993 and will be quickly followed by the remaining components. Materials for these components will also be monitored for U and Th content. Initial sampling of both raw materials and sample finished products indicate that very low levels of radioactivity can be expected.

Footnotes and References

[†] Engineering Division, Lawrence Berkeley Laboratory

Neural Network for Recognizing Čerenkov Radiation Patterns

D.W. Dong, Y. Chan, M.T.F. da Cruz, A. Garcíá, K.T. Lesko, R.M. Larimer, E.B. Norman, R.G. Stokstad, F.E. Wietfeldt and I. Žilim

The Sudbury Neutrino Observatory (SNO) is an underground Čerenkov detector equipped with 10,000 phototubes and a 1,000 tons D₂O target to detect solar neutrinos coming from the sun. Even though the basic behavior of the Čerenkov radiation is well known (the radiated photons are confined to a conic surface), the multiple collision of the source particle with the detector media and the reflection/refraction of the photons during transport greatly complicate the final observed results. How to identify and reconstruct the initial vertices for low energy signals in the presence of background are challenging problems.

A three layer feed forward neural network^{1 2} has been developed to distinguish between true and false Čerenkov radiation signals for SNO. The network consists of an input layer, two hidden layers, and an output layer. The first layer connections are developed by principal component analysis (PCA), i.e., receptive field connections for each neuron are the leading components of the input correlation matrix. The receptive fields have been designed to incorporate the actual 3-dimensional SNO geometry and the duration of the acceptance time window. The connections of the second and third layers are learned by back error propagation (BEP) on the first layer output.

Fig. 1 shows the performance of the network in terms of distinguishing valid events from random noise. Each event consists of a number of fired phototubes with known spatial and temporal distributions. The network has been trained with Monte Carlo generated mono-energetic electron

events at 3, 4, 5, 6, 7 MeV. For each true event, a background noise uniformly distributed in space and time, is deliberately added. At 3 MeV, the signal to noise ratio was taken to be 1, and at 7 MeV, 2. A false event consists of fired phototubes randomly distributed in both space and time, with the same average number of hits as the true events at the same energy. The network generalizes very well to a larger data set in the trained energy range and to higher energies. The performance approaches 100% correct around 8 MeV and above. At energies below this, the task becomes more difficult since the signal to noise ratio becomes smaller, but the network still achieves a better than 90% accuracy.

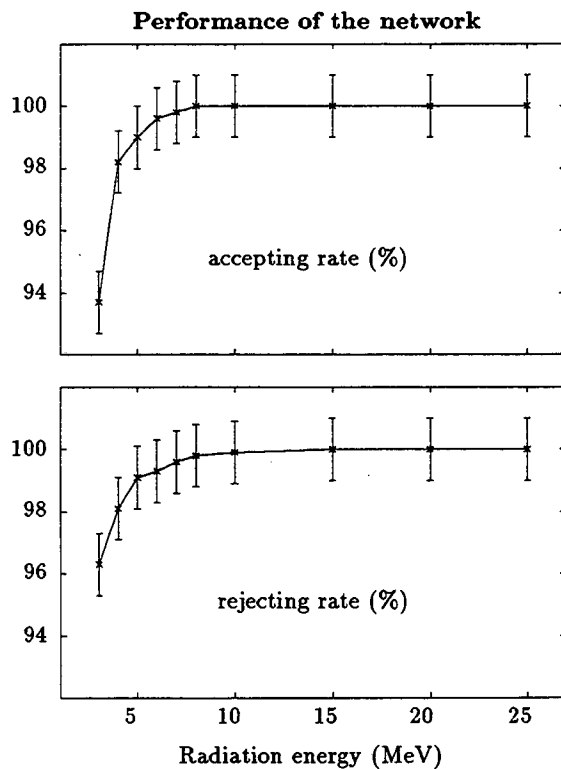


Fig. 1. The accepting rate (upper) for true events and the rejecting rate (lower) for false events at different radiation energies.

Footnotes and References

¹ Dong, D. W. and Chan, Y. D. 1993 Three layer network for identifying Čerenkov radiation patterns. *Submitted to WCNN'93*

² Dong, D. W. *et al* 1993 Neural network for recognizing Čerenkov radiation patterns. *LBL-33634*

Two-particle Correlation Functions in $^{14}\text{N}+^{27}\text{Al}$ Collisions at $E/A = 75\text{MeV}^*$

W.G. Gong, P. Danielewicz[†], C.K. Gelbke[†], S. Pratt[†]

Correlation functions of two light particles emitted with small relative momentum have been used to probe the space-time characteristics of heavy-ion reactions. We investigate whether the modified transport theory of reactions with a dynamic deuteron production[1] can account for both two-proton and two-deuteron correlations functions measured for $^{14}\text{N}+^{27}\text{Al}$ collisions at $E/A = 75\text{MeV}$.

Similar to a previous work[2], we have adopted a Skyrme potential corresponding to a stiff equation of state ($K = 380\text{MeV}$). Coulomb interactions were taken into account. Free nucleon-nucleon cross section was used for the in-medium nucleon-nucleon cross section. Koonin-Pratt formalism was used to calculate the two-particle correlation functions based upon the single particle phase space points predicted by the modified transport model.

Fig.1 shows two-proton (upper panel) and two-deuteron (lower panel) correlation functions for the collision $^{14}\text{N}+^{27}\text{Al}$ at $E/A = 75\text{MeV}$, respectively. The data (represented by symbols) were measured at the MSU K1200 cyclotron using a 50 element hodoscope. Both two-proton and two-deuteron correlations become stronger when the total momenta of two-particle pair get larger, which indicates that more energetic particles are emitted from sources of smaller space-time extent.

In the upper panel of Fig.1, the dashed curves were calculations from the Ref. [2], where nucleons were considered as emitted when the surrounding density fell below $\rho_e = \rho_0/8$. The solid curves are current calculations where particles were considered as emitted at the time of their last collision. The measured energy dependence of two-proton correlation functions can be reasonably reproduced by both calculations insensitive to the choice of particle emission criteria. In the lower panel, the solid and dashed curves are the calculated two-deuteron correlation functions corresponding to two gates on total momenta using the modified transport model. The agreement between measured and calculated correlation function for the low total-momentum gate P_1 is quite satisfactory. However, discrepancy in shape exists between data and calculation for the total-momentum gate P_2 which may be due to inaccurate description of two-deuteron relative wavefunction at small distance.

Footnotes and References

- * See Rapid Comm. of Phys. Rev. C, Feb. of 1993
- [†] NSCL, MSU, East Lansing, Michigan 48824
- ¹ P. Danielewicz and G.F. Bertsch, Nucl. Phys. A533,712(1991)
- ² W.G.Gong et al, Phys. Rev. Lett. 65,2114(1990)

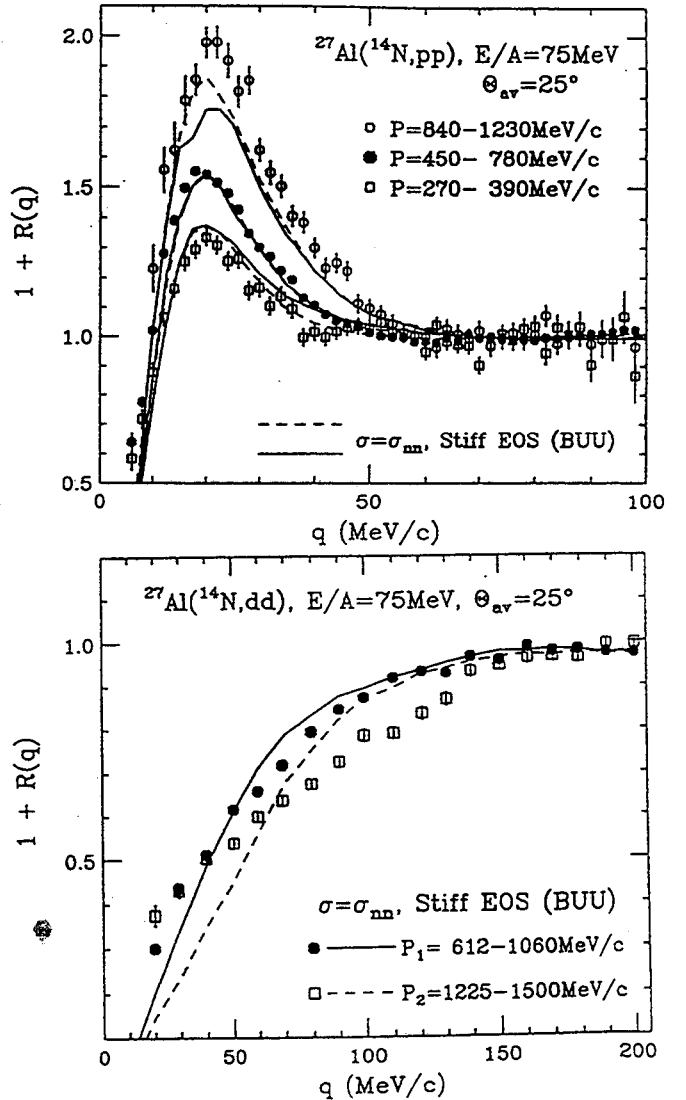


Fig.1. Two-particle correlation functions, for the collision $^{14}\text{N}+^{27}\text{Al}$ at $E/A = 75\text{MeV}$, shown for (a) two-proton (upper panel) (b) two-deuteron (lower panel). Symbol are data and curves are calculations explained in the text.

Performance of the LBL AECR Source at Various Frequencies*

Z.Q. Xie, C.M. Lyneis, S.A. Lundgren and D. Collins

Study the effects of frequency and radial magnetic field on an electron cyclotron resonance (ECR) ion source has been carried out on the LBL AECR source at 6.4, 10 and 14 GHz. Tests were done with a plasma chamber of 6.0 cm diameter and no radial pumping. The radial magnetic field is of 0.84 Tesla at the chamber surface which is very high for an ECR source running at 6.4 GHz. Pure oxygen was used as the working gas for a fair comparison.

The source was tested as a single stage, as well as with electron injection by an electron gun which takes the place of a conventional microwave-driven first stage.¹ Figure 1 shows that, higher frequency, with a higher axial magnetic field to ensure a closed ECR zone for electron heating, does give better performance. As demonstrated before and shown in Figure 2, at each frequency electron injection led to a factor of two increase in the high charge state oxygen beam intensity. The source performance of the source at 14 GHz is a factor of 3 to 5 compared to the source performance at the same frequency but with a plasma chamber of 7.0 cm diameter, radial field of 0.64 Tesla at the chamber surface and with radial pumping. Comparison of the performance at each frequency to other ECR sources running at lower radial magnetic fields shows that simply raising the radial field alone does not automatically improve the source performance.

Footnotes and References

*Condensed from contributions to the XIII International Conference on Cyclotron and their Applications, Vancouver, Canada, (1992).

1. Zuqi Xie, C.M. Lyneis, R.S. Lam, and S.A. Lundgren, Rev. Sci. Instrum. 62, 775 (1991).

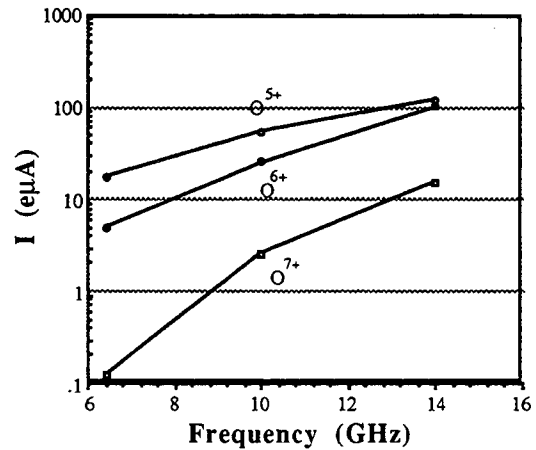


Fig. 1. High charge state oxygen ions produced by the AECR at a single stage mode at 6.4, 10 and 14 GHz.

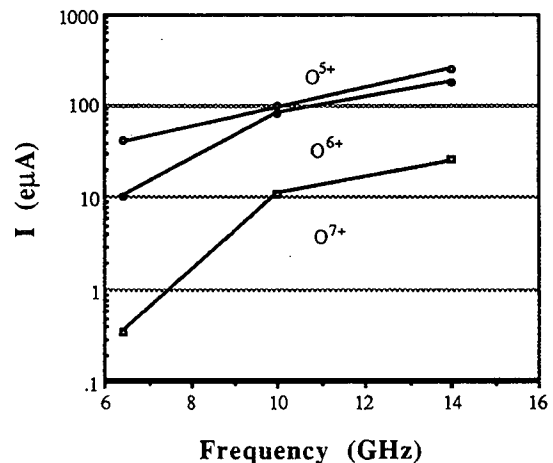


Fig. 2. High charge state oxygen ions produced by the AECR with electron injection at 6.4, 10 and 14 GHz.

Angular Distribution of ^{23}Mg Produced from 9.7 A MeV ^{24}Mg on Pt

K. Matsuta, S. Fukuda,† T. Izumikawa,† M. Tanigaki,† M. Fukuda,† T. Ohtsubo,†
Y. Nojiri,† T. Minamisono,† J.R. Alonso, G.F. Krebs, R. J. McDonald and T.J.M. Symons

Angular distributions of ^{23}Mg ($I^\pi=3/2^+$, $T_{1/2}=11.3$ s) produced in the $^{24}\text{Mg} + \text{Pt}$ collision have been observed at an energy of 9.7 A MeV as the first step towards quadrupole measurement of the nuclide.

A 2.5 μm thick Pt target was bombarded with a 9.7 A MeV ^{24}Mg primary beam extracted from the 88-inch Cyclotron to produce ^{23}Mg . The deflection angle of the reaction products was defined by a collimator and the energy of the product was selected by an energy degrader. The products were then implanted in a Pt foil. We tried isotope identification through $E-\Delta E$ measurements by Si detectors, but the method was not effective, especially for ^{23}Mg because of the serious admixture of the elastically scattered primary beam ^{24}Mg . On the other hand, the beta-ray time spectra were fairly effective for identification. Although there were also fast decaying and long lived components, the main component was ^{23}Mg , which decays with $T_{1/2} = 11.3$ s.

Angular distributions of the ^{23}Mg nuclei were measured through beta-ray observations as shown in the figure. Open circles are the data for the entire energy region, and closed circles are the data for just the quasi elastic region. As seen in the figure, the angular distribution has a clear peak at laboratory angle $\theta_L=25^\circ$. This result clearly shows the grazing character of the collision.

Since the grazing character of the collision assures the creation of polarization in the product nuclei, a considerable degree of polarization can be expected for the ^{23}Mg nuclei. Once we have polarization on this nuclide, nuclear moments of ^{23}Mg can be studied. Since

the magnetic moment of ^{23}Mg is known,¹ our goal is to measure the quadrupole moment of ^{23}Mg .

Footnotes and References

† Osaka Univ., Toyonaka, Osaka 560, Japan
1 M. Fukuda et al., To be published in the Proc. of the 9th Int. Conf. on Hyperfine Interactions, Aug. 17-21, 1992, Osaka, Japan ; submitted to the Phys. Lett.

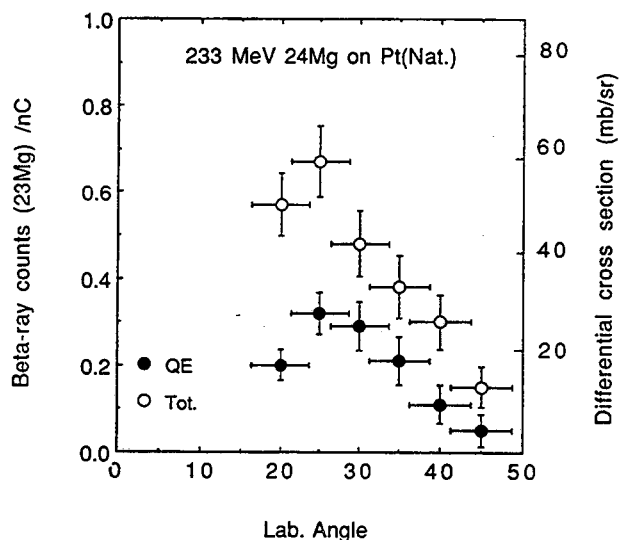


Fig. 1. Angular distributions of ^{23}Mg .

Cross sections are shown for both wide and narrow energy regions. Open circles are the data for all energies, and closed circles are for the quasi elastic region.

Controlling Surface Radioactivity at SNO

LBL-SNO Group

General information: The Sudbury Neutrino Observatory will have the lowest background radioactivity of any place on earth. Achieving a low background requires detector materials with low intrinsic radioactive content and correspondingly contamination-free surfaces. The main surface contamination will be the dust that permeates the nickel mine hosting SNO. The local mineral is norite, which contains about 5 ppm of Th. By contrast, the Th in the acrylic vessel holding the D₂O is about 1 ppt, or 5000 times smaller.

All detector components, construction equipment, and personnel must pass along a 2.5 km long tunnel leading from the mine shaft to SNO. The tunnel floor is covered with several inches of mine dust or mud. During the 18-month construction period, workers and car-sized containers will pass through this tunnel into the clean laboratory 10,000 times and 600 times, respectively. Yet, at the end of this period, at most 50 grams of dust may be present in the 2200 m³ sensitive region of the detector.

LBL has a major role in designing the program to control surface contamination. This involves systems and procedures to prevent dust from entering the laboratory, for purging the air of contamination, and for developing methods to measure particulate on surfaces.*

Recent progress: A concise summary of the work accomplished during this period is given by the list of SNO Scientific and Technical Reports (STR) on contamination control issued by our group. References 1-12 comprise this list.

There were major reviews of the contamination control program in March, 1992 and in November, 1992. The latter review included outside consultants.

In 1993 there will be increasing emphasis on implementing the procedures designed during

1992. The x-ray fluorescence spectrometer (for measuring small amounts of mine dust) will become operational and will be imported into Canada and installed in the mine.

References

1. **Establishing Clean Conditions in the Laboratory**, R.G. Stokstad, E.D. Hallman, and L. Moriarty, SNO-STR-92-47, July 14, 1992.
2. **Delivering Clean Components to the Cavity**, R.G. Stokstad, Ed. SNO-STR-91-066, January 17, 1992.
3. **Establishing a Cleanliness Program and Specifications for the Sudbury Neutrino Laboratory**, E.D. Hallman and R.G. Stokstad, SNO-STR-91-009, October 22, 1991.
4. **Final Cleanliness Measures: A Conceptual Plan**, R.G. Stokstad, SNO-STR-92-023, July 1, 1992.
5. **The Personnel Entry**, R.G. Stokstad, SNO-STR-92-51, July 14, 1992.
6. **Procedures for the Car Wash**, R. G. Stokstad, SNO-STR-92-52, July 14, 1992.
7. **Implementing the Cleanliness Program**, R.G. Stokstad, SNO-STR-92-079, September 28, 1992.
8. **Measurement of Surface Contamination**, R.G. Stokstad and E. Kong, SNO-STR-92-48, July 13, 1992.
9. **Contamination Control Study on Mine Dust**, R.G. Stokstad and E. Kong, SNO-STR-92-049, June 26, 1992.
10. **Thorium and Iron Content of Mine Dusts**, R.G. Stokstad, SNO-STR-92-078, October 15, 1992.
11. **Measurement of Mine Dust Deposited on Sanded Acrylic Surfaces under Bonding Conditions at the 4600' Laboratory**, Y. Hui, E. Kong, T. da Cruz, and R. Stokstad, SNO-STR-92-026, July 17, 1992
12. **Efficiencies of Removing Dust on Acrylic Plastic Surfaces by Non-agitated Deionized Water**, E. Kong, SNO-STR-92-83. October 23, 1992.

* See NSD annual report for 1991, LBL-31855, p. 81

Emission of ^{23}F and ^{24}Ne in Cluster Radioactivity of ^{231}Pa *

P. B. Price, R. Bonetti§, A. Guglielmetti§, C. Chiesa§, R. Matheoud§, C. Migliorino§, and K. J. Moody§

Using a track-recording phosphate glass detector with a standard deviation $\sigma_z = 0.23$ charge unit, we collected 2100 tracks of energetic clusters emitted from ^{231}Pa . Of these, 1348 survived cuts on energy, angle of incidence to the detectors, and c^2 . All but one of them are consistent with ^{24}Ne , and our measured branching ratio, $B(\text{Ne}/a) = (13.4 \pm 1.7) \times 10^{-12}$, for an alpha-decay half-life for ^{231}Pa of 3.28×10^4 yr. This value of B is a factor of 2.2 greater than was determined by Tretyakova *et al.*, who observed 252 Ne decays. We identify one event as ^{23}F , the nucleus predicted by cluster emission models to have the second highest branching ratio for emission from ^{231}Pa . This corresponds to a

branching ratio $B(\text{Ne}/\text{F}) = 1347+6440-940$, the 1 σ limits being governed by inverse Poisson statistics. Published models predict lower values of $B(\text{Ne}/\text{F})$, ranging from 3 to 400. Our event, if its 4 σ deviation from Ne is regarded as sufficient evidence for F, would be the first example of emission of an odd- Z cluster in spontaneous cluster radioactivity.

Footnotes and References

*Condensed from Phys. Rev. C **46**, 1939-1945 (1992).

§ Istituto di Fisica Generale Applicata, Universita degli Studi de Milano, Sezione di Milano, Italia

§ Nuclear Chemistry Division, University of California, Lawrence Livermore Laboratory, Livermore, CA

Search for Cluster Radioactivity of ^{237}Np *

K. J. Moody§, E. K. Hulet§, and P. B. Price

The few odd- A nuclides known to exhibit cluster radioactivity decay at rates hindered with respect to their even-even neighbors. For ^{237}Np , the most likely clusters are predicted to be ^{30}Mg and ^{32}Si . We have completed a rigorous search for cluster emission from ^{237}Np , with a null result. Our 90% confidence limit on the branching ratio with respect to alpha emission, $B(\text{cluster}/a) < 1.8 \times 10^{-14}$, is a factor 4.3 lower than the limit obtained by Tretyakova *et al.* The two experiments together place an upper limit of 1.5×10^{-14} on the branching ratio for emission of clusters with $10 \leq Z \leq 14$ from ^{237}Np .

Footnotes and References

*Condensed from Phys. Rev. C, **45**, 1392-1393 (1992).

§ Nuclear Chemistry Division, University of California, Lawrence Livermore Laboratory, Livermore, CA

BEVALAC EXPERIMENTS

Neutron Momentum Distribution from the Fragmentation of Neutron Rich Nuclei

T. Kobayashi,[†] I. Tanihata,[†] K. Yoshida,[†] T. Suzuki,[†] S. Shimoura,[‡] K. Sugimoto,[§] K. Matsuta,[§] S. Fukuda,[§] H. Wieman, W. Christie, and D.L. Olson

We have systematically studied the momentum distribution (MD) of projectile fragments and neutrons in coincidence for few-neutron-removal processes from ${}^6,8\text{He}$ and ${}^9,11\text{Li}$ projectiles on C and Pb targets. Measurements were performed at two incident energies: 800A MeV (LBL Bevalac) and 72A MeV (RIKEN Ring Cyclotron).

The MD of neutrons in coincidence with ${}^4,6\text{He}$ and ${}^9\text{Li}$ from ${}^6,8\text{He}$ and ${}^{11}\text{Li}$ at 800A MeV showed a two-Gaussian structure. The width of the narrow component is shown in Fig. 1. As seen in the figure, the width does not strongly depend on the separation energy of valence neutrons. A simple model based on sudden approximation with no correlation between valence neutrons does not explain this tendency, especially for higher separation energies such as the case of ${}^8\text{He}$ and ${}^9\text{Li}$. If one neutron is removed from the projectile, the intermediate state, such as ${}^5,7\text{He}$ or ${}^{10}\text{Li}$, is unstable against neutron emission. Therefore, the sequential decay mechanism via such an intermediate state is important. The solid line in Fig. 1 is an

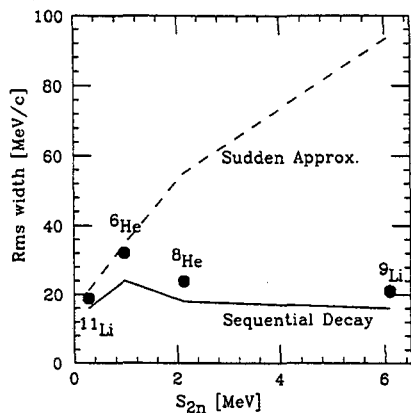


Fig. 1. The momentum width of neutrons for the two-neutron-removal process from ${}^6,8\text{He}$ and ${}^9,11\text{Li}$ projectiles on a C target as a function of the separation energy of valence neutrons.

estimate based on the sequential decay mechanism. It reproduces this general tendency. This is the first experimental indication that the sequential decay mechanism is important even for the two-neutron-removal process from neutron-rich nuclei.

The width of the neutron MD in coincidence with ${}^9\text{Li}$ from ${}^{11}\text{Li}$ is shown in Fig. 2 together with the GANIL data¹ for studying the dependence on incident-energy and target. The systematics showed two features: (1) target-independence, and (2) slight incident-energy dependence. The latter might result from probing the density distribution of ${}^{11}\text{Li}$ at a different radius due to a different nucleon-nucleon cross section; we need a more quantitative estimate.

Footnotes and References

[†]RIKEN, Saitama, Japan.

[‡]Univ. of Tokyo, Tokyo, Japan.

[§]Osaka Univ., Osaka, Japan.

1. R. Anne, et al., Phys. Lett. B 250 (1990) 19.

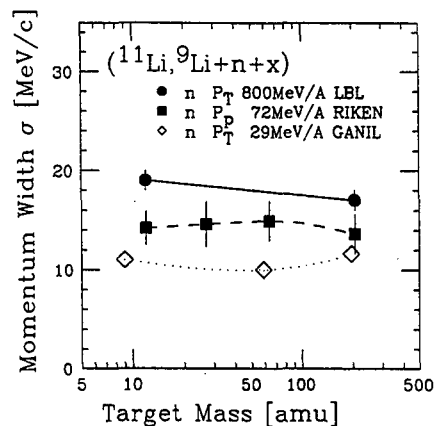


Fig. 2. The width of the neutron momentum distribution for the $({}^{11}\text{Li}, {}^9\text{Li})$ reaction on various targets at 29, 72, and 800 MeV/A.

Revelation of Thick Neutron Skins in Nuclei*

I. Tanihata,† D. Hirata,† T. Kobayashi,† S. Shimoura,‡ K. Sugimoto,§ and H. Toki**

Thick neutron skins (~ 0.9 fm) have been verified for the first time in ${}^6\text{He}$ and ${}^8\text{He}$ nuclei from a combined analysis of the interaction and fragmentation cross sections of ${}^{4,6,8}\text{He}$ incident reactions at 800A MeV.

Nuclear matter radii of ${}^{4,6,8}\text{He}$ determined by interaction cross section (σ_I) measurements showed that the radius increases drastically from $(1.57 \pm 0.05 \text{ fm})$ ${}^4\text{He}$ to $(2.48 \pm 0.03 \text{ fm})$ ${}^6\text{He}$.¹ Although they show quite a change in the matter radius it was not possible to determine whether the protons and the neutrons have different density distributions. Recently, Ogawa *et al.*² deduced an important relation between the interaction cross sections and the particle removal cross sections by applying the Glauber model to a loosely bound system. According to their result, if ${}^6\text{He}$ is described by a ${}^4\text{He}$ core and two neutrons, the interaction cross sections of ${}^6\text{He}$ and ${}^4\text{He}$ and the two-neutron removal cross section of ${}^6\text{He}$ with the same target are related as,

$$\sigma_{-2n}({}^6\text{He}) = \sigma_I({}^6\text{He}) - \sigma_I({}^4\text{He}), \quad (1)$$

where $\sigma_{-2n}({}^6\text{He})$ is the two-neutron removal cross section of a ${}^6\text{He}$ projectile. Here they used the fact that the ${}^5\text{He}$ nucleus has no particle stable state. This relation holds if the ${}^4\text{He}$ core in the ${}^6\text{He}$ nucleus is not modified and is essentially the same as the free ${}^4\text{He}$ nucleus. Although multiple scattering between a projectile and a target nucleon is included in the Glauber model, rescattering effects such as the one from a collision between the ${}^4\text{He}$ core and a knockout neutron from the ${}^6\text{He}$ are not included in the derivation. However this effect is considered to be small in the present case because of the extended peripheral nature of the reaction and the tight binding of ${}^4\text{He}$. This relation, in turn, provides a test how well a core persists in a nucleus from measurements of σ_I and σ_{-2n} .

Experimental values, at 800 A MeV with a C target satisfy Eq. (1) and thus indicate that the ${}^4\text{He}$ remains intact as the core in the ${}^6\text{He}$ nucleus. Similar formulation was made for a ${}^8\text{He}$ nucleus. It is found that ${}^8\text{He}$ is well described by a ${}^4\text{He}$ core and four neutrons orbiting outside the core. Assuming that ${}^4\text{He}$ forms a core in ${}^6\text{He}$ and ${}^8\text{He}$ nuclei, we have deduced the point-nucleon density distribution using the optical limit calculation of the Glauber model for the σ_I 's of ${}^4\text{He}$, ${}^6\text{He}$, and ${}^8\text{He}$ incident reactions. The resultant root-mean-square (rms) radii of the proton, the neutron, and the matter density distributions were determined. The rms radius of neutron, R_n^{rms} , is much larger than that of protons, R_p^{rms} , i.e. $R_n^{\text{rms}} - R_p^{\text{rms}} \approx 0.9$ fm for ${}^6\text{He}$ and ${}^8\text{He}$. Thus these nuclei have thick neutron skins.

A relativistic mean field (RMF) model is applied to ${}^6\text{He}$ and ${}^8\text{He}$ nuclei and shown to reproduce the neutron skin thicknesses very well. It is also shown that the RMF model predicts a gross linear dependence of the neutron skin thickness on the difference between the proton and the neutron Fermi energy in a wide range of nuclei. Possible observations of thick neutron skins in other nuclei, in particular in Na isotopes, are also discussed.

Footnotes and References

*Condensed from Phys. Lett. B **289** (1992) 261.

†RIKEN, Saitama, Japan.

‡Univ. of Tokyo, Tokyo, Japan.

§Osaka Univ., Osaka, Japan.

**Tokyo Metropolitan Univ., Tokyo, Japan

1. I.Tanihata, T. Kobayashi, O. Yamakawa, S. Shimoura, K. Ekuni, K. Sugimoto, N. Takahashi, T. Shimoda, and H. Sato; Physics Letters B **206** (1988) 592.
2. Y. Ogawa, K. Yabana, and Y. Suzuki, Niigata Univ. preprint NIIG-DP-91-3, submitted for publication in Nuclear Physics.

Proton-like Cross Section from 757 MeV/n La on La Collisions

*J. Bistirlich, R. Bossingham, H. Bossy, A. Chacon, T. Case,
K. Crowe, Y. Dardenne, J. Friedrich, W. McHarris, J. Rasmussen, M. Stoyer*

Discrepancies (factor of 2-3) have been reported between experimental results¹ and theoretical calculations^{2,3} for the invariant p-like cross section from 800 MeV/n La + La collisions. The theoretical calculations from six models were in general agreement with each other, but not with the experimental result at 20° polar lab angle. The invariant p-like cross section is defined as

$$\sigma_{inv} = \sum_{i=1}^n Z_i E_i \frac{d^3\sigma_i}{d^3k_i}, \quad (1)$$

where Z_i is the charge of the particle, while E_i and k_i are the energy and momentum per nucleon, respectively. The Lorentz invariant cross section $E_i d^3\sigma_i/d^3k_i$ is summed over the following proton containing fragments: H, ²H, ³H, ³He, and ⁴He. Since the model calculations were consistent, despite having varied assumptions, we set about verifying the experimental results on an independent spectrometer (Janus).

Figure 1 compares the resulting 60°, 40°, and 20° p-like cross sections with those previously measured. There is agreement at both 40° and 60°. However, there is a discrepancy (factor of 1.5) at 20°. The theoretical calculations⁴ were done at 800 MeV/n. Due to energy loss in materials in the beam line and the target, the energy of the beam was degraded to 757 MeV/n.⁵ The VUU calculation was then repeated⁶ for this lower beam energy; the comparison is shown in Fig. 2. There is agreement at 40°, at 60° there is disagreement in the low momentum range and

their still remains disagreement at the forward angles.

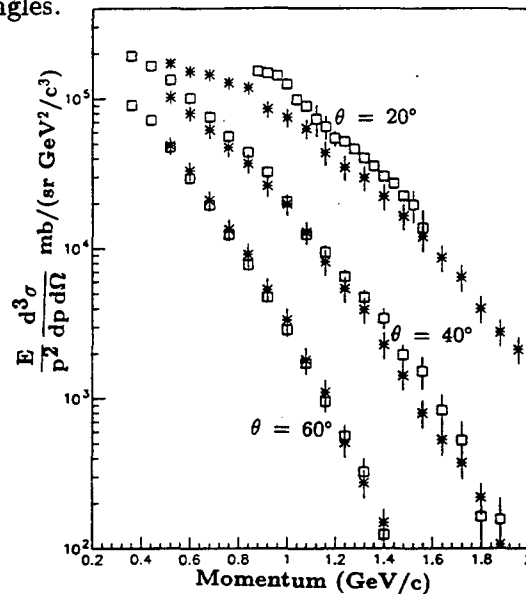


Fig. 1. Comparison of invariant cross sections of p-like particles from 757 MeV/n La + La collisions between present (\square) and previous ($*$) experimental results.

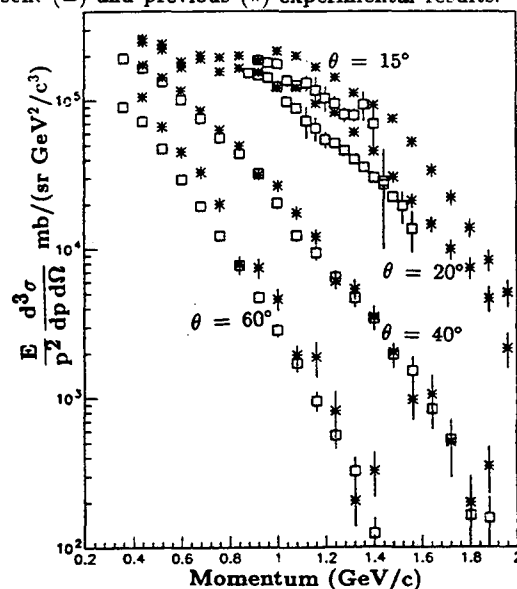


Fig. 2. Comparison of invariant cross sections of p-like particles from 757 MeV/n La + La collisions between present results (\square) and VUU calculations ($*$).

Footnotes and References

- ¹S. Hayashi *et al.*, Phys. Rev. C **38**, 1229(1988).
- ²J. Aichelin *et al.*, Phys. Rev. C **62**, 1461(1989).
- ³Y. Dardenne, Ph.D. thesis (unpublished) 1992.
- ⁴J. Aichelin *et al.*, Phys. Rev. C **62**, 1461(1989).
- ⁵J. Jiang, *et al.*, Phys. Rev. C **43**, 2353(1991).
- ⁶G. Batko, private discussions.

The EOS Experimental Program

Gulshan Rai and the EOS Collaboration

The EOS (Equation of State) experimental program was successfully completed at the Bevalac. Due to the inevitable closure of the Bevalac in February 93, priority was given to measurements at the highest extractable beam energies. The Bevalac delivered 1.2 GeV/A Au beam which is a record for the accelerator. The data obtained at this energy is presently unique and should yield very good physics.

The physics goals of the EOS program is to study the properties of nuclear matter under extreme conditions. Of particular importance is the Equation of State of nuclear matter away from equilibrium conditions. Since heavy ion collisions are accompanied by high temperature and density, these degrees of freedom offer the possibility of probing the unknown phase diagram of nuclear matter. The EOS experiment, by design, measured and identified most of the debris left over in a collision so that different aspects of the dynamics could be studied simultaneously. These studies range from nuclear flow, pion production and correlations, strangeness to multifragmentation and critical phenomena. The experiment used four major detectors. The EOS Time Projection Chamber (TPC), the Multiple Sampling Ionization Chamber (MUSIC II), the Time-of-Flight Wall, and the zero degree neutron spectrometer called MUFFINS. These detectors allowed nearly exclusive event-by-event characterization of the collisions.

A large amount of data was recorded on 8mm tapes using Exabyte tape drives. Just over 1000 tapes have been written containing almost 8 million interaction triggers. This represents approximately 3.5 terabytes of data. The best data acquisition rate was 80 events per beam spill. For central Au + Au collisions the data acquisition rate was on average 25 events per spill. An estimated 100 Gigabytes per day was recorded which exceeds, by far, most large particle physics experiments in operation now. The performance was realized by the pioneering development of the EOS TPC integrated circuit analogue and digital processing electronics mounted directly on the EOS TPC detector.

A summary of the data obtained in terms of the projectile, target and beam energy is

tabulated below. Complete analysis of the data is now underway.

Beam	Target	Energy GeV/A	Events
Au	Au	1.0	461 k
Au	C	1.0	541 k
Au	Al	1.2	11 k
Au	Au	1.2	361 k
Au	Be	1.2	35 k
Au	Ca	1.2	10 k
Au	C	1.2	12 k
Au	Cu	1.2	61 k
Au	La	1.2	39 k
Au	Nb	1.2	10 k
Au	U	1.2	11 k
Au	Au	0.25	181 k
Au	Al	0.4	11 k
Au	Au	0.4	47 k
Au	Au	0.6	252 k
Au	Au	0.8	246 k
Ca	Be	1.0	299 k
Ca	Ca	1.0	211 k
Ca	Ca	2.1	221 k
Ca	Au	0.8	13 k
Ca	Ca	0.8	22 k
Kr	Al	1.0	390 k
Kr	C	1.0	432 k
La	C	1.0	590 k
La	La	1.0	354 k
La	La	1.3	250 k
La	Be	0.4	38 k
La	La	0.4	30 k
La	La	0.8	266 k
Ni	Au	1.0	82 k
Ni	Cu	1.0	124 k
Ni	Cu	1.5	181 k
Ni	Au	1.9	147 k
Ni	Be	1.9	160
Ni	Cu	1.9	845 k
Ni	Cu	0.25	38 k
Ni	Au	0.4	115 k
Ni	Cu	0.4	270 k
Ni	Au	0.6	78 k
Ni	Cu	0.6	192 k
Ni	Cu	0.8	163 k

Footnotes and References

† NSD Annual Report (1989-90), LBL-30798

dE/dx Response and Particle Identification in the EOS Time Projection Chamber

A. Scott, S. Wang, D. Keane, and the EOS collaboration

Because the EOS TPC operates in an environment of very high track density, it differs from previous TPCs in having a pad plane with 100% area coverage, and does not have any readout for the anode wires. The pad plane measures $1.5 \text{ m} \times 0.96 \text{ m}$, with 128×120 pads. Fig. 1 is a scatter plot of truncated mean dE/dx versus momentum/charge for tracks with 40 or more useable dE/dx samples, produced in 250A MeV Au+Au collisions. About half of all found tracks in these events satisfy this condition. We find that the dE/dx response near minimum ionization does not accurately follow the Bethe-Bloch formula, but this effect fades above about five times minimum; it appears to be connected with the transition between tracks where the above-threshold signal is often collected on only one pad in a given row, and more strongly ionizing tracks where the signal is distributed over several pads in each row. The curves in Fig. 1 correspond to the Bethe-Bloch formula for the labeled fragment species, corrected for the above-mentioned effect. The dynamic range of the electronics is such that dE/dx saturates at about 90 times minimum ionization; the data in Fig. 1 indicate that fast ^{14}N fragments can be distinguished from saturated tracks.

Our currently-measured rms dE/dx resolution is 7-8% for minimum ionizing tracks traversing the full length of the chamber. Further refinements to the analysis software should lead to a limiting resolution of $\sim 5\%$. The identification of electrons, muons, and pions is more readily seen at higher beam energies. Fig. 2 shows the relevant region of dE/dx vs. p/Z for Au+Au at 1.2A GeV, this time without any condition on the number of dE/dx samples, and without any requirement that the track comes from the target. For the purpose of obtaining an uncontaminated pion sample, most of the electrons and muons seen in Fig. 2 can be rejected by a vertex cut.

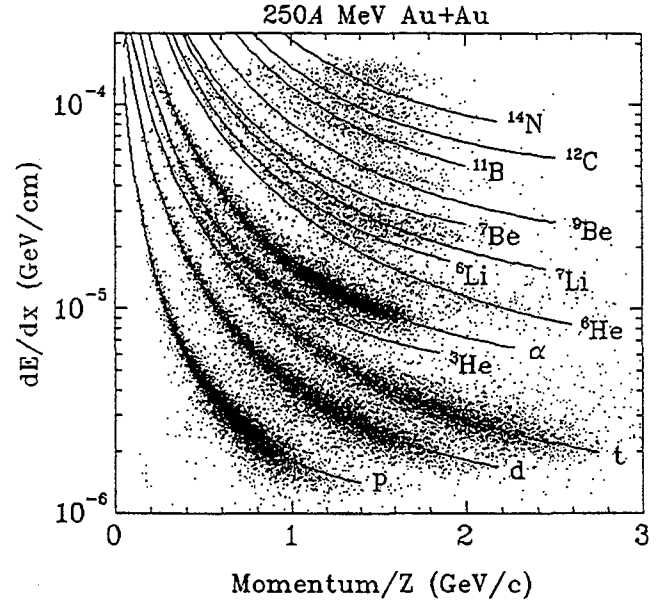


Fig. 1: Truncated (dE/dx) vs. p/Z for tracks with ≥ 40 samples, overlaid with Bethe-Bloch curves up to $Z = 7$.

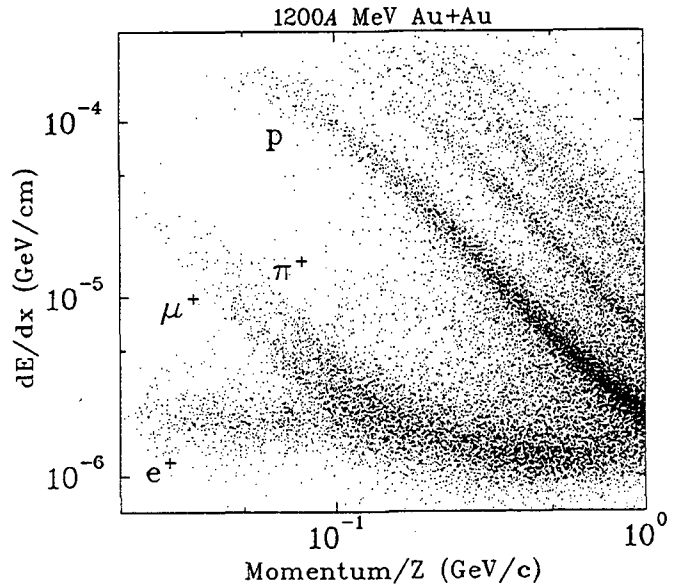


Fig. 2: As Fig. 1, but for a higher beam energy, and including all found tracks regardless of no. of dE/dx samples.

Study of Multifragmentation

The EOS Collaboration

Previous experimental data have been used to speculate that multifragmentation may be related to critical phenomena analogous to a liquid-gas phase transition in a van der Waals fluid. Such a phenomenon could occur when energy of the order of the total nuclear binding energy is deposited in the nucleus and shared among the nucleons. In the critical region, the highly excited nuclear matter fluctuates between a liquid phase (clusters of nucleons or fragments) and a vapor phase (nucleons). In nuclei such large scale density fluctuations could be detected in the behavior of the moments of fragment yields as described by Campi[†]. However, a precise analysis can only be carried in a complete experiment, i.e., measurements which span complete phase space and provide at least charge identification for every particle on an event-by-event basis.

In the EOS multifragmentation experiment we have used reverse kinematics where a heavy mass beam impinges on a light mass target. In this situation, all the collision fragments are swept into the acceptance covered by the EOS TPC, the Multiple Sampling Ionization Chamber (MUSIC II) and a Time-of-Flight (TOF) Wall. The experimental arrangement is shown in figure 1. We have used the MUSIC detector to identify the charge, Z , of all fragment nuclei heavier than Carbon. Figure 2 shows a histogram of Z obtained with the MUSIC detector for the reaction $\text{La} + \text{C}$ at 1 GeV/A beam energy. The charge resolution is about 0.2 units. The distribution of the summed charge observed together in the TPC and MUSIC detectors is found to be flat as a function of event multiplicity. Moreover, the average summed charge is equal to the value of the incident beam charge. With this combination of detectors we have, therefore, full geometrical acceptance and particle identification.

Approximately 300,000 events for each beam-target combinations have been recorded. We will carry out a significant moment analysis with fully reconstructed events.

Footnotes and References

[†] X. Campi, Proc. Int. School of Physics, Enrico Fermi, Course CXII, (1991), North Holland

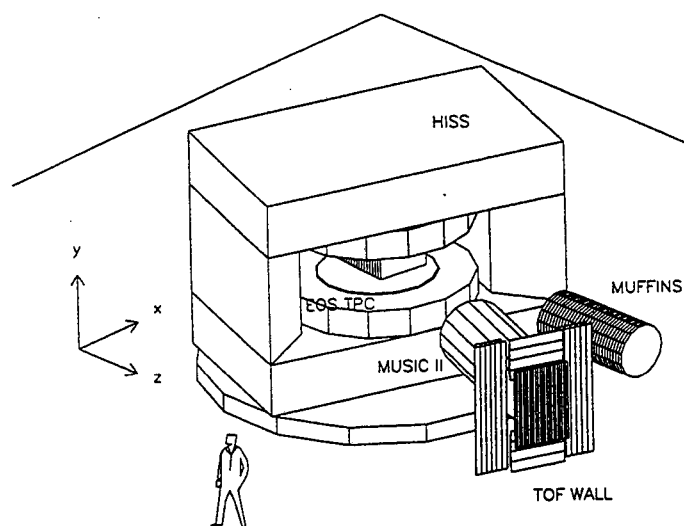


Fig. 1. The EOS experimental arrangement of principal detectors.

92/11/20 22.27

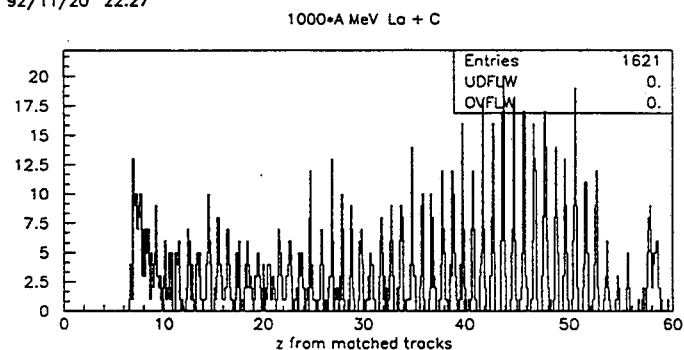


Fig. 2. Histogram of charge identification obtained from the MUSIC detector.

Preliminary Results of Collective Flow from Au + Au

M. Partlan and the EOS Collaboration

Collective flow is believed to be a signature of fluid-like behaviour in heavy ion collisions. This type of collective phenomena has been observed by the Plastic Ball¹ and the Streamer Chamber² groups. One of the goals of the EOS TPC is to extend the study of the development of collective flow to higher beam energies. For our preliminary study we have focused on the Au + Au excitation function at energies of 250, 400, 600, 800, 1000, 1200 MeV/A.

In figure 1 we show the mean transverse momentum per nucleon in the reaction plane as a function of normalized rapidity for the six different energies. The plots include all light fragments from semi-central events, multiplicity bin 3 (Mul 3) as defined by the Plastic Ball group. A measure of the flow is obtained by simply calculating the slope at mid rapidity of the 'S' shaped curve³. Here the error bars are statistical only.

In figure 2 we show the EOS flow excitation function along with the comparable Plastic Ball data. The two sets of data differ mainly at the higher beam energies, where EOS observes a continued increase in flow. However, we have not yet accounted for efficiency and acceptance of either detector. For EOS, we believe the corrections will have a minor effect on the results. We are in the process of studying the dependence of flow on multiplicity and fragment mass.

Footnotes and References

- 1 H. H. Gutbrod, A. M. Poskanzer, and H. G. Ritter, Rep. Prog. Physics 52, 2267 (1989)
- 2 R. E. Renfort et. al. Phy. Rev. Lett. 53, 763 (1984)
- 3 P. Danielewicz and G. Odyniec, Phys. Lett. B157, 146 (1985)

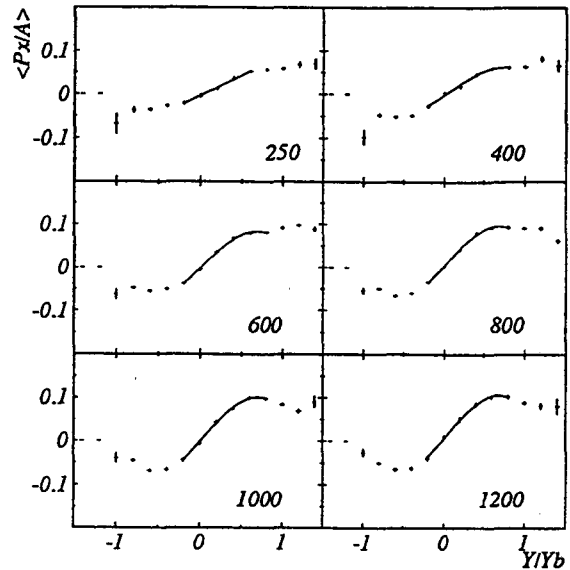


Fig. 1. Mean transverse momentum per nucleon vs. normalized rapidity for mid multiplicity events for the different energies of the Au+Au systems

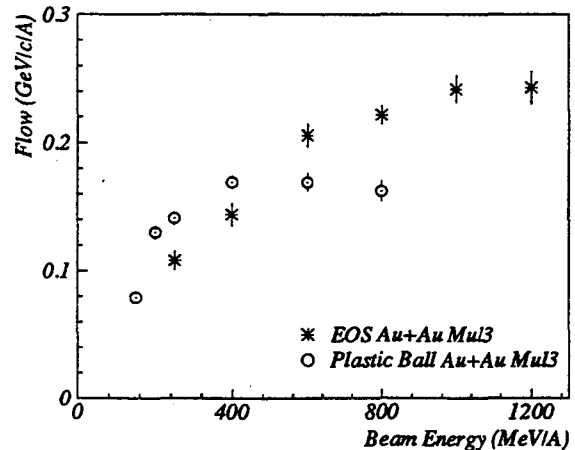


Fig. 2. Directed Flow versus beam energy for Au+Au semi-central events.

Relative Dielectron Yields in p+p and p+d Interactions from $E_{\text{beam}} = 1.0$ to 4.9 GeV

W.K. Wilson and the DLS Collaboration

Electron-positron pairs (dielectrons) are predicted to be penetrating probes of the hot compressed nuclear matter produced in the early stages of heavy-ion collisions. The initial measurements of dielectrons produced in Ca+Ca and Nb+Nb collisions for beam kinetic energies from 1-2 GeV/nucleon¹ have proven difficult to interpret due to a lack of knowledge of the fundamental nucleon-nucleon cross sections for the many processes which contribute to the dielectron yield. In June 1993, the Dilepton Spectrometer (DLS) Collaboration completed a four year long program to study dielectron production in nucleon-nucleon collisions using a liquid hydrogen target and proton beams.

In this report we present the ratio of the dielectron yield in p+d interactions to that in p+p interactions (pd/pp ratio) as a function of the beam energy from 1.0-4.9 GeV. The overall pd/pp ratio for the 4.9 GeV data set has already been published by the DLS collaboration². However, the beam energy dependence of the pd/pp ratio contained in the present report is expected to shed new light on the dominant processes leading to dielectron production in nucleon-nucleon collisions at these energies. The pd/pp ratio is a particularly clean observable since many of the effects of detector efficiency and acceptance are the same for both systems and thus cancel out of the ratio.

Proton beams of 1.03, 1.26, 1.60, 1.85, 2.07, and 4.9 GeV kinetic energy were provided by the Bevatron at Lawrence Berkeley Laboratory. Electron pairs were detected using the DLS, a twin arm magnetic dipole spectrometer. The details of the DLS hardware and performance have

been previously published³.

The pd/pp ratio measured for pairs with invariant masses greater than that of the π^0 , $m \geq 0.15$ GeV/ c^2 , is plotted in Fig. 1 as a function of the beam energy. The ratio decreases from 8.9 at 1.0 GeV to 2.1 at 4.9 GeV. The large ratio at 1.0 GeV suggests that dielectron production in the p+d system is dominated by a p+n process. Possible candidates include pn bremsstrahlung and subthreshold η production followed by Dalitz decay. The beam energy dependence of the ratio indicates that this p+n contribution decreases with respect to the other dielectron sources as the energy is increased.

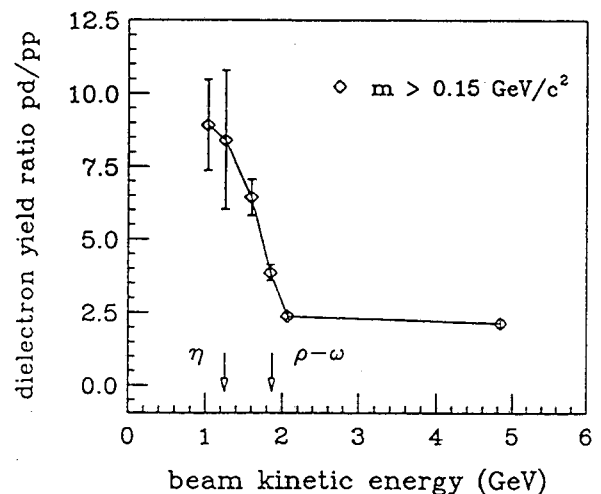


Fig. 1. The pd/pp dielectron yield ratio as a function of the beam energy. The energy thresholds for η and ρ - ω meson production are indicated by the two arrows. The line is only to guide the eye.

Footnotes and References

¹G. Roche et al., *Phys. Lett.* **226B**, 228 (1989); S. Beedoe et al., submitted to *Phys. Rev. C* (1992).

²H.Z. Huang et al., *Phys. Lett.* **B297**, 233 (1992).

Footnotes and References

³A. Yegneswaran et al., *Nucl. Instr. and Meth.* **A290**, 61 (1990).

Electron Pair Production in C+C, α +Ca and d+Ca Collisions

Charles J. Naudet and the DLS Collaboration

The Dilepton Spectrometer Collaboration (DLS) has just finished its program of measuring electron-pair production in nucleon-nucleon, nucleon-nucleus, and nucleus-nucleus collisions at the Bevalac. In p-Be collisions at 1.0, 2.1 and 4.9 GeV beam kinetic energy the invariant mass and transverse-momentum spectra and the total cross-sections have been studied in detail^{1,2}

In nucleus-nucleus collisions dileptons are expected to be a good probe of the hot and dense phase of the fireball. Calculations applicable to the Bevalac energy domain have shown the possible interesting effects in the mass structure can be understood in terms of the pion dispersion relation in nuclear matter³.

During the last year the DLS has collected over 2500 $e+e-$ pairs in Ca+Ca collisions at 1 GeV a factor of ten improvement in our statistics. Our last run in Jan. 93 has given us over 2500 $e+e-$ pairs in C+C and over 1000 pairs in each α +Ca and d+Ca.

Shown in Figure 1 A) is the preliminary invariant mass spectra for C+C collisions at 1 GeV kinetic beam energy. Figure 1 B) shows the preliminary invariant mass spectra for both the α +Ca and d+Ca systems. A large difference is observed at masses less than 400 MeV/c². Estimates of the Dalitz decay background and possible dominant subprocesses can be found in more detail elsewhere⁴.

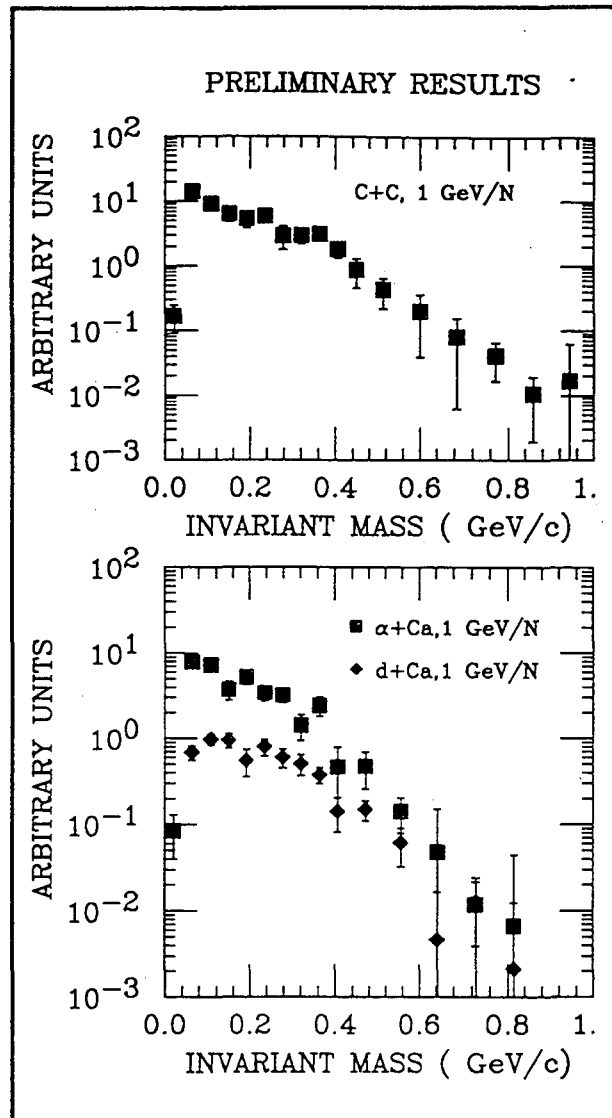


Figure 1. A) The preliminary $e+e-$ invariant mass spectra for C+C at 1 GeV B) The preliminary $e+e-$ invariant mass spectra for α +CA and d+CA at 1 GeV.

Footnotes and References

¹G.Roche et.al. Physc. ReV Lett. 61, 1069 (1988)

²C. Naudet et.al. Physc. ReV. Lett. 62, 2652 (1989)

³L.H. Xia Nucl. Phys. A485, 721 (1988)

⁴G. Roche et. al. Phys. Lett. B226, 28 (1989)

Dielectron Production in Ca+Ca Collisions, $E_{beam} = 1.05 \text{ GeV/A}$

R.J. Porter and the DLS Collaboration

Dielectrons produced in nucleus-nucleus interactions are potentially useful probes for studying the hot compressed nuclear matter stages of heavy-ion collisions. These electron-positron pairs suffer little secondary interactions with the hadronic medium of the collision and hence retain information about their production origins.

The Dilepton Spectrometer (DLS) Collaboration's initial measurements of dielectrons in $p+\text{Be}^1$ and $\text{Ca}+\text{Ca}^2$ systems established the existence for the signals in the energy region of 1-5 GeV/A. However, these measures have been difficult to adequately understand due to model dependent nucleon+nucleon source components as well as the statistical precision in the Ca+Ca data sets. To help rectify the first concern, the DLS collaboration recently concluded measurements in $p+p$ and $p+d$ interactions for several energies in the range provided by the Bevalac. Toward the second concern, an entire five week block running period was devoted to measurement of dielectrons produced in a single A+A system. This measurement in Ca+Ca collisions at 1.05 GeV/A was performed in September of 1992.

Along with obtaining a dramatic improvement in the statistical significance for this data, we also sought to tag the dielectron signal with a measure directly related to the collision's impact parameter. The DLS Multiplicity Array³, which gives a measure of the number of charge particles associated with the interaction, achieves this purpose. This allows us to examine the produced dielectron spectra concurrent with an estimation of the centrality of the Ca+Ca collision.

Some preliminary results from this measurement are shown in figure 1. The mass spectra in

figure 1A) contains about 2500 ± 150 true pairs. This represents about a factor of 10 increase in the size of the data sample over the previous Ca+Ca measure. The multiplicity spectra associated with the dielectron pairs is shown in figure 1B), as well as the distribution associated with minimum bias interactions. Both of these plots indicate the promising nature of this data for providing understanding of the mechanisms involved in such A+A collisions.

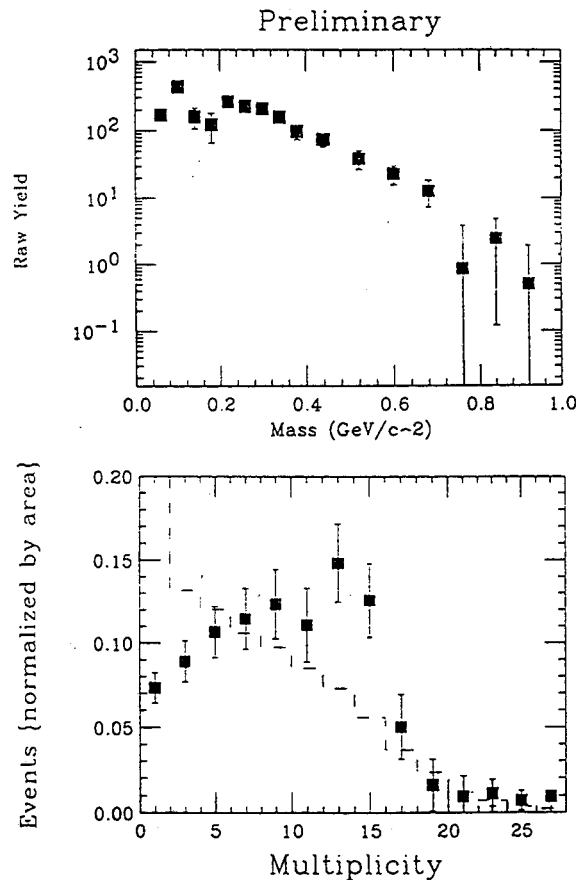


Figure 1. A) Preliminary true pair mass spectrum for Ca+Ca at 1 GeV/A. B) Multiplicity distributions for the dielectron sample (data) and for interactions which approximate a minimum bias sample (dashed histogram).

Footnotes and References

¹G. Roche et al., *Phys. Rev. Lett.* **61**, 1069 (1988);
C.Naudet et al., *Phys. Rev. Lett.* **62**, 2652 (1989)

²G. Roche et al., *Phys. Lett.* **B226**, 28 (1989)

³S. Beedoe et al., submitted to *Phys Rev. C* (1992).

Development of a Simple Device to Restandardize ECL Signals

H. S. Matis, B.T. Turko, J.E. Galvin, G. J. Zizka and the DLS Collaboration

Due to the beam structure of the Bevatron, rates in trigger counters can exceed 10 MHz. At this intensity, the electronics can affect the performance of the Dilepton Spectrometer (DLS).

In the original setup of the electronics, one output of a LeCroy 4416 discriminator went into a 4564 logic fan-in, while the other output went into 150 feet of twisted ECL delay cable and then into a LeCroy 2229 TDC. In order to reduce dead-time, the output of the discriminator had to be just larger than the coincidence width of the detectors which is 15 ns. As the signals were attenuated sufficiently by the ECL cable, the discriminator width had to be increased to 40-50 ns so that there was a reliable TDC signal.

Since a 50 ns signal would produce too many random triggers, we used a one-shot in the 4564 to reduce the coincidence width. Unfortunately, the one-shot would not re-trigger until several ns after the signal returned to its baseline and thus introduced significant deadtime into the trigger.

In order to correct for this effect, we had to study the rate-dependence of the trigger to properly normalize the cross-section. This correction is particularly difficult as the instantaneous rate, the significant observable, varies in an unpredictable way. To remove the one-shot from the system, we needed to find some way to detect the reduced ECL signals.

Nominally, differential ECL circuits have quiescent levels of -0.9 V and -1.7 V. A negative pulse is superimposed on the -0.9 V line and its complement on the -1.7 V line. If the absolute value of the pulse is less than one-half the difference of the two quiescent levels, then it can not be detected by standard electronics.

The solution of this problem was to build a resistive network which brought the quiescent voltage levels of the two ECL signals closer together. For instance if the two ECL levels are brought within several mV of each other, then a several mV signal can be detected.

The "restandardizer" consists of a variable resistor network to bring the levels close together and a HCMP96870 fast voltage comparator to generate a standard ECL pulse. Fig. 1 shows the device and describes how it is connected to the electronics.

We have made several tests on the bench and have used the device during the last two DLS runs. As expected the dead-time in the trigger decreased dramatically. In addition we have found no degradation in the DLS time-of-flight system. Once installed, the restandardizers performed flawlessly.

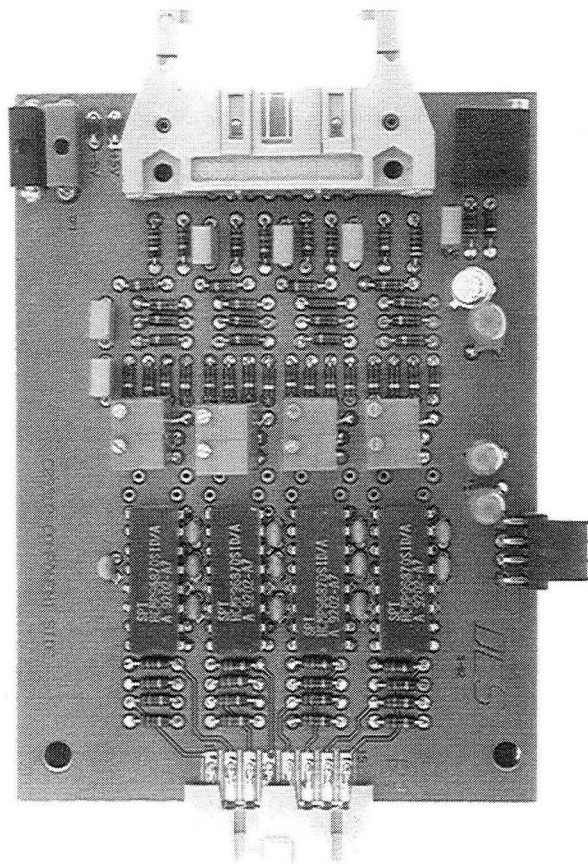


Fig. 1. Photograph of the eight channel restandardizer. The cable from the delay attaches to the top connector. The connector on the bottom directly plugs into the LeCroy 2229 TDC. A small power connector is located on the side. The sensitivity of all channels can be adjusted by the potentiometer on the upper right hand corner. The eight potentiometers in the center are for the individual channels.

Upper Limit on the Cross Section for Nuclear Charge Pickup by Relativistic Uranium Ions*

A. J. Westphal, P. B. Price, and D. P. Snowden-Ifft

We have searched for examples of nuclear charge pickup by relativistic uranium ions in targets of both uranium and phosphate glass. We find none, which allows us to set an upper limit of 7.7 mb per target atom at the 90% confidence level on the cross section for this process. An extrapolation of the approximately quadratic dependence on projectile charge of the cross section for charge pickup predicts a cross section which would be ~10 times larger. This breakdown in the scaling can be understood by the propensity of actinides to fission upon the deposition of sufficient excitation energy.

Footnotes and References

*Condensed from Phys. Rev. C 45, 2423-2426 (1992).

Sensitivity Study of CR-39 Plastic Track Detectors*

Y. D. He and P. B. Price

In support of our experiment to search for strangelets at the Brookhaven AGS, we felt it desirable to try to increase the sensitivity of CR-39 plastic track-recording detectors so as to be able to detect relativistic particles with Z as low as possible. We had samples containing antioxidant additives made by Tastrak (Bristol, UK) and we evaluated them by means of a Bevalac exposure. The results show that CR-39 containing 100 ppm Naugard antioxidant and no plastizer (DOS) has higher sensitivity than standard CR-39 plastic in the tested range of $Z/b = 7$ to 12. No nuclei with $Z \leq 5$ were recorded in any of the samples, indicating that the detection threshold of the calibrated

CR-39 samples was ≥ 6 when evaluated with an image processor at its normal setting.

We believe that some of the CR-39 made by Tastrak may actually record ions with Z/b as low as 4, provided it is etched for a short time so as not to produce a rough surface that prevents an image processor from being used. To detect shallow etchpits after a short etch time, one might be able to use an atomic force microscope, and work along these lines is being initiated.

Footnotes and References

* Condensed from a paper in Nucl. Tracks Radiat. Meas. 20, 491-494 (1992).

ULTRARELATIVISTIC EXPERIMENTS

The STAR Experiment at RHIC

The STAR Collaboration

The Solenoidal Tracker At RHIC (STAR) is the first experiment approved for construction at the Relativistic Heavy Ion Collider (RHIC). The STAR experiment will search for signatures of quark-gluon plasma (QGP) formation and investigate the behavior of strongly interacting matter at high energy density. The emphasis will be on two novel aspects of hadron production at RHIC: 1) *event-by-event correlations between global observables* - such as temperature, flavor composition, collision geometry, reaction dynamics, and energy or entropy density fluctuations; and 2) the use of *hard scattering of partons* as a penetrating probe of the quark-gluon plasma. These observables will be studied as a function of mass of the colliding system, impact parameter and incident energy, in order to understand the reaction dynamics at RHIC and to detect and conclusively identify the signatures of QGP formation.

To meet the design criteria¹ tracking, momentum analysis and particle identification of most of the charged particles at midrapidity are necessary. Particle identification of pions/kaons for $p < 0.7$ GeV/c and kaons/protons for $p < 1$ GeV/c, as well as measurement of decay particles and reconstruction of secondary vertices will be possible. A two-track resolution of 2 cm at 2 m radial distance from the interaction is expected. Momentum resolution of $\Delta p/p = 0.02$ at $p = 0.1$ GeV/c is required to accomplish the physics, and $\Delta p/p$ of a few percent at $p = 10$ GeV/c is sufficient to accurately measure the rapidly falling spectra at high p_t and particles from mini-jets and jets. The momentum resolution at low p_t will be limited by multiple scattering.

The configuration of the STAR experiment is shown in Fig. 1. Momentum measurements will be made at midrapidity over a large pseudo-rapidity range ($|\eta| < 2$) with full azimuthal coverage ($\Delta\phi = 2\pi$). Particle identification will be performed within $|\eta| < 1$. The detection

system will consist of a time projection chamber (TPC) and a silicon vertex tracker (SVT) inside a solenoidal magnet with 0.5 T field to enable tracking, momentum analysis, particle identification via dE/dx and location of primary and secondary vertices. Detectors will be installed to provide a collision geometry trigger. These include a central trigger scintillator barrel around the TPC, vertex position detectors near the beamline just outside the magnet, and calorimeters located in the region of the beam insertion magnets to selectively veto events according to the number of spectators. An electromagnetic calorimeter, for which supplemental funding is being sought, will be located inside the magnet coil and used to trigger on transverse energy and measure jet cross sections. A time-of-flight system surrounding the TPC for particle identification at higher momenta and external time projection chambers outside the magnet to extend the η coverage are anticipated as upgrades.

1. "Conceptual Design Report for the Solenoidal Tracker at RHIC", PUB-5347, LBL, June 15, 1992.

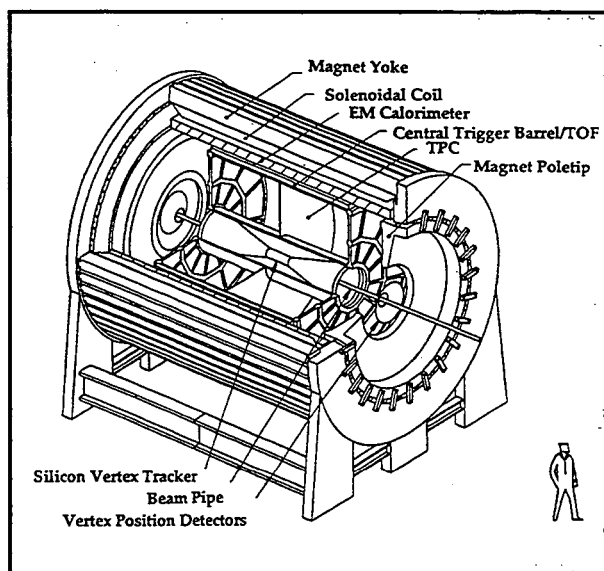


Fig. 1. Layout of the STAR experiment.

STAR Time Projection Chamber

H. Wieman, J. Bercovitz, † D. Cebra, W. Gong, ‡ E. Hjort, ‡ H. Huang, P. Jones, § D. Keane, J. Mitchell, R. Morse, G. Rai, I. Sakrejda, ‡ R. Scharenberg, D. Shuman, A. Sobel, R. Stone, ‡ B. Stringfellow and the STAR Collaboration

Work is progressing on the STAR TPC, a main component of the STAR detector system for use at RHIC. The TPC will provide tracking and dE/dx identification (for the thousands of charged particles emitted) in central heavy ion collisions at the RHIC collider.

The TPC is a solenoid design with a 50 m^3 drift volume that gives full azimuthal coverage and good acceptance for pseudo rapidity, $|\eta| \leq 1$. The active volume is 4 m long and has an inner radius of 0.5 m and an outer radius of 2.0 m.

The sectors on the endcaps are multiwire proportional chambers with pad readout. As shown in Fig. 1 the pads are arranged as a solid array of $6.2 \text{ mm} \times 19.5 \text{ mm}$ pads covering $r = 1.25\text{--}2.0 \text{ m}$. The continuous pad coverage provides both tracking and dE/dx in this outer region. At the inner region, $r = 0.5\text{--}1.25 \text{ m}$ the pad size is reduced to $2.9 \text{ mm} \times 11.5 \text{ mm}$ to improve the track resolution where the track density is highest. The drift gas is 10% $\text{CH}_4 + 90 \%$ Ar at one atmosphere. The electric field in the drift volume (130 V/cm) is maintained with a field cage of the ALEPH design. The maximum drift length is 2.1 m from the central cathode of the field cage to the read out chambers on the end caps. A relatively low magnetic field of 0.5 T has been chosen to extend the p_t acceptance down to 160 MeV/c. The TPC design includes a Nd-YAG laser system for spatial calibration of the drift volume. The laser is frequency quadrupled to provide ionizing UV beams for generating calibration tracks in the drift volume.

The design goal for tracking precision is 200 microns for the sagitta determination. This will provide a momentum resolution of 2.2% at momenta of 10 GeV/c. The peak of the pion p_t spectrum is 300 MeV/c. At this momentum the momentum resolution is limited by multiple scattering to 1.2%

The design and construction of the major elements of TPC will be done at LBL. Purdue will play a significant role in the testing and operation of the MWPCs. UC Davis will provide the laser system and Kent State will develop the anode voltage system for the MWPCs. Wayne State and Univ. of Texas (Austin) will assist in construction.

Initial testing of the TPC as a unit is scheduled for 1995. The scheduled date for operation of the complete STAR system in the beam at RHIC is 1997.

Footnotes and References

1. "Conceptual Design Report for the Solenoidal Tracker at RHIC", PUB-5347, LBL, June 15, 1992

† UC Davis

‡ Purdue

§ Kent State

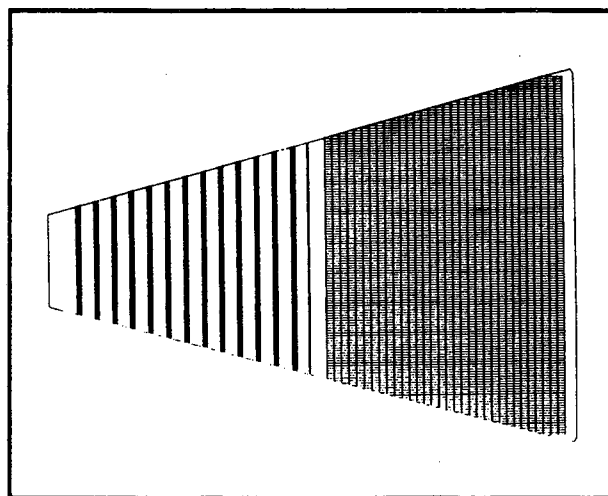


Fig. 1. Sector design for the pad plane read out of the STAR TPC. The outer radius region is a solid array of $6.2 \text{ mm} \times 19.5 \text{ mm}$ pads and the inner radius region is composed of separated pad row strips with $2.85 \text{ mm} \times 11.5 \text{ mm}$ pads.

The Silicon Vertex Tracker for STAR

W. Christie, S. Margetis, C. Naudet, G. Odyniec, J. Schambach, K. Wilson
and the STAR Collaboration

Over the last year significant progress has been made on the Silicon Vertex Tracking detector (SVT). The SVT is a tracking detector which, when coupled with the time projection chamber, will yield the position of the primary interaction vertex with high accuracy and precision, improve the momentum resolution and locate secondary vertices with a positional resolution better than 100 microns.

The SVT will play a pivotal role in strange particle detection, a primary goal of STAR¹. We have shown² that the high granularity and good position resolution of the SVT allow various strange particles (i.e. k_s^0 , Δ , Ξ^- , Ω^- , ...) to be detected via their weak decay into charged particles. In addition, the SVT will extend the STAR acceptance into the low- p_t domain.

The baseline SVT detector design consists of three cylindrical layers at radii of 5, 8, and 11 cm. Each layer is formed by connecting ladders (40 cm by 6 cm) together in a hexagonal pattern. Each ladder is composed of six silicon drift detectors (SDD)³ each 6.8 cm by 5.8 cm by 300 microns.

Over the last year the first prototype SDD detectors, see figure 1, were fabricated and tested. These detectors have recently been tested at LBL and were found to perform satisfactory over the entire active area giving proof of principle for the baseline SDD detectors.

The final detector design decisions are scheduled for the beginning of 1994 with the first 30 detectors to be produced in the following year. The design of the SDD will be centered at Brookhaven National Laboratory with LBL and Wayne State being primarily responsible for the testing of the detectors. In addition, LBL will be responsible for the device simulation code⁴, calibration and alignment of the detector and the GEANT simulations of the detector

capabilities. The expected date for operation of the baseline SVT detector is 1997.

Footnotes and References

¹ STAR, Conceptual Design Report, PUB-5347.

² S. Margetis, STAR-SVT note 9/20/91.

³ P. Rehak and E. Gatti, NIM 225 (1984) 608.

⁴ K. Wilson, STAR-SVT note 11/1/91.

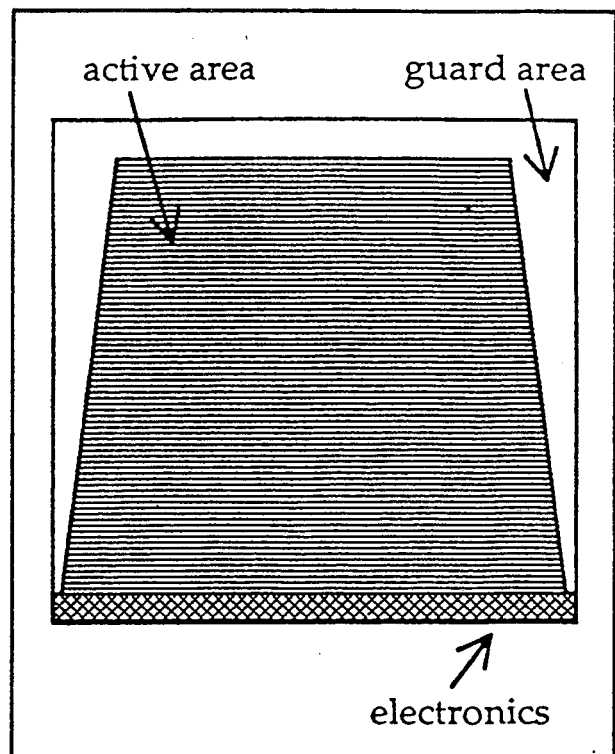


Figure 1.) The prototype 4-cm long SDD detector called STAR1-SDD detector.

A Simulation Package for the STAR Time Projection Chamber

P.G. Jones and I. Sakrejda and the STAR collaboration

A detailed Monte-Carlo simulation has been developed to aid the design of the STAR Time Projection Chamber (TPC). The geometry of the STAR detector and all the associated support structure is described using the GEANT program. The Lund-FRITIOF code has been used to generate the $\sqrt{s_{NN}} = 200$ GeV Au+Au events used as input to GEANT. The GEANT program outputs a list of track crossings for each TPC pad row and this forms the input to the FaSt TPC simulation program (FST).

FST has been designed to simulate the response of the TPC and the first level of the analysis software (the hit reconstruction algorithm). This has been achieved by parametrizing the width of the induced charged distribution on the pad row according to the pad response function¹ given by equation (1).

$$\sigma_{\text{prf}}^2 = \sigma_o^2 + \sigma_D^2 \lambda (1 + \tan^2 \alpha) + \sigma_\alpha^2 \tan^2 \alpha \quad (1)$$

The three terms in the pad response function are an intrinsic pad response (σ_o), a diffusion term (σ_D) proportional to the drift length λ and a crossing angle term (σ_α), where α is the track crossing angle perpendicular to the pad row. The values of the coefficients have been derived from previous measurements¹. This parametrization of the signal width enables the merging of near-by clusters to be modeled in the simulation.

The spatial resolution of each hit is similarly parametrized using the pad resolution function¹ shown by equation (2).

$$\sigma_{\text{res}}^2 = \sigma_A^2 + \sigma_B^2 \lambda \sec \alpha + \sigma_C^2 \cos \alpha \tan^2 \alpha \quad (2)$$

The three terms here are determined by the expected signal-to-noise ratio (σ_A), diffusion (σ_B) and the crossing angle of the tracks relative to the pads (σ_C). By utilizing these

parametrizations, FST models the expected detector two-track resolution and the space point resolution. The output analysis level of FST is that of reconstructed space points and this forms the input to the STAR tracking algorithm.

Track reconstruction is based on a Track Following method, which starts by using a simple extrapolation from the outermost pad rows to form short track segments. A helix fit is then performed on each segment and the segments are then extrapolated using the helix parametrization. Finally, a matching procedure is used to combine multiple track segments from single spiraling tracks (typically with transverse momentum, $p_T < 200$ MeV/c).

Figure (1), shows the transverse momentum resolution as a function of the transverse momentum calculated for the prototype TPC geometry using the full simulation and reconstruction software.

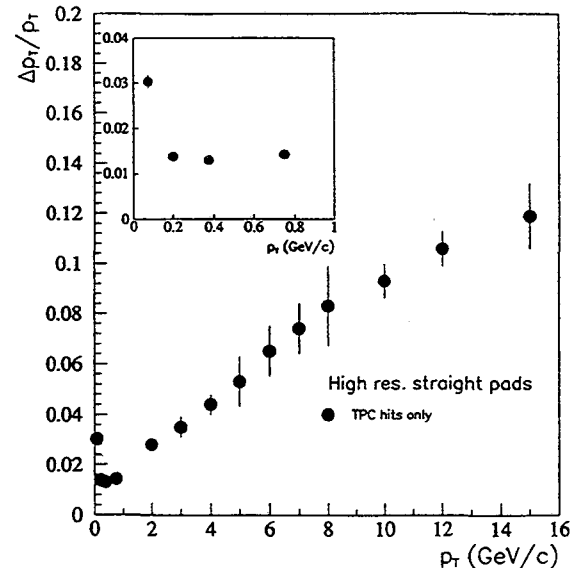


Fig. 1. The calculated transverse momentum resolution and a function of transverse momentum for the STAR TPC.

¹ The STAR CDR, LBL PUB-5347.

The SVT Resolution Simulator (SRS)

W.K. Wilson, S. Margetis, C. Naudet, G. Odyniec, and J. Walton

The SVT Resolution Simulator (SRS) provides the user with an estimate of the position resolution which can be expected from the Silicon Drift Detectors (SDD) ¹ in the STAR Silicon Vertex Tracker (SVT). The SRS code is intended to be used in conjunction with the output of GEANT simulations in order to study the impact of SDD resolution on tracking in STAR.

In the past ², we have assumed that the position resolution of the SDDs can be approximated by a gaussian distribution with a fixed standard deviation of 25 microns. Although this approach allowed useful preliminary simulations of the SVT performance to be conducted, it was unsatisfactory on several counts. The resolution of SDDs is not constant, but varies with the position of the hit respect to the anodes. The particle's angle of incidence and the amount of ionization it generates also influence the position resolution. Finally, in the previous system, there was no systematic way to investigate how changing the operating parameters of the SDDs, ie. drift velocity, anode pitch, etc., would change the performance of the SVT. The SRS code allows one to see the effects of different operating conditions on the resolution of the SVT for the variety of tracks which occur in the GEANT simulations of the STAR experiment.

The response of an SDD to a charged particle hit is parameterized in terms of the position of the hit relative to the anodes, angle of incidence of the track, and the number of electron-hole pairs generated. We have closely followed the model adopted by the PEP-4 group for parameterizing the response of their TPC ³. The details of the parameterization were obtained by studying the results of electron transport calculations.

Footnotes and References

¹Rehak et al., *Nucl. Instrum. Methods* A235, 224 (1985)

²G. Odyniec et al., *LBL Preprint LBL-31773* (1992)

³Aihara et al., *IEEE Trans. Nucl. Sci.* 30, 76 (1983)

The signals from the SDD anodes will be divided up into time buckets using a switched capacitor array (SCA). In the simulations, a sample is stored for each SCA time bucket which contains an integrated signal which is bigger than the uncertainty in the signal after subtraction of background noise. The position of the hit can be extracted from fits to the time dependence of the sample size. In Fig. 1 we show an example calculation using the SRS for typical SVT operating parameters. The resolution improves as the drift distance decreases until the distribution is too narrow to provide enough samples for an optimum fit. It will be interesting to see how the performance of the SVT is altered by this resolution distribution compared to the fixed 25 μm resolution assumed earlier.

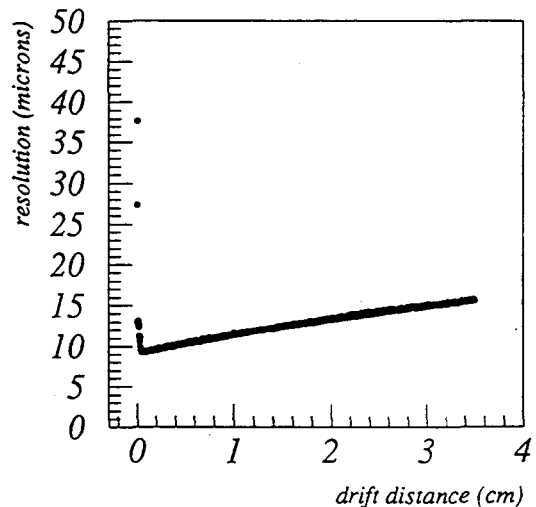


Fig. 1. The position resolution along the drift direction as a function of the drift distance as predicted by the SRS code.

Main Vertex Reconstruction in STAR

S. Margetis, D. Cebra and the STAR Collaboration

A Least Squares Method combined with a simple technique of outlier removal¹, has been used for main vertex fitting in simulated events for STAR. The accurate determination of the main vertex is essential for two reasons. First, it determines the interaction point and one can recalculate the momentum vector for each primary track at the vertex with the vertex point included in the fit. Second, it enhances the ability to discriminate between tracks coming from the primary or secondary vertices.

In the transverse plane, the real vertex can only be a few millimeters away from the central axis due to the small cross section of the beam.² For distances of this order of magnitude we can approximate the helices as straight lines. This linearization of the track model in the vertex neighbourhood has the advantage of leading to an analytical solution.

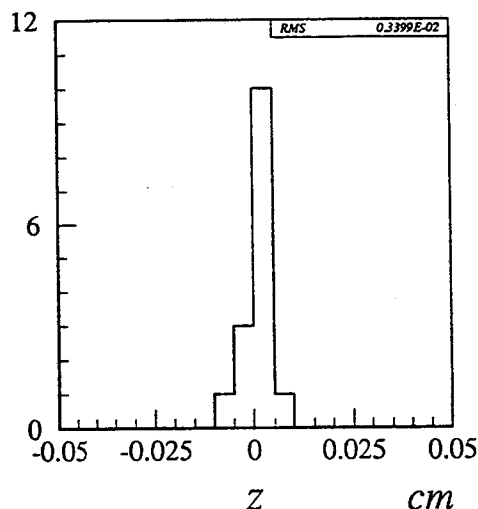
It is known that including in the fit tracks which are at large distances from the central cluster of tracks (outliers) has a strong influence on the results. We use a simple 'truncation' method in an iterative way to remove the outliers and therefore improve the 'robustness' of the fit. In this method we first use all reconstructed tracks to get an estimate of the vertex parameters. Then we use this result as a seed to the next iteration and we remove from the track pool all tracks with distances greater than a certain cut value. The new vertex is then used as a seed for the next iteration. The whole process converges after 3-4 iterations.

We ran the program on a set of 15 central Au+Au events at $\sqrt{s} = 200$ GeV/nucleon. The figure shows the distribution of the residuals for these events for the axis along the beam direction and the table summarizes the results of the

fit.

RMS (μm)	x	y	z
TPC	330	220	250
TPC+SVT	40	40	35

We observe that the resulting distributions have an RMS in the range 250-350 microns for the TPC and 30-40 microns for the TPC+SVT which reflects the accuracy of the fit. This high accuracy of defining the primary vertex is a result of two factors: the position resolution of the corresponding detectors and the number of tracks (degrees of freedom) used in the fit. This result, combined with the increase of the overall track length, makes the reconstructed vertex a valuable point in the track fitting process, improving the overall momentum resolution. Especially without the SVT in the experiment it makes a rather dramatic improvement ($dp/p = 9.6\%$ without, and 2.2% with the vertex included in the fit).³



Vertex resolution with the STAR TPC+SVT along the beam axis.

Footnotes and References

¹ STAR-Note #89

² Conceptual Design of RHIC, BNL 52195, May 1989

Footnotes and References

³ H. Wieman et al.; STAR Collab. meeting, BNL September 1992

Feasibility of Single-Event Bose-Einstein Correlations in STAR

R. J. Morse and The STAR Collaboration

It is anticipated that two-particle correlation studies will be an important tool as ultrarelativistic heavy-ion physics moves into the regime of RHIC energies ($\sqrt{s}/A = 200\text{GeV}$). The massive data sets envisioned for the large-acceptance major detectors at RHIC should prove well-suited to the type of high statistics, multidimensional analyses which current theoretical work indicates will be needed in order to discriminate between competing dynamical evolution scenarios for the reaction zone. However, more interesting is the possibility, due to the large expected charged particle multiplicity densities, of using single-event correlation functions as yet another variable in the event characterisation space at RHIC. Since detailed studies of the cross-correlations within this event characterisation space is a keystone of the physics program envisioned for the STAR detector, a study was conducted in order to determine, based purely upon the two-particle phase space accessible to the STAR detector, the feasibility of using single-event HBT as an event characterisation variable.

The results of this study are summarised in the following figures. Fig. 1 presents a nomogram of sensitivity to pion source parameters as a function of the number of events into the STAR acceptance assuming a particle-identified rapidity density of 200 and a lower p_t cut of 0.04 GeV/c for an assumed 10 fm source. This represents a conservative scenario from the viewpoint of charged particle multiplicity and source dimension. This indicates that on a single-event basis STAR can expect a 10 to 20% statistical sensitivity to the pion source parameters. Fig. 2 presents the result of a more speculative calculation in which the particle-identified rapidity density is increased to 500 and the source size is increased to 20 fm; the resulting single-event two-particle correlation function indicates a 27% statistical sensitivity to the pion source parame-

ters. It is concluded that for cases of up to 10 fm sources, source size can easily be used as an off-line event characterisation variable. In the more exotic case of a 20 fm source, the feasibility of single-event source size as an event classification variable would require either enhanced charged particle rapidity densities or the use of both positive and negative pions in the determination of the source size.

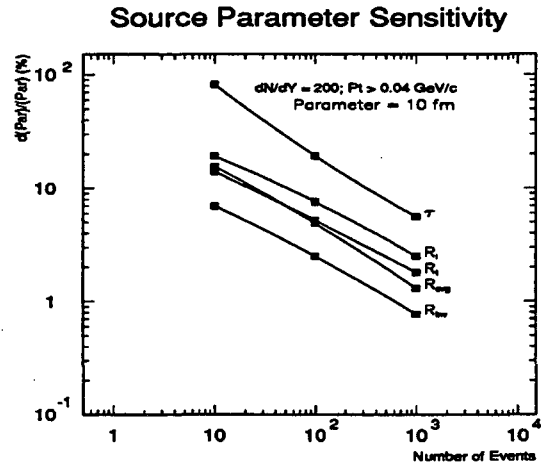


Fig. 1: Sensitivity to extracted source parameters versus number of events.

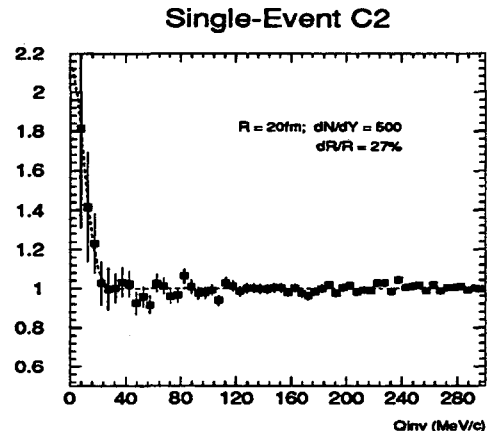


Fig. 2: Single-event correlation function for 20 fm source.

Temperature Dependence of the Gas Gain of Proportional Counters

W.G. Gong, A. Sobel, H. Wieman, E. Hjort, J. Mitchell

Temperature dependence of gas gain of a proportional counter is an important parameter for operating a large TPC detector. The effect was observed, however, it was not well documented in the literature. We decide to carry out this study using the EOS prototype chamber.

The gas gain was measured by reading out pulse height spectra on the anode wires using an ^{55}Fe X-ray source. The anode spectra were calibrated by injecting a known amount of charge through a precision capacitor. The ^{55}Fe peak position calibrated in terms of charge corresponded to the collected charges after the avalanche. The ratio of avalanche charges over the number of primary ionization electrons due to one X-ray defines the measured gas gain.

We heated the chamber by affixing heater tapes to the chamber wall and supporting aluminum block. Temperatures were read out by calibrated thermocouples attached by copper tapes at various locations to monitor the degree of thermal equilibrium around the chamber. However, the temperature readout closest to the avalanche region was used to represent our data. The maximum temperature reached was about 10°C above the room temperature. Figure 1 shows a typical measurement of gas gain at different temperatures for an anode voltage of 1350V . The rate of gain increase per degree is about 2.2%. Measurements taken at different anode voltage show variations of 1.7-2.5%.

The gas gain is typically expressed by $G = \exp(\int_{r_a}^r \alpha dr)$, where r_a is the anode radius, $r = r_a V/V_i$ is the distance from the axis to the point where the gas avalanche starts [1], and $\alpha = PA(\epsilon - I)$ is the Townsend coefficient (see Ref.[2] for details).

Under constant pressure of the gas volume, the increase of temperature reduces the gas number density. The mean-free-path of the electron in the gas then becomes larger. The electron will gain more kinetic energy under the acceleration of the electric field. It eventually leads to the gas gain increase. Mathematically,

$$\left(\frac{\Delta\alpha}{\Delta T}\right)_P = \left(\frac{keA}{\sigma^{ion}}\right) \frac{V}{r \cdot \ln(r_c/r_a)}, \quad (1)$$

assuming cylindrically distributed electrical field. Further integration gives an explicit expression for

the gas gain

$$G(V, T|P) = \exp\left\{CTV \ln\left(\frac{V}{V_i}\right)\right\}. \quad (2)$$

where $C = keA/(\sigma^{ion} \ln(r_c/r_a))$ is a constant. Empirically, $V_i = 514\text{V}$ and the gain increase by a factor of 2 when the voltage increases by 60V from $V_a = 1260\text{V}$ at $T = 300\text{K}$. We find that $C \approx 2 \times 10^{-5}(\text{KV})^{-1}$ for P-10 gas.

The open circles in Fig. 1 shows the calculated gain as a function of temperature. The calculations were multiplied by a factor of 8.4 to match the absolute gas gain and that factor may be attributed to the presence of field wire in our chamber. It appears that the measured temperature dependence of gas gain can be well reproduced.

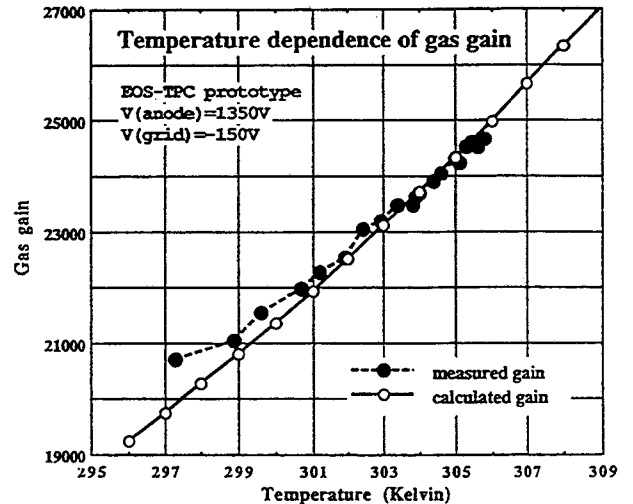


Fig.1: The temperature dependence of P-10 gas gain for EOS prototype chamber.

Footnotes and References

- ¹ M. E. Rose and S. A. Korff, Phys. Rev. 59 (1941) 850
- ² Y. Uozumi, et al Nucl. Instru. and Methods A324 (1993) 558

A $J^{PC} = 0^{++}$ Resonance at $1560 \text{ MeV}/c^2$ *

*K.M. Crowe, D.S. Armstrong, J. Bistirlich, R. Bossingham, H. Bossy, T. Case,
and the Crystal Barrel Collaboration*

One of the primary aims of the Crystal Barrel experiment at LEAR is to use low-energy $\bar{p}p$ annihilation to search for resonances that do not fit into the nonets of conventional mesons. Such resonances could include glueballs (bound states of gluons), hybrids (e.g. $q\bar{q}g$), mesonic “molecules” (4-quark states), or bound baryon-antibaryon states. One interesting nonet is the scalar ($J^{PC} = 0^{++}$), where there are already more low-mass candidate states than places in the lowest-lying nonet. Here we report on the observation of a scalar object with a mass of $1560 \text{ MeV}/c^2$ observed in $\bar{p}p$ annihilation at rest.

Data were taken with an all-neutral trigger, and, in off-line analysis, events with 6 photons in the final state were selected. Kinematic fits were then applied to isolate the reaction $\bar{p}p \rightarrow \eta\eta\pi^0$ ($\eta \rightarrow \gamma\gamma$, $\pi^0 \rightarrow \gamma\gamma$) from other possible channels. The data analyzed corresponded to 3×10^8 $\bar{p}p$ annihilations, and yielded 2.25×10^4 events which satisfied a confidence level of $> 10\%$ for the kinematic fit to $\eta\eta\pi^0$, and which had no fit with a confidence level $> 1\%$ for any background channel (e.g. $\pi^0\pi^0\pi^0$, $\eta\pi^0\pi^0$). A full Dalitz-plot analysis was then applied to these events.

A projection of the resulting Dalitz plot on the $\pi^0\eta$ invariant mass axis (Fig. 1a) clearly shows the presence of the $a_0(980)$ meson, and that on the $\eta\eta$ axis (Fig. 1b) appears to be dominated by the $f_0(1400)$ and by an enhancement around $1550 \text{ MeV}/c^2$. In the final χ^2 fit to the Dalitz plot, possible contributions were included from the $a_0(980)$, $a_2(1320)$, $f_0(1400)$, and $f_2(1515)$ resonances, as well as a state around $1550 \text{ MeV}/c^2$, the mass, width and spin-parity of which was allowed to vary. A reduced χ^2 of 1.15 for the fit to the Dalitz plot was achieved (see histograms in Fig. 1a and Fig. 1b). The fitted mass and

width of the ‘new’ resonance was determined to be $(1560 \pm 25) \text{ MeV}/c^2$ and $(245 \pm 50) \text{ MeV}/c^2$ respectively, and the spin-parity was unambiguously determined to be 0^{++} . Consistent results were also obtained in an analysis of the $\eta\eta\pi^0$ final state obtained from a 10γ final state (selecting $\eta \rightarrow 3\pi^0$ and $\eta \rightarrow \gamma\gamma$).

The interpretation of this resonance is unclear. A scalar resonance also decaying to $\eta\eta$ with similar mass and width has been observed in π^-p charge exchange reactions by the GAMS collaboration¹, and this particle is considered an excellent candidate to be a scalar glueball. However, the GAMS particle is observed to decay to $\eta'\eta$ with approximately 3 times higher branching ratio than to $\eta\eta$, while our data sets a limit on the $\eta'\eta$ branch of 4 times less than that for $\eta\eta$. Further searches for this resonance in other final states (e.g. $K\bar{K}$) are underway, and should help to clarify the situation.

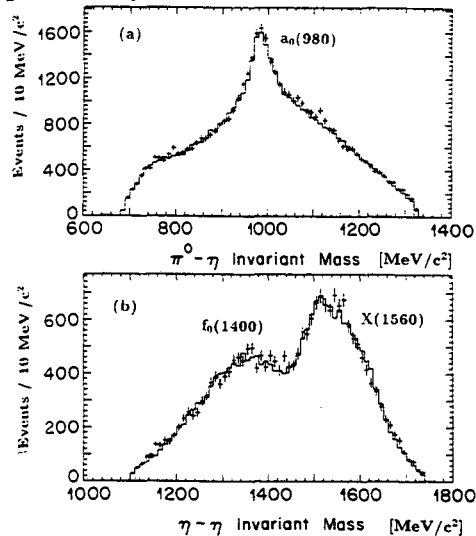


Fig. 1. (a) The $\eta\pi^0$ invariant mass spectrum. (b) The $\eta\eta$ invariant mass spectrum. The histograms are the final fit to the data.

Footnotes and References

*C. Amsler *et al.*, Phys. Lett. B291 (1992) 347.

Footnotes and References

¹F. Binon *et al.*, Nuovo Cimento A78 (1983) 313; D. Alde *et al.*, Phys. Lett. B201 (1988) 160.

The Pseudoscalar Mixing Angle from $\bar{p}p$ Annihilation at Rest*

*K.M. Crowe, D.S. Armstrong, J. Bistirlich, R. Bossingham, H. Bossy, T. Case,
and the Crystal Barrel Collaboration*

The isospin $I=0$ members of the lowest pseudoscalar meson nonet, the η and η' , are known not to be the pure SU(3) singlet and octet states $[(u\bar{u} + d\bar{d} + s\bar{s})/\sqrt{3}$ and $(u\bar{u} + d\bar{d} - 2s\bar{s})/\sqrt{6}$, respectively], but are rather linear combinations of these wave functions. This is due to the symmetry being broken because of the large strange quark mass. The linear combination is conventionally described by a mixing angle Θ_{PS} . It is also possible that the η and η' could mix with exotic states such as the lowest-mass 0^{-+} glueball, or with radial excitations.

The Crystal Barrel detector at LEAR has been used to determine the pseudoscalar mixing angle Θ_{PS} by comparison of various branching ratios for $\bar{p}p$ annihilation at rest into final states involving η and η' mesons. Θ_{PS} can be determined from these branching ratios using the assumption that the initial $\bar{p}p$ state only couples to the $(d\bar{d} + u\bar{u})$ component of the η and η' wavefunctions. Using this assumption, and also assuming, for example, that the η' is predominantly $s\bar{s}$ in nature, one expects that the ratio $r = \text{B.R.}(\bar{p}p \rightarrow \eta'X)/\text{B.R.}(\bar{p}p \rightarrow \eta X)$ (where $X = \pi^0, \omega, \eta, \gamma$) would be a small number, and neglecting phase space factors and dynamical corrections, it should be the same for all X . This assumption would be invalid, however, if the proton has a substantial $s\bar{s}$ component, as has been recently suggested.¹

An all-neutral trigger was used, and the final states selected were $\pi^0\eta$, $\pi^0\eta'$, $\omega\eta$, $\omega\eta'$, $\eta\eta$, $\eta\eta'$, $\gamma\eta$, and $\gamma\eta'$. Several of these channels have either never before been observed in $\bar{p}p$ annihilation at rest, or else had quoted errors several times larger than those of the present results. The ω

was observed through its $\pi^0\gamma$ decay mode, the η via its decay into either $\gamma\gamma$ or $\pi^0\pi^0\pi^0$, the η' through either the $\gamma\gamma$ or $\pi^0\pi^0\eta$ modes and the π^0 via its $\gamma\gamma$ decay.

The ratios of branching ratios were determined to be $r = 0.548 \pm 0.048, 0.652 \pm 0.069, 0.515 \pm 0.031$ and 0.69 ± 0.34 for $X = \pi^0, \eta, \omega$, and γ respectively (the $\eta\eta$ branching ratio has been multiplied by 2 to correct for the two identical bosons). These values of r need to be corrected for phase space and other possible dynamical factors before they can be used to extract Θ_{PS} . Various possible dynamical models were applied to the results, and each model was tested by examining the degree of consistency between the four dynamically-corrected values of r . Two models gave self-consistent values for Θ_{PS} from the four values of r . These were a model due to Vandermeulen² which yielded $\Theta_{PS} = -(17.3 \pm 1.8)^\circ$, and, perhaps surprisingly, the model suggested by Klempt,³ which was not to make any correction at all, and which yielded $\Theta_{PS} = -(18.4 \pm 0.7)^\circ$.

The present results for Θ_{PS} are in reasonable agreement with a recent determination of Θ_{PS} from a global fit to a large data set including $\gamma\gamma$ decays of the η and η' , J/ψ radiative decays, light meson radiative decays, mass formulae etc.,⁴ which gave $\Theta_{PS} \simeq -20^\circ$. This tends to support the assumptions used in our analysis, *i.e.* that there is no significant $s\bar{s}$ component in the nucleon at low momentum transfers, and that there is no need to consider mixing of the η and η' with other states.

Footnotes and References

*C. Amsler *et al.*, Phys. Lett. B294 (1992) 451; C. Amsler *et al.*, to be published.

¹e.g. R. Decker and D. Woitschitzky, Phys. Lett. B273 (1991) 301.

Footnotes and References

²J. Vandermeulen, Z. Phys. C 37 (1988) 563.

³E. Klempt, Phys. Lett. B244 (1990) 122

⁴F. Gilman and R. Kauffman, Phys. Rev. D36(1987)2761.

Correlations in $^{32}\text{S}+\text{S}$ and $^{32}\text{S}+\text{Au}$ Collisions at the CERN SPS

M.A. Bloomer, P. Jacobs, A.M. Poskanzer and the WA80 Collaboration

Most heavy ion experiments have used a scaled factorial moment analysis¹ to investigate intermittency in particle production from heavy ion collisions. The results of an high-statistics intermittency analysis of data taken at the CERN SPS with the WA80 Streamer Tube Detector, using 200 AGeV ^{32}S beams incident on S and Au targets, have been presented elsewhere.² It was found that a factorial moment analysis is extremely sensitive to a number of experimental effects, especially the two-track resolution. Even though the WA80 streamer tubes have a two-track resolution of ≤ 0.05 in $d\eta-d\phi$ space, the factorial moments exhibit distortions at scales much larger than this.

An alternative method to investigate the strength and scale of (η, ϕ) correlations in particle production is to calculate the two-particle correlation function. For the case of correlations in η this is defined as

$$C(\eta_1, \eta_2) = \frac{\rho_2(\eta_1, \eta_2)}{\rho(\eta_1)\rho(\eta_2)} \quad (1)$$

where $\rho_2(\eta_1, \eta_2)$ is the two-particle density function, which measures the joint probability of observing two particles with pseudorapidities (η_1, η_2) , and $\rho(\eta)$ is simply the pseudorapidity distribution.

We have performed a "standard" two-particle correlation analysis³ with the same data set used in the intermittency analysis, using the variables $d\eta$ ($\equiv |\eta_1 - \eta_2|$) and dR ($\equiv \sqrt{(\eta_1 - \eta_2)^2 + (\phi_1 - \phi_2)^2}$). The η - ϕ acceptance used to calculate all correlation functions was identical. Shown in Figure 1 is $C(dR)$. Simulated data incorporating Fritiof 1.7 and a de-

tailed model of detector response were analysed in the same fashion and are shown in the figure as grey bands of width $\pm 1\sigma$. The first few values of $C(dR)$ in all frames are outside the plotting limits, a consequence of the finite two-track resolution of the detector. Unlike $C(d\eta)$ (not shown), significant correlation peaks are observed in $C(dR)$ for $dR \leq 0.2$ in both central and peripheral collisions, though the peaks are much larger for peripheral collisions. The scale and strength of the correlations present in the data are reproduced reasonably well by the simulation.

From this we conclude that no correlated particle production is seen for correlation lengths $d\eta > 0.05$ or $dR > 0.05$ beyond that contained in Fritiof filtered through a model of the detector response. In addition, the correlation function analysis has considerable advantages over a factorial moment analysis, since it allows one to investigate particle correlations to the scale of the detector two-track resolution without bias.

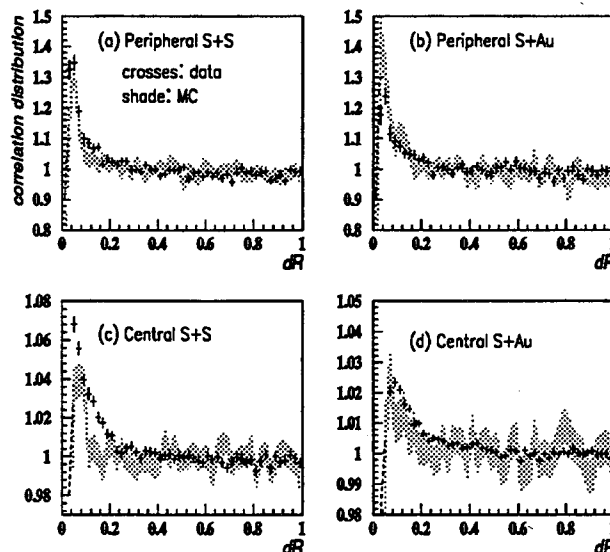


Figure 1: Two-particle correlation function versus dR .

Footnotes and References

¹A. Bialas and R. Peschanski, Nucl. Phys. B273 (1986) 703; A. Bialas and R. Peschanski, Nucl. Phys. B308 (1988) 857.

²M.A. Bloomer et al. (WA80 Collaboration), Nucl. Phys. A544 (1992) 543c; P. Jacobs et al. (WA80 Collaboration), Nucl. Phys. A545 (1992) 311c.

³for example, T. Abbott et al. (E802 Collaboration), Phys. Rev. Lett. 69 (1992) 1030.

Multiplicity Dependence of the Strangeness Production from the CERN Experiment NA-36

D. E. Greiner, C.R. Gruhn, I. Sakrejda, P.G. Jones and E.G. Judd

In the 1992 the CERN experiment NA36 published results¹ showing enhanced strangeness production at midrapidity in the collisions of 200 GeV/c per nucleon ³²S ions with a lead target. These results could suggest production of a new phase of matter - the Quark Gluon Plasma². There are no firm theoretical predictions for the conditions under which a transition to a different phase of matter would occur. Hence it is essential to correlate observed phenomena with global event parameters. One of the important global parameters is the event multiplicity that reflects centrality of the collision. Fig. 1 shows the correlation between the strangeness production and the number of negative particles produced in the event. Superimposed are the results of the strangeness production from the p+Pb collisions. Comparison indicates a factor of two enhancement in the ion induced reactions.

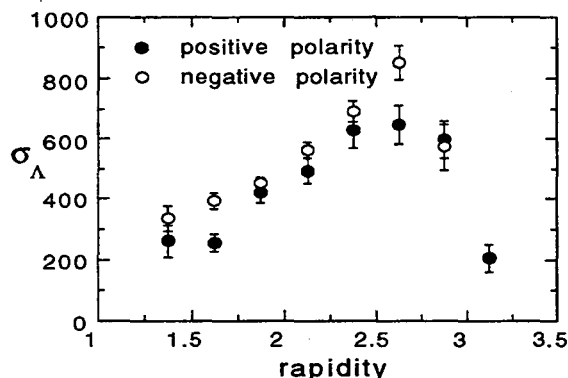


Fig. 2. Results obtained from the two independent sets of data show that corrections are well understood and under control.

¹ E. Andersen et al., Phys. Lett. B294 (1992) 127.

² J. Rafelski, H. Rafelski and M. Danos, Phys. Lett. B294 (1992) 131.

The initial rise of the Λ production with multiplicity observed in the S+Pb and p+Pb reactions suggests that the enhancement of the strangeness production could be related to the number of participants in the collision. Comparison with the Monte Carlo simulations based on the superposition of the p+p events (FRITIOF 7.0) shows a strong overall enhancement of the strangeness production in the nuclear interactions.

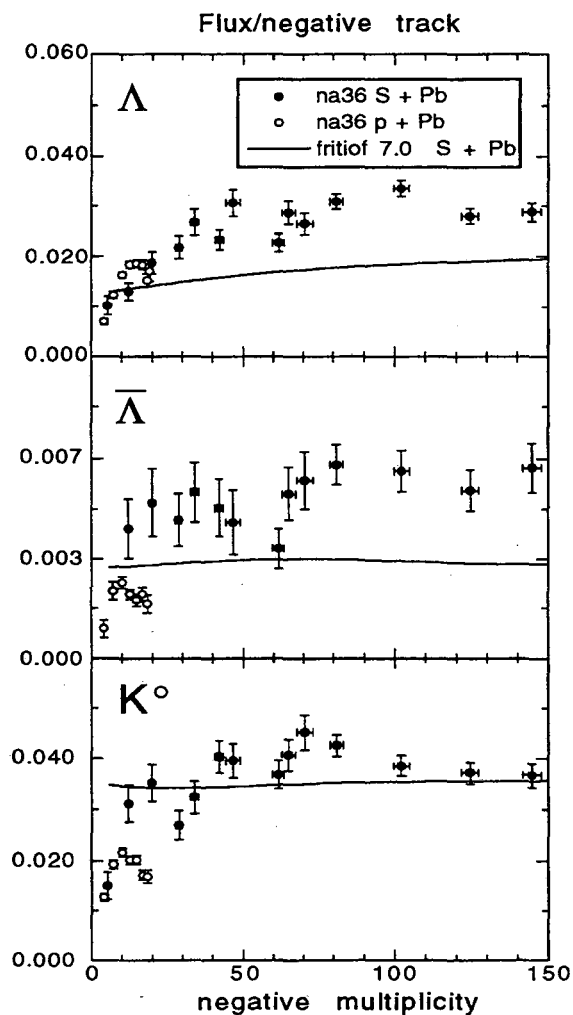


Fig. 1. Multiplicity dependence of the strangeness production.

Doubly Strange Baryons in CERN Experiment NA-36

D. E. Greiner, C. R. Gruhn, P. G. Jones, E. G. Judd and I. Sakrejda

The NA36 experiment at CERN has previously obtained some very interesting results on the production of singly strange, neutral, particles in S + Pb interactions at 200 GeV/c per nucleon.

The analysis has now proceeded to the next stage of extracting signals for doubly strange baryons, the Ξ^- and Ξ^+ . These particles are found from their decays to a singly strange baryon and a pion. This process has been completed for 60% of the data, and clear signals have been extracted. The results are shown in Figure 1 in the form of an Armenteros - Podolanski plot. The curves are at the correct kinematic positions for particles with a rest mass of the Ξ^- and Ξ^+ , ie 1.321 GeV.

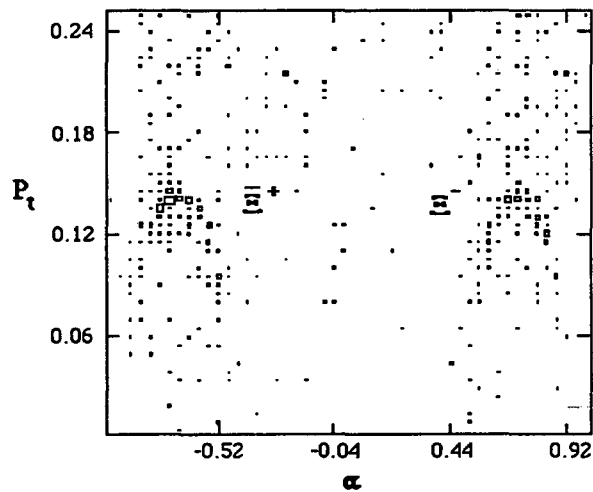


Figure 1

The invariant mass distributions are shown in Figure 2. Clear peaks, on a small flat background, can be seen in both cases. The statistics, however, are rather low, after background subtraction only $61 \pm 10 \Xi^-$ and $88 \pm 11 \Xi^+$ remain.

The process of correcting these yields for the experimental efficiency and acceptance is currently underway at LBL. Some first results have been extracted.

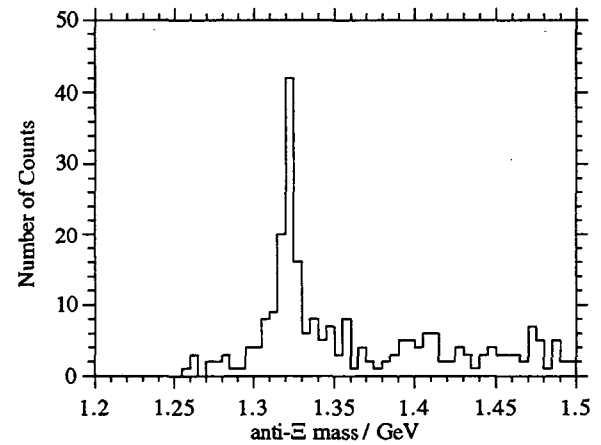
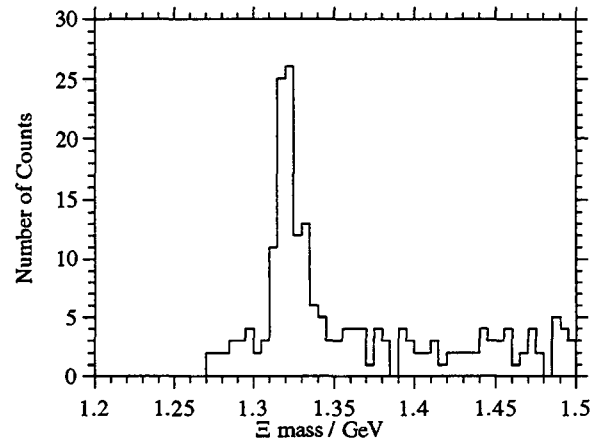


Figure 2

The $\Xi^+/\bar{\Lambda}$ ratio has been measured to be 0.05 ± 0.01 inside the experimental acceptance. This is consistent with the value of 0.06 ± 0.02 , obtained by the AFS collaboration in p + p interactions. But, it is inconsistent with the value of 0.33 ± 0.11 obtained by WA85. The NA36 results indicate that, while there is an enhancement in the production of both Ξ^+ and $\bar{\Lambda}$ in heavy ion collisions, doubly strange anti-baryons are not enhanced with respect singly strange ones. It is more likely, therefore, that the enhancement is due to increased stopping of the projectile, rather than quark-gluon plasma formation.

Antilambda Production near Midrapidity in central S + Au collisions at 200 GeV/nucleon.

NA35 Collaboration

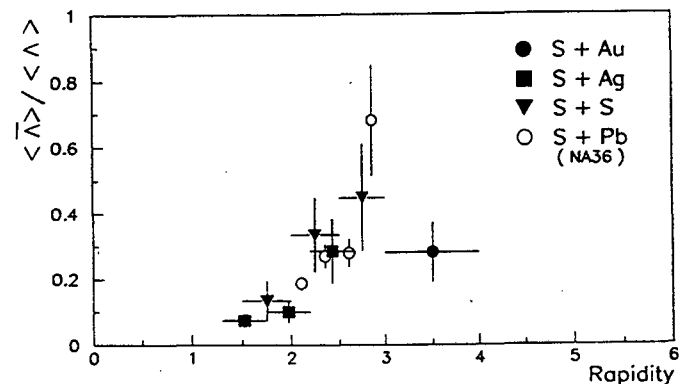
New data on neutral strange particle production in central S + Au collisions at 200 GeV/nucleon were obtained using a modified NA35 set-up, the so-called 'sweeper magnet configuration'. This modification was performed in order to extend the acceptance for Λ and $\bar{\Lambda}$ into the forward rapidity region ($3 < y < 4$).¹

The low momentum charged particles were removed from the streamer chamber by the sweeper magnet, which allowed the detection of the charged decays of Λ and $\bar{\Lambda}$ in the forward rapidity region. The sweeper magnet was 2 m long and situated 6.3 cm downstream from the target. In order to reduce the number of secondary particles in the streamer chamber, which do not come from the target but from interaction of primary particles with the sweeper magnet material, iron and steel slabs were built into the sweeper magnet. The vertical opening angle of the sweeper magnet was 2.5°. The streamer chamber was placed 3.61 m downstream from the target and the TPC was 3.46 m behind the streamer chamber. Because of the large distance between the target and the streamer chamber only Λ and $\bar{\Lambda}$ with large momenta (i.e. large γ -factor) will decay inside of the streamer chamber.

Central collisions were selected according to the energy deposited in the veto calorimeter ($\theta < 0.3^\circ$). The trigger cross section was 0.24 barn (6 % of total inelastic cross section). 40000 streamer chamber pictures were recorded. So far 1264 pictures were scanned and found (and measured) 1261 V^0 topologies. The single scanning efficiency is about 80 %. The average momentum error, $d(1/p)$, of the decay products is 0.0034.

Invariant masses are calculated for $p\pi^-$ (Λ), $\bar{p}\pi^+$ ($\bar{\Lambda}$) and e^+e^- (γ) pairs. In order to remove

the gammas from the sample, only decays for which the invariant mass of the e^+e^- pair is larger than 50 MeV were considered. The preliminary identification of Λ and $\bar{\Lambda}$ based upon the analysis of invariant mass and $\cos\theta_{cm}$ distributions yields 146 Λ s and 34 $\bar{\Lambda}$ s. (θ_{cm} is the angle between the Λ ($\bar{\Lambda}$) direction and the direction of p (\bar{p}) in the Λ ($\bar{\Lambda}$) rest frame.) The ratio $\bar{\Lambda}/\Lambda$ in the rapidity interval 3 to 4 is 0.28 ± 0.09 . This preliminary result is based upon the assumption that systematic losses of Λ and $\bar{\Lambda}$ are identical and that the p_T distribution of these particles is similar. In the figure the ratio ($\bar{\Lambda}/\Lambda$) in S + Au is compared to the ratios in S + S, S + Ag and S + Pb (NA36) collisions.



The ratio ($\bar{\Lambda}/\Lambda$) in S+Au events, compared to other data.

In the future only the streamer chamber pictures with antiproton candidate tracks which in addition do not point to the main vertex will be analyzed for $\bar{\Lambda}$. The \bar{p} candidates are identified by the measurement of the specific energy loss dE/dx of non vertex tracks in the TPC.

Footnotes and References

¹ J. Bartke et. al., *Z. Phys. C48*, 191(1990).

Impact Parameter Dependence of Bose-Einstein Correlations at 200 GeV/nucleon

The NA35 Collaboration

The NA35 TPC at the CERN SPS has been used in order to collect a data set of negative hadrons forward of rapidity 3 (nucleon-nucleon mid-rapidity) from minimum bias $E/A=200$ GeV S + Au collisions. We present preliminary results from a study of the dependence of the apparent pion source size upon event centrality, as inferred from the energy deposited into a veto calorimeter covering the beam fragmentation region (effective lab opening angle less than 0.3°).

During the Spring 1992 running period at CERN, a minimum bias data set was taken for the purpose of studying nuclear stopping power in $E/A=200$ GeV S + Au collisions; due to this triggering condition, these data were also amenable to a study of the dependence of pion source size as a function of event centrality. Fig. 1 illustrates the minimum bias veto energy spectrum for these collisions. Negative hadrons falling roughly between rapidities 3.7 and 4.7 and transverse momenta of 0.1 and 0.6 GeV/c were subjected to a two-particle correlation analysis; due to the limited statistics, correlation functions were only constructed in the one dimensional variable $q_{invariant}$. Fig. 2 presents the "radii" extracted in both the lowest veto energy (corresponding to most central collisions) and the highest veto energy (corresponding to the least central collisions) bins, presented as the lowest and highest cross-hatched regions in Fig. 1.

It has been observed that at AGS energies, the size of the source of pion production in heavy-ion collisions exhibits a dependence upon impact parameter in accord with a naive geometrical interpretation of two-particle correlation data.¹ This analysis is ongoing, but our results, presented in Fig. 2, appear to support this observation, i.e. for

identical colliding systems, the source sizes inferred for "central" events are observed to be somewhat larger than those inferred for "peripheral" events.

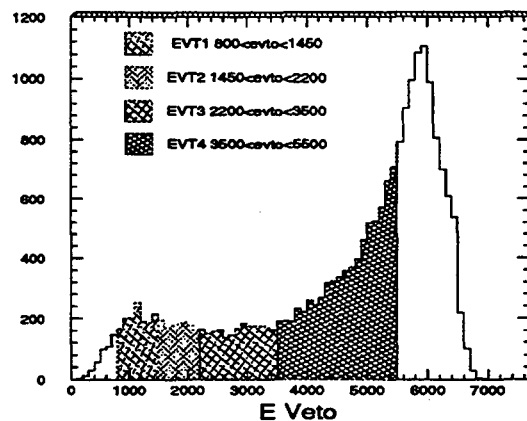


Fig. 1: This figure shows the minimum bias veto energy distribution from 200AGeV/c S+Au collisions.

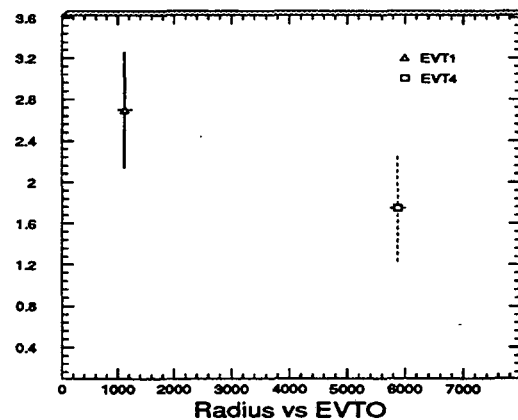


Fig. 2: This figure shows the dependence of the "invariant" source radius (in Fermi) upon veto energy. The source parameterisation is of the form $1 + \lambda \exp(-q^2 R^2/2)$

Footnotes and References

¹W. A. Zajc, et al., Nucl. Phys. **A544**, 237 (1992).

Electronics for the NA35 TPC

NA35 Collaboration

For the Spring 1992 sulphur beam run at the CERN SPS, the NA35 TPC was configured to maximize the track length in the detector (see Figure 1) in order to optimize pulse height resolution for the purpose of particle identification in the relativistic rise region. In this configuration, tracks could be measured by up to 60 TPC pad rows. In order to instrument 60 pad rows over a significant part of the TPC, additional electronics had to be constructed to supplement the original Aleph electronics. The collaboration decided to construct 6000 channels of modified EOS electronics for this purpose, giving a total of 11000 readout channels for the TPC. The modifications consisted of new printed circuit board layouts, shortening of the shaping time, expansion of the Switched Capacitor Array (SCA) from 256 to 512 time buckets, and an increase in the clock speed to 12.5 MHz.

These electronic channels were constructed, installed on the TPC, successfully integrated into the NA35 Data Acquisition system and used for physics during the Spring run. The pulse height resolution achieved as a function of number of samples is shown in Figure 2. The solid line is a fit to the data corresponding to the function $0.265N^{-0.43}$; this is in agreement with a semiempirical form derived previously.¹ An analysis is currently in progress to determine whether this pulse height resolution is sufficient at forward rapidities to identify protons and permit a measurement of stopping using *identified* protons, rather than positives minus negatives. Other TPC analysis projects in progress at LBL include $\pi\pi$ correlation functions and the identification of kinks (charged kaon decays) in the TPC volume.

In addition to generating physics, the NA35

TPC has served as a test bed for NA49 in various areas including electronics development and data analysis from TPCs outside of a magnetic field. The NA49 Main TPCs will have 90 pad rows. Extrapolation from Figure 2 shows that 90 samples will be sufficient to achieve the NA49 design goal of a pulse height resolution better than 4%.

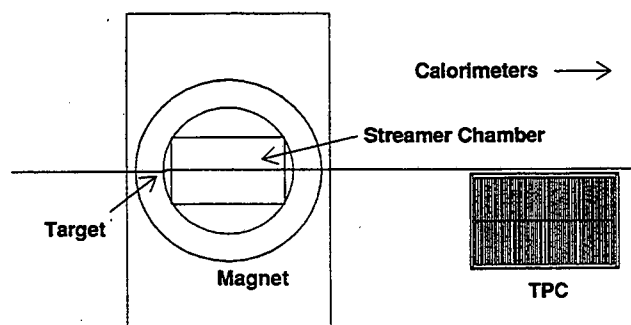


Fig. 1. NA35 layout showing TPC position suitable for relativistic rise dE/dx particle identification (Spring 1992). NA35 calorimeter not shown.

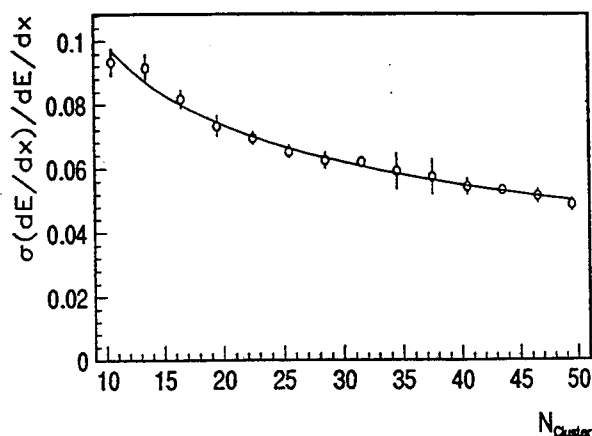


Fig. 2. Pulse height (dE/dx) resolution as a function of number of samples in the NA35 TPC. Solid curve: see text.

Footnotes and References

¹W.W.M. Allison and J.H. Cobb, *Ann. Rev. Nucl. Part. Sci.* **30**, 253 (1980).

The NA49 Experiment for Lead Beams at the CERN SPS

NA49 Collaboration

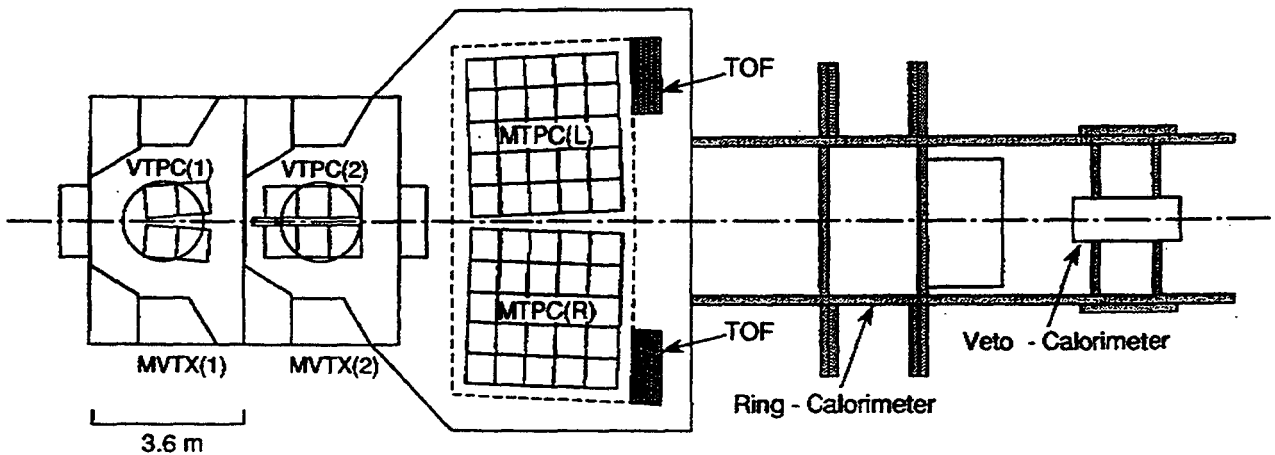
Lead beams at 160 GeV/nucleon will be available at the CERN SPS in the Fall of 1994. It is expected that central lead-lead collisions at the SPS will provide the highest energy density of *baryon-rich* nuclear matter available in the laboratory, and as such provide a unique opportunity to study such a state of matter.

The NA49 experiment is a major new facility designed to study many aspects of the collisions of such very heavy beams with heavy targets. It is a large acceptance, TPC-based experiment designed to track, measure the momentum, and identify most stable charged particles emitted into the forward half of phase space ($y > 2.9$). Physics goals include single particle spectra, high-statistics two particle correlation studies ($\pi\pi$, KK , pp) over a large portion of phase space, baryon stopping measurements, detection of singly and multiply strange particle decays, and intermittency. Because NA49 is a large acceptance device, the very high multiplicities produced in a central lead-lead collision create the interesting new possibility in NA49 of selecting events on the basis of several different features of the individual events (slope and $\langle p_T \rangle$ of pion p_T spectra, K/π , etc.), not just the usual criterion of centrality.

The layout of NA49 is shown in Fig. 1. The experiment consists of two dipole magnets, four

TPCs, two time-of-flight arrays, and forward calorimetry for triggering. Two TPCs are situated inside the dipole magnets (Vertex TPCs), and the others (Main TPCs) are situated in the field-free region. The Main TPCs are 3.6 m long, to achieve the pulse height resolution necessary ($<4\%$) to perform dE/dx particle identification in the relativistic rise region. The TOF arrays are situated in the region covering the momentum range 4–7 GeV/c, where adequate separation cannot be achieved by relativistic rise dE/dx . The first Vertex TPC is designed primarily to track mid-rapidity pions, which do not reach the Main TPCs, and the second Vertex TPC is designed primarily to detect neutral strange particle decays.

All TPCs are read out by capacitively coupled pad readout only. The sensitive volumes of the Main TPCs have dimensions $361 \times 361 \times 120$ cm³, with a total of 127,000 readout channels for both TPCs. The field cages for the Vertex TPCs have dimensions $235 \times 235 \times 80$ cm³, with 14,000 readout channels for the first Vertex TPC and 21,000 channels for the second. In total there are 161,000 readout channels in NA49.



Electronics for the NA49 TPCs

The NA49 Collaboration

We have developed new electronics for use with the large TPCs for CERN experiment NA49 (161,000 readout channels in total). These electronics can be seen as the natural next step in the evolution begun with EOS and NA35. The detector size, pad density, and cost considerations make it absolutely essential to have fully integrated front-end electronics and the highest possible performance in the data acquisition and compression system.

Two new integrated circuits have been developed for capturing and digitizing the chamber signals. A new 16-channel preamplifier/shaper IC combines the features of a previously developed low noise preamplifier circuit with a newly designed fully integrated 5-pole tunable shaping amplifier, and the 16-channel Switched Capacitor Array (analog store) chip used for NA35 has been augmented with A to D converters and double output buffers for every channel. Neither chip requires any external components, except for biasing and logical control functions

Figure 1 gives a schematic overview of the electronics chain. Two amplifier chips and two SCA/ADC chips are mounted on each Front-End

Board to service 32 pads. Control and Transfer (C/T) boards provide power and control signals and gather the data from 768 pads. This data is transferred via an optical fiber to data receiver modules located in the counting house.

To smooth out the SPS duty factor (5/19) and thus enhance the utilization of data compression hardware, each data channel has a 16 MByte input buffer capable of holding up to 32 events. This allows the embedded processors (Motorola 32-bit floating point Digital Signal Processors, DSP96002) to compact the data continuously rather than trying to keep up with the events only during the beam spill. Up to 40 events per beam spill will be recorded (2 events per second DC).

Activities at LBL include design and procurement of all custom ICs, design and fabrication of automated IC test equipment (including software), on-chamber C/T boards, and data receiver modules. Software is being produced to support the embedded DSPs, perform receiver board and C/T board diagnostics, and provide configuration control for the data acquisition system.

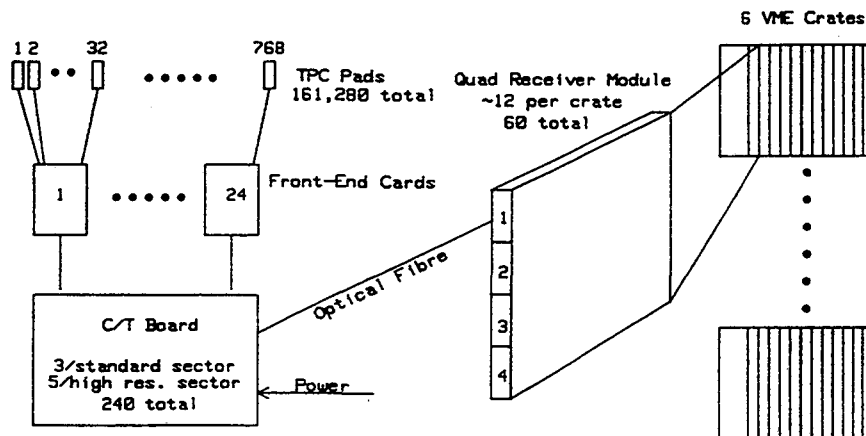


Fig. 1. Schematic Overview of TPC Electronics for NA49.

Advances in Solid State Nuclear Track Detectors*

P. B. Price

The review talk on which this paper was based was given at the most recent biennial international conference on principles and applications of solid state nuclear track detectors. About two-thirds of the attendees are usually from technologically underdeveloped countries.

Since the last opening talk that I have given in this series of conferences, several types of commercially available phosphate glasses with a wide range of sensitivities have been developed. Chief among these is BP-1, a barium phosphate glass with a high sensitivity and an unprecedented charge resolution.

CR-39, a polymeric track detector, has been found to respond differently at velocities below $10^{-2} c$, where nuclear stopping begins to dominate, than at high velocities, where electronic stopping dominates.

Atomic force microscopy has been shown to be a powerful new tool for the study of the etching process, using recoil tracks in mica and possibly other minerals.

CR-39 has been used to set limits on cold fusion rates in strong conflict with rates claimed by some electrochemists.

CR-39 and BP-1 have been used to study a number of topics in atomic and nuclear physics including charge pickup in relativistic nucleus-nucleus reactions, nuclear and electromagnetic spallation of relativistic heavy nuclei, the

determination of electron attachment and stripping cross sections for relativistic heavy nuclei, and cluster radioactivity.

CR-39 is being used to search for strangelets in nature and in ultrarelativistic nucleus-nucleus interactions at the Brookhaven AGS.

Several studies of cosmic ray composition carried on scientific spacecraft, including TREK, ANTIPODE, HIIS, and UHCRE, are obtaining new results using CR-39, polycarbonate, or BP-1 glass. The TREK experiment on the Mir Space Station involves Russian collaborators; two-thirds of the material will remain in space until 1995, after which it will be retrieved in a NASA Shuttle rendezvous with the Mir.

An experiment to search for weakly interacting massive elementary particles called WIMPs will use mica or another old mineral to detect very short tracks of nuclei that recoil when struck elastically by the WIMPs.

The most exciting thrust since the last SSNTD conference has been the development of new techniques such as AFM that permit one to identify nuclear particles at very low velocities, where nuclear stopping dominates.

Footnotes and References

*Condensed from keynote address at 16th International Conference on Solid State Nuclear Track Detectors held in Beijing, China, in September, 1992.

First Measurement of Cross Sections for Electron Capture and Stripping by Ultrarelativistic Ions*

Andrew Westphal and Y. D. He

We have made the first measurements of the equilibrium charge state and cross sections for orbital electron capture and stripping of ultrarelativistic ions with $g > 10$. We used gold ions with a mean kinetic energy of 10.8 A GeV at the Brookhaven AGS. Comparing our results with the theory of Anholt and Becker, we find that the ratio of the stripping cross section to the capture cross section differs from expectation by a factor of 2.3. The statistical significance is 10.5s. We find

that the capture cross section agrees with the prediction, but that the stripping cross section differs from theory by a factor of 2.0, with a significance of 3.5s. The discrepancy between our results and theory increases if we account for condensed matter effects.

Footnotes and References

* Condensed from a paper submitted to Phys. Rev. Lett.

Search for Abnormal Nucleus Production in Heavy-Ion Collisions *

Y. D. He and P. B. Price

A number of theorists including T. D. Lee and Gian-Carlo Wick have made quantitative speculations on the possibility of a second phase of nuclear matter that may be stable or metastable at much higher than normal nuclear densities. The few searches at the Bevalac in the 1970s led to negative results. Since the theories require the attainment of high densities, we thought it worthwhile to carry out a new search when the 11.4 A GeV ^{197}Au became available.

Our approach was to pass the gold beam through a thick Pb target and to search for tracks of density isomers having ionization rates corresponding to $Z/b > 82$ and velocity equal to or greater than the center-of-momentum velocity $b = 0.915$. Particles with this velocity would result from a completely inelastic collision of two nuclei of roughly equal masses.

In 10^9 collisions of 11.4 A GeV Au nuclei on a 1.27 cm Pb target we found nine events with large Z and velocities great enough to penetrate at least one mm-thick sheet of glass, but none of the nine had a velocity high enough to be considered a candidate for a density isomer. We believe that these events originated in beam-scraping interactions upstream of our target.

Our conclusion is that no nuclear products with $Z > 82$ and $b > b_{\text{CM}}$ were produced at an angle less than 140 mrad to the beam direction, allowing us to set an upper limit of 20 nb on the production cross section at 90% confidence level for abnormal nuclei with lifetime $\geq 10^{-9}$ sec.

Footnotes and References

*Condensed from a paper submitted to *Phys. Rev. Lett.* (in press).

Measurement of Cross Section for Charge Pickup by 11.4 A GeV Gold Ions *

Y. D. He and P. B. Price

In a systematic study, Ren *et al.*¹ found that the dependence of the inclusive cross section for nuclear charge pickup by relativistic projectiles in the energy interval 1 to 2 A GeV can be fitted by

$$\sigma_{DZ=+1} = a g_{PT} A_p^2 \quad (1)$$

where $g_{PT} = A_p^{1/3} + A_T^{1/3} - 1$ and $a = 1.7 \times 10^{-4}$ mb to within a factor two. To clarify the mechanism of relativistic charge pickup, we have made measurements at the AGS of charge pickup by 14.6 A GeV Si ions² and by 11.4 A GeV Au ions³ on seven targets ranging from CH₂ to Pb. We used BP1 phosphate glass detectors with a single-surface charge resolution of ~0.15 charge unit and an automated measurement system.

We found that the dependence of cross section on target mass is slightly steeper than in eq. (1); for a Au projectile it increases as $\sim A_T^{0.37}$. This dependence suggests that charge pickup occurs in peripheral reactions.

The dependence on projectile mass is much steeper than linear and not inconsistent with the A_p^2 dependence in eq. (1), which was established at ~1 A GeV.

The cross section decreases very weakly with energy in the interval 1 to 11.4 A GeV, in contrast to the rapid decrease from 0.6 to 0.8 A GeV.

Footnotes and References

* Condensed from a paper in Phys. Lett. B 298, 50-53 (1993).

1. Ren Guoxiao, P. B. Price and W. T. Williams, *Phys. Rev. C* 39, 1351 (1989).
2. P. B. Price and Y. D. He, *Phys. Rev. C* 43, 835 (1991).
3. Y. D. He and P. B. Price, Phys. Lett. B 298, 50 (1993).

Nuclear and Electromagnetic Fragmentation of 2.25-TeV ^{197}Au Nuclei*

Y. D. He and P. B. Price

We have made the first measurement of the total charge-loss cross section ($DZ \geq 1$) and partial cross sections ($DZ=1,2,3,\dots,9$) of 2.25-TeV ^{197}Au nuclei in six targets ranging from C to Pb. To disentangle the nuclear and electromagnetic contributions, we assumed that the nuclear contribution is energy-independent above 1 A GeV and given by ref. 1, and that the electromagnetic contribution increases with target charge as Z_T^d . The best fit to the data is with $d = 1.6 \pm 0.2$, which is consistent with experiments with lighter projectiles.

The electromagnetic partial cross sections in the Pb target exceed 40 mb for $DZ = 1, 2, 3$, and 4. For Pb the fractional contribution of electromagnetic fragmentation to the total charge-changing cross section is 15% for ^{16}O , 24% for ^{28}Si , and 20% for ^{197}Au at AGS energies. Thus, for Au the fraction is still substantial despite the large Coulomb barrier, which strongly favors neutron emission.

Tables and a figure give target and projectile factors for partial cross sections expressed as a sum of two terms, each of which is a product of a target factor and a projectile factor.

Footnotes and References

*Condensed from a paper submitted to Phys. Rev. Lett. (in press).

1. G. D. Westfall *et al.*, *Phys. Rev. C* **19**, 1309 (1979).

THEORY

Scale Dependence of Nuclear Gluon Structure*

K. J. Eskola

QCD-evolution of the parton distributions in heavy nuclei is studied with distributions constrained to conserve both baryon charge and momentum. The parton distributions at an initial scale $Q_0 = 2$ GeV are further constrained by the data on $\frac{1}{A}F_2^A/\frac{1}{2}F_2^D$ from deep inelastic lepton-nucleus collisions¹ and by the data on the anti(sea)quarks from the Drell-Yan lepton pair production in proton-nucleus collisions². For the gluon distributions, we consider two different Ansätze for gluon shadowing. The QCD-evolution is then computed using the first order Altarelli-Parisi-equations³, with and without the modifications due to small- x gluon recombination, calculated by Mueller and Qiu⁴. The main conclusion in each case remains the same: gluon shadowing vanishes much more rapidly than that of quarks and antiquarks, as shown by Fig. 1. In addition, the stronger the gluon shadowing, the slower does the shadowing of seaquarks vanish. The slow Q^2 dependence in the ratio $\frac{1}{A}F_2^A/\frac{1}{2}F_2^D$ is in accord with the experimental observations, especially also at small values of x and $4 \text{ GeV}^2 \lesssim Q^2 \lesssim 10 \text{ GeV}^2$.

As an application of the scale dependent nuclear modifications of the parton distributions, we compute the inclusive minijet cross sections $d\sigma_{\text{jet}}^{AB}/dp_T dy(y=0)$ in the range $2 \text{ GeV} \leq p_T \leq 10 \text{ GeV}$ at $\sqrt{s} = 200 \text{ GeV}$ and 6500 GeV . We conclude that at RHIC energies the scale dependent shadowing causes a relatively small depletion to the minijet cross sections in AB collisions at $p_T \lesssim 5 \text{ GeV}$, whereas at LHC energies -

depending on the strength of the still unknown gluon shadowing at the initial scale Q_0 - the depletion can be more than a factor 2.

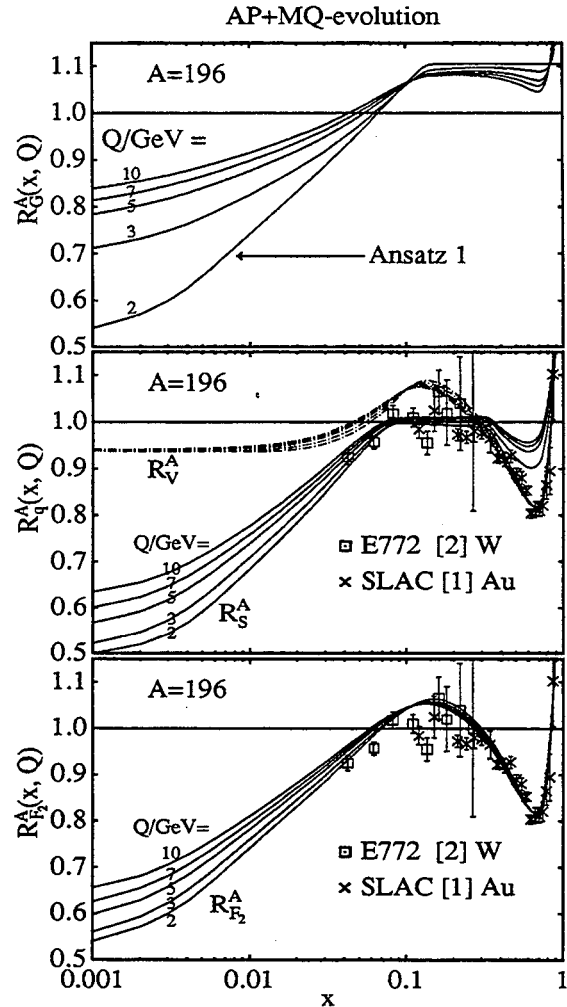


Fig. 1. The ratios of the parton distributions in $A = 196$ vs. free proton as functions of x at scales $Q = 2, 3, 5, 7, 10$ GeV. The evolution of the gluon ratio R_G^A , using our Ansatz 1 for gluon shadowing, is shown in the top figure, the sea(anti)quark ratio R_S^A and the valence quark ratio R_V^A in the middle, and the F_2 -ratio $R_{F_2}^A$ in the bottom figure.

Footnotes and References

- *LBL-32339, to appear in Nuclear Physics B
- ¹NM Collaboration, P. Amaudruz *et al.*, Z. Phys. C51 (1991) 387, R. G. Arnold *et al.*, Phys. Rev. Lett. 52 (1984) 727.
- ²D.M. Alde *et al.*, Phys. Rev. Lett. 64 (1990) 2479.
- ³G. Altarelli and G. Parisi, Nucl. Phys. B126 (1977) 298.
- ⁴A. H. Mueller and J. Qiu, Nucl. Phys. B268 (1986) 427.

Color Conductivity and the Evolution of the Minijet Plasma at RHIC*

K. J. Eskola and M. Gyulassy

In this paper we study possible consequences of color conductivity on the evolution of the minijet gluon plasma produced in $Au + Au$ at RHIC energies, $\sqrt{s} = 200$ AGeV. We also include effects of shear viscosity in the Navier-Stokes approximation¹. We start with minijet initial conditions at RHIC energies, as determined by first order perturbative QCD, with the scale dependent nuclear modifications to the parton densities included.² The plasma is then evolved according to the chromo-viscous-hydrodynamic equations with approximate longitudinal boost invariant initial conditions. In the context of the flux tube model for beam jet fragmentation,³ we show that the gluonic conductivity damps rapidly the background color field (see Fig. 1b). Ohmic heating keeps the energy density above the critical point slightly longer than in the case of free streaming but work done on viscous expansion reduces the final transverse energy by $\sim 25\%$ at RHIC energies.

The strongest effect of conductive flow in our calculation is the suppression of $q\bar{q}$ production from the background field shown in Fig. 1a. We emphasize that most of the minijets are gluons and the system is initially far from being in a chemical equilibrium with respect to quarks and gluons. The primary effect of color conductivity seems to be to hinder chemical equilibration by reducing the source of $q\bar{q}$ pairs. Without conductivity the background color field produces sufficiently many $q\bar{q}$ pairs that near ϵ_c chemical equilibrium

may be more nearly achieved. However, with the enhanced minijet conductivity the ratio of q to g densities remain far below equilibrium at least above the critical temperature.

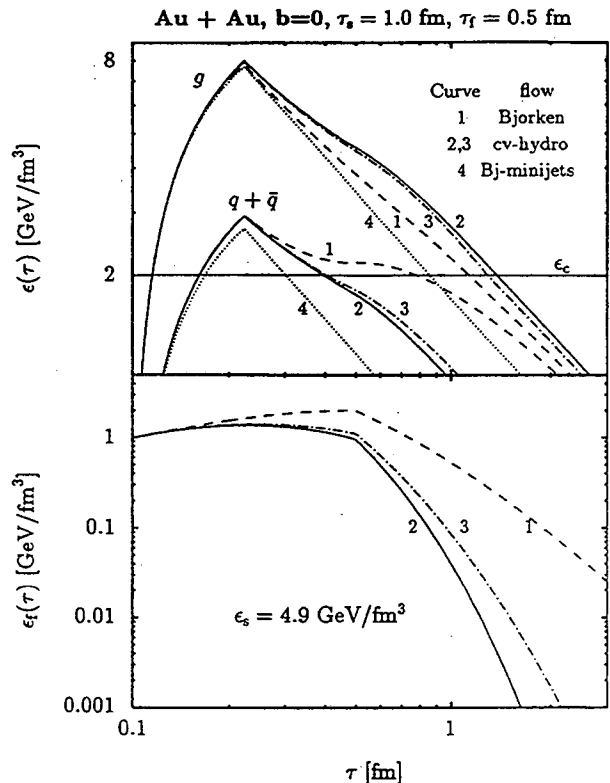


Fig. 1a. Evolution of the energy density of the minijet plasma with minijet initial conditions and decoupled fermions. Curves 1 correspond to non-conductive, non-viscous free flow. Curves 4 show the pure minijet contribution to curve 1. Curves 2 show the solution of the equations with the perturbative estimates for the viscosity and conductivity. Curves 3 show the solution when the momentum relaxation time τ_g is reduced by a factor of two. For curves 2 and 3 the gluon component is assumed to decouple at $\epsilon_c = 2 \text{ GeV/fm}^3$. Fig. 1b. The evolution of the field energy density in non-conductive (1) and conductive (2 and 3) cases.

Footnotes and References

*LBL-33150, CU-TP-586, submitted to Phys. Rev. C.

¹P. Danielewicz and M. Gyulassy, Phys. Rev. D31 (1985) 53.

²K.J. Eskola, *Scale Dependence of Nuclear Gluon Structure*, LBL-32339, to appear in Nucl. Phys. B.

³K. Kajantie and T. Matsui, Phys. Lett. B164 (1985) 373, Gatoff, A. K. Kerman and T. Matsui, Phys. Rev. D36 (1987) 114.

HIJING: A Monte Carlo model for multiple jet production in pp , pA and AA Collisions*

Xin-Nian Wang and Miklos Gyulassy

Combining perturbative-QCD inspired models for multiple jet production with low p_T multistring phenomenology, we develop a Monte Carlo event generator HIJING to study jet and multiparticle production in high energy pp , pA , and AA collisions. The model includes multiple minijet production, nuclear shadowing of parton distribution functions, and a schematic mechanism of jet interactions in dense matter. Glauber geometry for multiple collisions is used to calculate pA and AA collisions. The

phenomenological parameters are adjusted to reproduce essential features of pp multiparticle production data for a wide energy range ($\sqrt{s}=5$ -2000 GeV). Illustrative tests of the model on $p + A$ and light-ion $B + A$ data at $\sqrt{s}=20$ GeV/nucleon and predictions for Au+Au at energies of the BNL Relativistic Heavy Ion Collider ($\sqrt{s}=200$ GeV/nucleon) are given.

Footnotes and References

*Abstract of Phys Rev D44, 3501(1991)

Transverse flow due to minijets in $p\bar{p}$ collisions at $\sqrt{s}=1.8$ TeV*

Xin-nian Wang and Miklos Gyulassy

The multiplicity and flavor dependence of average transverse momentum of charged particles produced in high energy pp and $p\bar{p}$ collisions is studied in a PQCD inspired model. The experimentally observed transverse flow effect at $\sqrt{s}=1.8$ TeV is naturally explained in

the context of the fragmentation of multiple minijets which dominate the hadronic interaction mechanism at high collider energies.

Footnotes and References

*Abstract of Phys. Lett B282, 466 (1992)

Studying minijets via the p_T dependence of two particle correlation in azimuthal angle Φ *

Xin-Nian Wang

Following my previous proposal that two-particle correlation functions can be used to resolve the minijet contribution to particle production in minimum biased events of high energy hadronic interactions, I study the p_T and energy dependence of the correlation. Using HIJING Monte Carlo model, it is found that the correlation $c(\Phi_1, \Phi_2)$ in azimuthal angle Φ between two particles with $p_T^{cut} > p_T$ resembles much like two back-to-back jets as p_T^{cut} increases at high colliding energies due to minijet production. It is shown that $c(0,0)$ -

$c(0,\pi)$, which is related to the relative fraction of particles from minijets, increases with energy. The background of the correlation for fixed p_T also grows with energy due to the increase of multiple minijet production. Application of this analysis to the study of jet quenching in ultrarelativistic heavy ion collisions is also discussed.

Footnotes and References

*Abstract of Phys. Rev. D (in press); LBL-33499(1993)

Gluon Shadowing and Jet Quenching in $A + A$ Collisions at $\sqrt{s} = 200A$ GeV*

Xin-Nian Wang and Miklos Gyulassy

The sensitivity of moderate $p_T \leq 8$ GeV/c singles inclusive spectra in nuclear collisions to gluon shadowing and jet quenching is estimated using the HIJING Monte Carlo model. We show how the systematic study of the nuclear dependence of those spectra in $p + A$ can be used to determine the magnitude of gluon shadowing and how the

enhanced suppression in $A + A$ would provide information on the energy loss mechanisms in dense partonic matter.

Footnotes and References

*Abstract of Phys. Rev. Lett. 68, 1480 (1992)

Dynamical versus decay photons in $A + A$ Collisions at $\sqrt{s} = 200A$ GeV*

D.K. Srivastava M. Gyulassy and Xin-Nian Wang

Dynamical photons produced via $qg \rightarrow q\gamma$ and $q\bar{q} \rightarrow q\gamma$ processes in an equilibrated quark-gluon plasma are calculated in a hydrodynamic model for a wide range of initial conditions in ultra-relativistic heavy ion collisions. Electromagnetic decay photons are calculated via the Monte Carlo HIJING model including multiple minijet production. If rapid thermalization occurs and the decay photons can be subtracted with high

efficiency, the dynamical photons in the range $p_T > 2$ GeV may serve as a useful probe of the initial conditions in the plasma.

Footnotes and References

*Abstract of Phys. Lett. B276, 285 (1992)

†Variable Energy Cyclotron Centre, Calcutta, India

Interpretation of rapidly rotating pulsars*

F. Weibert and N.K. Glendinning

The minimum possible rotational period of pulsars, which are interpreted as rotating neutron stars, is determined by applying a representative collection of realistic nuclear equations of state. It is found that none of the selected equations of state allows for neutron star rotation at periods below 0.8 - 0.9 ms. Thus, this work strongly supports the suggestion that if pulsars with shorter rotational periods were found, these are likely to be strange-quark-matter stars. The conclusion that the confined hadronic phase of

nucleons and nuclei is only metastable would then be almost inescapable, and the plausible ground-state in that event is the deconfined phase of (3-flavor) strange-quark-matter.

Footnotes and References

*Abstract of Proceedings of 2nd International Symposium on Nuclear Astrophysics, Nuclei in the Cosmos, Karlsruhe, Germany, July 1992 (to be published)

†Institute for Theoretical Physics, University of Munich, Germany

Relativistic Mean-Field Calculations of Λ and Σ Hypernuclei*

N.K. Glendenning, D. Von-Eiff,† M. Haft,† H. Lenske† and M.K. Weigel†

Single-particle spectra of Λ and Σ hypernuclei are calculated within a relativistic mean-field theory. The hyperon couplings used are compatible with the Λ binding in saturated nuclear matter, neutron-star masses and experimental data on Λ levels in hypernuclei. The spin-orbit potentials for the hyperons and the

influence of the p-meson field (isospin dependent interaction) are discussed.

Footnotes and References

*Abstract of LBL-33031 submitted to Phys. Rev. C

†Sektion Physik der Ludwig-Maximilians, University of Munich, Germany

Application of the improved hartle method for the construction of general relativistic rotating neutron star models*

F. Weber† and N.K. Glendenning

Models of general relativistic rotating neutron stars, constructed from Hartle's perturbative "slow" rotation formalism of massive relativistic objects, are compared with their counterparts obtained from the exact solution of Einstein's equations. It is found that both methods, perturbative and exact, lead to compatible results down to rotational Kepler periods $P_K \approx 0.5$ ms, a value which is by far smaller than the smallest yet observed pulsar period. This finding rests on the reinvestigation of Hartle's method, (1) supplementing it by a selfconsistency condition inherent in the determination of the Kepler frequency, and (2) analyzing carefully sequences of star models near their end points. A collection of

17 representative neutron matter equations of state served as an input. Because of its simple structure, Hartle's method should prove to be a practical tool for testing models of the nuclear equation of state with data on pulsar periods. The form of an approximate empirical formula for the general relativistic Kepler frequency is obtained, and proportionality to the Newtonian expression arises in about equal parts from the equatorial flattening and the frame dragging.

Footnotes and References

*Abstract of Astrophys. J. 390, 541 (1992)

†Institute for Theoretical Physics, University of Munich, Germany

Neutron stars in the derivative coupling model*

N.K. Glendenning, F. Weber,† and S.A. Moszkowski‡

Properties of neutron stars derived from the hybrid derivative coupling model of nuclear field theory are studied. Generalized beta equilibrium with all baryon types to convergence is allowed. Hyperon couplings compatible with the inferred binding energy of the lambda hyperon in saturated nuclear matter predict a large hyperon population with neutrons having a bare majority population in a $1.5M_{\odot}$ neutron star. Among the properties studied are the limits on rotation

imposed by gravitation-radiation-reaction instabilities as moderated by viscosity. These instabilities place a lower limit on rotational periods of neutron and hybrid stars of about 1 ms.

Footnotes and References

*Abstract of Phys. Rev. C45, 844 (1992)

†Institute for Theoretical Physics, University of Munich, Germany

‡University of California at Los Angeles

Reconciliation of Neutron-Star Masses and Binding of the Λ in Hypernuclei*

N.K. Glendenning, S.A. Moszkowski,†

By relating scalar and vector couplings of the hyperons to the inferred empirical binding of the Λ hyperon in saturated nuclear matter, we obtain compatibility of this binding energy with neutron-star masses. Using the observational constraint of the lower bound on the maximum neutron-star mass and the upper bound of the couplings that are compatible with hypernuclear levels, we place bounds on the reduction in neutron-star mass that

hyperons produce. For the best current estimate of nuclear-matter properties, the reduction in mass due to conversion of nucleons to hyperons is $(0.71 \pm 0.15)M_{\odot}$. Neutrons comprise a slight majority population in neutron stars with mass $> 1.5M_{\odot}$.

Footnotes and References

*Abstract of Phys. Rev. Lett. 67, 2414 (1991)

†University of California at Los Angeles

Nuclear solid crust on rotating strange quark stars*

F. Weber,† and N.K. Glendenning

We calculate in general relativity the thickness, mass, and moment of inertia of the nuclear solid crust that can exist on the surface of a rotating strange quark star suspended out of contact with the quark core by an electric dipole layer on the core surface and the centrifugal force. Aside from the interesting properties of such stars, a particular question of great import to the viability of the strange matter hypothesis is whether strange stars can undergo the observed phenomena of pulsar glitches. We find that the nuclear crust can have a moment of inertia sufficiently large that a fractional change can account for the magnitude of pulsar glitches, even giant glitches. However, before testing a detailed model of the coupling of the crust and quark core, not an easy problem, we are not able to draw the

definite conclusion that strange stars can account for all phenomena associated with glitching such as the healing time and recurrence rate. The problem of understanding quakes on compact stars is, after all, akin to predicting earthquakes. We study the particular sequence of stars, both rotating and stationary, that have the maximum possible crust density, the neutron drip density. The sequence has a minimum mass of about $0.015M_{\odot}$ or about 15 Jupiter masses. Stars near this limit have crusts of thickness tens to hundreds of kilometers and are small and dark and so could be hiding places of baryonic matter.

Footnotes and References

*Abstract of Phys. Rev. Lett. 67, 2414 (1991)

†University of California at Los Angeles

First-order phase transitions with more than one conserved charge: Consequences for neutron stars*

Norman K. Glendenning

We consider how first-order phase transitions in systems having more than one conserved charge (multicomponent systems) differ from those in systems having only one. In general, the properties of the transition are quite different in the two cases. Perhaps most importantly the pressure varies continuously with the proportion of phases in equilibrium, and is not a constant in the mixed phase as in the example of the gas-liquid transition in familiar one-component systems. We identify the microphysics responsible for the difference. In the case that one of the conserved charges is the electric charge, a geometrical structure in the mixed phase is expected. As an example, possible consequences, are developed for the structure of a neutron star in

which the transition to quark matter in the core occurs. It is also pointed out that the general results pertain to relativistic nuclear collisions in the so-called stopping or baryon-rich domain where there are three conserved charges (baryon, electric, and strangeness), and impact the expected phase transition from confined hadronic matter to quark matter as regards signals that are supposedly driven by pressure. The physics discussed here is also relevant to the subnuclear gas-liquid transition that is under study in lower-energy nuclear collisions.

Footnotes and References

*Abstract of Phys. Rev. D46, 4 (1992)

Limiting rotational period of neutron stars*

Norman K. Glendenning

We seek an absolute limit on the rotational period for a neutron star as a function of its mass, based on the minimal constraints imposed by Einstein's theory of relativity, Le Chatelier's principle, causality, and lot-density equation of state, uncertainties in which can be evaluated as to their effect on the result. This establishes a limiting curve in the mass-period plane below which no pulsar that is a neutron star can lie. For example, the minimum possible Kepler period, which is an absolute limit on rotation below which mass shedding would occur, is 0.33 ms for a $M=1.442M_{\odot}$ neutron star (the mass of

PSR1913+16). A still lower curve, based only on the structure of Einstein's equations, limits any star whatsoever to lie in the plane above it. Hypothetical stars such as strange stars, if the matter of which they are made is self-bound in bulk at a sufficiently large equilibrium energy density, can lie in the region above the general-relativistic forbidden region, and in the region forbidden to neutron stars.

Footnotes and References

*Abstract of Phys. Rev. D46, 4161 (1992)

Neutron Stars, Strange Stars and the Nuclear Equation of State *

F. Weber[†] and N. K. Glendenning

This report consists of three parts. In part one, we review the present status of dense nuclear matter calculations, and introduce a representative collection of realistic nuclear equations of state which are derived for different assumptions about the physical behavior of dense matter (baryon population, pion condensation, possible transition of baryon matter to quark matter). In part two we review recently performed non-rotating and rotating compact star calculations performed for these equations of state. The minimum stable rotational periods of compact stars, whose knowledge is of decisive importance for the interpretation of rapidly rotating pulsars, are determined. In part three of this paper we investigate the amount of nuclear solid crust that can be carried by a rotating strange star, and answer the question whether such objects can give rise to the observed phenomena of pulsar glitches, which is at the present time the only astrophysical test of the strange-quark-matter hypothesis.

The indication of this work is that the gravitational radiation-reaction instability sets a lower limit on stable rotation for massive *neutron or hybrid stars* of $P \approx 0.8$ ms. Lighter ones having typical pulsar masses of $1.45 M_{\odot}$ are predicted to have rotational periods $P \gtrsim 1$ ms. This finding may have very important implica-

tions for the nature of any pulsar that is found to have a shorter period, say below $P \lesssim 0.5$ ms. Since our representative collection of nuclear equations of state does not allow for rotation at such small periods, the interpretation of such objects as rapidly rotating neutron or hybrid stars fails. Such objects, however, can be understood as rapidly rotating *strange stars*. The plausible ground-state state in that event is the deconfined phase of (3-flavor) strange-quark-matter. We find that the nuclear solid crust that can exist on the surface of a strange star (between R_{drip} and R_{surf} in Fig. 1) can have a moment of inertia sufficiently large that a fractional change can account for the magnitude of pulsar glitches. Furthermore low-mass strange stars can have enormously large nuclear crusts (up to ~ 400 km) which might considerably alter the cooling rate of strange stars and enables such objects to be possible hiding places of baryonic matter.

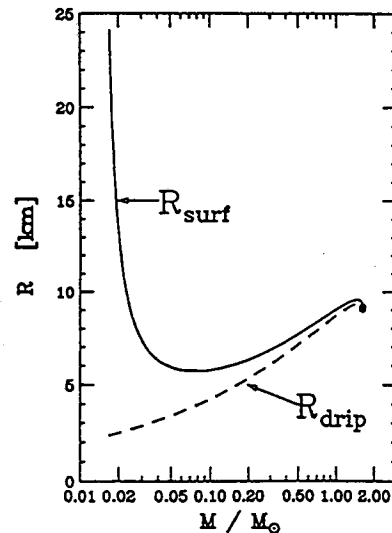


Figure 1: Radius versus mass of a strange star with nuclear crust.

Footnotes and References

*F. Weber and N. K. Glendenning, "Interpretation of Rapidly Rotating Pulsars", presented at the Second International Symposium on Nuclear Astrophysics NUCLEI IN THE COSMOS, Karlsruhe, Germany, July 6-10, 1992, (LBL-32562); F. Weber and N. K. Glendenning, "Neutron Stars, Strange Stars, and the Nuclear Equation of State", presented at the First Symposium on Nuclear Physics in the Universe, Oak Ridge, TN, September 24-26, 1992, (LBL-33066)

[†]Permanent address: Institute for Theoretical Physics, University of Munich, Theresienstr. 37/III, W-8000 Munich 2, F.R.G.

Early Cluster Recognition in Molecular Dynamics*

C. Dorso and J. Randrup

We have proposed a novel method for recognizing bound clusters in molecular dynamics simulations of nuclear collisions. Demanding that each particle in a given cluster be bound with respect to that cluster, we employ a Metropolis procedure (akin to simulated annealing) to maximize the cluster binding. Remarkably, the cluster structure can be identified approximately well before spatial separation occurs.

The "cost" associated with a given cluster decomposition $\mathcal{C} = \{C_1 C_2 \dots\}$ is thus taken as the corresponding clusterization energy, $E_{\mathcal{C}}$, *i.e.* as the sum of the energies of the individual clusters C_n , each one obtained by evaluating the total energy of that cluster in its own *CM* frame and disregarding its interactions with the rest of the system. The canonical probability corresponding to the particular cluster partition \mathcal{C} is then given by $P(\mathcal{C}) = e^{-E_{\mathcal{C}}/\tau}$, where τ is a prescribed "temperature" parameter.

In order to discuss the model we have made illustrative applications based on a simple molecular dynamics model developed earlier¹. In this model the total Hamiltonian is given by the free kinetic energy plus three types of two-body interaction: the Pauli potential (which serves to keep the nucleons apart in phase space), the nuclear potential (which is of a generalized Lennard-Jones form), and the Coulomb potential (for which we use point charges). This model gives a rough reproduction of the momentum distribution in a Fermi-Dirac gas, the binding energy of nuclear matter as a function of energy and temperature, and the size and binding of finite nuclei, and so it is sufficiently realistic to be useful for testing the proposed analysis method.

We have demonstrated that this method is very powerful in its ability to identify the ap-

proximate cluster structure already during the early stage when all clusters have considerable spatial overlap. The method is therefore of great practical utility in calculations of fragment production in heavy-ion reactions. Furthermore, the associated analysis demonstrates that the cluster structure is determined relatively early on in the process, at times when there is still considerable spatial overlap between the different preclusters. This feature has a bearing on our understanding of the fragment formation mechanism.

It should also be noted that the adopted criterion is by no means unique, and although all reasonable criteria will yield the same result when the clusters have separated sufficiently, they will generally differ at the early dense stage. Consequently, with the mathematical problem being somewhat fuzzy, the need for exact methods of solution therefore appears less compelling.

The proposed recognition method is not exact. However, the numerical simulations of fragment formation are statistical in nature and involve large samples of events. Therefore, what matters is the *distribution* of cluster decompositions and the recognition method is likely to be much better for this purpose.

We finally wish to draw attention to the fact that similar problems are encountered in other areas of physics, for example in the explosion of suddenly heated liquid drops. Indeed, our method can be regarded as a specific adaptation of the general concept of simulated annealing², which has already found application in a variety of areas, including mathematics, economics, and condensed matter physics³.

Footnotes and References

²S. Kirkpatrick, *J. Stat. Phys.* 34 (1984) 975

³*Simulated Annealing: Theory and Applications*, P.J.M. van Laarhoven and E.H.L. Aarts, D. Reidel Publishing Company, Boston (1987)

Footnotes and References

*LBL-33120: *Physics Letters B* (in press)

¹C. Dorso and J. Randrup, *Phys. Lett.* 215B (1988) 611

Simulating the Langevin force by simple noise in nuclear one-body dynamics*

M. Colonna^{ab}, G.F. Burgio^{ab}, Ph. Chomaz^a, M. Di Toro^b, and J. Randrup

^a) GANIL, Caen, France, ^b) LNS, Catania, Italy

For the purpose of addressing catastrophic phenomena in nuclear dynamics, we have explored the possibility of simulating the stochastic part of the collision integral in the Boltzmann-Langevin model by the numerical noise associated with the finite number of test particles in the ordinary *BUU* treatment. Considering idealized two-dimensional matter, for which it is practical to simulate the Boltzmann-Langevin equation directly, we have demonstrated that the number of test-particles per nucleon can be adjusted so that the corresponding *BUU* calculation yields a good reproduction of the spontaneous clusterization occurring inside the spinodal region. This approximate method may therefore provide a relatively easy way to introduce meaningful fluctuations in simulations of unstable nuclear dynamics.

Looking at the linear response to the Boltzmann-Langevin evolution, it is possible to demonstrate¹ that early on the average density fluctuation σ_k^2 associated with the unstable mode having wave number k satisfies an equation of motion of the form,

$$\frac{d}{dt}\sigma_k^2 \approx 2D_k + \frac{2}{t_k}\sigma_k^2, \quad (1)$$

where D_k is the source term arising from the stochastic nature of the collision integral.

It follows that the fluctuations of the mode k exhibit the following behaviour in time,

$$\sigma_k^2(t) \approx D_k t_k (e^{2t/t_k} - 1) + \sigma_k^2(0) e^{2t/t_k}, \quad (2)$$

where $\sigma_k^2(0)$ is the initial fluctuation. This result shows that the terms $D_k t_k$ and $\sigma_k^2(0)$ play sim-

ilar roles in the evolution. Therefore, it may be possible to replace the physical source term D_k by a suitable initial noise $\sigma_k^2(0)$ determined by the relation $\sigma_k^2(0) = D_k t_k$.

The numerical noise σ_k^2 scales as $1/\mathcal{N}$, and so it is possible to choose the number of test particles \mathcal{N} so as to reproduce the required magnitude of the physical source term D_k , for a particular value of the wave number k . Indeed, since in the *BL* lattice calculation we have $\sigma_k^2(0) = 0$, it follows from eq. (2) that asymptotically (*i.e.* for $t \gg t_k$) the magnitude of the fluctuations is determined by $D_k t_k$, whereas it is given by $D_k t_k/\mathcal{N} + \sigma_k^2(0)$ in the *BUU* test-particle simulation. Therefore, the matching of those two asymptotic evolutions determines the number of test particles \mathcal{N} .

We have then performed *BUU* calculations using a range of values for \mathcal{N} and compared the results with the corresponding lattice calculation. The results bear out our expectation that the time evolutions follow the form given in (2).

It must be noted that fluctuations are important *neither* before the system becomes unstable, since they are not amplified at this stage, *nor* after the fluctuations have grown to macroscopic size, because then their further development is dominated by the exponential amplification by the effective field. Therefore, the important physical conditions are those prevailing during a brief time window of the order of t_k after the system has entered the unstable region. By studying the physical properties of the system during the collision, and extracting the shortest amplification constant, it would be possible to determine that time window and to approximately match the numerical noise to the physical fluctuations over this time window.

Footnotes and References

*This work was supported by GSI, Darmstadt, Germany. Physical Review C (in press).

¹M. Colonna, Ph. Chomaz, and J. Randrup, LBL-33402: submitted to Nuclear Physics A.

Linear Response in Stochastic Mean-Field Theories and the Onset of Instabilities*

Maria Colonna[†], Philippe Chomaz[‡] and Jørgen Randrup[§]

We have shown that the application of linear-response theory to the Boltzmann-Langevin theory provides a relatively simple and complete understanding of the early development of the one-body phase-space density in nuclear matter, including its correlation function. Indeed, within such an approach it is possible to describe the time evolution of the correlated fluctuations created by the stochastic two-body collisions. This study is an extension of previous work¹.

The two-time correlation function contains no information on the spontaneous creation of fluctuations in the course of the evolution. However, for stable nuclear matter, it does exhibit the effects of both the Landau damping, due to the effective field, and the collisional damping. Moreover, for unstable systems, the two-time correlation function reflects the characteristic times for the amplification of existing fluctuations.

On the other hand, the evolution of the equal-time correlation function can be used to determine the source term governing the rate at which the unstable modes are agitated in the system. This has been illustrated the case of spinodal instabilities in idealized two-dimensional matter. In particular, the source term arising from the stochasticity of the basic nucleon-nucleon collision and the growth time associated with the self-consistent response of the effective field have been calculated on a grid inside the spinodal region in the density-temperature phase plane.

Footnotes and References

*Nuclear Physics A (submitted).

[†]INFN Sezione di Catania and LNS, Catania, Italy.

[‡]GANIL, B.P. 5027, F-14021 Caen, France.

[§]Supported by GSI, Darmstadt, Germany.

¹ J. Randrup and B. Remaud, NPA 514 (1990) 339; Ph. Chomaz, G.F. Burgio, and J. Randrup, PLB 254 (1991) 340; G.F. Burgio, Ph. Chomaz, and J. Randrup, NPA 529 (1991) 157; G.F. Burgio, Ph. Chomaz, and J. Randrup, PRL 69 (1992) 885.

The Boltzmann-Langevin equation reads:

$$\frac{\partial f}{\partial t} + \{f, H[f]\} = I[f] = \bar{I}[f] + \delta I[f], \quad (1)$$

where $f(\mathbf{r}, \mathbf{p}, t)$ is the one-body phase-space density. The left side is the collisionless Vlasov evolution and the right side represents the effect of the residual two-body collisions, which is decomposed into an average effect, $\bar{I}[f]$, and the fluctuating part $\delta I[f]$ (assumed to be Markovian).

To solve the Vlasov equation for nuclear matter, it is convenient to perform a Fourier transform with respect to the position \mathbf{r} . We may then look for particular solutions of the form $f_{\mathbf{k}}(\mathbf{p}, t) = f_{\mathbf{k},\omega}(\mathbf{p})/\exp(i\omega t)$, and we find the following dispersion relation for ω ,

$$1 = \frac{\partial U_{\mathbf{k}}}{\partial \rho} \int \frac{d\mathbf{p}}{h^D} \frac{(\mathbf{k} \cdot \mathbf{p})^2}{(\mathbf{k} \cdot \mathbf{p})^2 - m^2\omega^2} \frac{\partial f_0}{\partial \epsilon}. \quad (2)$$

The expansion on the eigenmodes has then only two terms for each value of \mathbf{k} ,

$$f_{\mathbf{k}}(\mathbf{p}, t) = A_{\mathbf{k}}^+(t)f_{\mathbf{k}}^+(\mathbf{p}) + A_{\mathbf{k}}^-(t)f_{\mathbf{k}}^-(\mathbf{p}). \quad (3)$$

Here the coefficients evolve according to the following equation of motion,

$$\dot{A}_{\mathbf{k}}^{\pm}(t) = \mp i\omega_{\mathbf{k}}A_{\mathbf{k}}^{\pm}(t) + B_{\mathbf{k}}^{\pm}(t), \quad (4)$$

which has been dubbed the *LaLime* equation. The first term represents the propagation of the mode in the self-consistent effective field, while the last term arises from the random part of the collision integral in (1). It has the following characteristic features,

$$\langle B_{\mathbf{k}}^{\kappa}(t) \rangle = 0, \quad \langle B_{\mathbf{k}}^{\kappa}(t)B_{\mathbf{k}'}^{\kappa'}(t') \rangle = 2D_{\mathbf{k}}^{\kappa\kappa'}\delta_{\mathbf{k}\mathbf{k}'}, \quad (5)$$

where $2D_{\mathbf{k}}^{\kappa\kappa'}$ is the phase-space diffusion coefficient expressed in terms of the collective modes.

Effect of N-Body Collisions on Subthreshold Kaon Production in High-Energy Nuclear Reactions*

Gustavo Batko, Jørgen Randrup, and Thomas Vetter†

We recently¹ generalized the standard *BUU* transport model to incorporate *N*-body collisions. We found that the total kaon yield is relatively unaffected by *N*-body collisions. However, one might expect that the inclusion of *N*-body collisions will enhance the yield of high-energy kaons in reactions at subthreshold bombarding energies. The model has now been further developed so as to allow the calculation of the energy spectra of kaons produced in nuclear reactions at relativistic energies.

Our starting point is the standard *BUU* model which is employed to provide a sequence of binary baryon-baryon collisions (primary collisions) events. For each such event it is determined how many additional baryons are located in the proximity, on the basis of the appropriate interaction range associated with the energy-dependent two-body interaction cross section $\sigma_{B_1 B_2}(\epsilon_{12})$. In this manner a "collision cluster" containing *N* baryons is identified, for that particular collision event.

In order to incorporate particle production in this model, we assume that the total energy available in the cluster, is first shared microcanonically between the *N* baryons in the cluster, before the two primary baryons produce the kaon.

The elementary process is of the form $B_1 B_2 \rightarrow BYK^+$, where *B* denotes the final baryon and the hyperon *Y* is either a Λ or a Σ , and it is furthermore assumed that the corresponding differential cross section $d^3\sigma_{B_1 B_2 \rightarrow K^+}(\epsilon_{12})/d\mathbf{p}$ is proportional to the phase space associated with the three particles in the outgoing channel. Since

Footnotes and References

*Nuclear Physics A546 (1992) 761; work supported by BMFT (Germany) and GSI, Darmstadt, Germany.

†Justus-Liebig-Universität Giessen, Germany.

¹Gustavo Batko, Jørgen Randrup, and Thomas Vetter, Nuclear Physics A536 (1992) 786.

we shall apply the model to the subthreshold regime, it suffices to include only those processes in which the emerging baryon *B* is a nucleon and the hyperon *Y* is a Λ particle (the Δ lies about 300 MeV higher in mass and the Σ mass is about 75 MeV above m_Λ , and their inclusion would anyway not affect our conclusions).

The effective differential cross section for a kaon production out of an *N*-body cluster is then obtained by averaging the elementary differential cross section over all the microcanonical momentum configurations of the *N*-body cluster.

The resulting model provides a conceptually simple, yet very general, scheme for taking account of the proximity of additional baryons in the nuclear medium. We wish to emphasize that the model developed represents a very simple extreme in which there is full equilibration between the two primary baryons and their cluster partners. Therefore, at least within the limitations of incoherent sequential scattering processes, it may be expected that the model will provide a useful upper bound on the effect of *N*-body collisions in nuclear reactions.

The various reactions contribute in a qualitatively similar manner to the invariant kaon multiplicity (considered as a function of the kaon kinetic energy): The inclusion of *N*-body collisions slightly enhances the kaon emission, with the effect growing with the kaon momentum. However, the differences between the spectra calculated from a pure binary and the full *N*-body simulation are, in all cases, remarkably small. This shows that, at least within the scope of the present model, the inclusion of *N*-body collision does not lead to a significant enhancement of the production of energetic mesons in the subthreshold energy regime.

BUU dynamics of unbound spherical nuclei*

Gustavo Batko and Jørgen Randrup

In recent years, extensive experimental efforts have been devoted to the collection and analysis of multifragment data in heavy-ion collisions at intermediate energies. A major goal is to probe the properties of nuclear matter at high density and temperature. However, the degree to which this can be attained depends on our ability to model the reaction dynamics adequately. Motivated by these efforts, we have studied the dynamical evolution of a nucleus that has been prepared in an excited but spherically symmetric configuration, generated either by compressing the ground state by a specified factor λ or by heating its local Fermi-Dirac momentum distribution. The systems considered all lie above the disassembly threshold and so it is energetically possible to disperse the system into its nucleon constituents. The dynamical evolutions have been calculated within the general framework of the Boltzmann-Ühling-Uhlenbeck model, using a commonly employed method of solution that propagates \mathcal{N} (≈ 100) A -body systems in the same effective one-body field. We have modified an existing code so as to ensure that the initial spherical symmetry is preserved, even when the system is situated in a mechanically unstable region of the phase diagram.

For moderate compressions the nucleus exhibits a weakly damped monopole oscillation, whereas for large initial compressions the radial motion induced by the release of the compressional energy is sufficient to cause the system to disperse into a dilute nucleon gas. For a range of intermediate values of the initial compression factor λ the expanded system lingers for a relatively long time in a hollow bubble-like configuration while continually radiating nucleons.

During this bubble stage the system is unstable against clusterization into fragments of

more favorable density. We illustrate this tendency towards spontaneous symmetry breaking by studying these situations with the standard *BUU* method which is endowed with considerable inherent irregularities since only a finite number of parallel systems \mathcal{N} are treated, and thus the unstable modes are readily triggered. The sensitivity of the *BUU* results to the numerical parameter \mathcal{N} is largest when the initial compression λ is near the critical value (*i.e.* that initial compression for which the nuclear cohesion exactly halts the outwards motion). On the other hand, when the dynamics keeps the system well away from instabilities (such as for sufficiently modest initial compressions), or only enters such regions sufficiently briefly (as during a rapid expansion), then there is relatively little trajectory branching and, accordingly, the *BUU* model is expected to yield a physically reasonable description of the macroscopic evolution.

Our present studies suggest the existence of a specific nuclear multifragmentation process by which an initially compressed nuclear system disassembles into several massive fragments. The characteristic feature is a decompression leading to an unstable hollow structure whose global evolution is sufficiently slow to allow the instabilities to manifest themselves, resulting in a clusterization of the structure into disjoint prefragments. Although our study has been carried out for an idealized spherical geometry, recent calculations indicate that such a scenario may be approximately reached in actual central heavy-ion collisions at intermediate energies [?]. This novel process displays an intricate interplay between the time scale for the global expansion dynamics and those for the triggering and amplification of the various unstable modes. The qualitative identification and quantitative exploration of this process would provide important new experimental information on nuclear dynamics.

Footnotes and References

*LBL-32722: Nuclear Physics A; supported by GSI.

Refinements of the Nucleon-Exchange Transport Model for the Emission of Hard Photons and Nucleons*

S.J. Luke^a, R. Vandenbosch^a, and J. Randrup

^a *Nuclear Physics Laboratory, University of Washington, Seattle, WA98195*

We have extended the nucleon-exchange transport model¹ to also include proton emission in addition to neutron emission. This extension is relatively straightforward, requiring only additional effects of the Coulomb barrier for the escaping protons and the effect of the Coulomb forces from both donor and receptor nuclei on the outgoing proton. The multiplicity of the pre-equilibrium protons is generally lower than that of the neutrons, because of the suppression from the Coulomb barrier, and the proton spectra are harder than the neutrons, due to the Coulomb push received by the receding proton.

We have also incorporated the effect of the known diffuse momentum distributions of the nucleons in the nuclear ground state. This has been done in a somewhat ad hoc manner, since it goes beyond the one-body nature of the model. The diffuseness used in our calculations is based on simulating the experimental ground-state nucleon momentum distribution, rather than by fitting pre-equilibrium particle emission spectra. It is therefore gratifying to find that the high-energy slopes of the calculated emission spectra are in good agreement with experiment. This extension is most important for low bombarding energy and for more asymmetric systems, at a given bombarding energy, as it increases the multiplicity and hardens the spectra most in these circumstances. For higher bombarding energies and more symmetric systems the energy dissipation at the early stage of the collision leads to hot nuclei with diffuse momentum distributions which dominate the contribution from the diffuse ground-state correlations.

Footnotes and References

*Submitted to Physical Review C

¹J. Randrup, Nucl. Phys. A327 (1979) 490; A383 (1983) 468; J. Randrup and R. Vandenbosch, Nucl. Phys. A474 (1987) 474

Furthermore, we have investigated changes in the expected *pn* nucleon-nucleon bremsstrahlung due to both the diffuse momentum distributions and quantum-mechanical effects on the elementary production mechanism. The latter has been treated classically in our earlier work². Suggestions have been made in the literature that quantum-mechanical effects are most important at higher nucleon-nucleon energies and for photons near the kinematical limit. The enhancements are typically less than a factor of two. When incorporated into the transport model they are most important for proton-induced reactions where it is possible to measure the photon emission near the kinematical limit.

Finally, we have pursued a suggestion³ that deceleration of the partners in the heavy-ion reaction during the transit time of an exchanged nucleon may modify the emission probability more for jets originating from the heavier reaction partner than for those originating from the lighter partner. This extension of the model involves solving for the propagation of the nucleons in the non-inertial frame of the decelerating and rotating host nucleus, thus considerably complicating the numerics. The results obtained are in the direction expected, but their effect on the residue velocity is modest. Predictions of mean residue velocities exhibit the correct trend with mass asymmetry but underestimate considerably the magnitude of the dependence. This is attributed to the known amounts of momentum carried away by complex particles, particularly α particles, which may arise from a variety of mechanisms.

Footnotes and References

²J. Randrup and R. Vandenbosch, Nucl. Phys. A490 (1988) 418

³Stuart Gazes, private communication (1990)

The Order to Chaos Transition in Axially Symmetric Nuclear Shapes*

J. Blocki,† F. Brut,‡ T. Srokiwski§ and W.J. Swiatecki

The transition from order to chaos for independent classical particles moving in variously deformed square well potentials (three dimensional "billards") is studied quantitatively by the method of Lyapunov exponents. The billards or containers are either variously elongated axially symmetric spheroids, spheres rippled according to Legendre Polynomials P_2 , P_3 , P_4 , P_5 and P_6 , or fission like shapes. The increase of the fractional volume of phase space corresponding to chaotic trajectories is studied as a

function of the deviation of the shapes from the sphere. The role of the particle's angular momentum about the symmetry axis in suppressing chaos is demonstrated.

Footnotes and References

*Abstract of Nucl. Phys. A545 (1992) 511c.

†Institute for Nuclear Studies, Swierk, Poland

‡Institut des Sciences Nucleaires, 38026 Grenoble-Cedex, France.

§Institute of Nuclear Physics, Krakow, Poland.

A Numerical Verification of the Prediction of an Exponential Velocity Spectrum for a Gas of Particles in a Time Dependent Potential Well*

J. Blocki,† F. Brut,‡ and W.J. Swiatecki

Using computer simulations we demonstrate that, as predicted, the velocity distribution for a gas of independent particles bouncing around chaotically in several types of deforming containers tends to an exponential function of the velocity. The generalized one-body dissipation formula for the heating up of such a gas, also derived earlier, is shown to give a good overall

account of the numerical results, although small deviations are apparent.

Footnotes and References

*Submitted to Nucl. Phys.

†Institute for Nuclear Studies, Swierk, Poland

‡Institut des Sciences Nucleaires, 38026 Grenoble-Cedex, France.

A Diffusion Equation for Energy in Ergodic Adiabatic Ensembles*

C. Jarzynski

This paper is concerned with systems evolving chaotically under a slowly time-dependent Hamiltonian, H . The principal result can be stated as follows. If we are given an ensemble of such systems, with initial conditions corresponding to different initial energies, and if we observe these systems as they evolve chaotically under the slowly changing H , then the distribution of energies $\eta(E, t)$ — defined so that $\eta(E, t) dE$ gives the number of systems with energy in an interval dE around E at time t — satisfies the following diffusion equation:

$$\frac{\partial \eta}{\partial t} = -\frac{\partial}{\partial E}(g_1 \eta) + \frac{1}{2} \frac{\partial^2}{\partial E^2}(g_2 \eta) \quad (1)$$

Here, g_1 and g_2 are functions of E and t for which explicit expressions are derived entirely in terms of the motion of systems of energy E evolving under the time-independent Hamiltonian obtained by “freezing” H at time t . Thus, the time-dependent problem is solved in terms of the solutions of a continuous sequence of time-independent problems.

The problem of systems evolving chaotically under a slowly time-dependent Hamiltonian has been considered in detail by Ott, Brown, and Grebogi¹. Ott has demonstrated that, for trajectories evolving under such a Hamiltonian, the volume of phase space enclosed by the instantaneous energy shell (surface of constant H) on which the trajectory is found, is an adiabatic invariant (i.e. is conserved in the limit of infinitely slow evolution of H). This quantity is the *ergodic adiabatic invariant*, Ω .

An important issue is the “goodness” of the ergodic adiabatic invariant, the extent to which its invariance is violated when the evolution of H is

not perfectly adiabatic. Considering an ensemble of trajectories with initial conditions distributed over a single energy shell of H , then allowing these trajectories to evolve for a time over which the Hamiltonian changes by order unity, the error in Ω may be measured by the moments of the final distribution of energies of this ensemble with respect to the energy predicted by the conservation of Ω . In the present paper, we apply our diffusion equation to solve for the rates of growth of the first two of these moments². The results which we obtain disagree with those obtained by Ott *et al.* using multiple-time-scale analysis.

We also derive explicit expressions for $\langle \Delta \Omega \rangle$ and $\langle (\Delta \Omega)^2 \rangle$ as functions of time, where $\Delta \Omega$ is the change in the value of Ω for a given system, and the brackets indicate an average over the ensemble. The quantities $\langle \Delta \Omega \rangle$ and $\langle (\Delta \Omega)^2 \rangle$ represent a more direct measure of the goodness of the ergodic adiabatic invariant Ω than the energy moments mentioned above.

We then consider two trivial cases of ergodic adiabatic Hamiltonians: in the first, a chaotic Hamiltonian undergoes uniform translational motion, in the second, uniform rotational motion. We show that the formalism of our theory correctly predicts that in both of these cases there will be no diffusion of energies (i.e. the diffusion coefficient in our equation works out to be zero).

Finally, we mention several areas, including heavy-ion dynamics and cosmic ray acceleration, in which the results of this paper may have applications.

Footnotes and References

*Published in Phys. Rev. **A46**, 7498 (1992).

¹E. Ott, Phys. Rev. Lett. **42**, 1628 (1979); R. Brown, E. Ott, and C. Grebogi, Phys. Rev. Lett. **59**, 1173 (1987), and J. Stat. Phys. **49**, 511 (1987).

Footnotes and References

²Higher moments grow at rates which are smaller by at least one order in a formally small “slowness parameter”, and are therefore not considered.

Theory of Rotational Population Patterns in Heavy-Ion Transfer Reactions: Even-Even Thorium Nuclei*

S. Y. Chu, J. O. Rasmussen, R. Donangelo, M. A. Stoyer, S. Frauendorf and Y. R. Shimizu

We developed and applied a straightforward Hamiltonian matrix diagonalization (HMD) method for rotor plus multinucleons to calculate the lowest several bands in $^{230,232,234}\text{Th}$. Neutron pair transfer strength distributions were calculated and compared between HMD and cranked Hartree-Fock-Bogoliubov plus Random Phase Approximation (CHFBRPA). Sudden-approximation methods were applied to estimate pair transfer population patterns in $^{206}\text{Pb} + ^{232}\text{Th}$ reactions. Band-crossing, pairing, and spin alignment properties were also discussed. We show here just the large combined proton and neutron calculation for ^{230}Th .

We shall not repeat the detail discussion of HMD method here, since it was given in Engeland reference¹. We differ in combining proton and neutron structure into very large matrices.

Fig.1 a-c show the results of the combined calculation. The dimensionality of the matrix has been decreased by an energy criterion that cuts out the less important configurations. Even so, the Hamiltonian matrix here has dimensionality of 19,098. The matrix is rather sparse, with 275,189 non-vanishing matrix elements. Parts of the code with the Lanczos algorithm require quadruple precision in the Sparcstations and double precision on the U.C Berkeley Cray in order to converge. The eight lowest roots were taken for the 16 diagonalizations at the 16 different spin values. The CPU time on the Sparcstation ELC was 73 hrs.

Footnotes and References

*Invited paper to be published in Proceeding of the Conference on Nuclear Physics in Our Time, Sanibel Island, Florida Nov. 1992, World Scientific Pub. Co., Singapore
¹ T. Engeland, *Proc. Nordic Winter School on Nuclear Physics (April 1983)* (World Scientific, Singapore, 1984) p. 155

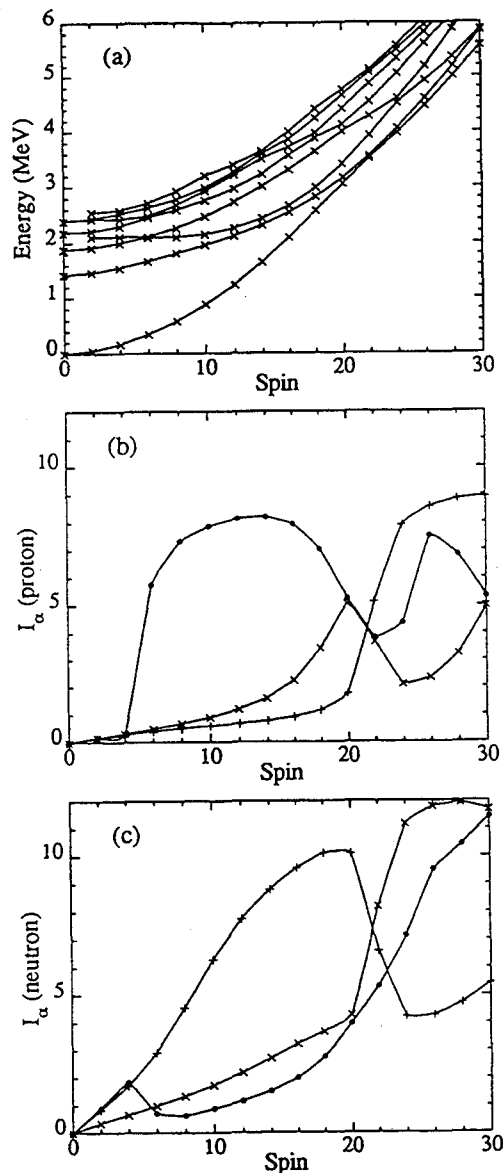


Fig.1 (a) HMD energies for the yrast and lowest seven even-parity bands in ^{230}Th . (b) proton spin alignment and (c) neutron spin alignment for yrast(x), yrare(+) and second excited band(•).

SEMINARS

Nuclear Science Division

Iwona Sakrejda LBL	Recent Results on Strangeness Production from the NA36 Experiment	January 21, 1992
Edward Shuryak SUNY	Theoretical Problems in High-Temperature QCD	January 27, 1992
Jay Davis LLNL	Inspection of Iraqi Nuclear Facilities under United Nations Resolution 687	February 3, 1992
Walter Loveland Oregon State University	The Production of Heavy Residues and Heavy Elements in Nucleus-Nucleus Collisions	February 24, 1992
Angela Olinto University of Chicago	Strange Goings-On in Neutron Stars	March 2, 1992
Baha Balantekin University of Wisconsin Madison	Solar Neutrino Physics with SNO and BOREXINO	March 4, 1992
Dr. Michael Musolf MIT	The Interpretation of Parity-Violating Electron Scattering Experiments	March 6, 1992
Dr. Jonathan Engle Bartol Research Institute	Dark Matter and Nuclear Physics	March 9, 1992
Dr. Xin-Nian Wang Duke University	High Transverse Momentum Aspects of RHIC and the Quark-Gluon Plasma	March 11, 1992
Dr. Tetsuo Hatsuda University of Washington	Hadrons in Hot/Dense QCD	March 12, 1992
Dr. Walter Muller GSI	Fragmentation of Gold Projectiles: From Evaporation to Vaporization	March 23, 1992
Dr. David Bowman MSU	Multifragmentation as a Probe of Nuclear Dynamics	March 30, 1992
Dr. Jim Vary Iowa State Ames Laboratory	Continuum Bound States in the Electron- Positron System and the GSI Phenomena	March 30, 1992
Dr. Craig A. Ogilvie GSI, Darmstadt	Nuclear Disassembly	April 1, 1992
Dr. Leslie J. Rosenberg Enrico Fermi Institute U. of Chicago	PeV Astrophysics with the Chicago Air Shower Array	April 6, 1992
Dr. Peter M. Jacobs Lawrence Berkeley Laboratory	Intermittency: Threat or Menace?	April 8, 1992

Dr. John Hardy Chalk River	Fermi-Beta Decay and the CVC Vector Coupling Constant: Test of CVC and the Standard Model	April 10, 1992
Dr. Claude Detraz GAMIL	Current European Nuclear Physics Projects — Which Ones and Why?	April 13, 1992
Dr. Jean-Antoine Scarpaci Institut de Physique Nucleaire Orsay	Nuclear Giant Resonance Studies at Orsay	April 20, 1992
Andrew Stuchbery Australia National University Canberra	Aspects of Magnetic Moments of Nuclear Excited States	May 11, 1992
Prof. Richard I. Steinberg Drexel University Philadelphia, PA	PERRY: A Long Base Line Reactor Neutron Oscillator Experiment and Solar Neutron Detector	May 22, 1992
Dr. Richard Hahn Brookhaven National Laboratory	Solar Neutrinos Observed by GALLEX	June 19, 1992
Dr. Norbert Porile Purdue University	Search for QCP in p - p Collisions at $s = \text{TeV}$	June 22, 1992
Dr. O. Dumitrescu Bucharest	Four-Nucleon Correlation and a New Superfluid Phase in Nuclei	July 20, 1992
Prof. Shiva Kumar Yale University	Anti-Proton Production	July 24, 1992
Dr. Lukesh Desai U.C. Irvine	Production and Detection of Strange Matter	July 28, 1992
Dr. Luis Egido Autonomous University of Madrid	Microscopic Description of the Electromagnet Decay of Hot Nuclei at High Angular Momentum	August 3, 1992
Dr. Zhiging Zhang LAL (Orsay)	New Measurement of Tau Branching Ratios with the ALEPH Detector at LEP	September 1, 1992
Dr. Brian Fujikawa UCB - LBL	Search for a 17 keV Neutrino in the Beta Decay of S-35	September 21, 1992
Dr. Valeria Perishina GSI	Theoretical Study of the Physico-Chemical Properties of Element 105	September 28, 1992
Dr. Walter Greiner University of Frankfurt	Clustering in the Quark-Gluon Plasma	October 5, 1992
Dr. Fred Wietfeldt LBL	Search for a 17-keV Neutrino in the ^{55}Fe Internal Bremsstrahlung Spectrum	October 12, 1992

Dr. Andrew Hime Los Alamos National Laboratory	Do Scattering Effects Resolve the 17-keV Conundrum?	October 26, 1992
Prof. Tadanori Minamisono Osaka University	Proton Halo of 8B Detected by Its Giant Quadrupole Moment	November 16, 1992
Dr. Craig Sangster LLNL	Two Fragment Correlations and Fragment Emission Timescales in Intermediate Energy Heavy Ion Collisions	November 23, 1992
Prof. M. Sakai Institute for Nuclear Studies University of Tokyo	Electron Lines from Positron Scattering on Heavy Targets	November 30, 1992
Prof. Yuri Oganessian Flerov Laboratory of Nuclear Reactions JINR, Russia	Experiments with Exotic Beams and Targets	December 3, 1992
Dr. Craig A. Stone San Jose State University	Exploring Nuclear Science with MacNuclide	December 4, 1992
Dr. Richard Tighe LBL	Entrance Channel Effects in Sub-Barrier Fusion	December 7, 1992
Dr. Hans Gutbrod GSI/CERN	WA98, the Other Pb Beam Experiment and the Concept for the LHC Ion Experiment	December 9, 1992
Dr. Peter Sonderegger CERN	Di-muon Production and the Elusive Quark-Gluon Plasma	December 14, 1992

Nuclear Theory

Keijo Kajantie Univ. of Helsinki	A Cosmological Z (3) Phase Transition in the QCD Sector of the Cosmic Fluid at 10 TeV	February 24, 1992
Angela Olinto Univ. of Chicago	Strange Goings-On in Neutron Stars	March 2, 1992
Baha Balantekin Univ. of Wisconsin, Madison	Solar Neutrino Physics and SNO and BOREXINO	March 4, 1992
Michael Musolf MIT	The Interpretation of Parity-Violating Electron Scattering Experiments	March 6, 1992
Jonathan Engel Bartol Research Institute	Dark Matter and Nuclear Physics	March 9, 1992
Xin-Nian Wang Duke Univ.	High Transverse Momentum Aspects of RHIC and the Quark Gluon Plasma	March 11, 1992
Tetsuo Hatsuda Univ. of Washington	Hadrons in Hot/Dense QCD	March 12, 1992
Yuki Asakawa Texas A&M	Novel Features in Dilepton Spectra from Hot Dense Matter	March 20, 1992
Dr. A.V. Selikhov Kurchatov Inst. Moscow	Collision Terms for a Quark-Gluon Plasma in a Semiclassical Limit	March 27, 1992
Dr. A.V. Selikhov Kurchatov Inst. Moscow	The Last Word on QCD Transport	May 27, 1992
Gongou Xu Lanzhou University Littlejohn & Co.	Topological Approach to the Study of Quantum Chaos	June 4, 1992
Biswarup Banerjee Tata Institute of Fund. Research	Quark-hadron Phase Transition, Primordial Nucleosynthesis and Supercooling of the Universe	June 10, 1992
Scott Chapman	The Effective Action of SU(N) at Finite Temperature	June 15, 1992
Dawei Dong LBL	Physics of Neurobiology	June 18, 1992
Prof. Horst Stocher U. of Frankfurt	Strangelet Production in AA	July 22, 1992

Raffaele Mattiello U. of Frankfurt	RQMD Dynamics for AA	July 24, 1992
Chris Jarzynski LBL	Report on Phys. Rev. paper by M. Wilkinson and E. Austin	August 12, 1992
Prof. Robert Vinh Mau University of Paris	Baryogenesis in the Early Universe	August 11, 1992
Dr. Ulrich Mosel University of Giessen	Dileptons-Probes for Hadronic Interactions in Dense Matter	August 25, 1992
Dr. S. J. Wang LBL	Level Dynamics: An Approach to the Study of Avoided Level-Crossing and Transition to Chaos	August 26, 1992
Dr. Walter Greiner Univ. of Frankfurt	Clustering in the Quark-Gluon Plasma	October 5, 1992
Dr. Scott Pratt MSU	Pion Lasers in Heavy Ion Collisions	October 29, 1992
Dr. Scott Chapman LBL	The QCD Effective Potential and Monopoles	November 6, 1992
Kari J. Eskola LBL	My Research Program, Goals, Motives, ...	November 16, 1992
Jorgen Randrup LBL	My Research Program, Goals, Motives, ...	November 23, 1992
W. Swiatecki LBL	My Research Program, Goals, Motives, ...	November 30, 1992
Prof. Lee Lindblom Cal Tech	Neutron Star Structure and the Equation of State (The Inverse Problem)	December 2, 1992
N.K. Glendenning LBL	My Research Program, Goals, Motives, ...	December 7, 1992
Dr. Klaus Geiger U. of Minnesota	Dilepton Emission from Cascading Partons in Ultrarelativistic Heavy Ion Collisions	December 9, 1992
Dr. Sean Gavin BNL	Evidence of High Densities from J/Psi Suppression	December 18, 1992
Jan Cernohorsky LBL	My Research Program, Goals, Motives, ...	December 14, 1992
Dr. Ramona Vogt GSI	My Research Program, Goals, Motives, ...	December 21, 1992

AUTHOR INDEX

Author Index

- Ahmad 46
Alonso 86
Anholt 31
Armstrong 113, 114
Azaiez 45
Baglin 26
Baisden 57
Bardayan 79, 80
Batchelder 72, 73, 74, 75, 78
Batko 140, 141
Bauer 68
Bazin 64
Bearden 46
Beausang 44, 47, 48
Beck 82
Becker 42, 43, 44, 45, 46, 47, 57
Bercovitz 106
Bertsche 30
Bilewicz 52
Bistirlich 93, 113, 114
Blocki 143
Bloomer 115
Blumenfeld 31, 65
Bonetti 88
Bossingham 93, 113, 114
Bossy 93, 113, 114
Bowman 67, 68
Bradley 65
Brinkman 42, 43, 45, 46
Browne 25, 26, 77
Brüchle 57
Brut 143
Burde 42, 43, 46, 48, 49
Burgio 138
Carlin 68
Carpenter 46
Case 93, 113, 114
Cebra 106
Cebra, 110
Cederwall 42, 45
Cerny 72, 73, 74, 75
Chacon 93
Champagne 81
Chan 26, 76, 77, 78, 79, 80, 82, 83
Chartier 67
Chiesa 88
Chomaz 138, 139
Christie 91, 107
Chu 145
Cizewski 44, 46
Clark 27, 30, 31
Collins 27, 85
Colonna 31, 63, 65, 66, 67, 68, 69, 71, 138, 139
Crowe 93, 113, 114
Crystal Barrel Collaboration 113, 114
Czerwinski 60, 61
D'Erasmus 70
da Cruz 26, 76, 77, 78, 79, 80, 81, 83
Daly 46
Danielewicz 84
Dardenne 93
Davidson 49
de Cruz 82
deBoer 43, 45
Deleplanque 42, 43, 44, 45, 46, 47, 48, 49
Delis 63, 65, 70
deSouza 68
Di Toro 138

Diamond 42, 44, 45, 46, 47, 48
Diamond, 43
DiToro 66
DLS Collaboration 10, 98, 99, 100, 101
Donangelo 145
Dong 83
Dorso 137
Dracoulis 49
Draper 42, 43, 44, 45, 46, 47
Duyar 42, 43, 45, 47
Duyer 46
Dycus 82
Eichler 54, 57
EOS Collaboration 11, 94, 95, 96, 97
Eskola 129, 130
Fabricius 49
Fallon 42, 45
Fiore 70
Firestone 25, 26
Fornal 46
Frauendorf 47, 145
Friedrich 93
Fukuda 86, 91
Gäggeler 54, 57
Galvin 101
Garbowski 46
Garcia 26
García 76, 77, 78, 79, 80, 82, 83
Garg 46
Gelbke 67, 68, 84
Glendenning 19, 132, 133, 134, 135, 136
Gober 57
Gong 68, 84, 106, 112
Goth 71
Gregorich 53, 55, 56, 57, 58, 60, 61, 62
Greiner 116, 117
Gruhn 116, 117
Guarino 65
Guglielmetti 88
Guy 27
Gyulassy 130, 131, 132
Haft 133
Halbach 30
Hall 60, 61
Hamilton 59, 60, 61
Hannink 50, 53
Hanold 63, 64, 65, 68, 70
He 102, 123, 124, 125, 126
Henderson 60, 61
Henry 42, 43, 44, 45, 46, 47
Hesselink 46
Hill 43
Hindi 78, 79, 80, 81
Hirata 92
Hjort 106, 112
Hoffman 50, 51, 52, 53, 54, 55, 56, 57, 58, 59, 60, 61
Hsi 67
Huang 106
Hughes 43, 45, 46
Hulet 88
Iori 65, 70
Izumikawa 86
Jacobs 115
Jäger 57
Janssens 46
Jarzynski 144
Jones 106, 108, 117
Jost 57
Judd 116, 117
Justice 70
Kacher 52, 53, 55, 56, 58, 60, 61
Kadkhodayan 53, 54, 55, 56, 57, 58, 60, 61

Kajiyama 82
Kalantar-Nayestanaki 46
Keane 95, 106
Kelley 43
Kelly 45, 46
Khoo 46
Kim 68
Kobayashi 91, 92
Koehler 82
Korten 45
Kovacs 54, 57
Kratz 57
Krebs 86
Kreek 53, 55, 56, 57, 58, 60, 61
Kuhnert 42, 43, 45, 46
Kunkel 30
Lane 53, 55, 56, 58, 59, 60, 61
Larimer 76, 77, 78, 79, 80, 81, 83
Latimer 26
Lauritsen 46
LBL-SNO Group 87
Lee 42, 45, 53, 55, 56, 57, 58, 60, 61
Lenske 133
Lesko 26, 76, 77, 78, 79, 80, 81, 82, 83
Leung 30
Leyba 60, 61
Li 30
Liang 46
Libby 65, 70
Lisa 67, 68
Luke 142
Lundgren 27, 85
Lynch 67, 68
Lyneis 27, 31, 85
Macchiavelli 43, 45, 48, 49
Madan 65
Mader 68
Manduci 71
Marchetti 65
Margetis 107, 109, 110
Mastinu 71
Matheoud 88
Matis 101
Matsuta 86, 91
Mayer 46
McDonald 27, 31, 86
McHarris 93
McMahan 27, 31, 65, 68
Meng 65
Meyerhof 31
Migliorino 88
Mignerey 65, 70
Milazzo 71
Minamisono 86
Mitchell 106, 112
Mohar 53, 56, 62
Molitoris 31
Moltz 72, 73, 74, 75, 78
Moody 88
Morenzoni 31
Moretto 31, 63, 65, 66, 67, 68, 69, 70
Moroni 70
Morretto 64
Morrisey 64
Morse 106, 111
Moszkowski 133, 134
NA35 Collaboration 14, 118, 119, 120
NA36 Collaboration 15
NA49 Collaboration 15, 121, 122
Naudet 99, 107, 109
Nessi 31
Neu 51, 53, 55, 56, 58, 60, 61

Nissius 46
 Nitsche 51
 Nitschke 41
 Nojiri 86
 Normal 26
 Norman 76, 77, 78, 79, 80, 81, 82, 83
 Nurnia 60, 61
 Odyniec 107, 109
 Ognibene 72, 73, 74, 75, 78
 Ohtsubo 86
 Oliveira 42, 43, 45, 46, 47, 49
 Olson 91
 Orr 64
 Ozeroff 82
 Pantaleo 70
 Partlan 97
 Paticchio 70
 Peaslee 65, 67, 68
 Pershina 57
 Phair 67, 68
 Plompen 46
 Porter 100
 Poskanzer 13, 115
 Pratt 84
 Price 88, 102, 123, 124, 125, 126
 Purgalis 82
 Rai 94, 106
 Randrup 137, 138, 139, 140, 141, 142
 Rasmussen 93, 145
 Reviol 46
 Ritter 9
 Roussel-Chomaz 65, 66
 Rowe 72, 73, 74, 75
 Roy 44, 47
 Rubel 42, 43, 45, 46, 47
 Russo 50
 Sakrejda 106, 108, 116, 117
 Santoruvo 65
 Schädel 57
 Schambach 107
 Scharenberg 106
 Schausten 57
 Schimpf 57
 Schwarz 67
 Scott 95
 Secondary Radioactive Beams Collaboration 11
 Sherrill 64
 Shimizu 145
 Shimoura 91, 92
 Shirley 26
 Shuman 106
 Silva 50, 51
 Singh 26
 Skulski 63, 67, 71
 Smith 82
 Snowden-Ifft 102
 Sobel 106, 112
 Sobotka 31
 Soramel 46
 Spooner 31
 Srivasta 132
 Srokiwski 143
 STAR Collaboration 16, 105, 106, 107, 108, 110,
 111
 Stephens 42, 43, 44, 45, 46, 47, 48, 49
 Stockstad 26
 Stokstad 76, 77, 78, 79, 80, 82, 83
 Stoller 31
 Stone 106
 Stoyer 42, 43, 44, 45, 46, 93, 145
 Stringfellow 106
 Sudbury Neutrino Observatory Collaboration 82

Sugimoto 91, 92
Sui 63, 65, 70
Sur 81
Suzuki 91
Swiatecki 143
Sylwester 53, 55, 56, 58, 60, 61
Symons 1, 86
Tanigaki 86
Tanihata 91, 92
Tighe 74, 75
Toki 92
Tsang 67, 68
Tso 63, 67, 69
Turko 101
Türler 55, 56, 57, 60, 61
Vandenbosch 142
Veeck 63, 71
Vermeulen 57
Vetter 140
Vo 43, 45, 46
Von-Eiff 133
WA80 Collaboration 115
Walton 109
Wang 45, 46, 95, 131, 132
Weber 132, 133, 134, 136
Weigel 133
Weiman 91
Westphal 102, 123
Wieman 106, 112
Wietfeldt 26, 76, 77, 78, 80, 83
Wietfeldt, 79
Williams 68
Wilson 98, 107, 109
Winger 64
Wohn 43
Wozniak 3, 31, 63, 64, 65, 66, 67, 68, 69, 70, 71
Xie 27, 85
Yoshida 91
Young 30
Zimmerman 57
Zizka 101
Žlimen 26, 76, 77, 78, 79, 80, 82, 83

Lawrence Berkeley Laboratory
Technical Information Department
University of California
Berkeley, California 94720

ABH456

LBL Libraries